BRNO UNIVERSITY OF TECHNOLOGY
VYSOKÉ UČENÍ TECHNICKÉ V BRNĚ

FACULTY OF MECHANICAL ENGINEERING
FAKULTA STROJNÍHO INŽENÝRSTVÍ

ENERGY INSTITUTE
ENERGETICKÝ ÚSTAV

ASSESMENT OF THE THERMAL ENVIRONMENT IN VEHICULAR CABINS
HODNOCENÍ TEPELNÉHO PROSTŘEDÍ KABIN AUTOMOBILŮ

DOCTORAL THESIS
DIZERTAČNÍ PRÁCE

AUTHOR — **Ing. Miloš Fojtlín**
AUTOR PRÁCE

SUPERVISOR — **prof. Ing. Miroslav Jícha, CSc.**
ŠKOLITEL

BRNO 2019

Abstract

People in developed countries spend substantial parts of their lives in indoor environments both during free time and while working. For this reason, there has been increasing interest in the quality of the indoor environment. The main emphasis of past research has been directed towards understanding the fields of human health, productivity, and comfort. One important contributor to all three fields is the thermal aspect of the environment, which is often represented by physical quantities such as air temperature, radiant temperature, air humidity, and air velocity. While weather-independent control of these parameters is possible via heating, ventilation, and air-conditioning systems (HVAC), a major limitation is that these systems are related to substantial energy consumption and carbon footprint. The complexity of thermal management is amplified in vehicular cabins because of their asymmetric and transient nature. Moreover, in electric vehicles, the available energy for microclimate management comes at the cost of driving range, and therefore, new solutions for more effective and human-centred ways of managing the indoor microclimate are sought.

One of the promising ways to address these issues is via local conditioning with the vehicle seats or auxiliary radiant panels operating in synergy with an HVAC unit. At the same time, the optimization and research tasks are being shifted towards virtual investigation to mitigate the need for costly and often ethically concerning human studies. To do so, models of human thermo-physiology and thermal sensation/comfort have been developed. Yet, for their reliable applications, many factors regarding high heterogeneity, clothing, the thermal mass of the adjacent surfaces, and active seat conditioning have not been resolved.

The aim of this thesis was to develop a methodology to assess human thermal sensation while in a sitting body position, including local conditioning factors such as heated and ventilated seats. A requirement of the method was applicability in both virtual and real indoor spaces. In the latter case, the focus was a thermal-sensation-driven feedback loop allowing for human-centred microclimate management.

The validity of the proposed methodology was demonstrated under typical cabin conditions (5–41 °C) and the findings from this PhD project are transferable to a broad variety of engineering fields. In passenger transport and occupational environments with higher heat strain, environmental engineers can benefit from a tool to identify sources of thermal discomfort and potential hazards of fatigue. Furthermore, the methodology can be of great merit to the rapidly developing electric vehicle industry, facilitating emphasis on energy efficient microclimate management. The virtual optimization of the conditioning strategies reduce the need for human studies, allow rapid prototyping, and have great potential to bring energy savings as well as increased driving range. Finally, the know-how presented is also applicable in built environments, where similar conditions apply.

KEYWORDS:

Modelling; Experiment; Heating; Ventilation; Seat; Human; Thermo-physiology; Fiala model; Equivalent temperature; Clothing; Seated position; Cabin; Vehicle; Car; Energy; HVAC; Thermal sensation; Thermal comfort

BIBLIOGRAPHIC CITATION:

FOJTLÍN, Miloš. *Assessment of the thermal environment in vehicular cabins*. Brno, 2019. Available from: https://www.vutbr.cz/studenti/zav-prace/detail/113758. Doctoral thesis. Brno University of Technology, Faculty of Mechanical Engineering, Energy Institute. Supervisor Miroslav Jícha.

Abstrakt

Ľudia žijúci vo vyspelých krajinách trávia väčšinu svojho života vo vnútorných prostrediach budov alebo dopravných prostriedkov. Z tohto dôvodu, záujem o výskum kvality vnútorných prostredím rastie, pričom hlavný dôraz je kladený na oblasti výskumu ľudského zdravia, produktivity a komfortu. Jedným z faktorov ovplyvňujúci kvalitu prostredí je ich tepelný aspekt, ktorý je najčastejšie popísaný teplotou vzduchu, radiačnou teplotou, vlhkosťou vzduchu a rýchlosťou prúdenia vzduchu. Zatiaľ čo tieto parametre je možné riadiť systémom pre vykurovanie, vetranie a klimatizáciu nezávisle na počasí, takéto zariadenia sa podieľajú na vysokej spotrebe energie a značnej uhlíkovej stope. V prostediach kabín áut a dopravných prostriedkov je riadenie parametrov tepelného prostredia komplikované z dôvodu ich asymetrickej a časovo premenlivej povahy. Táto situácia je obzvlášť kritická vo vozidlách na elektrický pohon s vlastnou batériou, kde je energia na úpravu vnútornej mikroklímy čerpaná na úkor dojazdu vozidla. Pre uvedené dôvody sa hľadajú nové, energeticky účinnejšie spôsoby pre úpravu tepelných prostredí a zabezpečenia tepelného komfortu.

Jedným z potenciálnych riešení sú zariadenia dodávajúce človeku teplo alebo chlad lokálne, ako napríklad vyhrievané a vetrané sedadlá a sálavé panely. Vzhľadom na to, že experimentálny výskum vnútorných prostredí je náročný s ohľadom na čas a potrebné vybavenie, trendy výskumu vplyvov takýchto zariadení na človeka smerujú k optimalizačným úlohám vo virtuálnych prostrediach pomocou modelov ľudksej termofyziológie a tepelného pocitu/komfortu. Avšak pre spoľahlivé výsledky modelovania sú potrebné presné vstupné parametre definujúce prostredie, odev, vplyv povrchov v kontakte s človekom (napríklad sedadlá) a pôsobenie systémov na lokálnu úpravu mikroklímy.

Cieľom tejto dizertačnej práce je vytvorenie metodológie na hodnotenie tepelných prostredí v kabínach automobilov s ohľadom na pozíciu v sede a využitím technológii na lokálnu úpravu tepelných prostredí. Jedným z požiadavkov na takúto metodológiu je jej aplikovateľnosť vo virtuálnych ale aj reálnych prostrediach. V prípade hodnotenia reálnych prostredí, cieľom je vytvorenie demonštrátora, ktorý by bol využiteľný ako spätná väzba pre riadenie systémov pre úpravu mikroklímy na základe požadovaného tepeleného pocitu.

Validita uvedenej metodológie bola demonštrovaná v typických podmienkach kabín automobilov (5–41 °C) a poznatky z tejto práce sú prenesiteľné do širokého spektra inžinierkych aplikácii. V oblasti osobnej dopravy a pracovných prostredí s vyššou tepelnou záťažou je táto metóda užitočná pre identifikáciu možných zdrojov diskomfortu. Navyše je táto metóda vhodná i pre rýchlo rastúci segment elektrických vozidiel, kde je možné sledovať tok energie potrebnej na dosiahnutie určitej úrovne komfortu a riešenie optimalizačných úloh za účelom úspory energie a predĺženie dojazdu. Obdobné aplikácie možno nájsť i v budovách a prostrediach s podobnými charakteristikami.

KĽÚČOVÉ SLOVÁ:

Modelovanie; Experiment; Vykurovanie; Vetranie; Sedadlo; Človek; Thermofyziológia; Fiala model; Equivalentná teplota; Odev; Pozícia v sede; Kabína; Vozidlo; Auto; Energia; HVAC; Tepelný pocit; Tepelný comfort

BIBLIOGRAFICKÁ CITÁCIA:

FOJTLÍN, Miloš. *Hodnocení tepelného prostředí kabin automobilů*. Brno, 2019. Dostupné také z: https://www.vutbr.cz/studenti/zav-prace/detail/113758. Dizertační práce. Vysoké učení technické v Brně, Fakulta strojního inženýrství, Energetický ústav. Vedoucí práce Miroslav Jícha.

Statement of originality

This PhD thesis presents original work performed within the author's PhD project, undertaken at Brno University of Technology in Brno, Czech Republic and the Swiss Federal Laboratories for Materials Science and Technology (Empa) in St. Gallen, Switzerland. The project was supervised by Prof. Miroslav Jícha and Dr. Jan Fišer from the Brno University of Technology together with Dr. Agnes Psikuta from Empa.

The content of this thesis was organised into two parts. Part A contains an introduction to the research field and a commentary to five scientific publications. Part B holds five appended scientific publications, each meeting distinct objectives, with the author of this thesis being the first author.

……...

Miloš Fojtlín

Acknowledgement

I would like to express my sincere gratefulness to everyone, who made it possible to finish this PhD thesis and to thank all the people who have supported me in my studies.

I would like to acknowledge the financial support of Brno University of Technology and Swiss Federal Laboratories for Materials Science and Technology, Empa in St. Gallen that made my scientific work possible. The exact funding sources were indicated in the papers appended in Section B.

I would like to thank Prof. Miroslav Jícha and Dr. Jan Fišer, my supervisors at Brno University of Technology, for involving me in a variety of research projects and your support when taking up the challenge of going abroad to open up new research topics. I am also grateful for your help in numerous administrative tasks at the University.

I would like to express my gratitude to Dr. Agnes Psikuta, who has been my supervisor and mentor at the Swiss Federal Laboratories for Materials Science and Technology Empa in St. Gallen, for your guidance, motivation, and enthusiasm that helped me to move over the obstacles, which happened to occur in the course of my PhD project and stay in Switzerland.

I am thankful to the members of the Laboratory for Biomimetic Membranes and Textiles at Empa: René Rossi and Simon Annaheim - for proofreading my manuscripts and providing valuable comments; Ankit Joshi – for sharing his expertise and his kind help; Braid MacRae – for helping me out with the English language; and all friends and colleagues from and around the office F1.23 – for endless flow of positive energy and humour, and for creating a stimulating working environment.

I would like to express my deepest gratitude to my parents, grandparents, and my brother, Braňo, for your love and invaluable support throughout my life.

Symbols and abbreviations

a, b	(-)	linear regression constants
A_{cl}	(m^2)	clothed body surface area
A_{sk}	(m^2)	nude body surface area
BMI	(kg/m^2)	body mass index
f_{cl}	(-)	clothing area factor
h_{cal}	($W \cdot m^{-2} K^{-1}$)	combined heat transfer coefficient
HF	($W \cdot m^{-2}$)	heat flux density
I_a	($m^2 K \cdot W^{-1}$)	adjacent air layer insulation
I_{cl}	($m^2 K \cdot W^{-1}$)	intrinsic clothing insulation
I_{tot}	($m^2 K \cdot W^{-1}$)	total insulation
Q	($W \cdot m^{-2}$)	sensible (dry) heat loss
$R_{e,a}$	($m^2 Pa \cdot W^{-1}$)	air water vapour resistance
$R_{e,cl}$	($m^2 Pa \cdot W^{-1}$)	basic water vapour resistance (evaporative resistance)
$R_{e,T}$	($m^2 Pa \cdot W^{-1}$)	total water vapour evaporative resistance
R_T	($m^2 K \cdot W^{-1}$)	total thermal insulation
t_{air}	(°C)	ambient air temperature
t_{eq}	(°C)	equivalent temperature
t_{rad}	(°C)	mean radiant temperature
t_s	(°C)	skin surface temperature

3D	three dimensional
BUT	Brno University of Technology
CFD	computational fluid dynamics
DTS	dynamic thermal sensation
e.g.	exempli gratia (*Latin, for the sake of an example*)
Empa	Swiss Federal Laboratories for Materials Science and Technology
FPCm	Fiala physiological and comfort model
GRG	generalized reduced gradient
HVAC	heating, ventilation, and air-conditioning
ISO	International Organization for Standardization
MTV	mean thermal vote
PhD	Philosophiae Doctor (*Latin, Doctor of Philosophy*)
PMV-PPD	predicted mean vote and predicted percentage of dissatisfied
RMSD	root mean square deviation
temp.	temperature
TSV	thermal sensation model by Jin et al.
TSZ	thermal sensation model by Zhang et al.
USA	United States of America
UTCI	Universal Thermal Climate Index

Table of content

PART A: A COMMENTARY TO THE SERIES OF SCIENTIFIC PUBLICATIONS 15

1 INTRODUCTION 17

1.1 CHALLENGES IN THE VEHICULAR MICROCLIMATE 17

1.1.1 Characteristics of the vehicular microclimate 17

1.1.2 Microclimate management 18

1.2 HUMAN PHYSIOLOGY WITH REGARDS TO THERMAL SENSATION AND COMFORT 19

1.2.1 Human thermoregulation 19

1.2.2 Perception of thermal sensation and comfort 20

1.3 FACTORS INFLUENCING THERMAL SENSATION 21

1.3.1 Environmental factors 22

1.3.2 Clothing 22

1.3.3 Seat 23

1.3.4 Metabolic heat production 24

1.3.5 Influence of body composition, age, and sex 25

2 ASSESSMENT OF THE THERMAL ENVIRONMENT IN VEHICULAR CABINS 26

2.1 MODELLING OF A HUMAN THERMAL RESPONSE 27

2.1.1 Overview of the thermo-physiological models 27

2.1.2 Input parameters for thermo-physiological models 28

2.2 ASSESSMENT OF THERMAL SENSATION 28

2.2.1 PMV-PPD model – global approach 28

2.2.2 Local thermal sensation models 29

2.2.3 Comments on thermal sensation scales and weighting factors 30

2.2.4 Manikin-based methods 30

2.2.5 Thermo-physiological human simulator 33

2.2.6 Computational fluid dynamics 33

2.3 VIRTUAL AND HARDWARE DEMONSTRATOR TO PREDICT THERMAL SENSATION IN A CABIN ENVIRONMENT 33

2.3.1 Concept of the methodology 33

2.3.2 Summary of the knowledge gaps 35

3 AIM AND OBJECTIVES 36

3.1 AIM AND THESIS 36

3.2 OBJECTIVES 36

3.3 STRUCTURE OF THE THESIS 37
3.4 THE MAIN AUTHOR'S CONTRIBUTION TO THE PUBLICATIONS 38
3.5 ASSOCIATED PAPERS NOT PRESENTED AS A PART OF THE THESIS 38

4 SUMMARY OF THE WORK CONDUCTED 40

4.1 OBJECTIVE 1 (PAPER I): DETERMINATION OF CAR SEAT CONTACT AREA FOR THERMAL SENSATION MODELLING 40
4.1.1 Summary of the main fidnings 41
4.2 OBJECTIVES 2 AND 3 (PAPER II): CLOTHING THERMAL PROPERTIES 42
4.2.1 Summary of the examined scenarios 43
4.2.2 Clothing and definition of body positions 44
4.2.3 Determination of seat thermal properties 45
4.2.4 Sensitivity analysis 45
4.2.5 Summary of the main findings 46
4.3 OBJECTIVES 4 – 6 (PAPER III): CONDITIONED SEATS 47
4.3.1 Development and validation of the seat heat transfer model 47
4.3.2 Coupling with thermo-physiological and thermal sensation models 48
4.3.3 Summary of the main findings 50
4.4 OBJECTIVES 7 – 8 (PAPERS IV AND V): DEVELOPMENT AND IMPLEMENTATION OF THE DEMONSTRATOR 51
4.4.1 Evaluation of the manikin measurement uncertainty 52
4.4.2 Development of the demonstrator 52
4.4.3 Integration of the demonstrator into the cabin 53
4.4.4 Summary of the main findings 53

5 CONCLUSIONS 55

5.1 FUTURE PERSPECTIVES 56
5.2 LIMITATIONS 56

6 REFERENCES 58

PART B: APPENDED PEER-REVIEWED SCIENTIFIC PUBLICATIONS 71

PAPER I 73

PAPER II 91

PAPER III 107

PAPER IV 141

PAPER V 151

Part A: A commentary to the series of scientific publications

1 Introduction

1.1 Challenges in the vehicular microclimate

An average European citizen spends of up to 90% of her/his lifetime indoors [1], in buildings and vehicles. This time spent indoors is one of the major reasons for elevated interest in understanding the interactions between humans and artificial environments. The fields of human health, productivity, and comfort have been central to this research attention. At the same time, new fields are emerging with a goal to reduce the energy expenditure and carbon footprint associated with microclimate management.

1.1.1 Characteristics of the vehicular microclimate

Vehicular cabins, including cabins of commercial and working vehicles, differ in many aspects from built environments. Key characteristics more typical of vehicular cabins include:

- a broad range of temperature (-20 ° to 60 °C) and air humidity (5 % to 100 %) [2], transient and asymmetric in nature;
- small air volume per person and consequent need for active ventilation and conditioning;
- solar irradiation and substantial heat exchange at skin induced by higher local air velocities and contact with adjacent surfaces (e.g. seats and steering wheel);
- fixed body position; and
- priority of auxiliary HVAC functions to prevent fogging and icing of the windows.

Weather related heat load can be amplified due to the nature of cabins (e.g. by the greenhouse effect or lack of air-conditioning) and leads to discomfort and thermal stress and strain. In private passenger transportation, the duration of a typical car trip is less than 20 minutes [3]. Such a short period of time is often insufficient for the HVAC unit to establish comfortable conditions. Inappropriate thermal conditions negatively impact a driver's performance [4] and health [5]. Thus, a state of thermal comfort is not only important for a pleasant thermal experience but also for prevention of driver fatigue and related hazards in traffic.

Notwithstanding, similarities between cabins and built environments also exist. The main denominators are a sitting body position and substantial body-contact with the seat. Additionally, heat stress and thermal asymmetry in buildings can be present in a variety of occupations. For these reasons, methodologies to assess cabin thermal environments can also apply to assess built environments.

1.1.2 Microclimate management

From the technological point of view, solutions to deliver comfortable microclimate conditions are available, mostly by well-established heating ventilation and air-conditioning (HVAC) systems. Nevertheless, HVAC systems are typically related to substantial energy consumption and production of environmental pollutants [6]. In steady conditions, vehicular cabin thermal management contributes to approximately 7 % of vehicle total energy consumption, yet, a four-fold rise may occur during peak loads [6,7]. New challenges have arisen, particularly with the development of battery-powered electric vehicles. Here, the vehicle's driving range is greatly reduced by the energy consumption of the HVAC system as the same battery source is used to propel the vehicle and the HVAC [7].

To sustain thermal comfort of occupants, alternative, less energy demanding and user-centred approaches are sought. Several studies examined the potential of mitigating thermal discomfort via radiative panels, localized ventilation, as well as heated and ventilated seats [8–14]. All studies confirmed that local conditioning broadens the boundaries of comfortable ambient conditions at lower energy consumption. This is mostly because of a reduced need to condition the whole environment around the occupant. Veselý et al. [8] concluded that 40 % annual energy savings could be achieved using a combination of the HVAC and local conditioning in the temperature range between 15 and 30 °C in buildings. Thus, similar trends in the cabin environment are expected too. Another advantage of localized conditioning is the potential to satisfy different needs of different occupants, thus, enhancing the human thermal experience, health, and performance.

Although technologies for personalized conditioning are available, their control is solely based on user interaction. The user reaction is delayed to a point when discomfort arises and is accompanied by negative effects such as rebound or overshoot [8]. Additionally, manual adjustments of the conditioning cause distraction and might have medical consequences when used improperly, such as low-temperature skin burns (*Erythema ab igne*) [15]. In the case of prolonged use of air-conditioning, mucous membrane irritation, fatigue, and headache are well-known symptoms. Although, their source is not clearly defined, it is usually ascribed to a combination of factors such as poor hygiene of the HVAC systems [16] and excessive cooling by a stream of cold, dry air.

The same regulatory principles can be found in up-to-date HVAC systems with a manual control. An automatic control regime takes into consideration one user input, temperature, and external system inputs such as exterior and interior temperatures, air humidity, and solar intensity, to treat and distribute the air in the cabin [17]. Nevertheless, this approach is based on proprietary empirical tuning of the HVAC system rather than on a well-founded method. The solution leading to enhanced, user-centred thermal experience can be achieved by continuous monitoring of local environmental and/or physiological parameters. Such data can be incorporated into a feedback control

loop for synergic operation of the HVAC and local conditioning technologies. To do so, a method that translates a measurable physical input into a local thermal sensation or comfort vote is needed.

1.2 Human physiology with regards to thermal sensation and comfort

1.2.1 Human thermoregulation

To sustain the vital functions of a human body, its core temperature has to be maintained within a relatively narrow temperature range of ~36.7 ± 0.5 °C [18]. This temperature maintenance can be achieved in spite of variability of the ambient environment by equalling the heat production and heat loss as well as by transferring the heat within the body. The two main thermoregulatory mechanisms are behavioural and autonomic. Behavioural thermoregulation relates to conscious changes in body position and clothing that influence the heat balance. Autonomic thermoregulation comprises physiological responses, such as vasomotion, shivering, and sweating, which help to conserve or to dissipate the body heat. From the thermoregulatory point of view, human skin is the most important element accounting for approximately 92 % of the heat exchange between the body core and the ambient environment. The rest is attributed to the respiratory heat exchange [19].

Vasodilatation and vasoconstriction, the widening and narrowing of specialised blood vessels, regulates skin perfusion, which acts as a fine regulatory mechanism to control convective and conductive heat exchange between the body core and the environment. Under warm conditions, vasomotion is supported by thermal sweating, which increases heat loss from the body by capitalising on the latent heat of vaporization. Conversely, cold-induced thermogenesis is initiated to increase the core temperature by shivering (involuntary muscle contraction) and brown fat thermogenesis [20]. While the active thermoregulation is sufficient in the majority of natural climatic conditions, its capacity is limited. Exceeding thermoregulatory limits may lead to adverse physiological effects causing health risks such as dehydration, frostbite, or death [5].

The thermoregulatory actions are controlled by the hypothalamus, where signals from temperature-sensitive neurons (receptors) present mainly in the skin, deep body tissues, and hypothalamus itself are integrated [21]. Vasodilatation and sweating (sudomotor response) are triggered by an increase in core temperature of ~0.3 °C [22]. Vasoconstriction, on the other hand, occurs if skin temperature drops below 35 °C and it is accompanied with shivering as the core temperature approaches 35 °C [23]. However, the thermoeffector thresholds are variable and depend on the initial thermal state of the body [24]. The likely explanation for this phenomenon is the presence of independent central controllers for thermally dependent thermoregulatory responses [24].

1.2.2 Perception of thermal sensation and comfort

The surrounding thermal conditions are sensed by peripheral cold- and warmth-sensitive receptors distributed within subcutaneous tissues. The second group of thermoreceptors, central receptors, are located along blood-vessels and in hypothalamus [25]. Although the density of the peripheral receptors is difficult to quantify, it could be expected to see a positive correlation between their number and sensitivity of hot and cold spots on the skin surface [26]. The distribution of such spots is not uniform over the human body and thus heating or cooling of different body parts is perceived differently [25,26].

Cabanac [27] described the sensory output by quadridimensional sensation. The first dimension is qualitative, describing the nature of the stimulus (thermal sensation); the second is quantitative, defining the intensity of the stimulus; the third is hedonic (pleasure) and may be absent; and the fourth expresses duration of the stimulus. Not all stimuli evoke pleasure or displeasure and mostly indifferent sensation is perceived under permanent flux inputs. However, the hedonic perception is influenced by the combination of factors such as the nature of the stimulus, the internal state of the subject, and the subject's history. Cabanac introduced the term *alliesthesia* [27] to express the variability of the hedonic component of sensation. Positive alliesthesia indicates a change towards more pleasurable sensation and vice versa for negative alliesthesia.

In thermal comfort studies, the thermal sensory perception has been simplified into two respective descriptors, thermal sensation and thermal comfort. The definition of the thermal sensation can be found in standards (e.g. ISO 7730 [28], ISO 10551 [29], and Handbook Fundamentals ASHRAE [30]) as "a conscious feeling commonly graded into the categories *cold, cool, slightly cool, neutral, slightly warm, warm, hot;* it requires subjective evaluation". The neutral thermal sensation is related to the thermal balance between a human body and the ambient environment. This heat exchange is, naturally, influenced by a number of factors, dominantly by metabolic activity, clothing, and the environmental parameters. When the human body is cooled at a higher rate than it is generating heat, one would perceive thermal sensation below thermo-neutrality and vice versa for thermal sensation above thermo-neutrality.

Thermal comfort, on the other hand, is defined as "that condition of mind which expresses satisfaction with the thermal environment and is assessed by subjective evaluation" [30]. Cabanac stated that state of thermal comfort is a stable state, as opposed to the dynamic pleasure, and can last indefinitely if the environment and the subject remain in stable conditions [27]. Moreover, the complexity of predicting thermal comfort is greater than that of thermal sensation since it depends on psychological, cultural, and other personal factors. It had been generally assumed that a neutral thermal sensation was essential to achieve thermal comfort [31]. This was contradicted, however, in the study by Humphreys and Hancock [32], where the participants voted for the desired thermal

sensation other than neutral in more than 40 % of cases. Nevertheless, the votes were typically in the close to thermo-neutral conditions, where only subtle thermoregulatory actions were needed such as vasomotion, rather than sweating or shivering.

Although humans are most productive in monotonous thermo-neutral settings [33], Kingma [34] expressed a hypothesis that such conditions are not automatically healthy. One of his major arguments was that the reduced need for thermoregulation also reduces the ability to cope with thermal challenges. Moreover, several indices were found that regular exposures to non-comfortable conditions have preventive effects against obesity and diabetes [35,36]. Therefore, benefits for both health and energy savings can be achieved when drifting away from the comfort zone in a controlled manner. Yet, further investigation in this field is necessary.

The next parameter closely related to thermal comfort is a perception of wet discomfort – skin wetness (sometimes addressed as skin wettedness). Skin wetness can be physically defined as the ratio of the actual sweat rate to the potentially evaporating amount of sweat. The local threshold for discomfort ranges between 0.3 to 0.4 units depending on a body part [37]. As there is no evidence of receptors sensing skin wetness directly, it has been shown that the perception of wetness is a learned skill based on complex thermal and tactile sensory experience [38]. From the perspective of a vehicular cabin, the risk of wet discomfort is highest at contact points (e.g. seat and steering wheel) and at body parts covered by impermeable clothing.

While the ultimate objective of indoor environment research is to find indices to design comfortable indoor environments, this is difficult without knowing the sources of discomfort. Since the perception of discomfort is subjective and is mainly related to the thermal sensation, it is meaningful to focus on the investigation of thermal sensation. Further, it is of major interest to allow individual occupants to have control over the fine adjustments of the local microclimate. Primarily, this creates the best prerequisites to mitigate the interpersonal differences in perception of comfortable conditions. Secondly, this also induces the positive alliesthesia, which is always perceived as comfortable. Besides, it was shown that the psychological aspect of having control over the environment automatically improved satisfaction with the indoor conditions [39,40].

1.3 Factors influencing thermal sensation

The thermo-neutral zone of a nude healthy adult at rest, where no major thermoregulatory actions are necessary, lies approximately within the range of ambient temperatures between 28.5 °C and 32 °C [41]. While this range can be explained by the evolution of humans and by their former natural habitat in Africa, the *position* of the neutral zone can be modulated by several factors. Two main categories of factors affecting the heat exchange and so the resulting thermal sensation are recog-

nized: environmental and personal [42]. Additionally, as individual body parts are unequally sensitive to warmth or cold [43], attention should be put to local definition of such factors, where applicable.

1.3.1 Environmental factors

Environmental factors are characterized by air temperature, mean radiant temperature, relative humidity, and mean air velocity. The environmental conditions can be determined using conventional methods. Otherwise, the desired environment can be simulated using tools with various levels of complexity, starting with analytical single-purpose models (e.g. a cabin model [44]) and ending with fine mesh CFD models [45].

With respect to the operating conditions of car cabins, environmental parameters are typically heterogeneous and change with time. In summer season, for instance, the range of comfortable conditions can be roughly characterized by air and mean radiant temperatures between 23 °C and 27 °C, relative air humidity between 30 % and 60 %, and air velocity below 0.4 $m \cdot s^{-1}$ [46]. However, thermal conditions after entering the cabin are usually different from the desired ones because of the previous cabin exposure to the weather. The HVAC is usually initiated after entering the cabin with consequent intensive cooling or heating. These situations may lead to activation of the thermoregulatory mechanisms and substantial discomfort.

1.3.2 Clothing

Clothing provides a barrier preventing heat and vapour transfer from the skin to the ambient environment or vice versa. For this reason, it is one of the most important personal factors influencing the thermal balance of a body and consequently thermal sensation. In the field of thermal comfort, clothing thermal properties are described by clothing area factor, intrinsic clothing insulation, and evaporative resistance. The clothing area factor f_{cl} represents a ratio of clothed area A_{cl} (m^2) to nude body surface area A_{sk} (m^2).

$$f_{cl} = \frac{A_{cl}}{A_{sk}} \tag{1}$$

Next, intrinsic clothing insulation I_{cl} ($m^2K \cdot W^{-1}$) describes the actual thermal insulation from the body surface to the outer clothing surface (including enclosed air-layers). The I_{cl} can be determined according to equation 2 [47], from the f_{cl}, the adjacent air layer insulation I_a ($m^2K \cdot W^{-1}$), and the total thermal insulation I_{tot} ($m^2K \cdot W^{-1}$). The last two parameters are defined as a temperature gradient from the skin to the ambient environment divided by a dry heat loss measured on a naked and clothed manikin, respectively.

$$I_{cl} = I_{tot} - \frac{I_a}{f_{cl}} \quad (2)$$

The last clothing parameter, the evaporative resistance $R_{e,cl}$ ($m^2Pa \cdot W^{-1}$), is defined in analogy to intrinsic clothing insulation (equation 3). Here the $R_{e,T}$ ($m^2Pa \cdot W^{-1}$) denotes total evaporative resistance and $R_{e,a}$ ($m^2Pa \cdot W^{-1}$) is vapour resistance of the boundary (surface) air layer around the outer clothing or, when nude, around the skin surface.

$$R_{e,cl} = R_{e,T} - \frac{R_{e,a}}{f_{cl}} \quad (3)$$

All three properties are highly dependent on a local air gap distribution [48,49], which is inherently shaped by a body position [50] as well as body movement [51,52]. In cabin environments, the number of possible body positions is reduced to a sitting position. However, the differences in clothing thermal properties between seated and standing body positions are known for global values (whole-body) [53–55]. However, the impact on local clothing parameters has not been examined in detail for individual body parts. Next, the effects of body movement are negligible as the driver and passengers usually do not perform any tasks involving considerable body motion.

With respect to the nature of the cabin environment, division of the human body should comprise at least six major body parts (head, torso, upper and lower limbs, hands, and feet) [56], although a more detailed division is common and dictated by its application. Nevertheless, the availability of local clothing properties is limited since conventional sources (e.g. ISO 9920 [47]) provide only global (whole-body) values having a unit clo (1 clo = 0.155 $m^2K \cdot W^{-1}$). Additionally, the state-of-the-art methods require dedicated equipment, such as a thermal manikin and a climatic chamber. The equipment purchase and maintenance costs make it inaccessible for many researchers. Alternative methods exists and can be classified accordingly: (a) analytical heat transfer modelling [57,58]; (b) regression modelling [59]; (c) empirical modelling, e.g. the UTCI model [60]; and (d) ISO based estimation [47,61,62]. However, the precision of such methods has not been assessed and therefore may be a source of an unknown error.

1.3.3 Seat

A seat plays a significant role in the thermal experience because of its large contact area with a human body, its considerable thermal mass, and potentially extreme initial temperature. Thus, the seat may become either a heat source or a heat sink, substantially influencing the local skin temperature and thermal sensation. Additionally, seats are frequently equipped with conditioning, such as seat heating and ventilation. Nevertheless, seats are currently approached as thermal and evaporative resistance [63–66] rather than an active component interacting with skin. While this approach might be sufficient in mild and static thermal environments (e.g. offices), it is clearly unsuitable in cabin conditions.

To resolve the dynamic thermal interaction at the occupant-seat interface, one can carry out measurements using dedicated heat flux blankets (e.g. blankets by Mahoele Messtechnik, Germany). However, the experimental approach is laborious and applicable only in laboratory conditions. Alternatively, the thermal interaction with seats can be calculated using laws of physics. However, such models are either proprietary (e.g. a module in THESEUS‑FE, Germany) or the models lack conclusive and transparent validation [67–69].

The next parameter related to seated position is the occupant-seat contact area, which conditions the resulting thermal interaction. However, human subject studies on this subject are scarce and the methods usually lack details [10,70]. As an alternative, one can find contact areas determined by circumscribing a thermal manikin seated on a seat [71,72]. Nevertheless, it is reasonable to expect that the contact area of a hard-shell and lightweight manikin body is not the same as that of a human body with compressible tissues. To allow for personalised calculations of heat exchange between the seat and its occupant, it is of major interest to find a relationship between the contact area and human anthropometry.

1.3.4 Metabolic heat production

Metabolic heat production is an influential factor, and results from thermogenesis induced by exercise (muscle activity), non-exercise activity (basal metabolism), and diet-induced thermogenesis (digestion of food) [41]. In thermal sensation/comfort research, the cold-induced thermogenesis (muscle shivering or non-shivering thermogenesis) [73] is usually avoided, since it is a mechanism activated *far* from thermo-neutral conditions. The metabolic heat production is typically related to surface skin area or body mass to reduce the interpersonal variability in its estimation. A metabolic rate of a healthy, sitting person at rest is 58.2 $W \cdot m^{-2}$, which is also a definition of a unit *met* [74].

Havenith et al. [74] classified three levels of determination of metabolic heat production. The first level uses tabular values, where the corresponding heat production is identified based upon a description of the activity. In the cabin conditions, while highway driving or resting, this is typically between 1 and 2 met [75]. Low metabolic production, on the other hand, also implies that even small changes in the environment may imbalance the thermal equilibrium.

In the second level, correlation of heart rate above 120 $beats \cdot min^{-1}$ with the heat production is defined. On the one hand, such a heart rate is above the normal range of activities in car cabins, which restricts the utilization of this method in situations with low metabolic production. On the other hand, this approach might be used to track metabolic history of the occupant, e.g. by a smart-watch. The third option is strictly related to laboratory conditions, where direct or indirect calorimetry measurements are required (for more information see [74]).

1.3.5 Influence of body composition, age, and sex

The last group of personal factors, including body composition, age, and sex, has a relatively minor impact on the thermo-neutral zone compared to the previous factors, but it may become relevant in greatly different populations. With regards to body composition, adipose tissues act as a natural barrier against heat dissipation from the core. The shift in the thermo-neutral zone can be as high as 5 °C if two populations having 5 mm and 30 mm of the subcutaneous fat layer, respectively, are compared [41]. Next, a study by Inoue et al. [76] demonstrated a decreasing ability to sense heat or cold with increasing age as well as higher sensitivity of females to innocuous warm and cold thermal stimulation than males independent of age. The justification for this trend is given in decreasing sensitivity of elderly to thermal stimuli as well as impaired control of neural vasoconstriction, which can be also related to the lower fitness level [41,76]. Finally, the differences between sexes are usually explained by body characteristics and endocrinal physiology with an upward shift of the thermo-neutral zone in women relative to men [77].

2 Assessment of the thermal environment in vehicular cabins

The prevailing ways to examine thermal comfort are field and climatic chamber studies [78]. However, with regards to the broad scope of possible situations in cabins, fully experimental research may become unfeasible. Experimental studies require dedicated equipment and a substantial amount of time and resources. Further, a possibility to obtain complete datasets comprising thermo-physiological, environmental, and comfort data from literature is also limited. The research papers are often written in a condensed way excluding details, which are crucial for interpreting, comparing, and generalising the results.

Methods capable of reliable predictions of thermal sensation both in the design phase as well as in already existing spaces have multiple valuable applications. Such methods afford the efficient optimisation of indoor spaces and virtual monitoring of the energy demands for comfortable conditions while decreasing the costs for prototyping and physical studies with human participants. In existing spaces, such methodology can be used for shifting the contemporary paradigm of microclimate management to the sensation-driven microclimate control. To achieve this, the factors influencing thermal sensation must be taken into consideration, most importantly the environment, clothing, and metabolic heat production. However, as covered above, the number of factors influencing thermal sensation is large and interpersonal differences in perception of thermal environment are inevitable.

An alternative to the elaborate experimentation is mathematical modelling of human physiology, developed with the intention to substitute for physical human studies [79,80]. Such models allow virtual investigation of a physiological response of the human body to various environmental stimuli. The major advantage of simulations is their versatility and instant availability of the results. However, only a limited amount of well-documented thermo-physiological models exist having sufficient accuracy of predicted parameters [81,82]. The thermo-physiological outputs can be coupled with thermal sensation and comfort models. Thermal sensation models relate objective parameters (e.g. skin and core temperatures) with a thermal sensation or comfort vote, to rate the thermal environment on a dedicated scale [83].

2.1 Modelling of a human thermal response

2.1.1 Overview of the thermo-physiological models

The efforts to replace a human by a computational model using the laws of thermodynamics date back to the beginning of the 20th century. One of the major applications for this is to obtain thermo-physiological data for thermal sensation modelling. An extensive overview of more than 20 models was described in the review paper by Katic et al. [80]. Increasing computational power gave rise to more complex and detailed models, comprising multiple tissue layers, body segmentation, and active thermoregulation. Although numerous models were proposed, their actual implementation is challenging because of the vast input parameters and working knowledge required. Additionally, a benchmark comparison of the performance of various models with respect to local predictions is scarce [80]. For this reason, the selection of a model is usually driven by its intended application, its availability, and range of available validation.

Depending on the intended model´s application and its complexity, the models can be divided into the following categories:

- one-, two-, or multiple-node models (node denotes the number of human tissue layers); and
- single- or multi-segment models (segment denotes a body part).

For automotive applications, it is reasonable to use multi-node and multi-segments models with a resolution of at least anterior and posterior aspects of the limbs, torso, and head. This is crucial for the investigation of local as well as transient thermal responses and consequent modelling of local thermal sensation. The most frequently cited and applied thermo-physiological models are the 65MN model by Tanabe et al. [84], the Berkeley model [85,86], and several Fiala-based models: ThermoSEM by Kingma [34], FPCm by ErgonSim [87], Fiala-FE by Theseus FE [88], FMTK by Pokorny et al. [89], and Human Thermal Module in TAITherm by Thermoanalytics Inc. [90].

An example of a well-documented, validated, and commonly used model is the Fiala physiological and comfort model (FPCm 5.3, Ergonsim, Germany) [91]. The model allows simulation of local time-dependent human thermal responses, such as skin and core temperatures and sweat rates. The model was validated in a range of ambient temperatures from 5 °C to 50 °C and exercise levels from 0.8 met to 10 met [81,82,92,93] in both symmetric and asymmetric thermal environments and conditions with constant ambient temperature, step change temperature, and temperature ramp. With regards to the local skin temperatures, the root-mean-square deviation and bias of the predictions was usually equal to a standard deviation of measurement.

The FPCm5.3 consists of active and passive systems characterising a simplified virtual body of an average unisex person (height 1.69 m, weight 71.4 kg, and skin surface 1.83 m^2), where a thermal in-

teraction between the body and the ambient environment takes place. The body was divided into 13 body segments representing major body parts. These were further divided into spatial sectors to allow detailed computing of heat exchange between the ambient environment and specific body parts. The active system is responsible for mimicking thermoregulatory actions that are present in a human body, such as sweating, shivering, and vasomotion [87].

2.1.2 Input parameters for thermo-physiological models

A chain is no stronger than its weakest link and this saying is also valid in modelling, where the *weakest link* is typically the quality of the input parameters, which then determine the quality of the outputs. The most commonly used input parameters in thermo-physiological modeling are environmental parameters (see Section 1.3.1), clothing thermal properties (see Section 1.3.2), and metabolic heat production (see Section 1.3.4). Alternatively, one can prescribe heat flux density or temperature, directly at the skin of a given body part. This can be used as a representation of conductive heat exchange to simulate the effects of seats and local conditioning.

Anthropology (height, weight, adipose tissue layers), age, sex, fitness level, and acclimitisation can be considered as a separate category of input parameters for thermo-physiological modelling. It is because of their impact on both passive and active components of the thermo-physiological models. As the majority of thermo-physiological models were created and validated for an average and often unisex person, efforts in thermo-physiological modelling are aimed towards a higher degree of personalisation. Several models and studies were developed over the past three decades to include the impact of these factors on the physiological response (e.g. [94–96]). Individualization might be beneficial if a known population is studied. However, the amount of validation cases for different groups of the subjects is significantly smaller than for an average population, which may already cause a great inherent error. Therefore, in applications, where the population is not specified, use of the average representation of human is likely to yield reliable results.

2.2 Assessment of thermal sensation

2.2.1 PMV-PPD model – global approach

One of the earliest and best-known models is the PMV-PPD model from ISO 7730 [28] predicting thermal sensation and a rate of discomfort based on environmental parameters (ambient temperature, mean radiant temperature, air velocity, relative air humidity), clothing (whole-body thermal insulation), and metabolic production. The range of the model's applicability covers moderate activities from 0.8 to 4.0 met, clothing in a range of 0 to 2 clo, air temperature within 10 °C and 30 °C,

and air velocity below 1 $m \cdot s^{-1}$. The model is valid in stationary conditions or conditions with minor fluctuations of one or more variables [28].

While the main advantage of this approach is its simplicity to obtain input parameters, the major drawback comes from the global thermal sensation output. In homogenous spaces without a local source of discomfort, for instance, contact heating or cooling by a seat, PMV-PPD can be successfully used. However, in the cabin conditions with characteristics previously described, it is meaningful to use an approach that would recognise thermal sensation locally, at major body parts. A local thermal sensation model may help to identify the local source of discomfort that can potentially skew the resulting global thermal sensation or comfort [97]. Thus, the source of discomfort can be addressed locally, rather than attempting to change the whole microclimate around a human body.

2.2.2 Local thermal sensation models

Numerous local thermal sensation models have emerged at the turn of the twentieth century. However, as discussed by Koelblen et al. [98,99] following a systematic study of the performance of thermal sensation models, a thorough validation of the models is usually missing and the functionality of the models is demonstrated on only a few exposures. For this reason, it is essential to understand the behaviour of models under asymmetric and transient thermal conditions.

With respect to the sitting body position, spatial asymmetry, and transient environment, three well-documented thermal sensation models come into consideration to evaluate cabins. Firstly, the model by Nilsson [100] based on heat transfer (MTV), being part of the ISO 14505 [64], was developed for automotive applications with a resolution of 18 body parts. In principle, this approach assumes that a certain heat flux from the skin corresponds to a thermal vote expressed on the 7-point Bedford scale. This scale combines thermal sensation votes with thermal comfort (much too cold, too cold, cold but comfortable, neutral, hot but comfortable, too hot, much too hot). The method is applicable under a range of ambient temperatures from 19 °C to 29 °C and metabolic heat production equivalent of sedentary activities, such as driving. The main advantage of MTV is its simplicity and possibility to couple with thermal manikin measurements. On the other hand, the model lacks a derivative component, and thus, it might not perform well in rapidly changing environments.

The second model dedicated to the vehicular cabins by Zhang (TSZ) [21,101], relates local skin and core temperatures (and their time derivatives) to thermal sensation at 15 body parts. These data are typically supplied from a thermo-physiological model. The local thermal sensation is predicted on the extended 9-point ISO scale, having two additional extreme thermal sensations votes (very cold and very hot). The model was developed in a range of air temperatures between 20 °C and 33 °C and is valid for seated metabolic production. The experiments to construct the model were carried out at the University of Berkeley in California, where, the climate is rather mild, throughout the

year, with hot summers. For this reason, subjects may perceive cool and cold thermal sensation differently than subjects acclimatized to cold environments, which was apparent in the study by Koelblen [98].

The third candidate, the model by Jin et al. (TSV) [102], uses local skin temperatures as inputs and yields local thermal sensation on the 7-point ISO scale (cold, cool, slightly cool, neutral, slightly warm, warm, hot) [28]. Although the TSV model contains no derivative component, it is claimed to be suitable for transient conditions with cooling as well as for stable thermal conditions. The model was developed on the Chinese population in conditions between 20 °C and 30 °C of ambient temperature wearing summer and winter indoor clothing sets of 0.4 clo and 0.9 clo, respectively. This, again, opens questions on applicability of the model on other populations, with different cultural and climatic background.

2.2.3 Comments on thermal sensation scales and weighting factors

One of the factors complicating the direct comparison of thermal sensation models is the existence of various thermal sensation scales. Firstly, there is no standardised procedure to unite the sensation scales, as discussed in a systematic comparison of thermal sensation models by Koelblen et al. [98]. Most importantly, Schweiker et al. [103] found that the relationship between temperature and subjective thermal sensation is non-linear depending on the type of scale used and most people do not perceive the categories of the thermal sensation scale as equidistant. For this reason, one has to be alert when comparing results from various scales. Yet, this topic remains open for investigation.

Next, the resolution of the model´s body parts may not be identical. In this case, various weighting coefficients can be used to calculate the whole-body thermal sensation or thermal sensation of a group of body parts. The most straightforward way is to use the surface area of the body parts as a weighting coefficient, which is mostly used in benchmark studies [98]. However, this weighting neglects the effect of prevailing thermal sensation on neighbouring body parts. To take this effect into consideration, Zhang [104] defined weighting factors as the ratios of overall thermal sensation change against local thermal sensation change during single-segment cooling or heating application. Later, this was changed to estimated values indicating the relative importance of local thermal sensation in predicting overall thermal sensation [105,106]. It has to be noted that each of the approaches yields different results.

2.2.4 Manikin-based methods

Thermal manikins are the-state-of-the-art devices applicable in various branches of clothing research and environmental engineering. The most frequent research applications can be found in

passenger transportation, workplaces, and homes. The most realistic quantification of heat and mass transfer is achieved by their human-like shape as well as by mimicking body motion and sweating. However, the manikin´s purchase costs are high and they can be substituted by a less complex device dedicated to a specific application such as: (a) a body part manikin (usually head, feet, torso, or hands); (b) an omnidirectional elliptical sensor [107]; and (c) a directional surface sensor [64]. However, the shape and size of the device matters and the results from two geometrically distinct devices may not be directly comparable [108].

Thermal manikins, body sectors, and sensors can operate in various control modes:

- constant surface temperature (usually 34 °C) corresponds to average skin temperature in close to thermo-neutral states under low metabolic production [108]. To determine evaporative or thermal clothing resistances of a clothing system constant surface temperature and constant sweat rate control mode is typically used. These procedures are well established and described in several standards, e.g. ISO 15 831 [109], ISO 9920 [47], or ASTM F2370-16 [110]. In environmental comfort research, the main advantage of this method is a rapid response to a change in the heat flux since the stored heat in the manikin is not changing and the imbalance is compensated by the manikin's heating system. This regulation mode was considered as unstable in previous decades [111]. However, this was resolved with computer controlled manikins, such as a Newton-type thermal manikin (Thermetrics, Seattle, USA [112]). The main methodological limitation, here, is the point when the manikin starts to gain heat from the ambient environment and its surface temperature cannot be controlled anymore. Again, a new generation of actively cooled manikins is in development to operate also under such conditions;
- constant heat flux control mode is technically the simplest approach that can be used to mimic certain metabolic heat production. Yet, the manikin's surface temperature can reach unrealistically high values compared to a human if insufficient cooling of the skin is present. This may also lead to unrealistic convective plume and heat losses from the manikin. More details about method can be found in the technical report FAT 109 [107]; and
- comfort temperature operation mode relates the skin temperature with the metabolic heat production according to the Fanger's linear equation [64]. The benefits of this method should stem from more realistic skin temperatures compared to a constant value. However, all of the three control modes are suitable only for examination of dry heat losses and, therefore, disregarding sweating.

Although measurement using a thermal manikin is the most realistic approach, yielding detailed information about heat exchange with the environment, this information alone is insufficient to describe thermal sensation or comfort. Therefore, a method translating the physical values into a sub-

jective perception is needed. Nilsson et al. [63,100,108] introduced the so-called clothing independent comfort zone diagram that relates equivalent temperature (t_{eq}) to thermal sensation and comfort for 18 body parts. The t_{eq} is defined as a temperature of an imaginary enclosure with the air temperature equal to the mean radiant temperature and with still air. Consequently, a manikin or subject would have the same heat exchange as if placed into the actual heterogeneous environment having the same clothing. This premise is valid only for matching body positions and metabolic heat production. The equivalent temperature can be determined for the whole body or for a segment accordingly:

$$t_{eq} = t_s - \frac{Q}{h_{cal}} \tag{4}$$

where t_s (°C) is the skin surface temperature, h_{cal} (W·m^{-2}K^{-1}) is the combined heat transfer coefficient, determined under calibration conditions, and Q (W·m^{-2}) is the sensible (dry) heat loss [64]. Nilsson worked with a presumption that the equivalent temperature correlates with the mean thermal vote (MTV). The clothing independent comfort zone diagram was developed experimentally by coupling the human subjective votes (MTV) to the equivalent temperature measured by a manikin exposed to identical environment. The diagrams are, thus, constructed on the premise that a human is equally sensitive to a heat loss independent of the clothing worn. The relationship between t_{eq} and MTV was described by a regression equation:

$$t_{eq,zone} = t_s - R_T(a + b \cdot MTV_{zone}) \tag{5}$$

where R_T (m^{2}K·W^{-1}) is the total thermal insulation; a and b are the linear regression constants [100].

The *clothing independence* stems from the possibility to measure the equivalent temperature by a nude manikin or an equivalent temperature sensor. With the aim of evaluating the MTV, the t_{eq} is plotted in a diagram corresponding to certain clothing set. This makes this method easy to apply. However, the price for simplicity is compensated with several methodological limitations:

- equation 5 is valid in conditions where no evaporation of sweat is present; only sensible (dry) heat loss is considered. In cabins, the risk of sweating is relatively high in warm conditions and at the less ventilated body parts such as at seats. Additionally, the sweat can already present before entering the cabin and cause higher rate of cooling compared to the model predictions;
- clothing is restricted to *indoor* (office) attire. This can be a major limitation in settings where highly insulating and impermeable garments are worn (e.g. rescue services and military);
- metabolic production of around 1.2 met, which suits driving or sitting light activities only. There is no consideration of other personal factors. In several occupations, intermittent driving is expected and this condition may not apply (e.g. delivery and rescue services).

2.2.5 Thermo-physiological human simulator

An alternative method exploits a thermal manikin coupled with a thermo-physiological model and is addressed as a *thermo-physiological human simulator* [79,113]. The human simulator is the most advanced approach and consists of a thermal manikin controlled in real time by a thermo-physiological model. The model is used to predict the manikin's skin temperature and sweat excretion based on the actual heat loss measured by the manikin in a given environment (alternatively skin temperature is measured to predict the heat loss) [79,113]. Additionally, the simulator can also be coupled with a dedicated local thermal sensation model for real-time predictions [114,115]. On the other hand, the coupling has high requirements on the heat flux measurement accuracy and it is prone to lateral heat fluxes between the body parts with different skin temperatures. At the same time, a validated thermo-physiological model is required [113,114], which makes this method the most demanding in terms of working knowledge and equipment.

2.2.6 Computational fluid dynamics

The indoor thermal conditions can be simulated using computational fluid dynamics (CFD) [116,117]. Usually, a virtual thermal manikin is placed into a mock-up environment containing all HVAC components to enhance realism of the simulation. In theory, arbitrary regulation mode of the virtual manikin could be used, but in reality, constant skin surface temperature is mostly used [63]. Despite technological progress, CFD is still a rare solution to investigate thermal interaction of a human with the ambient environment because of substantial computational power demands.

2.3 Virtual and hardware demonstrator to predict thermal sensation in a cabin environment

The focus of this section is to summarise knowledge gaps in modelling of human thermal physiology and thermal sensation as well as in their practical applications with regards to vehicular cabins. The emphasis is given to the investigation of a sitting body position and the use of local seat conditioning such as seat heating and ventilation. This summary should yield the specification of a validated modelling methodology, based on physical and physiological principles to evaluate thermal sensation. Next, similar principles should also be applicable in a physical demonstrator, which could be utilised in a thermal sensation-driven feedback control loop.

2.3.1 Concept of the methodology

The structure of the methodology to predict thermal sensation can be divided into virtual and physical approaches (Figure 1). In virtual environments, local boundary conditions describing the envi-

ronment, clothing, activity, and seat must be specified. These parameters are fed to a suitable thermo-physiological model, which yields an average human response in the form of physical quantities, such as skin temperatures, rectal temperature, sweat rates, or heat fluxes at the skin. Finally, the outputs from the thermo-physiological model are translated into the predicted thermal sensation vote using a dedicated model.

The second branch (Figure 1) represents an approach applicable in real cabin conditions. Here, it is of main interest to replace costly laboratory equipment, such as thermal manikins, with cost-effective sensors installed permanently in a cabin. The set of sensors should be able to determine the local heat flux by a given surface temperature (equivalent temperature) with comparable accuracy to the thermal manikin. Depending on the application, the sensor control mode has to be selected. The measured physical quantity is again converted to a local thermal sensation vote by a thermal sensation model.

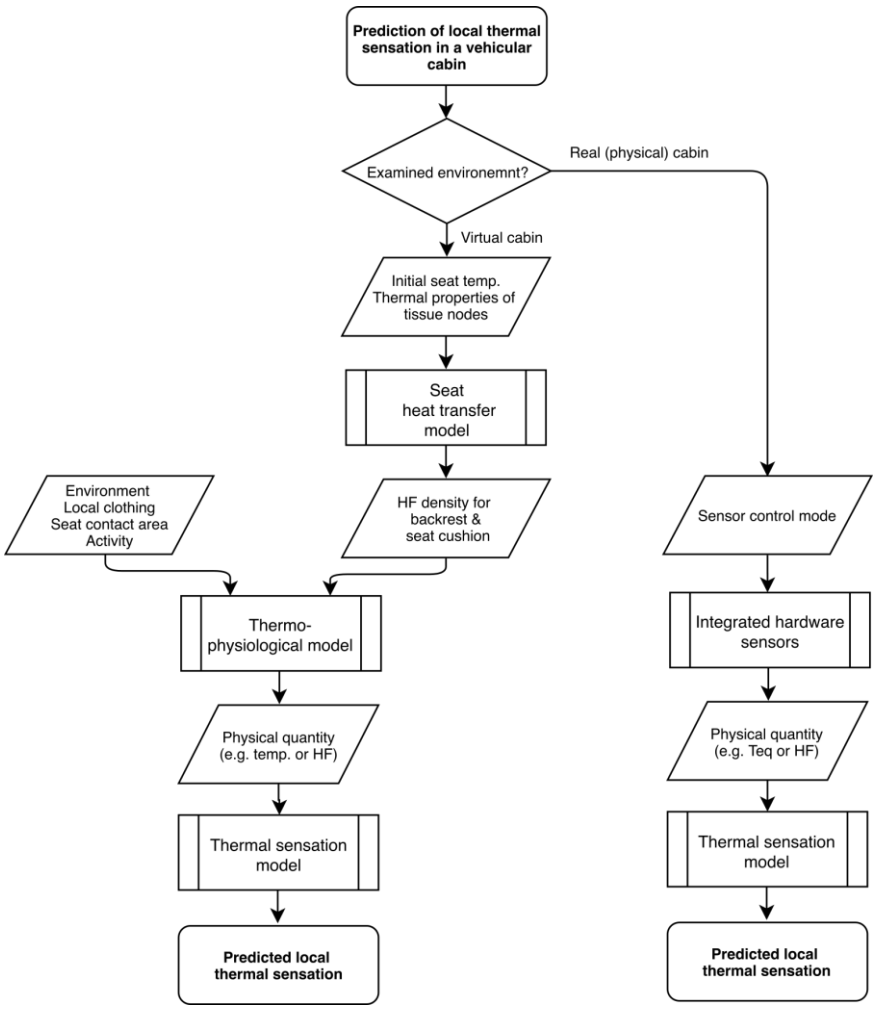

Figure 1. Structure of the methodology to predict thermal sensation in a vehicular cabin.

2.3.2 Summary of the knowledge gaps

Although the knowledge and technological advancements in the field of thermal comfort are extensive, their applicability in the cabin environment is still limited. The contemporary status and interaction of the three main components of the methodology is presented in Figure 2. Further, the most influential knowledge gaps on further development of the methodology are as follows:

- local clothing thermal properties, clothing area factor (f_{cl}), intrinsic clothing insulation (I_{cl}), and evaporative resistance ($R_{e,cl}$) for the sitting body position are unavailable in the literature and there is dependence on own manikin measurements;
- there is no realistic representation of a seat contact area in current thermo-physiological models and the contact area dependence on the body morphology is unknown;
- unavailable methodology for realistic representation of a seat conditioning and thermal diffusivity of a seat and its impact on human thermal response and thermal sensation in transient conditions; and
- a lack of a cost-effective hardware system capable of coupling with a suitable thermal sensation model for thermal sensation-driven HVAC applications.

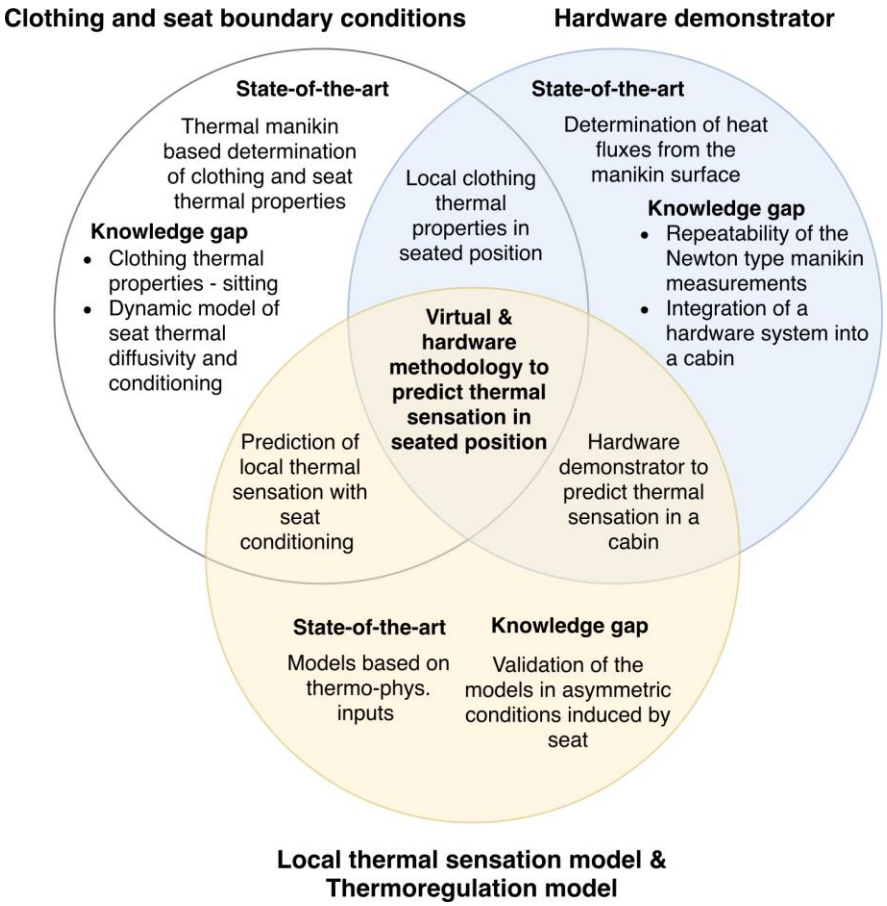

Figure 2. Summary of the state-of-the-art knowledge and knowledge gaps related to the three components of the methodology to to predict thermal sensation in a vehicular cabin.

3 Aim and objectives

3.1 Aim and thesis

The literature survey and knowledge about the specifics of predictions of thermal sensation in a vehicular cabin led to the formulation of the following thesis:

A set of tools comprising a seat heat transfer model, a realistic estimate of local clothing properties, a thermophysiological model, and a thermal sensation model can be used to evaluate thermal interactions between the human body and the surrounding environment. Further, this set of tools can be used to assess thermal sensation in the cabin environment using an objective parameter, such as equivalent temperature. These parameters can be measured in real-time and serve as advanced feedback for the thermal sensation-driven control of local conditioning technologies and HVAC.

Therefore, the aim of this thesis was to develop a methodology to assess human thermal sensation while in a sitting body position, including local conditioning factors such as heated and ventilated seats. A requirement of the method was applicability in both virtual and real indoor spaces. In the latter case, the focus was a thermal-sensation-driven feedback loop allowing for human-centred microclimate management. The particular interest is in an average thermal sensation response of a pool of adult healthy subjects, rather than individuals and/or children.

3.2 Objectives

The specific objectives of the PhD project have been formulated based on the aim of the work presented in Section 3.1 and the knowledge gaps presented in Section 2.3.2, and are as follows:

1. to develop a model relating the seat contact area to basic anthropometric measures (such as body height and weight) and to find a proper representation of the seat contact area in thermo-physiological models;
2. to assess differences between the sitting and standing body positions in the local clothing parameters (f_{cl}, I_{cl}, and $R_{e,cl}$);
3. to identify the impact of differences among typical approaches to determine local clothing parameters and to perform a sensitivity analysis of these on a simulated thermo-physiological response;
4. to develop and validate a model calculating heat transfer between a human body and a seat including local seat conditioning technologies (heating and ventilation);

5. to validate the predicted thermo-physiological responses using the local clothing and seat boundary conditions on a basis of original and literature experimental data;
6. to predict local thermal sensation using several thermal sensation models under steady, transient, and heterogenous conditions indiced by local conditioning and to identify the best performing thermal sensation model;
7. to develop a hardware demonstrator capable of exploiting the validated methodology to determine the equivalent temperature in a vehicular cabin; and
8. to implement the hardware demonstrator in a vehicular cabin and to demonstrate its functionality in a vehicular cabin against a reference, the Newton-type thermal manikin.

3.3 Structure of the thesis

The aim and objectives, outlined in the previous section, have been addressed in five peer-reviewed, scientific publications. The number of citations as of July 20 2019 is given in brackets (data from Google Scholar):

I **M. Fojtlín**, A. Psikuta, R. Toma, J. Fišer, M. Jícha, Determination of car seat contact area for personalised thermal sensation modelling, PLoS One. 13 (2018) 1–16. doi:https://doi.org/10.1371/journal.pone.0208599. (1 citation)

II **M. Fojtlín**, A. Psikuta, J. Fišer, R. Toma, S. Annaheim, M. Jícha, Local clothing properties for thermo-physiological modelling: Comparison of methods and body positions, Build. Environ. 155 (2019) 376–388. doi:10.1016/j.buildenv.2019.03.026. (0 citations)

III **M. Fojtlín**, A. Psikuta, J. Fišer, R. Toma, S. Annaheim, M. Jícha, R.M. Rossi. Thermal model of an unconditioned, heated and ventilated seat to predict human thermo-physiological response and local thermal sensation, Build. Environ. Under review.

IV **M. Fojtlín**, J. Fišer, M. Jícha, Determination of convective and radiative heat transfer coefficients using 34-zones thermal manikin: Uncertainty and reproducibility evaluation, Exp. Therm. Fluid Sci. 77 (2016) 257–264. doi:10.1016/j.expthermflusci.2016.04.015. (8 citations)

V **M. Fojtlín**, J. Fišer, J. Pokorný, A. Povalač, T. Urbanec, M. Jícha, An innovative HVAC control system: Implementation and testing in a vehicular cabin, J. Therm. Biol. 70 (2017) 64–68. doi:10.1016/j.jtherbio.2017.04.002. (3 citations)

Each of the presented papers is a stand-alone publication consisting of an introduction focused on its individual topic, a detailed description of the methods, results containing figures and tables, a thorough discussion of the results, and conclusions with respect to the topic of the paper. Each publication presents original work that is an integral part of this PhD thesis. A commented overview of the work with respect to the aim and objectives of this thesis is presented in Section 4.

3.4 The main author's contribution to the publications

I Conducted the majority of the experimental work, literature survey, data analysis, and writing of the manuscript.

II Conducted the majority of the experimental work, literature survey, data analysis, and writing of the manuscript.

III Contributed to the experimental study, developed the seat heat transfer model, carried out simulations with data analysis, and did the majority of the literature survey and writing of the manuscript.

IV Conducted the majority of the experimental work, literature survey, data analysis, and writing of the manuscript.

V Contributed to the innovative HVAC design requirements and experimental work, carried out the data analysis, and did the majority of the literature survey and writing of the manuscript.

3.5 Associated papers not presented as a part of the thesis

During the course of this PhD project, other research activities were carried out with the focus on an automotive cabin. The summary of publications unrelated to completing of the objectives indicated in Section 3.2 is presented below. The number of citations as of July 20 2019 is given in brackets (data from Google Scholar):

Peer-reviewed papers

J. Pokorný, J. Fišer, **M. Fojtlín**, B. Kopečková, R. Toma, J. Slabotínský, M. Jícha, Verification of Fiala-based human thermophysiological model and its application to protective clothing under high metabolic rates, Build. Environ. 126 (2017) 13–26. doi:10.1016/j.buildenv.2017.08.017. (3 citations)

Conference papers

M. Fojtlín, J. Pokorný, J. Fišer, R. Toma, J. Tuhovčák, Impact of measurable physical phenomena on contact thermal comfort, in: EPJ Web Conf., 2017. doi:10.1051/epjconf/201714302026. (2 citations)

M. Fojtlín, M. Planka, J. Fišer, J. Pokorný, M. Jícha, Airflow Measurement of the Car HVAC Unit Using Hot-wire Anemometry, in: EFM15 – Exp. Fluid Mech. 2015, EPJ Web of Conferences, 2016: p. 6. (8 citations)

J. Pokorný, F. Poláček, **M. Fojtlín**, J. Fišer, M. Jícha, Measurement of airflow and pressure characteristics of a fan built in a car ventilation system, in: EPJ Web Conf., 2016. doi:10.1051/epjconf/201611402097. (1 citation)

M. Fojtlín, J. Fišer, M. Jícha, Repeated determination of convective and radiative heat transfer coefficients using 32 zones thermal manikin, Extrem. Physiol. Med. 4 (2015) A160. doi:10.1186/2046-7648-4-S1-A160. (0 citations)

J. Fišer, A. Povalač, T. Urbanec, J. Pokorný, **M. Fojtlín**, Implementation of the equivalent temperature measurement system as a part of the vehicle Heating, ventilation and Air-conditioning unit, Extrem. Physiol. Med. 4 (2015) A159. doi:10.1186/2046-7648-4-S1-A159. (1 citation)

Conference proceedings (main author only)

M. Fojtlín, A. Psikuta, J. Fišer, M. Jícha, Modelling of conditioned automotive seats. The 18th International Conference of Environmental Ergonomics, July 2019, Amsterdam, Netherlands. Oral presentation.

M. Fojtlín, A. Psikuta, J. Fišer, J. Pokorný, R. Toma, M. Jícha, Effects of seated posture and automotive seat on human thermal response. The 12th International Meeting on Thermal Manikin and Modelling (12i3m), September 2018, St. Gallen, Switzerland. Oral presentation.

M. Fojtlín, J. Fišer, J. Pokorný, R. Toma, M. Jícha, An Innovative HVAC Control System: Comparison of the system outputs to comfort votes. The 17th International Conference of Environmental Ergonomics, November 2017, Kobe, Japan. Oral presentation.

M. Fojtlín and J. Fišer, Thermal manikin – utilisation in testing of protective equipment. 2nd International Conference on CBRN Protection (HAZMAT PROTECT 2016), November 2016, Kamenná, Czech Republic. Oral presentation.

M. Fojtlín, J. Fišer, J. Pokorný, A. Povalač, T. Urbanec, An Innovative HVAC Control System: Implementation and Testing in a Vehicular Cabin. Thr 11th International Meeting on Thermal Manikin and Modelling (11i3m), October 2016, Suzhou, China. Oral presentation.

4 Summary of the work conducted

4.1 Objective 1 (Paper I): Determination of car seat contact area for thermal sensation modelling

For this work, the methods were divided into parts comprising collection of relevant previously published data from the scientific literature, original experimental measurements, and the development of a model to predict seat contact area using basic anthropometric descriptors (e.g. weight, height, BMI, and total body surface area). In the literature, two prevailing approaches to investigate seat contact area were found. One of the methods, presented by Wu [71] and McCullough et al. [72], consists of manually circumscribing a manikin placed on a seat. The second method, by Park et al. [70], uses dedicated pressure distribution sensors covering the seat surface.

Each method has its limitations, either in the precision (uncertain contact boarders in circumscribing) or in the equipment accessibility. Moreover, the studies presented only generalised results, which are not suitable for development of a seat contact regression model. Therefore, a novel method was proposed that utilised easily accessible tools, and consisted of generating prints of a human silhouette on fine paper placed on an automotive seat. The printed shapes were digitalized using a digital camera and processed in graphical software to obtain the surface area separately for the backrest and the seat cushion. Additionally, compared to the circumscribing method, the print boarders are determined with much higher accuracy, particularly at the inaccessible body parts.

The actual prints were carried out on a sample of 13 participants covering approximately 82 % of the European population with regards to BMI (body mass index), ranging from the lower limit of normal weight (18.5 $kg \cdot m^{-2}$) to the upper limit of overweight (29.4 $kg \cdot m^{-2}$) [118]. To compare the contact area of human sample and a manikin, prints of the Western Newton-type thermal manikin (Thermetrics, WA Seattle, USA) were obtained using the same method. The seat for the investigation was selected from a middle-class passenger car, which might be likely equipped with a conditioning technology, such as seat heating and/or ventilation. Finally, the experimental results were compared to relevant scientific studies on human, manikin, and virtual manikin seat contact (full description in *Paper I*, Table 2).

Although the seat and body shape deformation is likely non-linear, a linear model was proposed to relate seat contact area with human anthropometry. This was done with respect to the range of the examined parameters, where the linearization was expected to have strong correlation and sufficient precision for the given application in thermo-physiology. Four easily accessible descriptors

were examined: body weight, height, surface area, and BMI. Admittedly, the last two predictors are power functions of weight and height, and therefore mathematically coupled, but their frequent occurrence in literature and their inclusion expand the applicability of the results.

To assess the accuracy of the linear models, the coefficient of determination, R^2, and root mean square deviation, RMSD, were calculated. The first parameter expresses proportion of the variation in the dependent variable that is explained by the model. The second parameter is used to measure the average difference between measured and predicted values. To predict the accuracy of the slope and intercept of the linear model, a 95% confidence interval was calculated for the best-fit line for the collected population. Finally, prediction intervals were calculated to estimate an interval in which future individual observations of contact area will fall with 95% probability [119].

4.1.1 Summary of the main fidnings

The results of the study revealed a mean average contact that equals 18 % of the human body surface area. It was also confirmed that this surface area was in agreement with the virtual body geometry of the human thermoregulatory model FPCm5.3 at posterior parts of thorax, abdomen, hips, and upper legs. This finding is crucial in further utilization of the FPCm5.3 for reliable investigation of seat conditioning on human thermo-physiology and thermal perception using a heat flux density boundary condition. Thus, the same amount of heat exchange can be guaranteed in simulations as in humans under the same conditions.

Next, four models to predict the total contact area based on human weight, height, body surface area, and BMI, respectively, were proposed. The best predicting capabilities were observed using two predictors, weight and body surface area, having the coefficient of determination of 0.86 and 0.83, respectively. Based on these findings, two models to predict the contact area for backrest (back) and seat cushion (buttocks), respectively, were developed using the weight and body surface area as two independent predictors. The applicability of the models is restricted to the ethnicities of European descent as well as to the scope of examined anthropometric measures. There is indication that differences exist in the distribution of muscles and adipose tissues among ethnicities, which influence the resulting contact area. Finally, it can be expected that a plateau exists for higher values of BMI, as the seat reaches its maximal contact surface area.

The cross comparison with data from literature revealed inconsistencies of using contemporary *hard shell* thermal manikins to investigate thermal effects of the seats. The seat contact area of the Newton type thermal manikin was found to be 35 % and 69 % smaller than that of a human at the seat cushion and backrest, respectively. These differences are due to the manikin´s low weight, rigid shell, and lack of spinal flexibility, which do not facilitate a human-like seat contact. The results from the manikin study by McCullough et al. [72] were well comparable to the humans. However,

the original study lacks details on both description of the manikin and the seat. More importantly, the authors of the manikin studies, using the circumscribing method, did not specify how they determined the contact margins in the inaccessible body parts such as buttocks and lower back.

We found very limited applicability of thermal manikins in evaluation of seat contact area and their actual use with automotive seats. The rigid construction of the figurine restricts the replication of natural contact with the seat, having no interaction with the seat at the mid back as well as significantly lower contact at the seat cushion compared to a human.

4.2 Objectives 2 and 3 (Paper II): Clothing thermal properties

The focus of *Paper II* was examining the local clothing parameters in a sitting body position and the most probable ways of their determination. However, high precision results are typically dependent on access to costly equipment, such as thermal manikins and a climatic chamber. Therefore, it is of particular interest to identify an alternative solution with sufficient accuracy comparable to the state-of-the-art methods.

The summary of examined scenarios is presented in Table 1, organised in descending order of sophistication. We selected a range of methods based on manikin measurements, analytical heat transfer modelling [57,58], regression modelling [59], empirical modelling, such as the UTCI model [60], and ISO based approaches [47,61,62]. A detailed description of the cases is provided in *Paper II*, Sections 2.3 – 2.9. Additionally, differences in the local clothing values between sitting and standing body positions were investigated in detail.

Table 1. Summary of the examined scenarios to determine clothing thermal properties.

Case	f_{cl} (-)	I_{cl} ($m^2K.W^{-1}$)	$R_{e,cl}$ ($m^2Pa.W^{-1}$)	Position	Segments
1	3D scanning	Manikin heat loss [109]	Manikin heat loss [110]	sitting	13
2	Photography [47]	Manikin heat loss [109]	Manikin heat loss [110]	standing	13
3	Physical model [57,58]	Physical model [57,58]	Physical model [57,58]	sitting	8
4	Physical model [57,58]	Physical model [57,58]	Physical model [57,58]	standing	10
5	Regression model [59]	Regression model [59]	Physical model [57,58]	standing	11
6	ISO based model [61]	ISO based model [61]	ISO based model [62]	standing	3
7	ISO database [47]	UTCI model [60]	ISO database [47]; Eq. 31	standing	7
8	ISO database [47]	ISO database [47]	ISO database [47]; Eq. 31	standing	1

4.2.1 Summary of the examined scenarios

Case 1 was composed as the reference case with the state-of-the-art methods used. The most realistic way to determine the f_{cl} is a three-dimensional (3D) scanning method. A dedicated scanner was used to digitalise the nude and clothed body surface of a sitting manikin (more details about the equipment can be found in [49]). Each measurement was repeated four times. The resulting scans were subsequently processed in software (Geomagic Control 2014, 3D Systems®, USA) to obtain the ratio of the clothed and nude manikin. This was done for 13 body parts, namely: *chest, back, abdomen, lumbus, anterior pelvis, buttocks, upper arm, lower arm (forearm), anterior thigh, posterior thigh, shin (anterior leg), calf (posterior leg), foot* to copy the body segmentation of the FPCm5.3 virtual manikin (ErgonSim, Germany [87]). This guarantees consistency of the inputs for thermo-physiological as well as thermal sensation modelling.

Determination of I_{cl} and $R_{e,cl}$ was carried out using a 34-zone Western Newton-type manikin (Thermetrics, Seattle, USA) seated onto an adjustable perforated plastic chair in a climatic chamber (detailed description of the chamber and the manikin in *Papers II* and *IV*). The experimental conditions were in accordance with ISO 15831:2004 [109]. The resulting I_{cl} was calculated according to equation 2 from Section 1.3.2. The evaporative clothing resistance $R_{e,cl}$ was determined using a prewetted tightly fitting, long sleeve overall [120,121]. The measurement was carried out at under isothermal conditions of 34 °C (skin temperature equal to ambient temperature), relative humidity of 18 % (partial water vapour pressure of 957 Pa), and air speed of 0.1 ± 0.05 $m \cdot s^{-1}$. The calculation of evaporative resistance was done according to heat loss method described in ASTM F2370 [110].

Case 2 was designed as a reference measurement in an upright standing body position under laboratory conditions, where a non-articulated thermal manikin and a camera are available. The local f_{cl} values were obtained according to the standard ISO 15831 [109] by superposition of photographs of a nude and dressed manikin using graphical software (CorelDRAW X8, Corel Corporation, USA). These were taken from four azimuth angles (front 0°, two side views 45°, 90°, and 180°) and a horizontal view of 0°. The experimental procedure to determine I_{cl} and $R_{e,cl}$ was identical with Case 1.

Cases 3 and 4 represented emerging methods to realistically and rapidly simulate f_{cl}, I_{cl}, *and* $R_{e,cl}$. The model exploits basic thermodynamic phenomena (conduction, radiation, and convection) and allows the calculation of local clothing parameters of multiple, layered garments. Most importantly, distribution of the heterogeneous air gaps entrapped in the clothing for a corresponding body part, both in sitting and standing positions, is accounted for. The clothing simulations were carried out using the in-house analytical clothing model developed at Empa [57,122].

Case 5 was based on a linear regression model by Veselá et al. [123], who related local values of f_{cl} and I_{cl} to clothing ease allowances. The models were constructed on data from single-layer garments and while in the standing position. However, we also investigated two-layer winter clothing.

Therefore, we applied principles from the study by Mark et al. [124], where the main findings indicated that the inner layer was negligibly influenced by the outer layer as long as the ease allowance of the outer layer was bigger than that of the inner one. This premise applies to the majority of casual clothing, including the clothing investigated in this study. The corresponding values of f_{cl} and I_{cl} were, thus, calculated according to the ease allowance of the outer layer. The methodology to calculate $R_{e,cl}$ was not presented in the study by Veselá et al. [123] and was adopted from Case 4 [57].

Case 6 exploited an algorithm for reverse calculations of all three local clothing parameters from their global values [61,62]. This approach was developed from global clothing databases by McCullough et al. [125] and ISO 9920 [47] valid for 106 garments. However, the resolution of the algorithm is limited to individual clothing items covering given body parts, such as trousers covering the whole lower limbs. As the method does not clarify an approach to calculate the resistances of multi-layered garments lying atop one-another, the clothing resistances were instead totalled to match the procedure of Veselá et al. [126]. The clothing area factors were determined for the outermost layer of the clothing ensemble.

Case 7 was based on estimation of clothing thermal parameters based on the ambient temperature [60]. The model has a resolution of 7 body parts (head, torso with upper arms, lower arms, hands, upper legs, lower legs, and feet). This model was applied despite its original focus on outdoor applications under the presumption of similar clothing preferences for indoor and outdoor environments based on two mild ambient temperatures of 24 °C (summer indoor clothing) and 21 °C (winter indoor clothing). These two temperatures were defined according to the PMV-PPD thermal sensation model [28] as thermo-neutral for the given clothing sets.

Case 8 was based on the clothing thermal properties listed in standard ISO 9920 [47]. From a practical perspective, this approach is of the main interest for a variety of engineering applications, since no dedicated equipment is required. The clothing thermal properties are presented in a form of global, whole-body values. By definition, the global values should be applied as a uniformly distributed insulation across the human body, which is typically not the case in reality. Two clothing sets were selected from the standard (Table A.2 [47]), *Ensemble 108* and *Ensemble 114* to represent summer and winter indoor clothing, respectively.

4.2.2 Clothing and definition of body positions

Since the research focus of this thesis was indoor environments, two ensembles were examined that correspond to the summer and winter seasons. The first clothing set represents summer indoor clothing, consisting of a collar shirt, light cotton jeans, briefs, socks, and leather sneakers. The second, winter set comprised a turtle-neck shirt as well as a cotton T-shirt worn underneath, heavier

cotton jeans, briefs, socks, and leather shoes. All garments were selected from the database by Psikuta et al. [127] and were used throughout the study to guarantee consistency of the method.

To analyse differences in local clothing thermal properties, two body positions were investigated. The sitting body position was selected to mimic driving, operating machinery, or office work. The specifications for the sitting were adopted from the work of Mert et al. [49] having an elbow angle of 120°, a hip angle of 110°, and a knee angle of 120°. Secondly, an upright standing position with hands down was examined since it is typically reported in the literature and was used to contrast the differences from one another (*Paper II*, Figure 1).

4.2.3 Determination of seat thermal properties

At this stage of the investigation, the seat was substituted with thermal and water vapour resistances since steady-state conditions were examined. Direct measurement of these two parameters with a thermal manikin does not yield realistic results, because of the manikin's rigid body construction and low body weight (see paper *Paper I*). As a result, the corresponding data was adopted from a study on aeroplane seats with similar construction to automotive seats, with moulded foam cushioning and leather covering. Using a stamp tester, a thermal resistance of 0.55 $m^2K \cdot W^{-1}$ [65] was measured for the seat, whilst an evaporative resistance of 100 $m^2Pa \cdot W^{-1}$ [65] was determined using the same seat in human trials. Finally, we estimated the seat clothing area factor to be 2.0 units based on the dimensions of the seat.

4.2.4 Sensitivity analysis

Comparison of the absolute values of clothing thermal properties is beneficial for the process of clothing development. However, in practical applications, it is of major interest to understand the impact of such differences on the human thermal response, which may be dampened [82]. Thus, the eight cases were supplied to the FPCm5.3 in order to reveal their impact on the development of thermo-physiological parameters such as local skin temperatures, core temperature, sweat production, and skin wettedness as well as the global thermal sensation indicated by DTS (Dynamic Thermal Sensation). The environmental conditions were selected as thermo-neutral with the following characteristics: operative temperature summer case ($t_{air} = t_{rad} = 24$ °C), operative temperature winter case ($t_{air} = t_{rad} = 21$ °C), air speed of 0.1 $m \cdot s^{-1}$, and relative humidity of 50 %. The metabolic production was selected with respect to the sitting body position as 1.3 met (driving or office work) and the simulations were carried out in a span of four hours with a five-minute simulation interval.

4.2.5 Summary of the main findings

The results of this study showed substantial variation among the methods for all examined clothing parameters, ranging from 13 – 43 % in f_{cl}, 35 – 198 % in I_{cl}, and 53 – 233 % in $R_{e,cl}$ of the reference value (Case 1). The most realistic results yielded the approaches based on analytical heat transfer modelling including realistic distribution of the air gaps (Case 3) [57,58] and the regression model (Case 5) [59] relating a garment ease allowance to the clothing insulation and clothing area factor. The least realistic approaches were the ISO based model (Case 6) [61,62] and the database values from the ISO standard itself [47]. The main reason for this lack of realism was a lack of method detail, in which the local values were lumped into larger areas, thus, neglecting the local extremes.

Altering the body position from standing to sitting causes a change in the orientation of several body parts and a redistribution of the air gaps. This also implies changes in all three clothing thermal parameters. While only minor changes were found for the global thermal and evaporative resistances [55], the local parameters showed much higher error margins:

- up to 31 % of the reference value (Case 1) for f_{cl} depending on body part;
- up to 80 % of the reference value (Case 1) for I_{cl} depending on body part; and
- up to 92 % of the reference value (Case 1) for $R_{e,cl}$ depending on body part.

There was a substantial influence of the discrepancies among the methods on predicted thermo-physiological responses. In mean skin temperature, the variation was within 0.6 °C and 1.3 °C in summer and winter clothing, respectively. This parameter is influential in thermal sensation models, where a considerable error in local thermal sensation can be expected in a range from 0.5 to 1.5 units depending on the thermal sensation model and its scale as demonstrated by Koelblen et al. [99] and Veselá et al. [126]. On the other hand, the differences in mean skin temperatures between the body positions were negligible, being within 0.3 °C.

The local thermo-physiological responses were clearly affected by the variation of the local clothing inputs. For example, relatively low differences in the clothing properties at the *chest* resulted in the absolute differences in skin temperatures of 0.5 °C among the methods and of 0.2 °C between the body positions. Quite the reverse, higher variability of input parameters, e.g. as at the *anterior thigh*, leads to a spread of the predicted local skin temperature of 1 °C and 2 °C in summer and winter clothing, respectively. The variability in input parameters also influenced the predicted amount of sweat as well as the onset of sweating. For instance, the sweat excretion amounted between 5 g (Case 7 winter clothing) and 138 g (Case 4 summer clothing) and the sweating onset varied between 60th (Case 8) and 190th minute (Case 7) using the winter clothing.

The error induced by clothing inputs, in this case, has no critical medical relevance such as uncompensated heat storage or dehydration. However, in thermal sensation and comfort studies, error in

the local clothing input can cause substantial error in the thermal sensation modelling. Next, this study confirmed our hypothesis that the whole-body clothing properties are neither suitable nor sufficient for local thermal sensation modelling. Two non-experimental methods, physical and regression modelling, were recommended to substitute resource demanding manikin measurements for a variety of engineering applications. Finally, a sensitivity study revealed a dominant influence of the thermal insulation on the predicted thermo-physiological parameters. Therefore, to get a high-quality prediction of physiological responses in a sitting position, it is crucial to always choose the most reliable method to determine the local thermal insulation, respecting the body position.

4.3 Objectives 4 – 6 (Paper III): Conditioned seats

Paper III addressed three major knowledge gaps in modelling of sitting exposures: (a) determination of heat exchange between the seat and its occupant; (b) validation of thermo-physiological responses under asymmetrical conditions induced by the seat; (c) prediction of thermal sensation under cold and hot environmental conditions using seat conditioning technologies such as seat heating and ventilation. Next, the findings from *Papers I* and *II* also contributed to reliable thermo-physiological simulations by determination of the seat contact area and by the use of the most accurate methods for determining the clothing thermal properties in a sitting body position.

4.3.1 Development and validation of the seat heat transfer model

The seat heat transfer model was developed using the fundamental principles of heat transfer. The aim of the model was to provide sufficient approximation of the heat exchange between a seat with a considerable thermal mass and an adjacent body part such as the buttocks and back. A thermal system comprising human body tissues, clothing layers, and seat construction layers was designed and solved under the following presumptions:

- dominant heat flux in a direction perpendicular to the plane of the seat;
- neglected convection, evaporation, and radiation between the internal calculation nodes due to the high evaporative resistance of the seat and the negligible convection and radiation in the highly compressed layers of clothing and seat. Although the cooling in the ventilated seat is caused by sweat evaporation, in practical applications, it is not feasible to determine all necessary parameters for psychrometric calculations in the seat contact (e.g. air velocity, relative humidity, air temperature). The evaporative cooling was, thus, represented by a heat sink or a possibility to prescribe a time-dependent temperature profile at the seat surface, yielding equivalent heat flux as if the evaporation was considered;

- neglected evaporation and radiation at the exterior calculation nodes (back of the seat) due to high evaporative resistance of the seat and partial shading of the back of the seat resulting in major simplification of the calculation;
- constant thermal properties of all human tissues, clothing, and seat construction layers;
- uniform thickness (but not the same) of all tissue, clothing, and seat construction layers;
- no thermoregulatory actions in the human tissues for a simplified solution; and
- solution using the finite-difference method with a discrete time step of 0.05 s.

The model yields calculated heat flux separately for the seat cushion and backrest. The model's validation was performed against original experimental measurements of heat flux, under cool (t_{air} of 18 °C) and hot (t_{air} of 41 °C) environmental conditions in the climatic chamber at Brno University of Technology. The validation procedure comprised unconditioned, seats heated to constant surface temperature, and ventilated seats. Details about the validation cases and participants can be found in Table 2, Cases 18 °C and 41 °C.

Table 2. Complete overview of the cases used for validation of the methodology.

	Case	Pre-condition 60 min t_{air} (°C)	Chamber 30min t_{air} (°C)	Seat conditioning	Males Uncond. / Cond.	Females Uncond./ Cond.	BMI M/ F (kg.m^{-2})	Available data for validation
This study	18 °C	22.5	18	Uncond./ Heated const. temp.	8 / 14	2 / 6	25 / 23	8 skin temp.**; backrest & seat cushion temp. and HF; TS votes
	41 °C	25	41-25*	Uncond. / Ventilated	7 / 7	2 / 2	26 / 28	8 skin temp.; backrest & seat cushion temp. and HF; TS votes
Oi et. al [10]	5 °C	22	5	Uncond./ Heated const. HF	8 / 8	-	18.6 / -	Skin temp. at backrest & seat cushion
	10 °C	22	10	Uncond./ Heated const. HF	8 / 8	-	18.6 / -	Skin temp. at backrest & seat cushion
	15 °C	22	15	Uncond./ Heated const. HF	8 / 8	-	18.6 / -	Skin temp. at backrest & seat cushion
	20 °C	22	20	Uncond./ Heated const. HF	8 / 8	-	18.6 / -	Skin temp. at backrest & seat cushion

t_{air} – ambient air temperature; BMI – body mass index; temp. - temperature, HF – heat flux density, TS – thermal sensation.

*25°C reached after 20 min of exposure; **skin temperatures unavailable for unconditioned case

4.3.2 Coupling with thermo-physiological and thermal sensation models

In the next step, the seat heat transfer model outputs were coupled with the FPCm5.3 to obtain the predicted thermo-physiological response for the body parts in contact with the seat as well as for the rest of the body. Local skin temperatures were available for comparison to predictions at eight body sites (forehead, right scapula, left upper chest, right upper arm, left forearm, left hand, right anterior thigh, and left calf; segmentation from the ISO 9886:2004 [128]). The measurements were

carried out with the use of a junction semiconductor device, iButton (also known as a silicon diode temperature sensor, Maxim Integrated, USA, accuracy ± 0.5 °C), attached to the participants' skin by medical tape (Hypafix 16002, BSN Medical GmbH, Germany). To calculate mean skin temperature, the eight skin temperatures were averaged using the weighting coefficients from the standard.

The range of validation cases of the skin temperatures in the seat contact was extended using data from a paper by Oi et al. [10] at ambient temperatures of 5 °C, 10 °C, 15 °C, and 20 °C (details in Table 2). The seat used in the study was a front automotive seat heated by silicone rubber heating pads placed underneath the leather upholstery. The heating was reported as a constant heat flux of 268 $W \cdot m^{-2}$ delivered both to the seat cushion and backrest [10]. The thermal interaction with the seat was modelled using the seat heat transfer model based on the description from the paper.

In the final step of this study, the thermo-physiological predictions were used to predict thermal sensation. In total, the performances of three local thermal sensation models were investigated:

- the model by Nilsson (MTV) [100] was used due to its standardisation (part of the ISO 14505 standard [64]) and possible coupling with equivalent temperature sensors. The model uses a seven-point Bedford scale that combines thermal sensation votes with thermal comfort (much too cold, too cold, cold but comfortable, neutral, hot but comfortable, too hot, much too hot) that correlate with a heat loss from a given body part or equivalent temperature. The range of applicable conditions covers ambient temperatures from 19 °C to 29 °C;
- the model by Zhang (TSZ) [21,101], which was developed for automotive applications and predicts local thermal sensation using an extended nine-point ISO scale with two additional extreme thermal sensation votes (very cold, very hot). The model requires local skin and core temperatures as inputs. The range of applicability is between air temperatures of 20 °C and 33 °C; and
- the model by Jin et al. (TSV) [102], which yields a local thermal sensation on the seven-point ISO scale (cold, cool, slightly cool, neutral, slightly warm, warm, hot) [28]. The model was developed based on a sample from the Chinese population and is applicable in the temperature range from 20 °C to 30 °C.

In each step of the methodology, the accuracy of all predicted parameters (heat flux, seat temperatures, skin temperatures, and thermal sensation votes) was assessed by means of RMSD and bias. Predictions were assumed to have high precision if the RMSD and bias were within the standard deviation of the measurement.

4.3.3 Summary of the main findings

The proposed seat heat transfer model successfully predicted development of the heat fluxes at the seat-occupant interface. Throughout the exposure, the typical error of the calculated heat flux oscillated between 3 % and 10 % and the RMSD and bias were within two standard deviations of the measurement, with somewhat lower precision in the highly transient period after taking the seat. Psikuta et al. [129] stated that an error of 2 % has a negligible impact on the development of mean skin and core temperatures being less than ±0.18 °C and ±0.01 °C, respectively. Since the discrepancies in the predicted heat flux were close to these margins, a sufficient precision of the seat heat transfer model for coupling with FPCm5.3 was concluded.

Thus, in the next step, the seat heat transfer model was coupled with the FPCm5.3 to predict the temperatures in the contact with the seat as well as skin temperature in the non-contacting body part. Again, we found a good agreement between the predictions and measurements in terms the RMSD and bias. These findings were supported by the RMSD and bias being lower than the standard deviation of the measurement and, at the same time, within typical inter- and intra-human variations in skin temperatures (approximately 1 °C) [81]. Such precision is also sufficient for reliable thermal sensation modelling [99,126].

The outliers were discussed in *Paper III*, where the highest inaccuracies were found in the 5 °C case with seat heating. The error was attributed to a combination of factors including a brief description of the experiment from the literature, the neglected lateral heat losses, and constant thermal properties of the tissues in the seat heat transfer model. In this case, the error was proportional to decreasing ambient temperature, which peaked at 2.6 °C in the 5 °C case.

The benefits of the model were displayed against two simplified assumptions. For the unconditioned seat, the seat was assumed as thermal insulation and evaporative resistance. In the heated case, the seat was replaced with a heat generation boundary condition without dissipation to the ambient environment. These simplifications yielded not only four-times higher errors than that of the proposed methodology but also unrealistic development of the skin temperatures.

The best performing thermal sensation models, in general, were MTV and TSZ, in which the RMSD and bias were within two standard deviations of the human votes having an average of 1.1 units. The two standard deviations of the thermal sensation votes were selected to cover 95 % of their dispersion due to the relatively low number of participants (details of this are given in Table 2). The worst performance was found in the TSV model. Here, the RMSD and bias exceeded two standard deviations in more than half of the body parts examined. Furthermore, TSV did not respond either to the temperature step change or to the cooling ramp, which is not acceptable in any application.

Although the skin temperatures were predicted accurately at the seat contact, the predicted thermal sensation was clearly less accurate than for body parts without seat contact. Since the TSZ contains a derivative component, it performed well in the transient conditions (the first six minutes of the exposure), with an RMSD and bias within two standard deviations. Nevertheless, after this period, TSZ drifted towards higher thermal sensation votes and exceeded the two standard deviations limit. In the first six minutes of the cool exposure, the MTV model tended to over-estimate the effects of the cold seat by up to 2.3 units. This error was mainly because of the high initial cooling rates (up to 150 $W \cdot m^{-2}$) and no derivative component of the model. The remaining part of the cool exposure (18 °C) typically followed the trends of the experimental data. Under hot conditions, on the other hand, the accuracy of the predictions by MTV was the best out of the three models, having the RMSD and bias of approximately one standard deviation.

The lower accuracy of the thermal sensation predictions in the contact can be attributed to several dominant factors. Firstly, the range of temperatures that can occur during contact is wider than that without contact. Thus, the thermal sensation models were at or beyond their limit of applicability. Next, Oi et al. [10] concluded that comfortable skin temperatures at the seat contact are higher by lower ambient temperatures, what can influence thermal sensation voting and acceptability of locally higher skin temperatures. Similar findings were also demonstrated by Zhang et al. [130] for heated and cooled seats in a range of ambient temperatures of between 15°C and 45°C. Nevertheless, none of the examined models captures this dependence. For the aforementioned reasons, further refinement of current thermal sensation models is needed to achieve more consistent predictions.

4.4 Objectives 7 – 8 (Papers IV and V): Development and implementation of the demonstrator

In this part of the thesis, we examined the idea to develop a hardware demonstrator consisting of several cost-effective equivalent temperature sensors and their integration into a vehicular cabin in proximity of an occupant. The demonstrator is aimed to be an integral part of the cabin interior, rather than a manikin or a dedicated laboratory instrument. The spatial distribution of the directional equivalent temperature sensors was expected to provide detailed information about the local effects of the environment on the occupant. Further, the equivalent temperature was shown correlate with thermal sensation [56,100] (see Section 2.2.4) and thus, could be translated into a local thermal sensation vote. Such system input could be used to evaluate thermal sensation in real time and serve as a basis for thermal-sensation-driven HVAC control.

4.4.1 Evaluation of the manikin measurement uncertainty

The Newton-type manikin was used for the calibration of the equivalent temperature system in the actual cabin environment. However, no detailed statistical analysis of repeated manikin measurements was available. For this reason, we carried out a study on measurement uncertainty of the Newton-type manikin in typical laboratory conditions in both sitting and standing position (*Paper IV*). The experimental data were obtained from three independent repetitions of measurements in steady conditions inside a climatic chamber with a calibration box to ensure homogenous environmental conditions. A series of tests were carried out to reveal statistically significant differences (95% confidence) among repeated measurements of radiative and convective heat transfer coefficients as follows:

- Kolmogorov-Smirnov test for normal distribution of data. Normality is a fundamental premise for the calculation of succeeding tests. The assumption of normality was satisfactory for all cases except for the head;
- Bartlett test for homogeneity of variances. Homogeneity is accepted if the variances of studied populations are sufficiently equal. This criterion is also essential premise for the test for the means. The assumption of homogeneity of variance was satisfactory for most of the body parts, but not for the posterior forearms, upper thighs, and calves; and
- test for the means using one-way ANOVA. The test revealed statistically significant differences of the means for most of the body parts. Therefore, A and B type uncertainty evaluation was further expressed.

The A type uncertainty evaluation represents a statistical analysis of series of independent observations having normal distribution. The typical expanded uncertainty (95% confidence level) was found below 8 % of the mean. The B type uncertainty is determined by means other than statistical analysis of series of independent observations. It is a function of partial uncertainties that enter the calculation of the studied physical value (e.g. measurement of air and manikin's surface temperatures, heat flux etc.) [131]. The typical expanded uncertainty (95% confidence level) was found below 4 % of the mean. These findings are in line with other manikin studies and are within boundaries for reliable manikin applications [79]. Therefore, we found the Newton-type manikin suitable for calibration of the equivalent temperature system.

4.4.2 Development of the demonstrator

The modular system of equivalent temperature sensors was designed and produced (full description in *Paper V*) based on the criteria defined by the intended application of the sensors:

- precision of temperature measurement and heating temperature stability better than 0.1 °C;

- sufficient heating power to start up from temperature of -20 °C within 2 minutes – achieved by maximal heating power of 1000 $W \cdot m^{-2}$;
- stable control characteristics in the typical conditions, approximately from 20 to 100 $W \cdot m^{-2}$;
- small size (20 × 20 × 10 mm) allowing unobtrusive installation in the cabin; and
- system modularity, with the ability to add or remove an arbitrary number of sensors.

4.4.3 Integration of the demonstrator into the cabin

Sixteen t_{eq} sensors were distributed in the vicinity of the driver to capture the orientation of 16 body parts (*Paper V*, Figure 2). Nevertheless, the optimal placement and orientation of the sensors was in some cases restricted. This was most critical for upper and lower limbs, where the sensors could not be placed with the same spatial orientation. To mimic segmental equivalent temperature (such as output from a manikin) one or more sensors were allocated in an aggregation map to each body part. The aggregation map served as a platform, in which the individual signals were scaled (calibrated) according to the manikin measurements under the same conditions.

To eliminate weather disturbances from the ambient environment, the calibration was carried out in climatic chamber conditions under three basic conditions:

- a cold case, 10 °C, no solar irradiation;
- neutral case, 20 °C, no solar irradiation; and
- hot case, 25 °C, solar simulator set to 700 $W \cdot m^{-2}$, 70° elevation, facing the left (driver) side.

The calibration procedure began with a preconditioning of the experimental vehicle in a climatic chamber until stable conditions in the cabin were reached. At the same time, the Newton-type manikin was seated at the driver's seat and was operating with a constant surface temperature of 34 °C. Next, the vehicle was started and the proposed system of equivalent temperature sensors was initiated. The cabin microclimate was managed by the on-board HVAC system, which was set to a control regime 'Automatic 22°C'. Each trial lasted for one hour and for the calibration purposes, the last five minutes of the measurement period were evaluated. All the examined cases were pooled to find optimal scaling coefficients for the aggregation map. To do so, the differences between the equivalent temperature obtained from the manikin and the system were minimized by the GRG (generalized reduced gradient) optimization scheme.

4.4.4 Summary of the main findings

In steady conditions and at the majority of body parts, the system of equivalent temperature sensors was capable of determining the t_{eq} with precision better than 1 °C. In cold conditions, the system underestimated t_{eq} by 1.9 °C for the lower legs. Conversely, in neutral conditions, the system

overested t_{eq} by 1.8 °C for the anterior thighs. In hot conditions, the prediction accuracy of the system was the highest. In general, the limbs are the most challenging body parts to determine their corresponding equivalent temperature using the flat-surface sensors. It is because of their cylindrical shape and positioning in the cabin. Next, the sensors were not equipped with guarding (heated) surfaces that would prevent lateral heat losses from the measurement surface to the body of the sensor. The guarding was substituted by thermal insulation, but this was not sufficient since we found a decreasing trend in the accuracy of the measurement with decreasing ambient temperature. At the same time, guarding is essential for examination of rapid changes in t_{eq} to avoid the influence of the thermal capacity of the sensor's body.

The comfort zone diagram by Nilsson [100] is used to relate the equivalent temperature to mean thermal vote of a given body part. The *width* of the zones depends on the clothing and body part sensitivity. However, to cross one zone, such as to go from hot but comfortable down to cold but comfortable, a difference in the equivalent temperature of at least 3 °C is needed. For this reason we concluded sufficient precision of the demonstrator for its further applications.

5 Conclusions

As formulated in the objectives, this project presents a model to calculate seat contact area; clothing thermal properties in a sitting body position; method to address local seat conditioning; and a physical demonstrator integrated into a cabin. This PhD thesis has demonstrated the applicability of certain methods to predict thermal sensation in a sitting body position with regards to the respective factors typical of vehicular-cabin environments.

The summary of the main conclusions from individual studies is as follows:

- the seat contact area of an average person is approximately 18 % of the total body area;
- The seat contact area in FPCm5.3 can be realistically represented by posterior parts of the thorax, abdomen, hips, and thighs;
- within a range of the typical European population, the seat contact area can be described using linear equations and predicted based on weight and/or total skin surface;
- thermal manikins without adjustments are not suitable for research of contact microclimate;
- two-fold differences exist in local clothing thermal properties between the standing and sitting positions and these differences have substantial impact on local predicted thermo-physiological responses;
- physical modelling with a realistic air-gap distribution and regression modelling was found to be sufficient for replacing the state-of-the-art measurements of clothing thermal properties. This applies to indoor (*office*) clothing for summer and winter season;
- the seat heat transfer model significantly contributed to the improvement of predicted thermo-physiological responses and thermal sensation for the contact body parts with or without conditioning;
- uncertainty of the Newton-type thermal manikin was defined and was found sufficiently accurate to be used for calibration of the on-board equivalent temperature measurement system; and
- the modular system of directional equivalent temperature sensors was shown to determine equivalent temperatures for individual body parts in the cabin to the precision of ±1°C.

The knowledge gaps addressed in this thesis were mostly related to the quality of input parameters and extension of the applicability of already existing methods. This brought the modelling approach much closer to realistic applications and tackling challenges in engineering, rather than creating "just another" model of thermal sensation or thermo-physiology. The engineering community can benefit from the prompt calculations of both physical variables and consequent subjective

thermal sensation for a given environment with a known error. This ability for rapid calculation enables the effective evaluation of human interactions with indoor spaces, reducing the dependence on costly, logistics-intensive, and labour-intensive human subject studies.

5.1 Future perspectives

One of the most influential contemporary motivations for thermal comfort research is to efficiently create comfortable and healthy conditions with respect to low energy consumption and other environment impacts. These demands are still conflicting. However, the proposed methodology can be used to carry out parametric studies focused on investigating strategies to mitigate the energy consumption using local conditioning technologies or by changing the construction of the cabin (e.g. altering the position of air inlets, glazing, and shading). Such knowledge is of major interest in the field of battery powered electric vehicles, where the microclimate management operates at the cost of driving range.

The system of inexpensive equivalent temperature sensors demonstrated an opportunity to shift traditionally laboratory based equipment into a consumer market. In asymmetric and transient thermal environments, such a device can be used for personalisation of the thermal experience and zoning with much higher accuracy than any commercially available solution. Furthermore, the user can define his/her thermal expectation from the HVAC system in more natural way, via a desired thermal sensation for individual body parts, rather than a desired ambient temperature. This would likely lead to an enhanced thermal experience and higher thermal comfort. Indeed, it was shown that the psychological aspect of having control over the environment automatically improved satisfaction with the indoor conditions [39,40].

Additionally, computational methods can be also used for academic purposes. Here, the thermophysiological model with realistic input data can be applied to reconstruct studies from the literature as well as field-based studies where thermal sensation was investigated, but no thermophysiological data were collected. Very often, this is the case because specialised equipment and approval of an ethical board is needed to carry out research with human participants. Therefore, such efforts would contribute to extending the pool of exposures and could serve as a basis for refinement of local thermal sensation modelling.

5.2 Limitations

The complexity of the mechanisms behind human thermal perception is much higher than the contemporary understanding. Because of this, many parameters influencing thermal perception are not considered by the models. Thus, the major weakness of thermal sensation modelling is still a gener-

alisation of the results, which cover only a certain population and certain conditions with typical accuracy better than one thermal sensation unit.

The predictive power of the examined thermal sensation models was lowest at the body parts in contact with the seat. The range of skin temperatures under seat contact is much wider than the rest of the body exposed to the ambient conditions, either because of the initial seat temperature or because of the seat conditioning. Moreover, in highly asymmetric conditions, the local exposure may significantly affect local thermal sensations of an unexposed body parts [106] and comfortable skin temperatures are higher with lower ambient temperatures [10]. However, none of the examined models captures these effects and subsequent extension is required.

The proposed seat heat transfer model was developed to calculate realistic heat exchange between the seat and its occupant. In order to reduce number of input parameters and, at the same time, potential sources of uncertainty, the cooling effects of latent heat of sweat vaporisation was replaced by a heat sink or a possibility to prescribe a time-dependent temperature profile at the seat surface, yielding equivalent heat flux as if the evaporation was considered. While thermal sensation models require only inputs such as skin and core temperatures or heat flux, the neglect of the water propagation restricts the investigation of discomfort induced by skin wetness.

Finally, several limitations of the method should be noted for the hardware demonstrator. The equivalent temperature approach captures the sensible heat only. This might not be sufficient for hot conditions where a larger amount of sweat is likely to be excreted by a human body and, thus, evaporation starts to play a dominant role in cooling. In such case, the predictions would be inaccurate. Next, in hot conditions, the method can be used only up to the temperature of the heated surface. Beyond this limit, the sensor receives heat from the ambient environment and is no longer capable of heat flux measurements. On the other hand, Nilsson [108] commented that the sensor could be used in a passive thermometer mode, when the surface temperature can be approximated to the equivalent temperature. Finally, this methodology is applicable under transient ambient conditions. However, a transient state can arise also on the side of the human with regards to metabolic heat production and prior environmental exposures. Under human-centred transients, it is likely to see a substantial error in predictions of thermal sensation.

6 References

[1] European Commission, How Europeans spend their time, Office for Official Publications of the European Communities, Luxembourg, 2004.

[2] X. Cheng, Z. Tan, X. Wang, R. Tay, Air quality in a commercial truck cabin, Transp. Res. Part D Transp. Environ. 11 (2006) 389–395. doi:10.1016/j.trd.2006.07.005.

[3] M. Cisternino, Thermal climate in cabins and measurement problems, in: Assess. Therm. Clim. Oper. Cabs, Semin. Florence; JTI-Rapport, Swedish Institute of Agricultural and Environmental Engineering, Florence, 1999: pp. 15–23.

[4] H.A.M. Daanen, E. Van De Vliert, X. Huang, Driving performance in cold, warm, and thermoneutral environments, Appl. Ergon. 34 (2003) 597–602. doi:10.1016/S0003-6870(03)00055-3.

[5] R.A.I. Lucas, Y. Epstein, T. Kjellstrom, Excessive occupational heat exposure: A significant ergonomic challenge and health risk for current and future workers, Extrem. Physiol. Med. 3 (2014) 1–8. doi:10.1186/2046-7648-3-14.

[6] R. Farrington, J. Rugh, Impact of Vehicle Air-Conditioning on Fuel Economy, Tailpipe Emissions, and Electric Vehicle Range: Preprint, Natl. Renew. Energy Lab., Golden, CO. (2000) 1–12. http://www.nrel.gov/docs/fy00osti/28960.pdf.

[7] K.R. Kambly, T.H. Bradley, Estimating the HVAC energy consumption of plug-in electric vehicles, J. Power Sources. 259 (2014) 117–124.

[8] M. Veselý, W. Zeiler, Personalized conditioning and its impact on thermal comfort and energy performance - A review, Renew. Sustain. Energy Rev. 34 (2014) 401–408. doi:10.1016/j.rser.2014.03.024.

[9] M. Veselý, P. Molenaar, M. Vos, R. Li, W. Zeiler, Personalized heating – Comparison of heaters and control modes, Build. Environ. 112 (2017) 223–232. doi:10.1016/j.buildenv.2016.11.036.

[10] H. Oi, K. Tabata, Y. Naka, A. Takeda, Y. Tochihara, Effects of heated seats in vehicles on thermal comfort during the initial warm-up period, Appl. Ergon. 43 (2012) 360–367. doi:10.1016/j.apergo.2011.05.013.

[11] H. Oi, K. Yanagi, K. Tabat, Y. Tochihar, Effects of heated seat and foot heater on thermal comfort and heater energy consumption in vehicle, Ergonomics. 54 (2011) 690–699.

doi:10.1080/00140139.2011.595513.

[12] H. Zhang, E. Arens, M. Taub, D. Dickerhoff, F. Bauman, M. Fountain, W. Pasut, D. Fannon, Y. Zhai, M. Pigman, Using footwarmers in offices for thermal comfort and energy savings, Energy Build. 104 (2015) 233–243. doi:10.1016/j.enbuild.2015.06.086.

[13] W. Pasut, H. Zhang, E. Arens, Y. Zhai, Energy-efficient comfort with a heated/cooled chair: Results from human subject tests, Build. Environ. 84 (2015) 10–21. doi:10.1016/j.buildenv.2014.10.026.

[14] M. Luo, E. Arens, H. Zhang, A. Ghahramani, Z. Wang, Thermal comfort evaluated for combinations of energy-efficient personal heating and cooling devices, Build. Environ. 143 (2018) 206–216. doi:10.1016/j.buildenv.2018.07.008.

[15] B.B. Adams, Heated car seat-induced erythema Ab igne, Arch. Dermatol. 148 (2012). doi:10.1001/archdermatol.2011.2207.

[16] M.J. Mendell, Commentary: Air conditioning as a risk for increased use of health services, Int. J. Epidemiol. 33 (2004) 1123–1126. doi:10.1093/ije/dyh264.

[17] S. Daly, Automotive Air-conditioning and Climate Control Systems, Elsevier Ltd, Oxford, UK, 2006.

[18] Stanislav Trojan, Lékařská fyziologie, Grada Publishing a.s., 2003.

[19] K.C. Parsons, Human thermal environments, Taylor & Francis, LONDON AND NEW YORK, 2010. doi:10.4324/9780203302620_chapter_1.

[20] R.J. Brychta, K.Y. Chen, Cold-induced thermogenesis in humans, Eur. J. Clin. Nutr. 71 (2017) 345–352. doi:10.1038/ejcn.2016.223.

[21] H. Zhang, E. Arens, C. Huizenga, T. Han, Thermal sensation and comfort models for non-uniform and transient environments: Part I: Local sensation of individual body parts, Build. Environ. 45 (2010) 380–388. doi:10.1016/j.buildenv.2009.06.018.

[22] A.P. Gagge, R.R. Gonzalez, Mechanisms of Heat Exchange: Biophysics and Physiology, in: Handb. Physiol. - Environ. Physiol., 4, 2010: pp. 45–83. doi:10.1002/cphy.cp040104.

[23] J.W. Castellani, A.J. Young, Human physiological responses to cold exposure: Acute responses and acclimatization to prolonged exposure, Auton. Neurosci. Basic Clin. 196 (2016) 63–74. doi:10.1016/j.autneu.2016.02.009.

[24] N.A.S. Taylor, Å. Nykvist, N. Powers, J.N. Caldwell, Thermoeffector threshold plasticity: The impact of thermal pre-conditioning on sudomotor, cutaneous vasomotor and thermogenic thresholds, J. Therm. Biol. 83 (2019) 37–46. doi:10.1016/j.jtherbio.2019.05.001.

[25] M.A. Heller, W. Schiff, eds., The Psychology of Touch, Physiology Press, New York, London, 2009.

[26] M. Nakamura, T. Yoda, L.I. Crawshaw, S. Yasuhara, Y. Saito, M. Kasuga, K. Nagashima, K. Kanosue, Regional differences in temperature sensation and thermal comfort in humans., J. Appl. Physiol. 105 (2008) 1897–1906. doi:10.1152/japplphysiol.90466.2008.

[27] M. Cabanac, Sensory Pleasure, Q. Rev. Biol. 54 (1979) 1–29.

[28] International Organization for Standardization, ISO 7730 Ergonomics of the thermal environment — Analytical determination and interpretation of thermal comfort using calculation of the PMV and PPD indices and local thermal comfort criteria, Geneva, 2005.

[29] International Organization for Standardization, ISO 10551, Assessment of the influence of the thermal environment using subjective judgement scales, European Committee for Standardization, Brussels, 1995.

[30] American Society of Heating Ventilation and Air-Conditioning Engineers (ASHRAE), ASHRAE Fundamentals Handbook, SI, Atlanta, 2001.

[31] Fanger PO, Thermal comfort: analysis and applications in environmental engineering., Danish Technical Press, Copenhagen, 1970.

[32] M.A. Humphreys, M. Hancock, Do people like to feel "neutral"?. Exploring the variation of the desired thermal sensation on the ASHRAE scale, Energy Build. 39 (2007) 867–874. doi:10.1016/j.enbuild.2007.02.014.

[33] L. Schellen, W.D. van Marken Lichtenbelt, M.G.L.C. Loomans, J. Toftum, M.H. de Wit, Differences between young adults and elderly in thermal comfort, productivity, and thermal physiology in response to a moderate temperature drift and a steady-state condition, Indoor Air. 20 (2010) 273–283. doi:10.1111/j.1600-0668.2010.00657.x.

[34] B. Kingma, Human thermoregulation: a synergy between physiology and mathematical modelling, PhD thesis, Maastricht University, 2012. http://arno.unimaas.nl/show.cgi?did=28096.

[35] W.D. van Marken Lichtenbelt, M.J.W. Hanssen, J. Hoeks, A.A.J.J. van der Lans, B. Brans, F.M. Mottaghy, P. Schrauwen, Cold acclimation and health: effect on brown fat, energetics, and insulin sensitivity, Extrem. Physiol. {&} Med. 4 (2015) 1–2. doi:10.1186/2046-7648-4-S1-A45.

[36] F. Johnson, A. Mavrogianni, M. Ucci, A. Vidal-Puig, J. Wardle, Could increased time spent in a thermal comfort zone contribute to population increases in obesity?, Obes. Rev. 12 (2011) 543–551. doi:10.1111/j.1467-789X.2010.00851.x.

[37] T. Fukazawa, G. Havenith, Differences in comfort perception in relation to local and whole body skin wettedness, Eur. J. Appl. Physiol. 106 (2009) 15–24. doi:10.1007/s00421-009-0983-z.

[38] D. Filingeri, D. Fournet, S. Hodder, G. Havenith, Body mapping of cutaneous wetness perception across the human torso during thermo-neutral and warm environmental exposures., J. Appl. Physiol. 117 (2014) 887–97. doi:10.1152/japplphysiol.00535.2014.

[39] M. Frontczak, P. Wargocki, Literature survey on how different factors influence human comfort in indoor environments, Build. Environ. 46 (2011) 922–937. doi:10.1016/j.buildenv.2010.10.021.

[40] M. Tarantini, G. Pernigotto, A. Gasparella, A Co-Citation Analysis on Thermal Comfort and Productivity Aspects in Production and Office Buildings, Buildings. 7 (2017) 36. doi:10.3390/buildings7020036.

[41] B. Kingma, A. Frijns, W.D. van Marken Lichtenbelt, The thermoneutral zone: implications for metabolic studies, Front. Biosci. E4. (2012) 1975–1985. https://pdfs.semanticscholar.org/7dee/d798dd2fbfd98687f36231130a557a0e86f2.pdf.

[42] M. Simion, L. Socaciu, P. Unguresan, Factors which Influence the Thermal Comfort Inside of Vehicles, Energy Procedia. 85 (2015) 472–480. doi:10.1016/j.egypro.2015.12.229.

[43] N. Gerrett, Y. Ouzzahra, B. Redortier, T. Voelcker, G. Havenith, Female thermal sensitivity to hot and cold during rest and exercise, Physiol. Behav. 152 (2015) 11–19. doi:10.1016/j.physbeh.2015.08.032.

[44] J. Pokorny, J. Fiser, M. Jicha, Virtual Testing Stand for evaluation of car cabin indoor environment, Adv. Eng. Softw. 76 (2014) 48–55. doi:10.1016/j.advengsoft.2014.06.002.

[45] T. Han, K.-H. Chen, B. Khalighi, A. Curran, J. Pryor, M. Hepokoski, Assessment of Various Environmental Thermal Loads on Passenger Thermal Comfort, SAE Int. J. Passeng. Cars - Mech. Syst. 3 (2010) 830–841. doi:10.4271/2010-01-1205.

[46] A. Alahmer, M. Omar, Vehicular Cabins' Thermal Comfort Zones - Fanger and Berkley Modeling, Veh. Eng. 1 (2013) 19–32.

[47] International Organization for Standardization, ISO 9920 Ergonomics of the thermal environment - Estimation of thermal insulation and water vapour resistance of a clothing ensemble, (2007).

[48] E. Mert, A. Psikuta, M.A. Bueno, R.M. Rossi, Effect of heterogenous and homogenous air gaps on dry heat loss through the garment, Int. J. Biometeorol. 59 (2015) 1701–1710. doi:10.1007/s00484-015-0978-x.

[49] E. Mert, A. Psikuta, M. Bueno, R.M. Rossi, The effect of body postures on the distribution of air gap thickness and contact area, Int. J. Biometeorol. 61 (2017) 363–375. doi:10.1007/s00484-016-1217-9.

[50] E. Mert, A. Psikuta, M.A. Bueno, R.M. Rossi, The effect of body postures on the distribution of air gap thickness and contact area, Int. J. Biometeorol. (2016) 1–13. doi:10.1007/s00484-016-1217-9.

[51] Y. Lu, F. Wang, X. Wan, G. Song, C. Zhang, W. Shi, Clothing resultant thermal insulation determined on a movable thermal manikin. Part II: effects of wind and body movement on local insulation, 59 (2015) 1487–1498. doi:10.1007/s00484-015-0959-0.

[52] Y. Lu, F. Wang, X. Wan, G. Song, Clothing resultant thermal insulation determined on a movable thermal manikin . Part I : effects of wind and body movement on total insulation, 59 (2015) 1475–1486. doi:10.1007/s00484-015-0958-1.

[53] G. Havenith, R. Heus, W.A. Lotens, Resultant clothing insulation: a function of body movement, posture, wind, clothing fit and ensemble thickness., Ergonomics. 33 (1990) 67–84. doi:10.1080/00140139008927094.

[54] G. Havenith, R. Heus, W.A. Lotens, Clothing ventilation, vapour resistance and permeability index: Changes due to posture, movement and wind, Ergonomics. 33 (1990) 989–1005. doi:10.1080/00140139008925308.

[55] Y.S. Wu, J.T. Fan, W. Yu, Effect of posture positions on the evaporative resistance and thermal insulation of clothing, Ergonomics. 54 (2011) 301–313. doi:10.1080/00140139.2010.547604.

[56] I. Holmér, H. Nilsson, M. Bohm, O. Norén, Equivalent temperature in vehicles – conclusions and recommendations for standard, in: Assess. Therm. Clim. Oper. Cabs, Semin. Florence; JTI-Rapport, Swedish Institute of Agricultural and Environmental Engineering, Florence, 1999: pp. 89–94.

[57] A. Joshi, A. Psikuta, M.-A. Bueno, S. Annaheim, R.M. Rossi, Analytical clothing model for sensible heat transfer considering spatial heterogeneity, Int. J. Therm. Sci. 145 (2019) 14. doi:doi.org/10.1016/j.ijthermalsci.2019.05.005.

[58] A. Psikuta, Local air gap thickness and contact area models for realistic simulation of thermal effects in clothing, Int. J. Biometeorol. (2018) 1–14. doi:https://doi.org/10.1007/s00484-018-1515-5.

[59] S. Veselá, A. Psikuta, A.J.H. Frijns, Local clothing thermal properties of typical office ensembles under realistic static and dynamic conditions, Int. J. Biometeorol. 62 (2018) 2215–

2229. doi:10.1007/s00484-018-1625-0.

[60] G. Havenith, D. Fiala, K. Blazejczyk, M. Richards, P. Bröde, I. Holmér, H. Rintamaki, Y. Benshabat, G. Jendritzky, The UTCI-clothing model, Int. J. Biometeorol. 56 (2012) 461–470. doi:10.1007/s00484-011-0451-4.

[61] P.A. Nelson, D.A.;Curlee, J.S.;Curran, A.R.;Ziriax, J.M.; Mason, Determining localized garment insulation values from manikin studies : computational method and results, Eur J Appl Physiol. 95 (2005) 464–473. doi:10.1007/s00421-005-0033-4.

[62] J.S. Curlee, An approach for determining localized thermal clothing insulation for use in an element based thermoregulation and human comfort code, Master Thesis, Michigan Technological University, 2004.

[63] H.O. Nilsson, I. Holmér, Comfort climate evaluation with thermal manikin methods and computer simulation models., Indoor Air. 13 (2003) 28–37. doi:10.1034/j.1600-0668.2003.01113.x.

[64] International Organization for Standardization, EN ISO 14505-2 Ergonomics of the thermal environment - Evaluation of thermal environments in vehicles - Part 2: Determination of equivalent temperature, (2006) 25.

[65] V.T. Bartels, Thermal comfort of aeroplane seats: Influence of different seat materials and the use of laboratory test methods, Appl. Ergon. 34 (2003) 393–399. doi:10.1016/S0003-6870(03)00058-9.

[66] M. Scheffelmeier, E. Classen, Development of a method for rating climate seat comfort, IOP Conf. Ser. Mater. Sci. Eng. 254 (2017). doi:10.1088/1757-899X/254/18/182010.

[67] G. Karimi, E.C. Chan, J.R. Culham, I. Linjacki, L. Brennan, Thermal Comfort Analysis of an Automobile Driver with Heated and Ventilated Seat, SAE Tech. Pap. 2002-01-0222. (2002). doi:10.4271/2002-01-0222.

[68] G. Karimi, E.C. Chan, J.R. Culham, Experimental Study and Thermal Modeling of an Automobile Driver with a Heated and Ventilated Seat, SAE Tech. Pap. O3 DHM-12. (2003) 12. doi:10.4271/2003-01-2215.

[69] K. Shin, H. Park, J. Kim, K. Kim, Mathematical and Experimental Investigation of Thermal Response of an Automobile Passenger With a Ventilated Seat, (2008) 529–539. doi:10.1115/imece2006-14770.

[70] S.J. Park, S.N. Min, M. Subramaniyam, H. Lee, Y.K. Shin, C.H. Jang, S.H. Hwang, Driving Posture Measurement using 3D Scanning Measuring Technique, SAE Int. J. Passeng. Cars - Mech. Syst. 8 (2015) 2015-01–1392. doi:10.4271/2015-01-1392.

[71] T. Wu, W. Cui, B. Cao, Y. Zhu, Q. Ouyang, Measurements of the additional thermal insulation of aircraft seat with clothing ensembles of different seasons, Build. Environ. 108 (2016) 23–29. doi:10.1016/j.buildenv.2016.08.008.

[72] E.A.. McCullough, B.W.. Olsen, S.. Hong, Thermal insulation provided by chairs, ASHRAE Trans. Soc. Heat. Refrig. Airconditioning Engin. 100 (1994) 795–804. http://www.cbe.berkeley.edu/research/other-papers/McCullough et al 1994 Thermal insulation provided by chairs.pdf.

[73] M.J. Vosselman, G.H.E.J. Vijgen, B.R.M. Kingma, B. Brans, W.D. Van Marken Lichtenbelt, Frequent extreme cold exposure and brown fat and cold-induced thermogenesis: A study in a monozygotic twin, PLoS One. 9 (2014). doi:10.1371/journal.pone.0101653.

[74] G. Havenith, I. Holmér, K. Parsons, Personal factors in thermal comfort assessment: Clothing properties and metabolic heat production, Energy Build. 34 (2002) 581–591. doi:10.1016/S0378-7788(02)00008-7.

[75] B.E. Ainsworth, W.L. Haskell, M.C. Whitt, M.L. Irwin, A.M. Swart, S.J. Strath, O.W. L, Compendium of Physical Activities: an update of activity codes and MET intensities, Med. Sci. Sport. Exerc. 32 (2000) 498–516.

[76] Y. Inoue, N. Gerrett, T. Ichinose-Kuwahara, Y. Umino, S. Kiuchi, T. Amano, H. Ueda, G. Havenith, N. Kondo, Sex differences in age-related changes on peripheral warm and cold innocuous thermal sensitivity, Physiol. Behav. 164 (2016) 86–92. doi:10.1016/j.physbeh.2016.05.045.

[77] H. Kaciuba-Uscilko, R. Grucza, Gender differences in thermoregulation, Curr. Opin. Clin. Nutr. Metab. Care. 4 (2001). doi:10.1097/00075197-200111000-00012.

[78] R.J. De Dear, T. Akimoto, E.A. Arens, G. Brager, C. Candido, K.W.D. Cheong, B. Li, N. Nishihara, S.C. Sekhar, S. Tanabe, J. Toftum, H. Zhang, Y. Zhu, Progress in thermal comfort research over the last twenty years, Indoor Air. 23 (2013) 442–461. doi:10.1111/ina.12046.

[79] A. Psikuta, K. Kuklane, A. Bogdan, G. Havenith, S. Annaheim, R.M. Rossi, Opportunities and constraints of presently used thermal manikins for thermo-physiological simulation of the human body., Int. J. Biometeorol. 60 (2015) 435–446. doi:10.1007/s00484-015-1041-7.

[80] K. Katic, R. Li, W. Zeiler, Thermophysiological models and their applications: A review, Build. Environ. 106 (2016) 286–300. doi:10.1016/j.buildenv.2016.06.031.

[81] N. Martínez, A. Psikuta, K. Kuklane, J.I.P. Quesada, R.M.C.O. de Anda, P.P. Soriano, R.S. Palmer, J.M. Corberán, R.M. Rossi, S. Annaheim, Validation of the thermophysiological model by Fiala for prediction of local skin temperatures, Int. J. Biometeorol. 60 (2016) 1969–

1982. doi:10.1007/s00484-016-1184-1.

[82] A. Psikuta, D. Fiala, G. Laschewski, G. Jendritzky, M. Richards, K. Blazejczyk, I. Mekjavič, H. Rintamäki, R. de Dear, G. Havenith, Validation of the Fiala multi-node thermophysiological model for UTCI application, Int. J. Biometeorol. 56 (2011) 443–460. doi:10.1007/s00484-011-0450-5.

[83] B. Koelblen, A. Psikuta, A. Bogdan, S. Annaheim, R.M. Rossi, Thermal sensation models: A systematic comparison, Indoor Air. 27 (2016) 1–10. doi:10.1111/ina.12329.

[84] S.I. Tanabe, K. Kobayashi, J. Nakano, Y. Ozeki, M. Konishi, Evaluation of thermal comfort using combined multi-node thermoregulation (65MN) and radiation models and computational fluid dynamics (CFD), Energy Build. 34 (2002) 637–646. doi:10.1016/S0378-7788(02)00014-2.

[85] C. Huizenga, Z. Hui, E. Arens, A model of human physiology and comfort for assessing complex thermal environments, Build. Environ. 36 (2001) 691–699. doi:10.1016/S0360-1323(00)00061-5.

[86] S. Tanabe, M.E. ASHRAE Arens, M.H. ASHRAE Zhang TL Nladsen Member A SHRA E FS Bauman, P. Member ASHRAE, T. Madsen, Evaluating thermal environments by using a thermal manikin with controlled skin surface temperature, Ashrae. 100 Part 1 (1994) 39–48. https://escholarship.org/uc/item/22k424vp.

[87] ErgonSim, FPC - model user manual,Version 2.5, (2013) 60. www.ergonsim.de.

[88] S. Paulke, Finite element based implementation of fiala's thermal manikin in THESEUS-FE, VTMS 8 - Veh. Therm. Manag. Syst. Conf. Exhib. Nottingham, United Kingdom. (2007) 559–566. http://www.theseus-fe.com/ths_content/publications/slides/20070523_slides_vtms_finite-element-based-implementation-of-fialas-thermal-manikin-in-theseus-fe_en.pdf.

[89] J. Pokorný, J. Fišer, M. Fojtlín, B. Kopečková, R. Toma, J. Slabotínský, M. Jícha, Verification of Fiala-based human thermophysiological model and its application to protective clothing under high metabolic rates, Build. Environ. 126 (2017) 13–26. doi:10.1016/j.buildenv.2017.08.017.

[90] M. Hepokoski, A. Curran, D. Dubiel, Improving the accuracy of physiological response in segmental models of human thermoregulation, in: S. Kounalakis, M. Koskolou (Eds.), XIV Int. Conf. Environemntal Ergon. Nafplio, Nafplio, 2011: pp. 102–103. https://www.researchgate.net/profile/Petros_Botonis/publication/270647588_THE_EFFECT_OF_SKIN_SURFACE_MENTHOL_APPLICATION_ON_RECTAL_TEMPERATURE_D

URING_PROLONGED_IMMERSION_IN_COOL_AND_COLD_WATER/links/54b199fb0cf220c63cd12836.pdf#page=360.

[91] D. Fiala, G. Havenith, Modelling Human Heat Transfer and Temperature Regulation, in: Mechanobiol. Mechanophysiology Mil. Inj., Springer, Berlin, 2015: pp. 265–302. doi:10.1007/978-3-319-33012-9.

[92] D. Fiala, K.J. Lomas, M. Stohrer, Computer prediction of human thermoregulatory and temperature responses to a wide range of environmental conditions, Int. J. Biometeorol. 45 (2001) 143–159. doi:10.1007/s004840100099.

[93] D. Fiala, A. Psikuta, G. Jendritzky, S. Paulke, D.A. Nelson, W.D. van Marken Lichtenbelt, A.J.H. Frijns, Physiological modeling for technical, clinical and research applications, Front. Biosci. S2. (2010) 939–968.

[94] G. Havenith, D. Fiala, Thermal indices and thermophysiological modeling for heat stress, Compr. Physiol. 6 (2016) 255–302. doi:10.1002/cphy.c140051.

[95] W.D. Van Marken Lichtenbelt, A.J.H. Frijns, D. Fiala, F.E.M. Janssen, A.M.J. Van Ooijen, A.A. Van Steenhoven, Effect of individual characteristics on a mathematical model of human thermoregulation, J. Therm. Biol. 29 (2004) 577–581. doi:10.1016/j.jtherbio.2004.08.081.

[96] W.D. Van Marken Lichtenbelt, A.J.H. Frijns, M.J. Van Ooijen, D. Fiala, A.M. Kester, A.A. Van Steenhoven, Validation of an individualised model of human thermoregulation for predicting responses to cold air, Int. J. Biometeorol. 51 (2007) 169–179. doi:10.1007/s00484-006-0060-9.

[97] Z. Fang, H. Liu, B. Li, M. Tan, O.M. Olaide, Experimental investigation on thermal comfort model between local thermal sensation and overall thermal sensation, Energy Build. 158 (2018) 1286–1295. doi:10.1016/j.enbuild.2017.10.099.

[98] B. Koelblen, A. Psikuta, A. Bogdan, S. Annaheim, R.M. Rossi, Thermal sensation models: A systematic comparison, Indoor Air. 27 (2016) 1–10. doi:10.1111/ina.12329.

[99] B. Koelblen, A. Psikuta, A. Bogdan, S. Annaheim, R.M. Rossi, Thermal sensation models: Validation and sensitivity towards thermo-physiological parameters, Build. Environ. 130 (2018) 200–211. doi:10.1016/j.buildenv.2017.12.020.

[100] H.O. Nilsson, Thermal comfort evaluation with virtual manikin methods, Build. Environ. 42 (2007) 4000–4005. doi:10.1016/j.buildenv.2006.04.027.

[101] Y. Zhao, H. Zhang, E.A. Arens, Q. Zhao, Thermal sensation and comfort models for non-uniform and transient environments, part IV: Adaptive neutral setpoints and smoothed

whole-body sensation model, Build. Environ. 72 (2014) 300–308. doi:10.1016/j.buildenv.2013.11.004.

[102] Q. Jin, X. Li, L. Duanmu, H. Shu, Y. Sun, Q. Ding, Predictive model of local and overall thermal sensations for non-uniform environments, Build. Environ. 51 (2012) 330–344. doi:10.1016/j.buildenv.2011.12.005.

[103] M. Schweiker, X. Fuchs, S. Becker, M. Shukuya, M. Dovjak, M. Hawighorst, J. Kolarik, Challenging the assumptions for thermal sensation scales, Build. Res. Inf. 45 (2017). doi:10.1080/09613218.2016.1183185.

[104] H. Zhang, Human thermal sensation and comfort in transient and non-uniform thermal environments, PhD thesis, University of California, Berkeley, 2003.

[105] H. Zhang, E. Arens, C. Huizenga, T. Han, Thermal sensation and comfort models for non-uniform and transient environments, part III: Whole-body sensation and comfort, Build. Environ. 45 (2010) 399–410. doi:10.1016/j.buildenv.2009.06.020.

[106] Y. Zhang, R. Zhao, Effect of local exposure on human responses, Build. Environ. 42 (2007). doi:10.1016/j.buildenv.2006.07.014.

[107] R. Schwab, FAT Schriften Reihe Nr. 109, Einfluss der Sonneneinstrahlung auf die thermische Behaglichkeit in Kraftfahrzeugen, Druckerei Henrich GmbH, 1994. https://www.vda.de/.

[108] H.O. Nilsson, Comfort climate evaluation with thermal manikin methods and computer simulation models., PhD Thesis, University of Gavle, 2004.

[109] International Organization for Standardization, ISO 15831 Clothing - Physiological effects - Measurement of thermal insulation by means of a thermal manikin, (2004) 11.

[110] ASTM, F2370-16 Standard Test Method for Measuring the Thermal Insulation of Clothing Using a Heated Manikin, (2015) 1–7. doi:10.1520/F1291-15.1.

[111] N. a G. Martinho, M.C.G. Silva, J. a E. Ramos, Evaluation of thermal comfort in a vehicle cabin, Proc. Inst. Mech. Eng. Part D J. Automob. Eng. 218 (2005) 159–166. doi:10.1243/095440704772913936.

[112] Thermetrics, Newton Thermal Manikin - product brochure, Prod. Broch. (n.d.) 2. http://www.thermetrics.com/sites/default/files/product_brochures/Newton Manikin Thermetrics 2015.pdf (accessed March 2, 2018).

[113] A. Psikuta, J. Allegrini, B. Koelblen, A. Bogdan, S. Annaheim, N. Martínez, D. Derome, J. Carmeliet, R.M. Rossi, Thermal manikins controlled by human thermoregulation models for energy efficiency and thermal comfort research – A review, Renew. Sustain. Energy Rev. 78

(2017) 1315–1330. doi:10.1016/J.RSER.2017.04.115.

[114] B. Koelblen, A. Psikuta, A. Bogdan, S. Annaheim, R.M. Rossi, Human simulator – A tool for predicting thermal sensation in the built environment, Build. Environ. (2018). doi:10.1016/j.buildenv.2018.03.050.

[115] E. Foda, K. Siren, A thermal manikin with human thermoregulatory control: Implementation and validation, Int. J. Biometeorol. 56 (2012) 959–971. doi:10.1007/s00484-011-0506-6.

[116] W. Liu, T. Zhang, Y. Xue, Z. Zhai, J. Wang, Y. Wei, Q. Chen, State-of-the-art methods for inverse design of an enclosed environment, Build. Environ. 91 (2015) 91–100. doi:10.1016/j.buildenv.2015.02.041.

[117] W. Liu, S. Mazumdar, Z. Zhang, S.B. Poussou, J. Liu, C.H. Lin, Q. Chen, State-of-the-art methods for studying air distributions in commercial airliner cabins, Build. Environ. 47 (2012) 5–12. doi:10.1016/j.buildenv.2011.07.005.

[118] European Commission, Eurostat - Statistics Explained. Overweight and obesity - BMI statistics, (2014) 1–9. http://ec.europa.eu/eurostat/statisticsexplained/%0Ahttp://ec.europa.eu/eurostat/statistics-explained/index.php/Overweight_and_obesity_-_BMI_statistics (accessed March 10, 2018).

[119] X. Yan, X. Gang Su, Linear Regression Analysis: Theory And Computing, World Scientific Publishing, Singapore, 2009.

[120] M.G.M. Richards, R. Rossi, H. Meinander, P. Broede, V. Candas, E. den Hartog, I. Holmér, W. Nocker, G. Havenith, Dry and Wet Heat Transfer Through Clothing Dependent on the Clothing Properties Under Cold Conditions, Int. J. Occup. Saf. Ergon. 14 (2015) 69–76. doi:10.1080/10803548.2008.11076750.

[121] F. Wang, C. Gao, K. Kuklane, I. Holmer, Determination of Clothing Evaporative Resistance on a Sweating Thermal Manikin in an Isothermal Condition : Heat Loss Method or Mass Loss Method?, Ann. Occup. Hyg. 55 (2011) 775–783. doi:10.1093/annhyg/mer034.

[122] E. Mert, A. Psikuta, M.-A. Bueno, R.M. Rossi, Effect of heterogenous and homogenous air gaps on dry heat loss through the garment, Int. J. Biometeorol. 59 (2015) 1701–1710. doi:10.1007/s00484-015-0978-x.

[123] S. Veselá, A. Psikuta, A.J.H. Frijns, Local clothing thermal properties of typical office ensembles under realistic static and dynamic conditions, Int. J. Biometeorol. (2018) 15. doi:10.1007/s00484-018-1625-0.

[124] A. Mark, The impact of the individual layers in multi-layer clothing systems on the

distribution of the air gap thickness and contact area, Master Thesis, Albstadt-Sigmaringen University of Applied Science, 2013.

[125] E. McCullough, B. Jones, A comprehensive data base for estimating clothing insulation., ASHRAE Res. Proj. Reoprt RP-411. (1985) 162.

[126] S. Veselá, B.R.; Kingma, A.J. Frijns, Local thermal sensation modeling: a review on the necessity and availability of local clothing properties and local metabolic heat production., Indoor Air. 27 (2017) 261–272. doi:10.1111/ina.12324.

[127] A. Psikuta, E. Mert, S. Annaheim, R.M. Rossi, Local air gap thickness and contact area models for realistic simulation of human thermo-physiological response, Int. J. Biometeorol. (2018) 1–14. doi:https://doi.org/10.1007/s00484-018-1515-5.

[128] European Committee for Standardization, EN-ISO 9886:2004, Ergonomics - evaluation of thermal strain by physiological measurements., Brussels, 2004.

[129] A. Psikuta, M. Richards, D. Fiala, Single-sector thermophysiological human simulator, Physiol. Meas. 29 (2008) 181–192. doi:10.1088/0967-3334/29/2/002.

[130] Y.F. Zhang, D.P. Wyon, L. Fang, A.K. Melikov, The influence of heated or cooled seats on the acceptable ambient temperature range, Ergonomics. 50 (2007) 586–600. doi:10.1080/00140130601154921.

[131] Joint Committee for Guides in Metrology (JCGM), J.C.F.G.I.M. Jcgm, Bipm, Iec, Ifcc, Ilac, Iso, Iupac, Iupap, Oiml, J.C.F.G.I.M. Jcgm, Joint Committee for Guides in Metrology, J.C.F.G.I.M. Jcgm, B. Drive, F.-- Issue, B. Drive, T. Williams, C. Kelley, J. Campbell, R. Cunningham, D. Denholm, G. Elber, R. Fearick, C. Grammes, L. Hart, L. Hecking, T. Koenig, D. Kotz, E. Kubaitis, R. Lang, A. Lehmann, A. Mai, M. Bastian, E.A. Merritt, P. Mikul, T. Tkacik, J. Van Der Woude, J.R. Van Zandt, A. Woo, J. Zellner, B. Drive, W.M. Parkway, Evaluation of measurement data — An introduction to the "Guide to the expression of uncertainty in measurement" and related documents, Int. Organ. Stand. Geneva ISBN. (2008). doi:10.1016/0263-2241(85)90006-5.

Part B: Appended peer-reviewed scientific publications

Paper I

PLOS ONE

RESEARCH ARTICLE

Determination of car seat contact area for personalised thermal sensation modelling

Miloš Fojtlín[1,2☯], **Agnes Psikuta**[1☯*], **Róbert Toma**[2‡], **Jan Fišer**[2‡], **Miroslav Jícha**[2‡]

1 Laboratory for Biomimetic Membranes and Textiles, Empa Swiss Federal Laboratories for Material Science and Technology, St. Gallen, Switzerland, **2** Department of Thermodynamics and Environmental Engineering, Energy Institute, Faculty of mechanical engineering, Brno University of Technology, Brno, Czechia

☯ These authors contributed equally to this work.
‡ These authors also contributed equally to this work.
* agnes.psikuta@empa.ch

Citation: Fojtlín M, Psikuta A, Toma R, Fišer J, Jícha M (2018) Determination of car seat contact area for personalised thermal sensation modelling. PLoS ONE 13(12): e0208599. https://doi.org/10.1371/journal.pone.0208599

Editor: Adam W Potter, US Army Research Institute of Environmental Medicine, UNITED STATES

Received: July 24, 2018

Accepted: November 20, 2018

Published: December 11, 2018

Data Availability Statement: All relevant data are within the paper and its Supporting Information files.

Funding: The part of work conducted at Empa was supported by the [HEAT-SHIELD project within EU Horizon 2020 program] under Grand [RIA 668786-1]. Part of the work conducted at Brno University of Technology was supported by the [Ministry of Education project Youth and Sports of the Czech Republic] under the "National Sustainability Programme I" [LO1202 Netme Centre Plus]; and

Abstract

A lot of daily activities are conducted in a sedentary posture. This includes a thermal interaction between the human and the seat that has implications on thermal perception and comfort. These interactions are investigated by simulating heat and mass transfer, thus, reducing a need for costly and time demanding subject studies. However, it is not clear, from the available literature, what portion of the body surface area is actually affected by the seat with respect to human anthropometry. The aim of this study was to develop a predicting function of the seat contact area based on anthropometric parameters. The results showed strong linear correlation between the contact area obtained by printing a body silhouette on paper placed at the seat and body weight, height, body surface area, and body mass index. The body surface area and the body weight were identified as the best predictors for the contact area.

Introduction

Western lifestyle is bound to seated posture during work, travelling or leisure time with more than 50% of wake time spent sitting [1,2]. For this reason, the effects of sitting on health and comfort have been investigated in detail [3–6]. Moreover, the state of comfort is closely related to vigilance and well-being that is needed to ensure productive conditions at a workplace or safe and enjoyable experience while driving or travelling [7–9].

Various aspects of comfort and discomfort in an office environment in sitting were examined by Zhang et al. [10]. Office features with the highest importance to office workers were ascribed to chair comfort (12% of responses) and effects of an ambient microclimate (11% of responses). Moreover, similar conclusions were found in an airplane passenger comfort study, where again the best predictor for general comfort on the flight was found the seat comfort [9].

One of the aspects of comfort is thermal comfort that expresses satisfaction with the thermal environment. In addition to a clothing resistance, the seat creates thermal and water vapour barrier at the contact body parts. As a result, the seat's high thermal insulation and low water

the [Brno University of Technology] under the project Reg. No. [FSI-S-17-4444]. The funders had no role in study design, data collection and analysis, decision to publish, or preparation of the manuscript.

Competing interests: The authors have declared that no competing interests exist.

vapour permeability affect local microclimate at the body surface that may lead, under certain circumstances, to a local discomfort, sweating, and perception of wetness [11–13].

A very specific application of seats are the ones used in vehicular cabins that are often exposed to a broad variety of outdoor conditions ranging from temperatures below 0 ˚C to over 50 ˚C. On one hand, cabins are typically equipped with heating ventilation and air-conditioning system (HVAC) to create a comfortable environment [14]. On the other hand, the HVAC is usually activated right after entering the cabin and its response time is insufficient to satisfy passengers' needs and expectations immediately. Hence, the seats may be equipped with contact heating and ventilation systems to compensate rapidly for the extreme conditions and to help overcome adverse effects of excessive heating or cooling of the body through accumulated heat in the seat causing thermal discomfort. Such seat constructions have to be tested in the process of their development with regards to thermal comfort in human studies. Because of high cost and time requirements of human trials, there is a substantial effort to simulate human thermal perception virtually [15–17]. For this reason, numerous virtual manikins or reference models of human anthropometry were developed to reproduce average observed characteristics of a human for human thermal physiology simulations. The most frequently referenced models are the 65MN model by Tanabe et al. [18], the Berkeley thermoregulation and comfort model [19,20], and several Fiala-based models—ThermoSEM by Kingma [21], FPCm by ErgonSim [22], Fiala-FE by Theseus FE [23], FMTK by Pokorny et al. [24], and Human Thermal Module in TAITherm by Thermoanalytics Inc., Michigan, USA [25].

The virtual manikins are usually composed of basic geometric solids, such as cylinders or spheres, representing individual body parts. This division is generally dictated by the resolution needed for proper simulation of human thermoregulation in conjunction with clothing, e.g., changes of skin temperature during vasomotory response, sweating patterns, or typical clothing body coverage. In addition, some models are further divided into sectors facing environment or neighboring body parts, such as anterior, posterior, inferior and/or superior sectors. Such fine resolution of body segmentation allows a much more precise determination of the environmental influence, for instance, projected area factors for detailed direct and diffuse solar radiation and longwave radiation analysis. The summary of the parameters of individual models is presented in Table 1. Despite the clearly defined segmentation of the virtual manikins, it is not clear if the surface area of the assumed sectors in contact with the seat correspond to the seat contact area of a human with the equivalent anthropometry (e.g. height, weight). This is especially critical for the identification of the contact body parts and their surface area involved in seat heating or ventilating. Moreover, skin sensitivity to a thermal stimulus is neither homogeneous over the surface of a human body, nor is the distribution of sweating [26–29]. As a result, there is a need to specify the total seat contact area with a resolution of at least two major body parts—seat and back, both having distinct physiological and perceptual responses.

To the best of our knowledge, there is no standard methodology for determining contact area between the body and the seat, and a variety of different methods has been applied. Park et al. carried out a study on seat pressure distribution and preferred driving position of Korean drivers wearing tightly fitting clothing [3]. This was done using dedicated seat pressure blankets with resolution of eight and nine segments on the seat and back, respectively. The test subjects consisted of 10 males and 10 females in body weight groups of: < 59 kg, 60 to 79 kg, >80 kg. Each weight group was evaluated individually, however, there were missing details about subjects' heights and mean, maximal, and minimal body weights in each weight category.

Another method to determine seat contact area is to draw a border line around a seated manikin on paper placed on the seat [30,31]. The first manikin study employed thermal

Table 1. Examples of virtual manikins.

Source	Body parts/ body sectors	Sex	Weight (kg)	Height (m)	Total skin area (m^2)
FPCm [22]	13/41	Unisex	71.4	1.70	1.83
65MN [18]	10/-	Male	74.4	-	1.87
ThermoSEM [21]	10/22	Unisex	73.4	1.73	1.85
Berkeley thermoregul. and comfort model [19,20]	10/-	Female	-	-	1.47
FMTK [24]	12/32	Unisex	73,5	1.71	1.85
Human Thermal Module in TAITherm* [25]‡	13/41	Male	78.6	1.76	1.95

Pair body parts are counted as one.

*50^{th} percentile male body was selected;

‡Help desk, ThermoAnalytics Inc., Michigan, USA.

https://doi.org/10.1371/journal.pone.0208599.t001

manikin Fred (height of 1.79 m, body surface area of 1.8 m^2, unknown weight) placed on various office chairs. In the second study, an Asian Newton type thermal manikin (height and weight of 1.70 m and 65 kg) was employed to examine contact area on airplane seats [31].

In some cases the method was not explicitly stated and the seat contact area was stated as aside information, e.g. study by Oi et al. [28], who presented the seat contact area based on a pool of eight Japanese males sitting on an automotive seat. The group of volunteers was rather homogenous with mean body weight of 57.2 kg (SD ± 3.2 kg) and height of 1.75 m (SD ± 0.01 m). Clothing in the study comprised of long pants, a long sleeved shirt, and a light jacket.

To sum up, the anthropometric data for human subjects was often presented in a narrow range or there were even missing details about subjects' body weight or height, which makes it impossible to compare various literature sources using objective parameters. In addition, the use of thermal manikins on seats seems not to be representative of human contact area because of their low body weight, unrealistic weight distribution, a rigid body surface without local skin resilience, and no spinal flexibility. Another parameter that is often missing in literature is the precise description of the examined seat and subjects' clothing. Studies by McCullough [30] and Wu et al. [31] have demonstrated positive correlation between the seat contact area and thermal insulation of clothing. However, the practical use of these results is limited, as they both used thermal manikins.

Another possibility would be to use commercially available seat testers that are dedicated for realistic testing with respect to weight distribution and geometry of the contact parts, e.g. manikin STAN (Thermetrics, Seattle, WA, USA) [32]. However, contact areas examined with this device have not been found in the scientific literature. All the above mentioned issues prevented reliable utilization of literature data in thermophysiological simulations.

The aim of this study was to develop a model describing the body contact area with the automotive seat in relation to body characteristics, such as body weight and height. Human subjects and the Western type Newton thermal manikin were seated on a serial-production automotive seat and the contact area was examined separately for the seat and the back using a modified method based on the study by Park et al. [3]. Finally, the results were compared to the available literature data for both humans and thermal manikins. Since the contact area is crucial not only for accurate manikin measurement of thermal effects of seats, but also necessary for setting up the boundary conditions in simulations using human thermoregulation and thermal perception models, we have also addressed the body resolution of humanoids used in such models. The findings from this study are applicable in clothing, indoor, and transportation research.

Methodology

Measurement principle

The methods comprise experimental determination of the seat contact area of human subjects as well as a thermal manikin. The determination of seat contact area for this study was based on printing of a human or manikin silhouette on paper placed on an automotive seat (see sections *Seat* and *Protocol* for more detailed characterisation). The method is proposed because of its relative simplicity and no need for special equipment. In addition, a higher resolution of this approach is expected compared to the circumscribing method, especially on inaccessible parts for circumscribing, e.g. lower back and pelvis area.

After the printing, the paper prints were immediately laid flat and photographed using a 50 mm lens from a distance of 1.3 m. The area of seat print images were determined using graphical software CorelDRAW X8 (Corel Corporation, Ottawa, Canada) by manual tracking of the print borders. The number of the print pixels was compared to the number of pixels of a known reference area in the picture. Additionally, the actual prints were divided into two weight groups split by the median of the sample (80 kg) to visualize potential differences in the shapes of the seat prints depending on the subjects' weight.

Human subjects

The research was approved by Ethical committee at Department of Biomedical Engineering at Brno University of Technology (document EK:01/2018, approved on 5. January 2018) and all 13 subjects (12 males and 1 female) agreed to enter the experiment voluntarily signing a written informed consent. The subjects cover a majority of European population (approximately 82%) in terms of body mass index (BMI) ranging from the lower limit of normal weight (18.5 kg/m^2) to the upper limit of overweight (29.4 kg/m^2) [33], and represented the white ethnic group with average characteristics: body weight of 80.6 kg (SD 11.7 kg), height of 1.80 m (SD 0.05 m), body surface area of 1.99 m^2 (SD 0.02 m^2) calculated according to the Du Bois equation [34], BMI of 24.8 $kg.m^{-2}$ (SD 3.0 $kg.m^{-2}$), and age of 30.5 (SD 3.4 years). The participants were instructed to wear a pair of long cotton pants, underwear, and T-shirt with normal fit (Fig 1A). The individual in Fig 1A has given written informed consent (as outlined in PLOS consent form) to publish these case details.

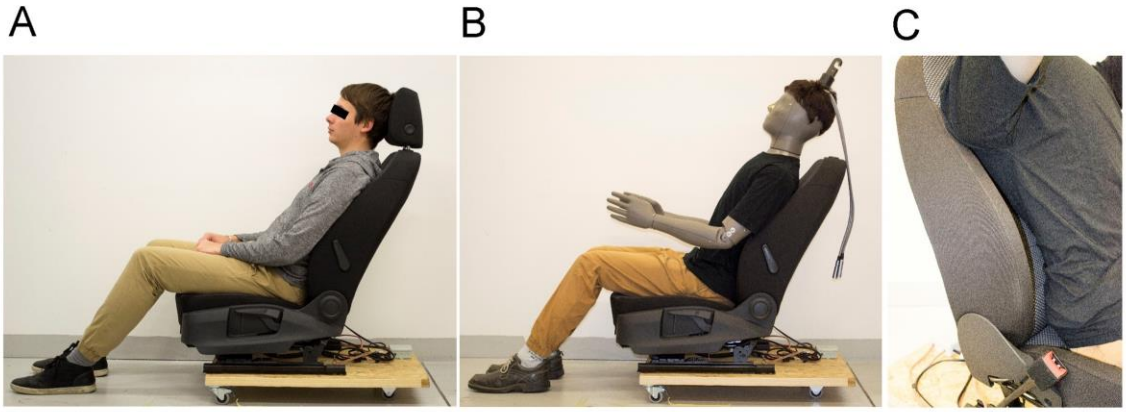

Fig 1. Illustration of the seating position. A human subject (A), the Newton manikin (B), and the detail of insufficient contact of the manikin's lower back with the back rest (C).

https://doi.org/10.1371/journal.pone.0208599.g001

Thermal manikin

The Newton type thermal manikin (Thermetrics, WA Seattle, Western type manikin) was employed for comparison of the contact area with the one measured by human subjects using the same method. The manikin body size corresponds to a 1.79 m tall western male. The construction of the manikin is intentionally lightweight (27.5 kg), thus, having lower thermal inertia and allowing easier manipulation in its typical application in clothing research. Here, it is necessary to easily dress, undress, and set the manikin in the desired position. For this reason, the manikin is also equipped with ten movable joints (ankles, knees, hips, elbows, shoulders). However, it does not allow spinal flexing and its surface is rigid (Fig 1B).

Seat

The seat used for the study represented a serial-production front seat of a middle class passenger car. The construction of the seat consists of metal chassis, polyurethane cushioning, and polyester upholstery. The thicknesses of the seat and back rest cushioning are approximately 5.5 and 4.5 cm, respectively, and the participants rated the stiffness of the seat as medium (scale: *soft*, *medium*, *hard*). The setup of the seat was fixed in all trials (details in Figs 1 and 2) with the adjustable lumbar support set to maximum. Height of the front lip of the seat was approximately 37 cm above the floor. The trunk-thigh angle was set to 110˚ based on the preferred driving posture of a bodyweight group ranging from 60 to 79 kg [3].

Protocol

The method to determine the seat contact area separately for the buttocks and the back was firstly validated using water based paint applied to a plastic foil attached to the back, buttocks, and lower thighs of the participant. Next, the person sat down on the seat covered by two separate sheets of paper (specific weight of the paper 80 $g.m^{-2}$) and stood up again after approximately 15 seconds. The subjects were asked to sit in a comfortable position, but without slouching and with fully rested thighs on the seat (Fig 1). The print of the contact area of the body on the paper padding of the seat was then used for further processing. Finally, the paint was replaced by spraying water directly on the participants' clothing. The aim of this was not to soak the clothing, but to create a thin film of water droplets on the clothing that was later transferred to the paper with mitigated effects of lateral wicking. The specific weight of the paper used in this study was approximately 40 $g.m^{-2}$ to improve uptake of the water, and hence, leaving a clear print border. The finer paper is also capable of copying the seat surface deformations without major buckling. These changes were sufficient to identify the contact area on the paper with better time efficiency and no contamination hazards. The contact area of the Western type manikin was determined using the same method and clothing (all garments size M). In this case, the head rest of the seat was removed to allow the manikin to support its back on the seat, since the neck does not flex (Fig 1B).

Cross-comparison with literature data

In the final step, the experimental results were compared to the findings from literature. This was done to assess differences among data from the human, manikin, and virtual manikin studies using various approaches and the possibility to use virtual thermal manikins for simulations with a seat contact. Despite not having the realistic contact areas from the seat tester STAN, the surface areas of its active parts were assumed for the comparison. Next, for the Fiala virtual manikin [22], following segments were selected to stand for contact surfaces: back—the sum of posterior thorax and posterior abdomen, and buttocks—the sum of posterior hips and

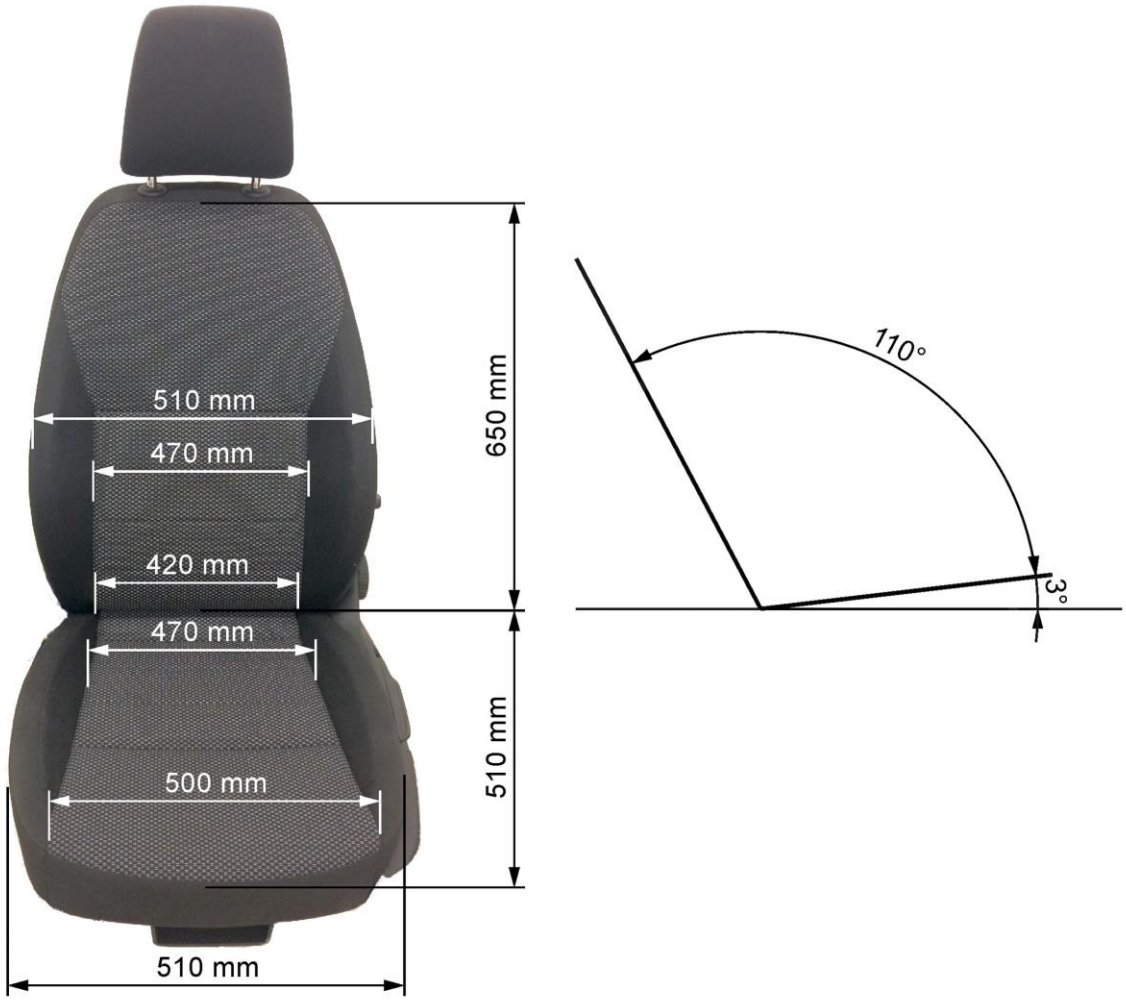

Fig 2. Projected dimensions of the seat used in this study.

https://doi.org/10.1371/journal.pone.0208599.g002

posterior upper legs. In case of the TAITherm virtual manikin [25], the back contact was selected to consist of back and a half of upper abdomen with assumption of manikin symmetry. Finally, the buttocks contact was assumed to be posterior thighs and a half of lower abdomen. An overview of the cases and selected clothing is shown in Table 2.

Model description and statistical analysis

The collected data was evaluated in the Microsoft Excel (Microsoft Corporation, Redmond, WA, USA) and the linear regression model was proposed to fit the data from the seat prints with predictors, namely: weight, height, body surface area, and BMI. This was done despite the

Table 2. Overview of the cases for cross-comparison with the literature data.

Study	Subjects	Ethincs	Seat	Clothing	Method
This study	12 M; 1F	White	Automotive	Normal fit—T-shirts, Trousers	Printing a silhoutte
Park et al., 2015	10 M; 10 F	Korean	Automotive	Tightly fitting outfit	Pressure sensitive blankets
Oi et al., 2012	8 M	Japanese	Automotive	Shirt, Jacket, Trousers	Unknown
Wu et al., 2016;	Asian Newton	Asian	Airplane	Shorts, T-shirt	Circumscribing
McCullough, 1994	Manikin Fred	Unknown	Executive chair	Trousers, Shirt	Circumscribing
This study	Western Newton	White	Automotive	Normal fit—T-shirts, Trousers	Printing a silhoutte
Fiala virtual man. [22]	Unisex	Global	-	Nude	Posterior parts
TAITherm virtual man. [25]	Male	White	-	Nude	Posterior parts
STAN seat tester ‡	Male	White	-	Nude	Active areas of the manikin

M-males, F-females.

‡Help desk, ThermoAnalytics Inc., Michigan, USA.

https://doi.org/10.1371/journal.pone.0208599.t002

non-linear behaviour of the seat and body deformation that affects resulting contact area. However, in the examined range of the predictors (see section *Human subjects* for the details), linearisation of the interaction of the human body with the seat is expected to have strong correlation and sufficient precision for the given application in thermophysiology. Further, both body surface area and BMI are power functions of weight and height, but both were included in this study as additional parameters because of their frequent occurrence in literature and praxis. Finally, selected cases from literature (Table 2) were added to the comparison, wherever applicable, with respect to the scope of the published parameters.

Next, the coefficient of determination R^2 was calculated to express the proportion of the variation in the dependent variable that is predictable from the independent variable. Further, the root mean square deviations *RMSD* between the measured data and predictions were expressed to assess the accuracy of the models. Finally, two intervals were defined for the linear regression models. Firstly, a confidence interval for the best-fit line for the collected population with 95% confidence level was plotted. This allowed visualisation of margins for the slope and intercept for each regression model. Secondly, prediction intervals were calculated to estimate an interval in which future individual observations of contact area will fall with 95% probability [35].

Results

Fig 3 relates total seat contact area to two basic anthropometric measures, body weight and height, and two derived measures, total body surface area and BMI. The average total seat contact area is 18% of the body surface area. Fig 4 shows the predictive functions of the seat and back contact area separately in relation to body weight and body surface area being selected on the basis of the highest R^2 values and the lowest values of *RMSD*. The points marked with violet colour stand for human studies, whereas green and red markers represent manikin and virtual manikin studies, respectively. Error bars indicate the standard deviation if reported in the original source. A special case is the study by Park et al. (2015), in which neither the actual mean values of each bodyweight group were presented, nor the upper and lower weight limits. Thus, we interpreted the results from the study as areas (Figs 3A, 4A and 4C). Moreover, 95% confidence intervals were plotted for each linear regression model with dotted lines, and the dashed lines depict prediction intervals covering 95% of the population (Figs 3 and 4). The complete dataset on which this publication is based, is provided in the supporting information file S1 Dataset.

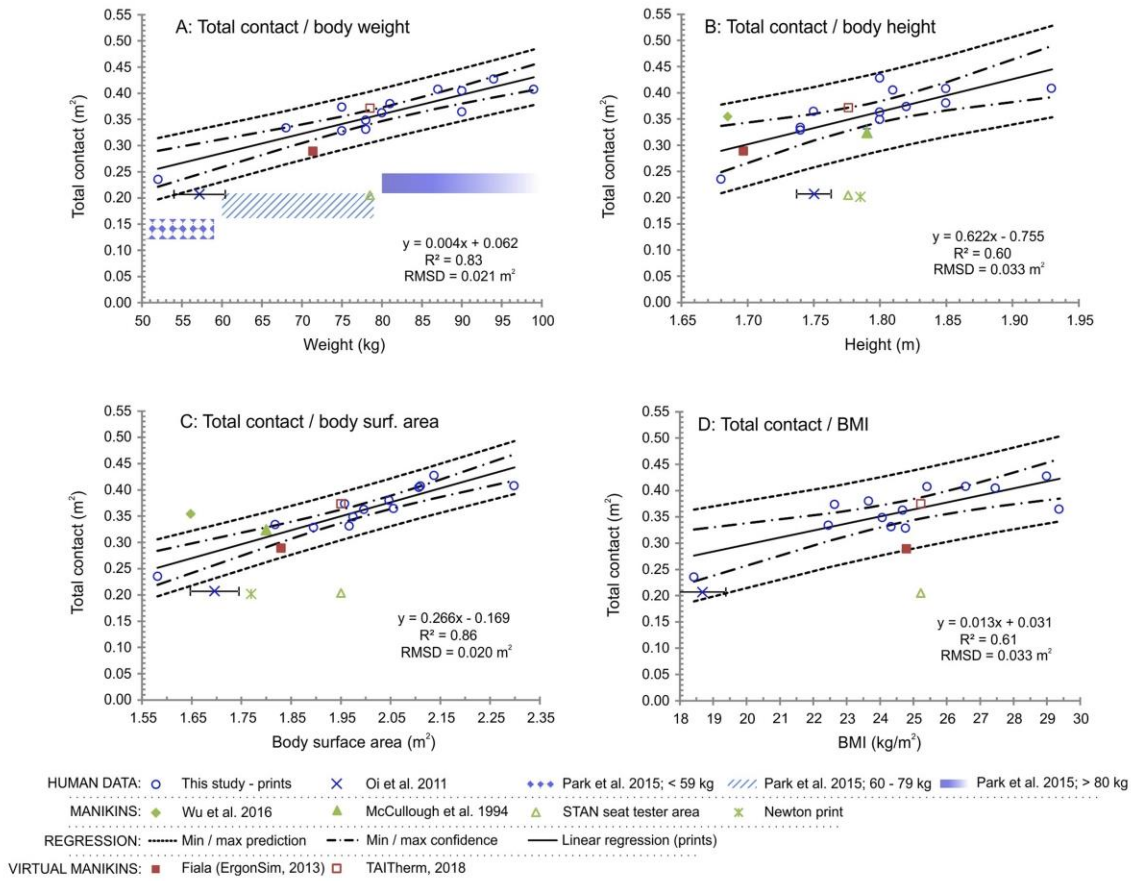

Fig 3. Total seat contact area. The total seat contact area dependent on body weight (A), body height (B), total body surface area (C), and Body Mass Index (D).

https://doi.org/10.1371/journal.pone.0208599.g003

Discussion

Total contact area predictions

Body weight and total skin area were identified as the best predictors for the total contact area. The values of R^2 ranged from approximately 0.60 (body height, BMI) to 0.86 (body weight, body surface area). Correspondingly, the values of *RMSD* were of 57% lower if body weight and body surface area were used as predictors compared to body height and BMI. This indicates that changes in body weight or body surface area have a greater impact on the changes in total contact area than height or BMI within the scope of this study.

Next, if we intuitively presume that the height has a dominant effect on the print length and the weight on the print width, a partial support for this statement could be found in Fig 5. The back prints exhibit greatest standard deviation in the lumbar width (SD 0.08 m, min/max width 0.24/0.49 m), as opposed to the back length (SD 0.06 m, min/max length 0.36/0.57 m). Similarly, the variability of the seat print width is greater (SD 0.05 m, min/max width 0.43/0.61

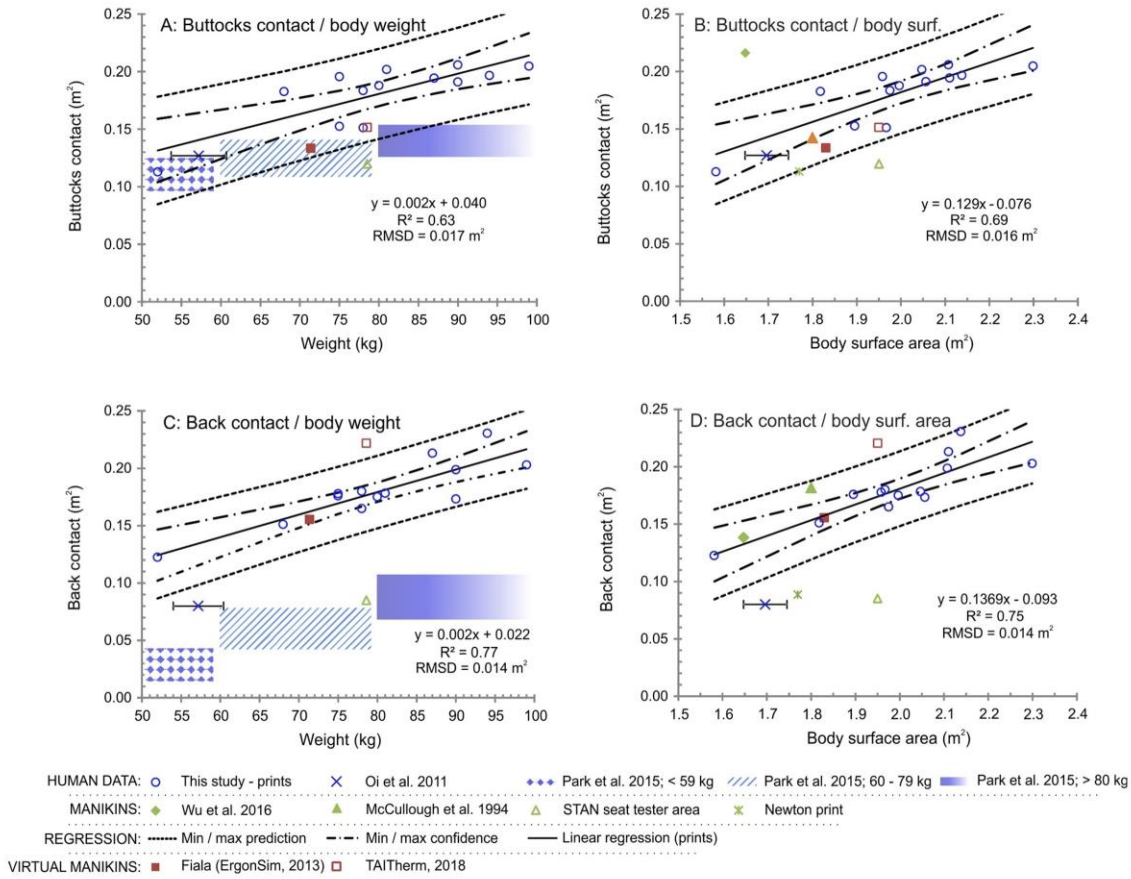

Fig 4. Local body contact areas. Contact areas at back and seat dependent on body weight (A and C), and total body surface area (B and D), respectively.

https://doi.org/10.1371/journal.pone.0208599.g004

m) than the seat print length (SD 0.03 m, min/max length 0.37/0.48 m). On the other hand, since the seat width is 0.51 m and several prints exceeded this size, we can also assume that higher weight contributes to a greater imprint of a person into the seat, thus, leaving a larger print area in all directions.

Secondly, total body surface area calculated according the Du Bois equation has the highest explanatory power as opposed to the BMI. In both skin area and BMI formulas, the weight has a lower power than the height, but the weight has a greater impact on the result in a range of meaningful values for adult seat occupants, e.g. from 45 to 120 kg. These values were calculated using the limits for underweight and overweight (from 18 to 30 kg/m^2) and a likely range of the occupants' body height (from 1.6 to 2.0 m). Most importantly, the interpretations of the formulas are different. The BMI can be explained as a screening tool for indication of high body fat content, calculated as weight over square of height, and its nature has been criticized for not capturing the distribution and proportion of lean mass and body fat [36]. This is likely

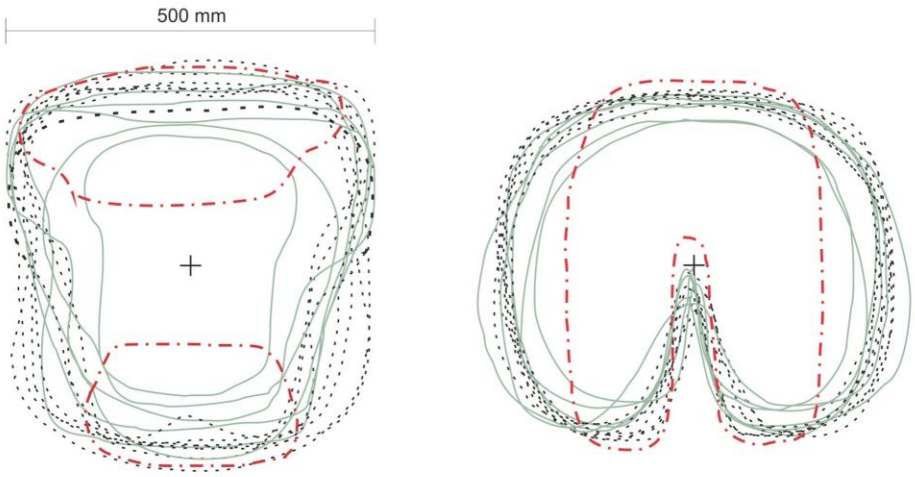

Fig 5. Centred shapes of the seat prints. Back prints (left) and buttocks prints (right). Dashed line indicates a subjects group with body weight of more than 80 kg, continuous line with less than 80kg, and red dotted line depicts the contact of the Western Newton type manikin.

https://doi.org/10.1371/journal.pone.0208599.g005

the cause for the relatively low R^2 of 0.61 if compared to the straightforward parameter, such as the skin surface area (R^2 = 0.86).

Local contact area predictions

The models for the local contact surface with the buttocks and back were based on the body weight and body surface area as they showed the best predicting capabilities out of the examined parameters. In both cases, the models for back contact area have smaller values of RMSD and higher R^2 compared to the seat area models, in other words, the models for back are more accurate.

In Fig 5, the prints for seat and back are divided into two weight groups split by median of the sample (80 kg). The shoulder width remains in the majority of cases almost identical and is outlined by width of the seat, whereas, in most of the cases under 80 kg, the lumbar contact has narrower contours (Fig 5 left). This shaping reflects the distribution of muscles and body fat with increasing weight, where the larger fat deposits occur in the lumbar region [37]. On the other hand, the differences in the print shape and size are less pronounced in case of the buttocks (Fig 5 right).

Finally, literature on an apparel design discusses several predominant male and female body types based on the proportions of hips-waist-back dimensions, lengths of the limbs and crotch [37,38]. The variability of the body shapes is also projected into the seat prints, where a contact area of two subjects with a similar anthropometric measure is not identical. For instance, in Fig 5 left, the widest seat print belongs to a person weighing less than 80 kg with muscular thighs that leave wider print than ones of heavier subjects with less developed musculature at thighs. This also explains differences between lower and upper prediction lines that are, in the best-case scenarios, of around 0.10 m^2 for total contact (Fig 3C), 0.07 m^2 for seat (Fig 4B) and 0.06 m^2 for the back (Fig 4C).

Cross-comparison with literature data

The findings from this study were compared to two human studies, two manikin studies, and two virtual manikin geometries. The first human study by Oi et al. [28] yields the total contact area of 33% lower compared to the mean prediction of this study. Yet, these values are on the edge of the prediction intervals unless the height was used as a predictor (Fig 3). Next, the seat contact area is below the mean predictions too, but within the confidence and prediction intervals (Fig 4A and 4B). The situation is different on the back, where the local contact is of 68% lower compared to mean predictions and out of prediction intervals in all cases (Fig 4C and 4D). The consistency of the seat contact and mismatch of the back contact areas point out potential differences in the seat involved in the study that was described only as an automotive seat. Secondly, the discrepancies might be caused by differences in body shapes between the Japanese and white ethnicities. Possible explanation of this hypothesis may be found in the Nakanishi and Nethery [39] who examined differences in anthropometry of Japanese and white-American university male students. Significantly lower girths in Japanese at all body parts that build a contact with a seat were found, but no significant differences in percentage of body fat. Wang et al. [40] carried out a study on differences between Asians and white males and females in range from 18 to 94 years. The main findings show the Asians having lower BMI, while having an increased amount of adipose tissues than the white of both sexes. This can be explained by a different muscle constitution between the ethnicities that may be the cause for significant differences in the back contact area, and less pronounced differences in the seat contact.

The seat contact areas from the second human study by Park et al. [3] were presented in three body weight categories and the results are again below predictions of this study (Figs 3A, 4A and 4C). The mean contact area on the back for 70 kg person is substantially lower of about 0.1 m^2 compared to predictions from this study (difference of 169%). On the other hand, the seat contact area intersects with the lower prediction intervals (Fig 4A). The first likely explanation for the mismatch may stem from the focus on driving conditions by which the contact area distribution is asymmetric and variable, thus, being lower than that of a rested person. The decrease of the contact is caused by the use of the right leg and arms to control the vehicle [3]. Secondly, the subjects in the study were Korean with differences in the anthropometry when compared to the white [40]. Thirdly, the contact area was examined by pressure sensitive blankets with a resolution of 1296 sensing points, and size of 45 × 45 cm, whereas the print sizes in this study exceeded 45 cm in the majority of cases. Therefore, the blankets might not have been sufficient to cover all possible contact areas, especially on the back and in high body weights, where the dimensions of the prints are the greatest (Fig 4C).

Next, data from both Asian, Western Newton type manikins, and the seat tester STAN shows great discrepancies (Figs 3 and 4). The STAN has its contact area below predictions, however, this is expected since the assumed contact areas are not actual prints, but active sensing areas of the device. The seat contact area of the Asian type manikin is greater by 58% compared to the predicted mean from this study and is out of the prediction interval, whereas the back contact area matches the confidence and predictions intervals. Admittedly, the ratio between seat and back was not presented in the original paper and was adopted from literature being equal to 60:40 [28]. Yet, this does not have an impact on the total contact area that is still relatively high compared to the predictions (Fig 3C). The disagreement may stem from a different way of determining the contact area. This was neither explained in detail, nor was it explained how the contact area on inaccessible parts was identified (e.g., lower back and hips). For instance, authors may have taken into consideration the contact border line wherever the clothing touches the seat. In this study, the contact was ascribed to areas determined by both

applying a pressure and moisture from the clothing. Additionally, the authors have not explained how they adjusted the manikin parameters given by the manufacturer, such as 1.69 m and 27.5 kg of manikin body height and weight, respectively [41]. The additional weight and its distribution were not explained in the paper and may have contributed to a larger seat contact. Finally, the examined seat was an airplane seat with unspecified dimensions and setup.

The Western type manikin, used in this study, has smaller seat and back contact areas of 35% and 69%, respectively, if compared to the mean human predictions. This is rather anticipated with regards to the rigid and lightweight manikin body construction (27.5 kg for manikin as compared to approximately 65 kg human of a similar anthropometry), and consequently, lower print area. In reality the manikin touches the back rest only at the upper back and hip level with an air gap covering the whole lumbar area. These findings are supported by Fig 1C, where the gap is photographed, and also by the shape of the manikin prints in Fig 5 (red dotted line).

Another manikin study presented by McCullough [30] shows a good match with the total and local predicted values. In this case the weight of the manikin is unknown, but with respect to the year 1994 when the paper was published, the manikin could have been made of metal with consequently higher construction weight. This might imply more realistic immersion to the seat, resulting in the larger contact area with the seat. Further, the manikin might have had different curvature on the back that allows better contact with the seat. The seat involved in the study was executive chair with a similar shape to the car seat.

The total and local contact areas of the Fiala virtual manikin match the predictions well and are in all cases within the prediction lines (Figs 3 and 4). Such findings are favourable to the further utilization of the virtual manikin in the simulation of the local effects of the seat on the thermo-physiology and human thermal perception. The TAITherm manikin has similarly good match with human observations in case of the total contact and buttocks, whereas the back contact area is above prediction lines.

Virtual manikins with verified contact area could be effectively used to predict effects of seat heating or ventilation on a human. On the other hand, despite the match of the proposed contact parts of the virtual humanoid and human contact area, it is still questionable, whether the humanoid geometry is adequate for the seat simulations. Today, the humanoids used in thermophysiological models are usually composed of basic solids, e.g. cylinders (Table 1), whereas the shape of the back contact is rather conical in majority of cases (Fig 5). Greater contact area is thus at the upper back rather than on its lower part. Insight into the seat contact opens up opportunities to refine the segmentation on contact parts with respect to different level of sensitivity to hot and cold stimuli [27] and distribution of sweat [29].

Practical implications

As discussed in section *Local contact area predictions*, the differences between the lower and upper prediction lines are not negligible. This may have further impact on practical applications of the results, such as additional thermal insulation provided by the seat, seat heating or ventilation, etc. To demonstrate this, by example, we considered a seat heating of 268 $W.m^{-2}$ [28] and uniformly distributed power over the surface of the seat. The total contact heating power for the virtual manikin anthropometry would be 77 W. For a human with the same skin area, the range of the heating power is between 72 and 98 W. Such variation should be accounted for in representation of simulation results and it needs to be explored further what would be the influence of this variability on the human thermo-physiological response in a specific application.

The study captures the range of predominant European weight in terms of BMI (Details in section *Human subjects*) and the extremes were not examined. With regards to finite dimensions of the seat, it is expected that the upper limit of contact area exists as the seat gets filled with the body with increasing BMI. Therefore, an extrapolation of the results, especially in direction of higher body weights, might not be valid.

Another implication of the findings is in utilisation of thermal manikins in measurement of seat thermal properties. This study shows that different manikins and approaches of determining seat contact area yield different results. Therefore, it is advisable to ensure similar contact of the manikin to the one of humans before performing any measurements, e.g. by applying an additional weight to the figurine.

Limitations and sources of error in the experimental work

The resolution of the proposed method is limited by wicking and soaking of the water into the paper. However, the amount of applied water was controlled and kept low to eliminate these effects. Next, the seat print borderline was circumscribed manually in graphical software (Details in section *Protocol*), therefore, the borderline might not be copied perfectly. However, the contribution of these two sources of error is expected to be negligible compared to the variations in human data.

Finally, the sample of participants is relatively low, but it corresponds to the aim of this study to provide an overview into the problematics of seat contact area with regards to thermophysiological simulations, which was not as clear as to present. A consistent and robust method to carry out contact area measurements for any population and seat of interest was proposed. This allowed us to discuss and compare various approaches from the literature sources in a broader context.

Conclusions

To conclude, linearity between the contact area and body weight, height, skin surface area, and BMI was found within the scope of this study. The most reliable and precise predictors for the contact areas are the body weight and the body surface area. Next, the numerical results are valid for the white ethnicity and might not be applicable in other ones, e.g. in the Asians because of differences in body constitution. Further, the cross-comparison shows inconsistencies in determination of the contact area using thermal manikins. The reasons for this are possible differences in methodologies, manikins' rigid structure, low body weight, and no spinal flexibility of the manikins. In case of the virtual manikin used in the human thermoregulation model by Fiala, it was verified that posterior thorax, abdomen, hips, and upper legs can be used as representatives of the seat contact area.

Supporting information

S1 Dataset. Summary of the data for the publication.
(XLSX)

Acknowledgments

The authors gratefully acknowledge help of the participants in the study from both Brno University of Technology and Empa Swiss Federal Laboratories for Material Science and Technology. The authors would like to thank Prof. Dr. René M. Rossi and Dr. Simon Annaheim for constructive criticism of the manuscript, and Mgr. Ivana Bachurová for valuable comments on the data evaluation.

Author Contributions

Conceptualization: Agnes Psikuta.

Data curation: Miloš Fojtlín.

Formal analysis: Agnes Psikuta, Jan Fišer, Miroslav Jícha.

Investigation: Miloš Fojtlín, Agnes Psikuta, Róbert Toma, Jan Fišer.

Methodology: Miloš Fojtlín, Agnes Psikuta, Róbert Toma.

Project administration: Jan Fišer, Miroslav Jícha.

Resources: Agnes Psikuta, Miroslav Jícha.

Supervision: Agnes Psikuta, Jan Fišer, Miroslav Jícha.

Validation: Miloš Fojtlín, Róbert Toma.

Visualization: Miloš Fojtlín.

Writing – original draft: Miloš Fojtlín.

Writing – review & editing: Miloš Fojtlín, Agnes Psikuta, Róbert Toma, Jan Fišer, Miroslav Jícha.

References

1. Matthews CE, Chen KY, Freedson PS, Buchowski MS, Beech BM, Pate RR, et al. Amount of time spent in sedentary behaviors in the United States, 2003–2004. Am J Epidemiol. 2008; 167: 875–881.
2. Thorp AA, Healy GN, Winkler E, Clark BK, Gardiner PA, Owen N, et al. Prolonged sedentary time and physical activity in workplace and non-work contexts: a cross-sectional study of office, customer service and call centre employees. Int J Behav Nutr Phys Act. 2012; 9: 128. https://doi.org/10.1186/1479-5868-9-128 PMID: 23101767
3. Park SJ, Min SN, Subramaniyam M, Lee H, Shin YK, Jang CH, et al. Driving Posture Measurement using 3D Scanning Measuring Technique. SAE Int J Passeng Cars—Mech Syst. 2015; 8: 2015-01-1392. https://doi.org/10.4271/2015-01-1392
4. Hatoum O, Ghaddar N, Ghali K, Ismail N. Experimental and numerical study of back-cooling car-seat system using embedded heat pipes to improve passenger's comfort. Energy Convers Manag. Elsevier Ltd; 2017; 144: 123–131. https://doi.org/10.1016/j.enconman.2017.04.047
5. Kumar AR, Fredericks TK, Butt SE. Using a psychophysical approach to identify a user's self selected thermal comfort on a task chair. Int J Ind Ergon. Elsevier Ltd; 2015; 46: 36–43. https://doi.org/10.1016/j.ergon.2015.01.005
6. Daeijavad S, Maleki A. Proper farm tractor seat angles for the right posture using FEM. Comput Electron Agric. Elsevier B.V.; 2016; 124: 318–324. https://doi.org/10.1016/j.compag.2016.02.025
7. Daanen HAM, Van De Vliert E, Huang X. Driving performance in cold, warm, and thermoneutral environments. Appl Ergon. 2003; 34: 597–602. https://doi.org/10.1016/S0003-6870(03)00055-3 PMID: 14559420
8. Wilder D, Magnusson ML, Fenwick J, Pope M. The effect of posture and seat suspension design on discomfort and back muscle fatigue during simulated truck driving. Appl Ergon. 1994; 25: 66–76. https://doi.org/10.1016/0003-6870(94)90067-1 PMID: 15676952
9. Rankin WL, Space DR, Nagda NL. Passenger Comfort and the Effect of Air Quality. Am Soc Test Mater. 2000; 269–290. https://doi.org/10.1520/STP14499S
10. Zhang L, Helander MG, Drury CG. Identifying Factors of Comfort and Discomfort in Sitting. Hum Factors J Hum Factors Ergon Soc. 1996; 38: 377–389. https://doi.org/10.1518/001872096778701962
11. Cengiz TG, Babalik FC. The effects of ramie blended car seat covers on thermal comfort during road trials. Int J Ind Ergon. 2009; 39: 287–294. https://doi.org/10.1016/j.ergon.2008.12.002
12. Cengiz TG, Babalik FC. An on-the-road experiment into the thermal comfort of car seats. Appl Ergon. 2007; 38: 337–347. https://doi.org/10.1016/j.apergo.2006.04.018 PMID: 16759628

13. Matsuoka T, Nishimatsu T, Yamazaki J, Kanai H, Ishizawa H, Toba E, et al. Influence of Wadding Thickness on Sitting Comfort of Automotive Seat. Sen'i Kikai Gakkaishi (Journal Text Mach Soc Japan). 2005; 58: T142–T146.
14. Fojtlín M, Fišer J, Pokorný J, Povalač A, Urbanec T, Jícha M. An innovative HVAC control system: Implementation and testing in a vehicular cabin. J Therm Biol. 2017; https://doi.org/10.1016/j.jtherbio.2017.04.002 PMID: 29074027
15. Pokorný J, Fišer J, Fojtlín M, Kopečková B, Toma R, Slabotínský J, et al. Verification of Fiala-based human thermophysiological model and its application to protective clothing under high metabolic rates. Build Environ. Elsevier Ltd; 2017; https://doi.org/10.1016/j.buildenv.2017.08.017
16. Koelblen B, Psikuta A, Bogdan A, Annaheim S, Rossi RM. Thermal sensation models: A systematic comparison. Indoor Air. 2016; 27: 1–10. https://doi.org/10.1111/ina.12329 PMID: 27564215
17. Croitoru C, Nastase I, Bode F, Meslem A, Dogeanu A. Thermal comfort models for indoor spaces and vehicles—Current capabilities and future perspectives. Renew Sustain Energy Rev. Elsevier; 2015; 44: 304–318. https://doi.org/10.1016/j.rser.2014.10.105
18. Tanabe SI, Kobayashi K, Nakano J, Ozeki Y, Konishi M. Evaluation of thermal comfort using combined multi-node thermoregulation (65MN) and radiation models and computational fluid dynamics (CFD). Energy Build. 2002; 34: 637–646. https://doi.org/10.1016/S0378-7788(02)00014-2
19. Huizenga C, Hui Z, Arens E. A model of human physiology and comfort for assessing complex thermal environments. Build Environ. 2001; 36: 691–699. https://doi.org/10.1016/S0360-1323(00)00061-5
20. Tanabe S, Arens ME, Zhang TL Bauman FS, Madsen T. Evaluating thermal environments by using a thermal manikin with controlled skin surface temperature. Ashrae. 1994; 100 Part 1: 39–48. Available: https://escholarship.org/uc/item/22k424vp
21. Kingma B. Human thermoregulation: a synergy between physiology and mathematical modelling [Internet]. PhD thesis. Maastricht University. 2012. http://arno.unimaas.nl/show.cgi?did=28096
22. ErgonSim. FPC—model user manual,Version 2.5. 2013. p. 60.
23. Paulke S. Finite element based implementation of fiala's thermal manikin in THESEUS-FE [Internet]. VTMS 8—Vehicle Thermal Management Systems Conference and Exhibition. 2007. pp. 559–566. http://www.theseus-fe.com/ths_content/publications/slides/20070523_slides_vtms_finite-element-based-implementation-of-fialas-thermal-manikin-in-theseus-fe_en.pdf
24. Pokorný J, Fišer J, Fojtlín M, Kopečková B, Toma R, Slabotínský J, et al. Verification of Fiala-based human thermophysiological model and its application to protective clothing under high metabolic rates. Build Environ. 2017; 126.
25. Hepokoski M, Curran A, Dubiel D. Improving the accuracy of physiological response in segmental models of human thermoregulation. In: Kounalakis S, Koskolou M, editors. XIV International Conference on Environemntal Ergonomics, Nafplio. Nafplio; 2011. pp. 102–103. https://www.researchgate.net/profile/Petros_Botonis/publication/270647588_THE_EFFECT_OF_SKIN_SURFACE_MENTHOL_APPLICATION_ON_RECTAL_TEMPERATURE_DURING_PROLONGED_IMMERSION_IN_COOL_AND_COLD_WATER/links/54b199fb0cf220c63cd12836.pdf#page=360
26. Filingeri D, Fournet D, Hodder S, Havenith G. Body mapping of cutaneous wetness perception across the human torso during thermo-neutral and warm environmental exposures. J Appl Physiol. 2014; 117: 887–97. https://doi.org/10.1152/japplphysiol.00535.2014 PMID: 25103965
27. Inoue Y, Gerrett N, Ichinose-Kuwahara T, Umino Y, Kiuchi S, Amano T, et al. Sex differences in age-related changes on peripheral warm and cold innocuous thermal sensitivity. Physiol Behav. Elsevier Inc.; 2016; 164: 86–92. https://doi.org/10.1016/j.physbeh.2016.05.045 PMID: 27237043
28. Oi H, Tabata K, Naka Y, Takeda A, Tochihara Y. Effects of heated seats in vehicles on thermal comfort during the initial warm-up period. Appl Ergon. Elsevier Ltd; 2012; 43: 360–367. https://doi.org/10.1016/j.apergo.2011.05.013 PMID: 21683338
29. Smith CJ, Havenith G. Body mapping of sweating patterns in athletes: A sex comparison. Med Sci Sports Exerc. 2012; 44: 2350–2361. https://doi.org/10.1249/MSS.0b013e318267b0c4 PMID: 22811031
30. McCullough E.A.; Olsen B.W.; Hong S. Thermal insulation provided by chairs. ASHRAE Trans Soc Heat Refrig Airconditioning Engin. 1994; 100: 795–804. Available: http://www.cbe.berkeley.edu/research/other-papers/McCullough%20et%20al%201994%20Thermal%20insulation%20provided%20by%20chairs.pdf
31. Wu T, Cui W, Cao B, Zhu Y, Ouyang Q. Measurements of the additional thermal insulation of aircraft seat with clothing ensembles of different seasons. Build Environ. Elsevier Ltd; 2016; 108: 23–29. https://doi.org/10.1016/j.buildenv.2016.08.008
32. Thermetrics. Seat Test Automotive Manikin. In: Product brochure [Internet]. 2015 [cited 2 Mar 2018] p. 2. http://www.thermetrics.com/sites/default/files/product_brochures/STAN%20Manikin%20Thermetrics%202015.pdf

33. EUROSTAT. European Health Interview Survey. Almost 1 adult in 6 in the EU is considered obese. Eurostat Press Off. 2016; 2014: 1–5. Available: http://ec.europa.eu/eurostat/documents/2995521/7700898/3-20102016-BP-EN.pdf/c26b037b-d5f3-4c05-89c1-00bf0b98d646

34. Du Bois D, Du Bois EF. A formula to estimate the approximate surface area if height and weight be known. Arch Intern Med (Chic). Arch Intern Med (Chic).; 1916; 17: 863–871. https://doi.org/10.1001/archinte.1916.00080130010002

35. Yan X, Gang Su X. Linear Regression Analysis: Theory And Computing. Singapore: World Scientific Publishing; 2009.

36. Barnes R. Body shape and weight distribution: the Body Volume Index (BVI) and the Body Mass Index (BMI). Designing Apparel for Consumers. Elsevier; 2014. pp. 58–77. https://doi.org/10.1533/9781782422150.1.58

37. Robinet P, Carrier S. 11 –Male and female consumers: segmenting consumers in the apparel market by body shape and other factors. Designing Apparel for Consumers. 2014. pp. 221–234. https://doi.org/10.1533/9781782422150.2.221

38. Bellemare J. 10 –Males: understanding sizing requirements for male apparel. Designing Apparel for Consumers. 2014. pp. 189–220. https://doi.org/10.1533/9781782422150.2.189

39. Nakanishi Y, Nethery V. Anthropometric comparison between Japanese and Caucasian American male university students. Appl Human Sci. 1999; 18: 9–11. https://doi.org/10.2114/jpa.18.9 PMID: 10191547

40. Wang J, Thornton JC, Russell M, Burastero S, Heymsfield S, Pierson RN. Asians have lower body mass index (BMI) but higher percent body fat than do whites: comparisons of anthropometric measurements. Am J Clin Nutr. American Society for Nutrition; 1994; 60: 23–28. Available: http://ajcn.nutrition.org/cgi/content/short/60/1/23

41. Thermetrics. Newton Thermal Manikin—product brochure. In: Product brochure [Internet]. [cited 2 Mar 2018] p. 2. http://www.thermetrics.com/sites/default/files/product_brochures/Newton%20Manikin%20Thermetrics%202015.pdf

Paper II

Building and Environment 155 (2019) 376–388

Contents lists available at ScienceDirect

Building and Environment

journal homepage: www.elsevier.com/locate/buildenv

Local clothing properties for thermo-physiological modelling: Comparison of methods and body positions

Miloš Fojtlín[a,b], Agnes Psikuta[a,*], Jan Fišer[b], Róbert Toma[b], Simon Annaheim[a], Miroslav Jícha[b]

[a] Empa Swiss Federal Laboratories for Material Science and Technology, Laboratory for Biomimetic Membranes and Textiles, St. Gallen, Switzerland
[b] Brno University of Technology, Faculty of Mechanical Engineering, Energy Institute, Department of Thermodynamics and Environmental Engineering, Czech Republic

ARTICLE INFO

Keywords:
Clothing
Thermal insulation
Evaporative resistance
Sitting
Clothing area factor
Thermal sensation

ABSTRACT

Thermo-physiological modelling has become a frequently used and valuable tool for simulations of thermoregulatory responses in a variety of applications, such as building and vehicular comfort studies. To achieve reliable results, it is necessary to provide precise inputs, such as clothing thermal parameters. These values are usually presented in a standing body position and scarcely reported locally for individual body parts. Moreover, as an air gap distribution is both highly affected by a given body position and critical for clothing insulation, this needs to be taken into account. Therefore, the aim of this study was to examine eight probable approaches to assess the clothing parameters using state-of-the-art measurements, analytical and empirical models, and estimation. Next, we studied the effects of the eight clothing inputs on predicted thermo-physiological response under the same environmental conditions conducted with the Fiala model. Secondly, the study focuses on differences between seated and standing positions, both using two clothing sets representing typical European, indoor, summer and winter ensembles. The results show clear differences in clothing thermal properties between sitting and standing positions on both lower limbs and torso. The outputs of the eight examined methods showed discrepancies between them, in the range of up to 200%. The discrepancies from the eight clothing inputs were also propagated in the results of thermo-physiological responses. These varied significantly in terms of their impact on predicted thermal sensation, highlighting the importance of using adequate inputs for modelling.

1. Introduction

Efforts to minimize energy expenditure for heating ventilation and air-conditioning (HVAC) in a variety of indoor environments – such as transportation and occupational settings – with help of local conditioning technologies are a subject to substantial research attention [1–4]. Effects of localised heating and cooling on a human thermo-physiological response are usually investigated in human or thermal manikin studies [5,6]. Alternatively, one can utilise validated thermo-physiological models that allow prompt simulations of human thermo-physiological responses and reduce the need for costly physical studies [7–9]. In addition, these responses can be further translated into the prediction of thermal sensation or thermal comfort using dedicated models [10].

At the same time, to accurately simulate thermal interactions between the human body and the surrounding environment, using thermo-physiological models, there is a need for precise inputs defining: the environmental conditions, metabolic activity, and clothing [11]. Clothing governs heat and mass transfer between the human body and the ambient environment. Local clothing thermal properties may vary considerably over the body, thus, having a major impact on the development of skin temperatures, sweating, and perception of thermal sensation and comfort [12]. Yet, these properties, namely intrinsic clothing insulation (I_{cl}), evaporative clothing resistance ($R_{e,cl}$), and clothing area factor (f_{cl}), are rarely reported in literature [11]. Moreover, previous research has shown that body posture change has a significant impact on the resulting global clothing properties [13–15], however, only globally as an average for the whole body. The findings by Mert et al. [16,17] show differences in air gap thicknesses between sitting and standing positions that change relative to localised body parts and directly influence the local thermal and evaporative resistance of a garment. Nonetheless, the impact of variations between body postures on the human thermo-physiology has not been investigated and the majority of authors provide the local clothing properties applicable only for the standing body position [18–25].

The most realistic method to determine local clothing thermal properties is the use of a thermal manikin with detailed body segmentation [5]. Nevertheless, the accessibility of this apparatus is

* Corresponding author. Empa Swiss Federal Laboratories for Material Science and Technology, Lerchenfeldstrasse 5, 9014, St. Gallen, Switzerland.
E-mail address: agnes.psikuta@empa.ch (A. Psikuta).

https://doi.org/10.1016/j.buildenv.2019.03.026
Received 6 December 2018; Received in revised form 14 March 2019; Accepted 16 March 2019
Available online 25 March 2019

restrictive on the account of the high costs of both the device and the necessity of additional equipment, including a climatic chamber. Therefore, other ways to obtain clothing properties can be found in the literature, which do not require specialised equipment. The most common approach is to choose a desired ensemble from an exhaustive database of clothing from standard ISO 9920 [18]. According to the definition of the *clo* unit, measured using a standing thermal manikin, all three clothing parameters are presented as global values for the whole-body (in essence virtual insulation covering the whole body) [18]. As a matter of fact, the uniform distribution yields unrealistic physiological responses, since the local extremes are averaged and the mean value is prescribed even for body parts without clothing in reality, typically face and hands [17,26]. To address this problem, Curlee [19] and Nelson et al. [23] developed a method to calculate local clothing parameters based on global parameters from McCullough et al. [24] and ISO 9920 [18] valid for 106 garments. This approach was presented only for single-layer clothing and the resolution of the model is limited to a single value for parts covered by the garment. Yet, there are obvious differences within air gaps, between some of the body parts considered by the model [16,17].

Another option is to estimate local clothing properties based on empirical formulae relating outdoor temperature and clothing insulation, such as the UTCI clothing model [20]. The data for the model was gathered from several independent studies on clothing habits of Europeans. The model has a resolution of 7 body segments, applicable for a standing person, and temperatures from approximately −30 °C to 32 °C [20]. The paper also presents compensation of thermal insulation for an increased air-speed.

Local air gap thickness mainly affects local clothing parameters and because of this, one of the emerging methods to precisely examine these parameters is three-dimensional (3D) body scanning. This allows detailed assessment of the mean local air gap thicknesses, percentage of clothing contact area, and calculation of clothing area factors [27,28]. With the use of this information, prediction of thermal clothing insulation is possible based on basic laws of physics, using dedicated models for major body parts [29,30].

The optimal number of body segments for thermo-physiological modelling is conditioned by the specific application. The standard ISO 14505–2 [31] addresses cabin environments with seated positions and proposes segmentation of at least 16 body parts (11 parts if right-left symmetry is assumed for limbs) where distinct thermal conditions are expected, such as shade or a seat. Another standard ISO 15831 [32] recommends at least 15 segments (9 parts if right-left symmetry is assumed for limbs), and the most cited thermo-physiological models have similar resolutions to the ISO 15831 of up to 19 segments, with an additional spatial subdivision [33]. Similarly, the prevailing local thermal sensation models, such as models by Zhang [34,35], Jin [36], and Nilsson [37], have resolution covering major body parts of up to 13 segments assuming right-left symmetry. It is therefore reasonable to use a number of clothing segments equal to the number of segments of thermo-physiological and thermal sensation models to achieve the most realistic simulation of heat and mass transfer between the body and the environment.

Other parameters that are bound to the seated position are the thermal properties of the seat. Their determination requires specific instrumentation that can mimic contact pressure of a seated person, such as a seat tester STAN (Thermetrics, USA) [38] or a stamp tester as presented by Bartels [39]. The additional pressure is important because of the compression of seat layers, as well as the consequent changes in their thermal properties [39] and contact area with the body. Therefore, a measurement using a thermal manikin without realistic weight distribution and seat contact yields unrealistic results [40]. Values of additional thermal insulation provided by chairs were presented by McCullough et al. [41] and Wu et al. [42], both used thermal manikins, however, without explaining whether and how the realistic contact was achieved.

The next parameter that is often neglected is the clothing fit and the associated air gap distribution, which influences resulting thermal and evaporative resistance [17]. Standard ISO 9920 recommends using clothing with normal fit, whereas ISO 14505 recommends tightly fitting clothing to get repeatable results. Thus, there is a need for an objective parameter that would describe fit of the clothing, for example, clothing ease allowance (*EA*) that is defined as a difference between girths of the body and clothing at given body landmarks. This parameter was found to be strongly correlated with air gap thickness, and hence, clothing thermal and evaporative resistance [21,27,43].

The aim of this study is to examine typical approaches of obtaining the local clothing thermal properties for simulations of physiological and perceptual responses with respect to their use in spatially heterogeneous conditions. Next, the focus is on differences between seated and standing body positions that to the best of our knowledge have not been addressed locally. The impact of the differences is shown by means of simulated thermo-physiological responses that are directly linked to thermal sensation. The application of the findings is in passenger transportation and a range of occupational settings, including but not limited to professional driving, machinery operation, and the office environment.

2. Methods

2.1. Study design

The study included the determination of clothing thermal properties for two clothing sets based on distinct approaches comprising measurement, modelling, and estimation of clothing properties. Thus, this study provides relevant information for laboratories following different approaches and with potential access to equipment listed in Table 1. *Cases 1* and *2* are assumed as references for sitting and standing positions, respectively, because of the state-of-the-art methods used. Moreover, the consistency of the methodology was achieved using the same clothing throughout the study.

The second part of the work is focused on the investigation of the sensitivity of the thermo-physiological model by Fiala [46] (FPCm5.3, Ergonsim, Germany) to changes in boundary clothing conditions. The model was chosen on a basis of its broad validation documentation [47–49]. The study focuses on the seated position in a neutral steady

Table 1
Overview of the examined cases and methods to determine clothing area factor (f_{cl}), intrinsic clothing insulation (I_{cl}), evaporative clothing resistance ($R_{e,cl}$). Right-left symmetry is assumed.

Case	f_{cl} (−)	I_{cl} ($m^2K.W^{-1}$)	$R_{e,cl}$ ($m^2Pa.W^{-1}$)	Position	No. of segments
1	3D scanning	Manikin heat loss method [32]	Manikin heat loss method [44]	sitting	13
2	Photography [18]	Manikin heat loss method [32]	Manikin heat loss method [44]	standing	13
3	Physical model [30,45]	Physical model [30,45]	Physical model [30,45]	sitting	8
4	Physical model [30,45]	Physical model [30,45]	Physical model [30,45]	standing	10
5	Regression model [21]	Regression model [21]	Physical model [30,45]	standing	11
6	ISO based model [23]; Table 1	ISO based model [23]; Table 1	ISO based model [19]; Appendix A	standing	3
7	ISO Database [18]; Table. A2	UTCI model [20]	ISO Database [18]; Formula 31	standing	7
8	ISO Database [18]; Table. A2	ISO Database [18]; Table. A2	ISO Database [18]; Formula 31	standing	1

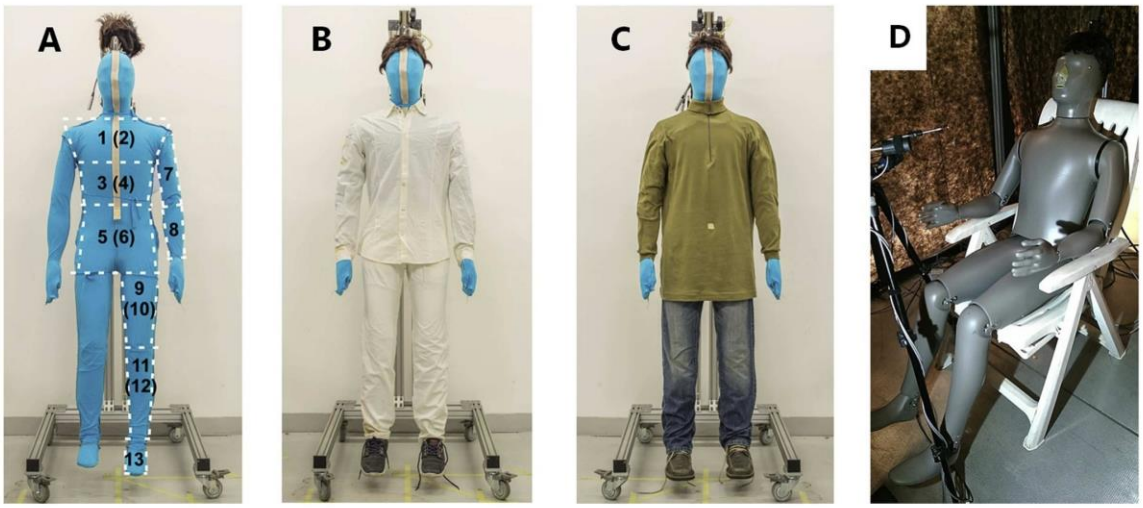

Fig. 1. Illustration of the manikin used and the clothing sets applied. A – segmentation of a nude manikin with an artificial skin, posterior parts in brackets; B – summer indoor clothing; C – winter indoor clothing; D – seated position. *Note: segmentation from* Fig. 1A *– 1 Chest, 2 Back, 3 Abdomen, 4 Lumbus, 5 Anterior pelvis, 6 Buttocks, 7 Upper arm, 8 Lower arm, 9 Anterior thigh, 10 Posterior thigh, 11 Shin, 12 Calf, 13 Foot.*

environment that is typical for a broad variety of indoor environments, and should serve as a benchmark for comparison of the eight individual approaches.

2.2. Definition of clothing sets and body positions for the study

The clothing sets included in this study represent typical indoor summer and winter clothing and were selected from the database of clothing presented by Psikuta et al. [27]. Most importantly, the focus was on the consistency of the clothing ease allowances (defined as the difference between the girth of clothing and a nude manikin at relevant body landmarks) throughout the study, as they affect resulting clothing area factor, thermal resistances, and evaporative resistances. The summer set consists of a collar shirt, light cotton jeans, briefs, short socks, and leather sneakers (Fig. 1 B). The winter set was comprised a turtle-neck shirt with a T-shirt worn underneath, heavier cotton jeans, leather shoes, as well as the same underwear as in the summer case (Fig. 1C). Detailed descriptions and the ease allowances of the clothing are given in Table 2.

A seating position typical of postures adopted for driving, operating of machinery, or office work, was adopted from the work of Mert et al. [28] in which an elbow angle of 120°, hip angle of 110°, and knee angle of 120° are specified (Fig. 1D). The thermal manikin was seated on a plastic chair with openings accounting for approximately 40% of its surface. The standing upright position with hands down (Fig. 1) is typically reported in literature and was used to quantify the differences in comparison to the sitting position.

2.3. Case 1 – 3D scanning and heat loss method in seated position

The first studied case was considered as a reference case providing highest precision for determination of clothing thermal parameters in the seated position. The clothing area factor was measured by a 3D body scanning technique combined with post-processing software, which allows for the quantification of nude and dressed surface areas of individual body regions in a given position [17,27,50]. Details of the methodology and equipment were adopted from the study by Mert et al. [28]. The surface area was quantified four times for each clothing set,

Table 2
Overview of clothing and *ease allowance (EA)* related to the size of a western type Newton thermal manikin.

	Indoor summer set			Indoor winter set				Both sets
Type	Smart shirt	Jeans light	Sneakers	Shirt	T-shirt	Jeans	Shoes	Briefs
Item in Psikuta et al. [27]	21	45	–	3	24	33	–	31
Fit	Regular	Regular	Regular	Regular	Regular	Loose	Regular	Regular
Fibre content (%)	100 CO	100 CO	Leather	100 CO	95 CO/5 EL	100 CO	Leather	100 CO
Specific weight (g/m^2)	137	179	Size	227	176	366	Size	145
Fabric structure	Plain weave	3/1 twill	EUR 42.5	Interlock	Single jersey	3/1 twill	EUR 42.5	1 × 1 rib
EA chest (cm)	14.5	–	–	10.5	11.5	–	–	–
EA waist (cm)	24.0	–	–	30.0	22.0	–	–	–
EA hips (cm)	13.0	8.0	–	12.0	10.0	14.0	–	−4.0
EA biceps (cm)	9.0	–	–	4.0	–	–	–	–
EA lower arm (cm)	8.0	–	–	2.5	–	–	–	–
EA thigh (cm)	–	6.0	–		–	3.0	–	–
EA lower leg (cm)	–	6.0	–	–	–	7.0	–	–

Notes: CO – cotton, EL – elastane.

as well as for an undressed flexible manikin [28]. This manikin has, however, a different body geometry than the western Newton type thermal manikin (Thermetrics, USA) used to measure thermal and evaporative resistances. The differences in griths at given body land marks were typically of 2 cm, having the maximum of 6 cm at *Upper arm*. Linear interpolation was therefore used to compensate for the discrepancies between the manikins girths and consequently clothing ease allowances based on the clothing presented in Mert et al. [28]. This was done according to the findings by Vesela et al. [21], where the linear relationship between the garment ease allowance and f_{cl} was demonstrated.

The local intrinsic clothing thermal (I_{cl}) and evaporative resistances ($R_{e,cl}$) were determined using the 34 zones Newton type manikin in a climatic chamber (detailed description of the chamber and the manikin in Fojtlín et al. [51]). The manikin was seated onto an adjustable plastic chair with perforation wearing the garments listed in Table 2. The 34 zones were merged into 13 segments (Fig. 1A) to represent body segmentation of the Fiala model with resolution of upper and lower limbs, anterior and posterior torso. The measurement of both clothing sets and clothing resistances was executed three times independently, including dressing and undressing of the manikin.

The test conditions for the local intrinsic thermal resistances were adopted from ISO 15831 [32], which establishes requirements of a 34 °C manikin skin temperature, as well as air, mean ambient, and radiant temperatures of 24 °C, and relative humidity of 50%. The air speed in the test was 0.1 ± 0.05 m/s that suits the target application in indoor environments with low air velocities. The calculation of the thermal resistances was done using the heat loss method according to Equation (A.3a) from ISO 15831 [32].

The evaporative clothing resistance was determined using a tightly fitting, long sleeve overall (Fig. 1A) that was pre-wetted and worn only during evaporative resistance measurements [52,53]. The fabric for the overall was selected according to the recommendations from the study by Koelblen et al. [54] with thickness of 0.92 ± 0.03 mm, specific weight of 208 g/m, and fibre composition of 95% cotton and 5% elastane. The measurement was carried out at isothermal conditions of 34 °C (skin temperature equal to ambient temperature), relative humidity of 18% (partial water vapour pressure of 957 Pa), and air speed of 0.1 ± 0.05 m/s. This setup allowed measurements in steady state conditions for at least 20 min to ensure reliable calculation of evaporative resistance. The calculation of evaporative resistance was done using the heat loss method described in ASTM F2370 [44].

2.4. Case 2 – photographic and heat loss method in standing position

Case 2 represents an example of experimental approach when an upright standing, non-articulated manikin (Fig. 1A) and a camera are available. The methodology to determine *Icl* and *Re, cl* is identical with *Case 1*, whilst the calculation of f_{cl} is based on superposition of photographs of nude and dressed manikin using graphical software (CorelDRAW X8, Corel Corporation, USA) according to the standard ISO 15831, Equation (A7) [32]. In this case, the western Newton type thermal manikin was photographed using a full frame camera with a 35 mm lens placed 4.33 m in front of the manikin from four azimuth angles (front 0°, two side views 45°, 90°, and 180°) and a horizontal view of 0°. The standard [32] suggests using one additional horizontal angle of 60°, however, this was not feasible due to the ceiling clearance limitation of the laboratory. Although the original method was proposed to calculate the whole body f_{cl}, we divided the manikin's body into *Upper arm, Lower arm, Chest, Abdomen, Anterior hip, Back, Lumbus, Posterior hip, Upper leg, Lower leg, and Foot*, before determining their local values.

2.5. Cases 3 and 4 – analytical heat transfer model

Cases 3 and 4 represent one of the emerging methods to realistically and rapidly simulate f_{cl}, I_{cl}, *and* $R_{e,cl}$, taking the air gap thickness and contact area into account for a corresponding body part both in seated and standing positions. All three local clothing parameters were calculated using the in-house analytical clothing model developed at Empa [30,43]. The model exploits basic thermodynamic phenomena (conduction, radiation, and natural convection) and allows the calculation of local clothing parameters of multiple, layered garments. The physical model resolution is equal to the number of input parameters that were calculated according to the linear regression model proposed by Psikuta et al. [27] in *Case 4*. The model yields corresponding air gap thickness and contact area, in standing positions, based on the ease allowances of clothing (Table 2) for 14 body parts excluding feet. However, the upper and lower chest as well as upper and lower back were averaged (area weighed) into two respective body parts to match the segmentation in Fig. 1A and the body resolution of the thermal manikin.

In *Case 3*, the resolution of the model was reduced to eight parts, since the four body parts in contact with the seat were not considered. The air gap thickness and contact area were taken from the database of garments in the seated position by Mert et al. [16] (positions U5, L4). The air gap thickness and contact area were obtained by linear interpolation based on the ease allowances.

2.6. Case 5 – regression and analytical heat transfer models

Case 5 represents an approach based on predictions of local f_{cl} and I_{cl} on clothing ease allowances proposed by Vesela et al. [21]. This allows simple calculation of the clothing properties based on readily available parameters. The regression models were derived from single layer garments in standing position. Yet, the behaviour of the multilayer clothing was described in the study by Mark et al. [55] using the 3D scanning technique. The main findings indicate that the inner layer is negligibly influenced by the outer layer as long as the ease allowance of the outer layer is bigger than that of the inner one. Further, for the majority of casual clothing, it can be assumed that the representative f_{cl} and I_{cl} can be calculated according to the ease allowances of the outer garment, and was also performed in this study. The overview of the ease allowances is given in Table 2. The methodology to calculate $R_{e,cl}$ was not presented in the study by Vesela et al. [21] and was adopted from *Case 4* [30].

2.7. Case 6 – ISO 9920 based model

Curlee [19] and Nelson et al. [23] developed a method to calculate all three local clothing parameters valid for 106 garments from McCullough et al. [24] and ISO 9920 [18]. However, the resolution of the algorithm is limited to individual clothing items covering given body parts, such as a shirt covering the whole torso and arms. As the method does not clarify an approach to calculating the resistances of multiple, layered garments lying atop one-another, the clothing resistances were instead totalled to match the procedure of Vesela et al. [11]. The clothing area factors of the outer layers were calculated as described in section 2.6.

Following clothing was selected for this study from Appendix A [19]:

- Summer clothing: Long sleeve collar shirt (broadcloth); Straight long fitted trousers (denim); Soft soled athletic shoes; Calf length dress socks.
- Winter clothing: Long-sleeve turtleneck (thin knit); Short sleeve collar shirt (broadcloth); Straight long lose trousers (denim); Hard soled athletic shoes; Calf length dress socks.

2.8. Case 7 – empirical model

The UTCI clothing model predicts local thermal insulation for 7 body parts (head, torso with upper arms, lower arms, hands, upper legs,

lower legs, feet) [20]. Despite the model's focus on outdoor applications, we assumed similar clothing preferences for indoor and outdoor environments based on two mild ambient temperatures of 24 °C (summer indoor clothing) and 21 °C (winter indoor clothing). These two temperatures were defined according to the PMV-PPD thermal sensation model described in the ISO 7730:2005 [56] as a thermo-neutral environment for activity level representing office work or driving at 1.3 met, clothing insulation according to ISO 9920 of 0.62 (summer) and 1.01 clo (winter), and air speed of 0.1 m/s.

2.9. Case 8 – estimation based on ISO 9920

Standard ISO 9920 [18] provides an exhaustive list of civil, working, and non-western clothing properties determined by a standing thermal manikin. Therefore, this approach is of main interest for a variety of engineering applications where there is no dedicated equipment available. The I_{cl} and f_{cl} are presented as a resultant insulation prescribed to all body parts, even to those parts, which are not covered by the clothing in reality. Similarly, the $R_{e,cl}$ was calculated as a whole body value according to Equation (31) from the standard [18] as intrinsic thermal insulation multiplied by a constant of 0.18.

Two clothing sets were selected from the standard (Table A.2) [18] based on the closest match of the description of the garments as follows:

- Summer clothing: *Ensemble 108* – briefs, long-sleeve shirt, fitted, trousers, calf-length socks, shoes.
- Winter clothing: *Ensemble 114* – briefs, T-shirt, shirt, loose trousers, round-neck sweater, calf-length socks, shoes.

2.10. Determination of seat thermal properties

As a consequence of the seat, the body segments in contact with it experience increased thermal and water vapour resistances. Direct measurement of these parameters with the Newton type manikin is not accurate because of the manikin's rigid body construction and low body weight, which inhibit the resulting contact area from imitating the interaction of a representative body and seat [40]. As a result, lower compression of seat layers and smaller contact area with differences in shape are expected for manikins when comparing to humans. For this reason, the corresponding data was adopted from the study on aeroplane seats with similar construction to automotive seats, with moulded foam cushioning and leather cover. Using a stamp tester, a thermal resistance of 0.55 m^2K/W (Fig. 7 in Ref. [39]) was measured for the seat, whilst an evaporative resistance of 100 m^2Pa/W [39] was determined using the same seat in human trials. Finally, we estimated the seat clothing area factor to be 2.0 units based on the dimensions of the seat.

2.11. Thermo-physiological simulations

Benchmark tests of clothing thermal properties are helpful in the development and evaluation of clothing systems, but thermo-physiological responses do not show a similar sensitivity to clothing properties as can be detected by benchmark tests [48]. Therefore, the eight studied cases were used as separate inputs for thermo-physiological modelling under the same environmental conditions to quantify the resulting differences in physiological responses among the methods.

To do so, two setups corresponding to summer ($t_{air} = t_{rad} = 24°$) and winter ($t_{air} = t_{rad} = 21°$) indoor environments with an ambient air speed of 0.1 m/s, and relative humidity of 50% were carried out using the broadly validated Fiala model FPCm 5.3 [46]. The metabolic production of 1.3 met was selected from a database presented by Ainsworth et al. [57] as an average from reading, typing, and driving. The simulations were run for 4 h with a 5 min simulation interval to reveal the development of thermo-physiological response in a long steady exposure.

In the simulations, the clothing thermal properties of shoes were obtained from *Case 2 and* considered in f_{cl} for *Cases 1,3,4,5*, I_{cl} for *Cases 3,4,5*, and $R_{e,cl}$ for *Cases 3,4,5,6*. Additionally, the simulations account for the thermal effects of the seat (Section 2.10). The seats were applied as the clothing boundary conditions to posterior thighs, posterior hip, posterior abdomen, and posterior thorax of the virtual humanoid according to the findings from Fojtlín et al. [40]. This was done for *Cases 1* to *7*, whereas the eighth case was executed according to the directions from ISO 9920 [18], such that an additional thermal insulation of 0.039 $m^2K.W^{-1}$ was added to the whole-body resistance. As the standard does not clarify how to treat f_{cl} and $R_{e,cl}$, the values were unchanged for *Case 8* in the standing position.

Firstly, to assess the effects of clothing boundary conditions, we examined mean skin and rectal temperatures to provide a global overview of the body thermal state. Secondly, the cumulative sweating was investigated to quantify the amount of liquid sweat excreted from the whole body. Next, to measure the development of local parameters, skin temperatures were examined at Chest and Anterior thighs, which were selected because of their dominant surface area that is not in the contact with the seat and their distinct susceptibility to change air gap thickness with the change of position. Furthermore, dynamic thermal sensation (*DTS*) was calculated to predict whole body thermal sensation on the 7-point scale ranging from - *3 Cold*, through *0 Neutral*, to *3 Hot* [56]. Finally, skin wettedness was examined at *Chest* and can be considered as a perception of wet discomfort being physically defined as the ratio of the actual sweat rate to the potentially evaporating amount of sweat.

3. Results

3.1. Comparison of the methods

Local clothing properties f_{cl}, I_{cl}, and $R_{e,cl}$ were divided into four groups of body parts, namely anterior and posterior torso, and upper and lower limbs (Figs. 2 and 3). Furthermore, Figs. 2 and 3 show the local clothing properties obtained from all examined methods for a given body part in one plot. A result from one body part is connected with a dashed line for easier tracking of its development depending on the method. The results from methods having body parts resolutions lower than reference (13) were either left blank, if missing, or presented as one value for related body parts, for instance lower leg from UTCI model [20] covers *Shin* and *Calf*. Where applicable in Figs. 2 and 3, error bars represent standard deviation of the repeated measurements. The differences between repeated manikin measurements in I_{cl} fell within the recommended 4% [32], thus, the standard deviation was too small to be visualised and was not plotted. Despite the anatomically unrealistic contact of the manikin with the seat [40], the I_{cl} and $R_{e,cl}$ from the contact area in *Case 1* (Figs. 2 and 3 – *Back, Lumbus, Buttocks, and Anterior thighs*) are shown for full overview. Because of the limitations of the 3D scanning method in the contact area, in *Case 3*, the f_{cl} was calculated based on an increase of the skin surface area by the thickness of the fabrics. As reference body geometry we used a virtual humanoid from the Fiala thermo-physiological model [46]. Further, the I_{cl} and $R_{e,cl}$ was estimated as thermal and evaporative resistances of the fabrics only.

Assuming that *Case 1* (manikin measurement in seated position) is the most accurate method, the variation between all the methods for both clothing ensembles was as follows:

- 13–43% of the reference value for clothing area factor (f_{cl}) depending on body part;
- 35–198% of the reference value for intrinsic thermal insulation (I_{cl}) depending on body part;
- 53–233% of the reference value for intrinsic evaporative resistance ($R_{e,cl}$) depending on body part.

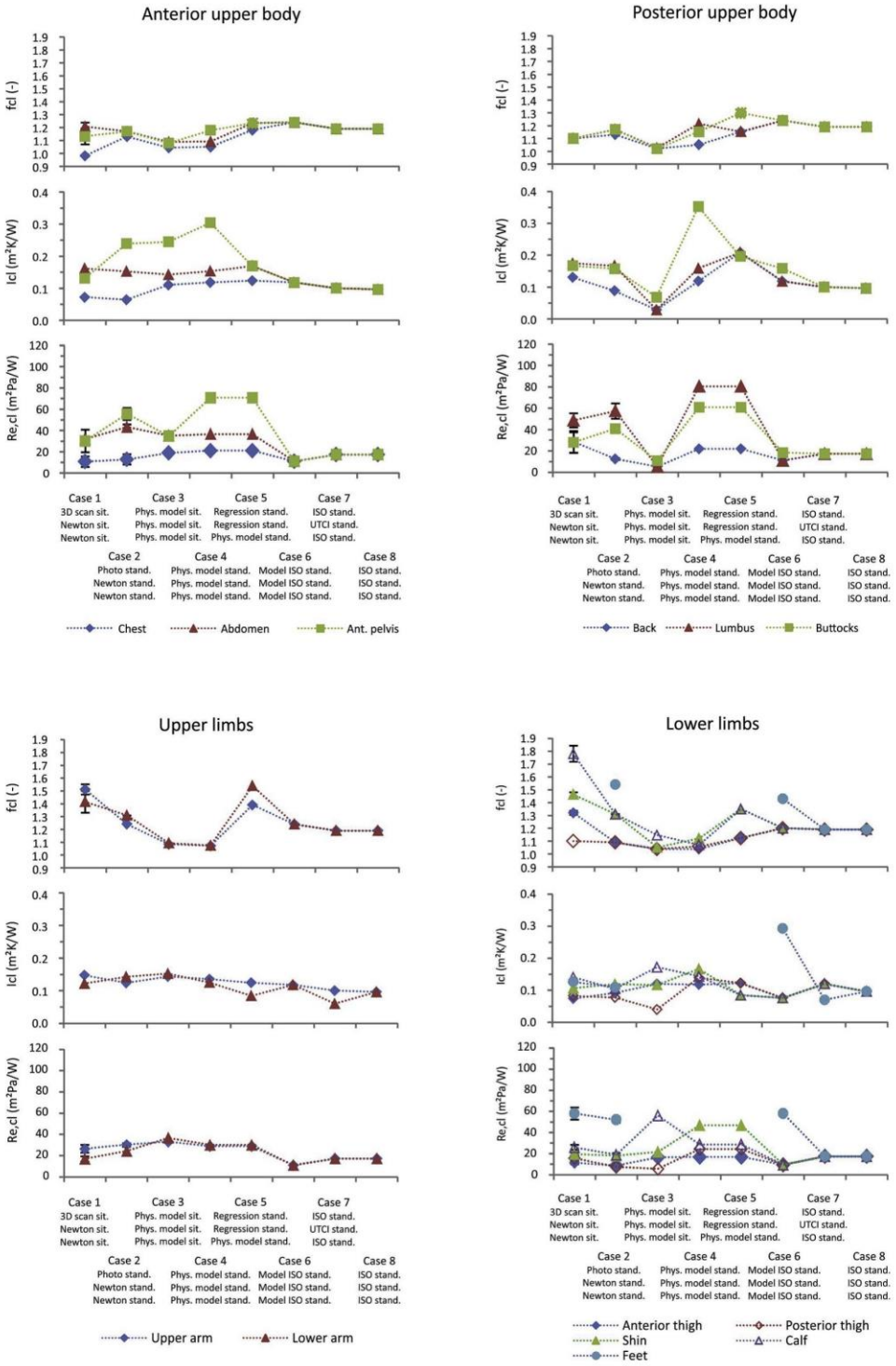

Fig. 2. The clothing thermal properties of the summer indoor clothing set shown for 13 body parts excluding the seat thermal properties. Error bars depict standard deviation.

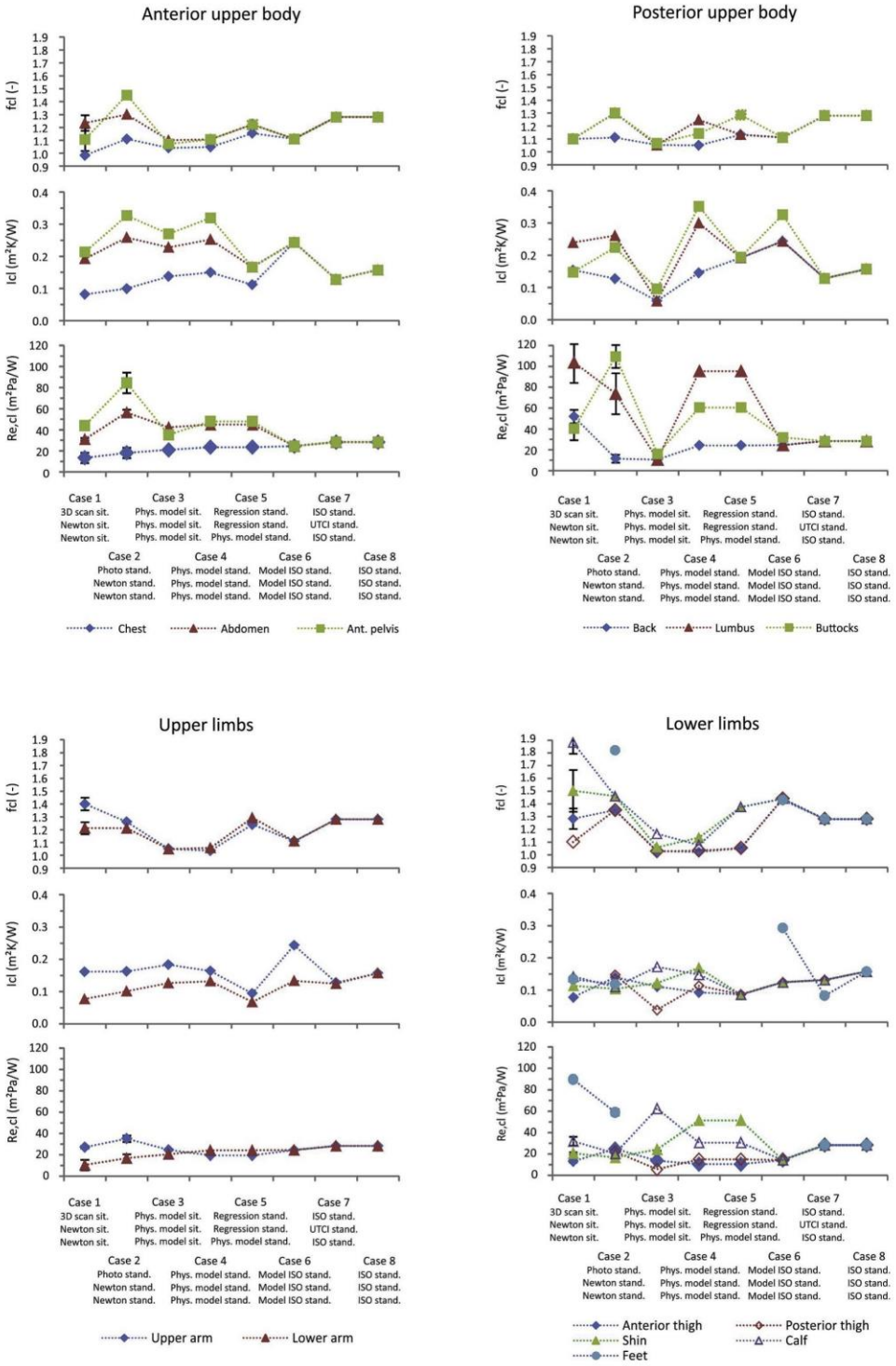

Fig. 3. The clothing thermal properties of the winter indoor clothing set shown for 13 body parts excluding the seat thermal properties. Error bars depict standard deviation.

These variations were found to be very similar for both clothing ensembles with somewhat higher values for the looser, multilayer winter ensemble (Figs. 2 and 3). When comparing 6 cases based on standing body position only (*Cases 2, 4, 5, 6, 7,* and *8*, Table 1), their variation was as follows:

- 6–36% of the reference value for clothing area factor (f_{cl}) depending on body part;
- 32–204% of the reference value for intrinsic thermal insulation (I_{cl}) depending on body part;
- 45–232% of the reference value for intrinsic evaporative resistance ($R_{e,cl}$) depending on body part.

3.2. Differences in manikin measurements between sitting and standing body positions

The differences between parameters for both sitting and standing positions are depicted in Fig. 4 for selected representative body parts with and without a major change in their orientation. The body parts in contact with the seat were considered without the seat thermal insulation. The following difference margins between sitting and standing positions were found, namely:

- up to 31% of the reference value (*Case 1*) for f_{cl} depending on body part;
- up to 80% of the reference value (*Case 1*) for I_{cl} depending on body part;
- and up to 92% of the reference value (*Case 1*) for $R_{e,cl}$ depending on body part.

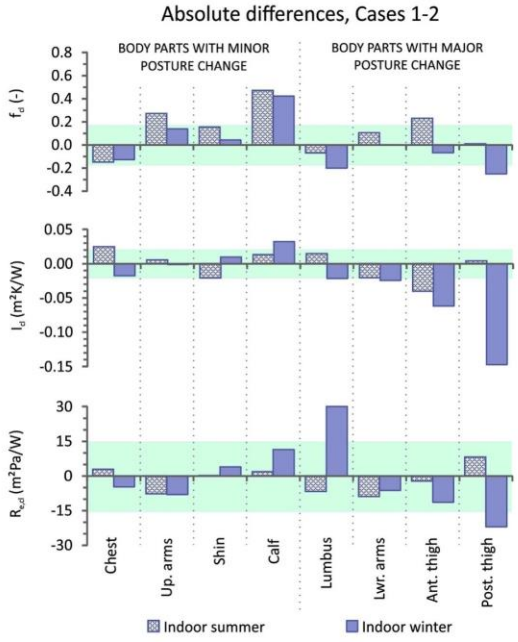

Fig. 4. Absolute differences between clothing thermal properties between the positions (Cases 1–2) for summer and winter indoor clothing, respectively. The transparent field depicts a range of three standard deviations of the methods used in Case 1 covering 99.7% of observations being ± 0.17 units for f_{cl}, ± 0.02 m^2K/W for I_{cl}, and ± 15 m^2Pa/W for $R_{e,cl}$.

3.3. Effects of the clothing and body position on thermo-physiology

The results for the whole-body and local thermal responses from thermo-physiological simulations are depicted in Fig. 5, separately for summer and winter scenarios. In total, eight responses were plotted such as mean skin temperature, rectal temperature, skin temperature at chest, skin temperature anterior thigh, cumulative sweating, dynamic thermal sensation (DTS), and skin wettedness at *Chest*. Each line represents a development of a given simulated response corresponding to one of the examined methods to determine the clothing properties. To differentiate between sitting and standing body positions, the sitting positions are represented within the plots by continuous lines, whilst standing positions are denoted by dashed lines.

4. Discussion

4.1. Comparison of the methods

In this study, we compared six various methods to obtain clothing area factor, seven methods for intrinsic thermal insulation, and five methods for intrinsic evaporative resistance determination. These methods were combined into eight distinct cases corresponding to different availabilities of advanced equipment to determine the clothing properties in an exemplary laboratory. In theory, all the examined methods should yield the same results. Contrary to this, large differences of more than 200% were found for all three clothing parameters and body parts covered by the clothing (Figs. 2 and 3) assuming that *Case 1* (manikin measurement in seated position) is the most accurate reference method (13–43%, 35–198%, and 53–233% of the reference value for clothing area factor (f_{cl}), intrinsic thermal insulation (I_{cl}) and intrinsic evaporative resistance ($R_{e,cl}$), respectively, depending on body part).

It is worth to mention that this variation cannot be predominantly attributed to the body position. When comparing 6 cases based on standing body position only (*Cases 2, 4, 5, 6, 7,* and *8*, Table 1), their variation was slightly lower, such as 6–36%, 32–204%, and 45–232% of the reference value for clothing area factor, intrinsic thermal insulation, and evaporative resistance, respectively, depending on body part.

The error in f_{cl} was greater at the limbs (0.16–0.81 units of difference among the methods) than at the torso (0.15–0.38 units of difference among the methods). The median of error among all cases was 0.36 units, whereas the most outstanding difference was observed at calves of up to 0.81 units (Fig. 3, *Case 3*). Here, the method assumes a cylinder as a base shape wrapped by clothing which includes the average air gap thickness. This does not fully represent the real situation of the hanging trouser leg in the sitting position. Regarding I_{cl} and $R_{e,cl}$, amongst the methods tested the upper limbs presented the best matching predictions, resulting in differences of 0.05–0.15 m^2K/W and 15.8–25.7 m^2Pa/W, respectively. The rest of the body parts did not show any clear trends in prediction accuracy, having average differences among the methods in I_{cl} and $R_{e,cl}$ of 0.14 m^2K/W and 38.8 m^2Pa/W respectively, with the greatest span of predictions of 0.2 m^2K/W in I_{cl} and of 60.1 m^2Pa/W in $R_{e,cl}$ at *Anterior pelvis*.

The predictions of all clothing parameters were the most realistic in *Cases 3, 4,* and *5* compared to the reference values from *Case 1*. Presumably, the rest of the methods poorly capture changes in the clothing parameters because of their limited body resolution. *Cases 1* and *2* were carried out with resolutions of 13 segments as well as *Cases 3, 4,* and *5,* whereas the methods used in *Cases 6, 7,* and *8* work with body segmentation of three, seven, and one components, respectively. Thus, distinct body parts (such as *Chest*, *Abdomen*, *Ant. Pelvis, Back, Lumbus, and Arms* in *Case 6*) are lumped into one segment that yields an averaged value in *Case 6* of 0.12 m^2K/W for summer clothing and of 0.24 m^2K/W for winter clothing when neglecting local extremes. Area weighted average from the same segments from the more detailed *Case 2* shows comparable results of 0.15 m^2K/W and 0.20 m^2K/W in summer

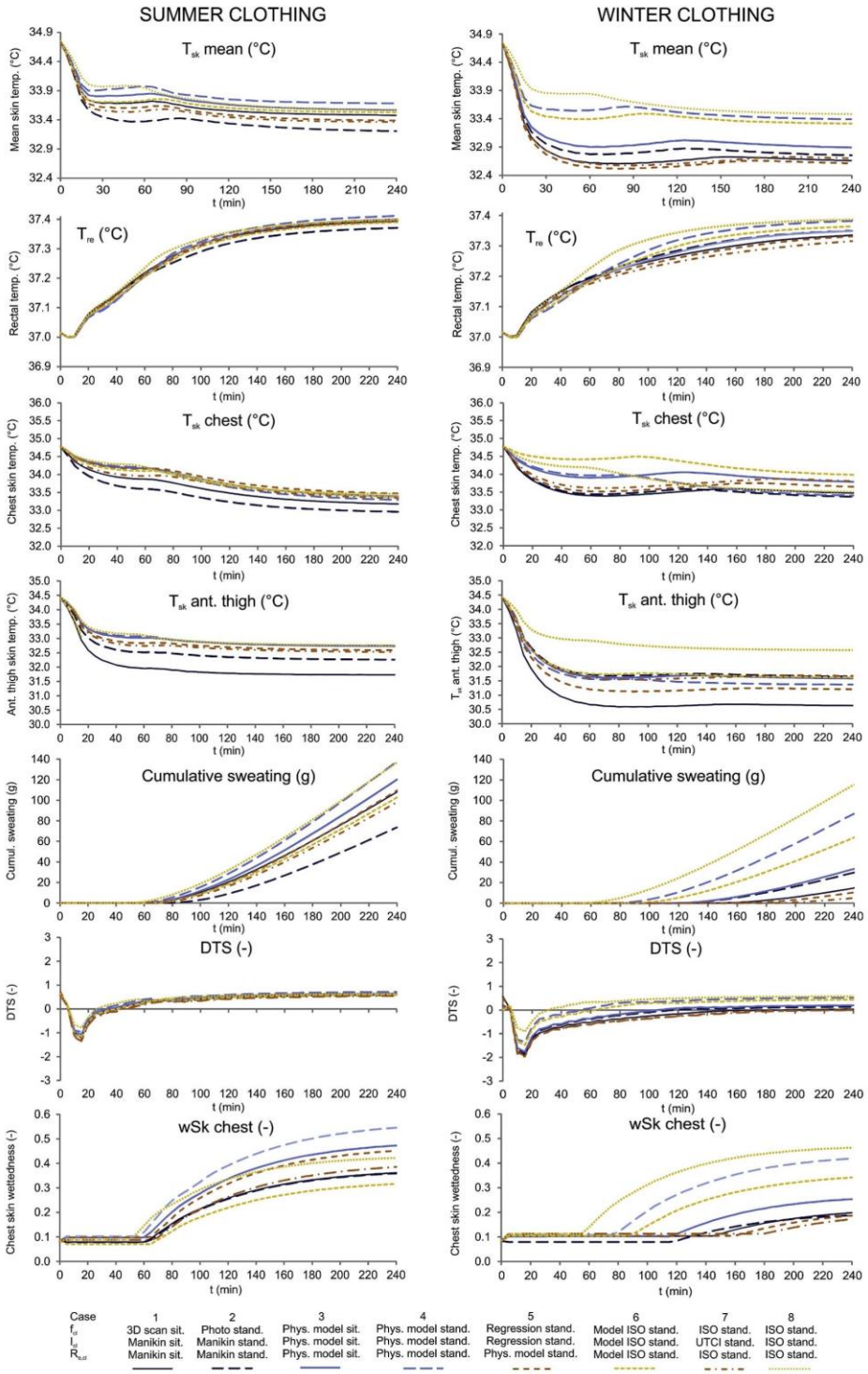

Fig. 5. Results of the thermo-physiological simulations separately for summer and winter clothing.

and winter clothing, respectively. At the same time, the local values in *Case 2* differ substantially from their average, with extremes at *Chest* and *Anterior Pelvis* of 0.06 m^2K/W and 0.24 m^2K/W for summer clothing and of 0.10 m^2K/W and 0.33 m^2K/W for winter clothing, respectively. Therefore, it is essential to account for local extremes.

4.2. Differences in manikin measurements between sitting and standing positions (cases 1 and 2)

The change of body position implies a change in orientation for several regions of the body to varying extents. This is particularly evident when one considers the significant degree of thigh reorientation, when contrasted to the minor reorientation of the chest when moving between standing and sitting positions. The differences in all three clothing thermal properties for both positions were found and are depicted in Fig. 4 for selected representative body parts with and without a major change in their orientation. The least pronounced deviations (of up to 31%) were discovered in f_{cl}. Despite slight postural changes at *Calf* and *Upper arm*, here, an error in f_{cl} was three standard deviations higher than of other typical measurements (Fig. 4).

Although minor variations would be expected due to slight postural changes, it was found that the an error in f_{cl} at the *Calf* and *Upper arm* was three standard deviations higher than of other typical measurements. Despite minor changes were expected only because of the minor posture change, we found the opposite in f_{cl} at the *Calf* and *Upper arm*, being higher than three standard deviations of typical measurement (Fig. 5). The error at *Calf* can be explained by the hanging trouser leg in the seated position yielding a difference of approximately 0.5 f_{cl} units. The discrepancy at *Upper arm* is plausibly related to methodological differences between *Cases 1* and *2*.

The photographic method is based on the projection of a three-dimensional object to a two-dimensional plane. Whilst there is an expected loss of detail in the clothing topography through this approach in *Case 2*, the 3D scanning method of *Case 1* accounts for clothing folds which affect total clothing surface area. Thus, the error between the scanning and the photography is of 0.28 f_{cl} units for summer and 0.12 f_{cl} units for winter clothing. However, it is difficult to generalise the methodological error because the number and the size of the folds vary over the body surface. Next, in the sitting position, the 3D scanning method yields f_{cl} at *Chest* lower than 1 as opposed to the photographic method. The probable reason for this is the anatomic curvature of the flexible manikin's chest [16] that has a greater surface area than the stretched flat garment that covers the chest, whereas the Newton thermal manikin (*Case 2*) has simplified concave chest curvature. Thus, its skin surface is smaller than the surface of the outer garment yielding f_{cl} greater than 1.

The results in I_{cl} and $R_{e,cl}$ from *Cases 1* and *2* exhibit greater variation (of up to 80% and 92%, respectively) and correspond to a redistribution of the mean air gap thicknesses between the positions reported by Mert at al. [28], and its consequent impact on thermal and evaporative resistances as reported by Psikuta et al. [45]. In compliance with these two studies, we found decrease in I_{cl} and $R_{e,cl}$ greater than three standard deviations of measurement at *Anterior pelvis*, *Anterior thighs*, *Abdomen,* and *Lower arm* (Fig. 4). At these parts, air gaps collapse and the I_{cl} of two-layer winter clothing might be equalled to standing summer clothing. This underlines the importance of distinguishing between the body orientations and using local values.

4.3. Effects of the clothing and position on thermo-physiology

Differences in local clothing properties may be integrated by human thermoregulation and, thus, result in minimal discrepancy of global parameters such as mean skin or core temperatures. The variation of mean skin temperatures among the eight methods was within 0.6 and 1.3 °C in summer and winter clothing, respectively. This rather remarkable error can be related to a considerable change in local thermal sensation from approximately 0.5 to 1.5 units, depending on the thermal sensation model, and its scale as demonstrated by Koelblen and Veselá et al. [11,58]. However, the differences between the body positions were marginal within 0.3 °C. Finally, we found minor impact of the eight clothing inputs on the predicted rectal temperature of less than 0.1 °C.

The local thermo-physiological parameters show substantial variation that corresponds to variation in the clothing inputs even if applied in a neutral, steady, and uniform environment (Fig. 5). In reference to *Case 1*, the approaches whose results which most closely matched were found to be the same as in the investigation on the clothing thermal properties, namely *Case 3* (modelling based on air gap thicknesses in sitting) and *Case 5* (regression model based on air gap thickness). The worst performing approach was *Case 8* based on the whole-body estimation of clothing parameters and the ISO based model from *Case 6* (Fig. 5). It seems to be not possible to recover any local data based on whole body values with reasonable accuracy when local data is necessary, as shown by performance of *Case 6*.

Next, the development of the local skin temperatures is clearly affected by the variation of local clothing thermal properties. For instance, relatively low differences in the clothing properties at *Chest* (Figs. 2, 3 and 5) result in the absolute differences in skin temperatures of 0.5 °C among all methods and of 0.2 °C between the body positions (Fig. 5). On the contrary, higher variability of input parameters, such as at *Anterior thighs*, leads to a spread of the predicted local skin temperature of 1 and 2 °C in summer and winter clothing, respectively. Next, cumulative sweating indicates low to mild sweat excretion that amounts between 5 g (*Case 7* winter clothing) and 138 g (*Case 4* summer clothing). The onset of sweating varied substantially in the winter clothing between 60th (*Case 8*) and 190th minute (*Case 7*).

The precise predictions of the sweat amount and onset of sweating can enhance a proper prediction of skin wettedness linked to so-called wet discomfort from sweating. At the end of the exposure, this parameter ranged from 0.03 to 0.61 and from 0.06 to 0.71 in summer and winter clothing, respectively. The highest values were always found in the contact parts with the seat and the lowest for bare body parts, such as hands. The variability of predictions can be demonstrated on *Chest*, where the threshold for discomfort of 0.42 units [59] was exceeded in the winter clothing tests of *Cases 4* and *8* (value reached in 210 min and 145 min, respectively), and in the summer clothing *Cases 3* (125 min), *4, 5,* and *8* (185 min). The threshold was not reached in the *Cases 1* and *2* (Fig. 5).

Although, the examined deviations in thermo-physiological parameters are not critical in regards to medical relevance, such as uncompensated heat storage or dehydration, they negatively influence accuracy of thermal sensation prediction. The benchmark value for the assessment of thermal sensation was adopted from ISO 7730 [56] as ± 0.5 units (thermal environment category B corresponding to less than 10% of dissatisfied occupants with the thermal environment). The whole-body thermal sensation index *DTS* showed minor variations between the methods which was within 0.2 units for summer clothing and significant discrepancies were found in the winter scenario of up to 0.6 units (*Cases 4, 7, 8* compared to *Case 1*, Fig. 5). Yet, the contribution of the position change, demonstrated in *Cases 1* and *2*, did not reveal any significant differences in *DTS* (below 0.1 units). However, it can be expected to see major differences in the local thermal sensation predictions.

The whole body values are not sufficient for local modelling and the seated posture induces a drop in thermal and evaporative resistance due to collapse of air layers underneath the clothing. Furthermore, the previously discussed variability of the thermo-physiological responses induced by the clothing inputs urges the use of precise local clothing parameters. Only then with these parameters can reliable simulations of thermo-physiological responses be conducted. In addition, the discrepancies between the predictions may inflate for conditions further away from thermo-neutrality and cause even larger errors in

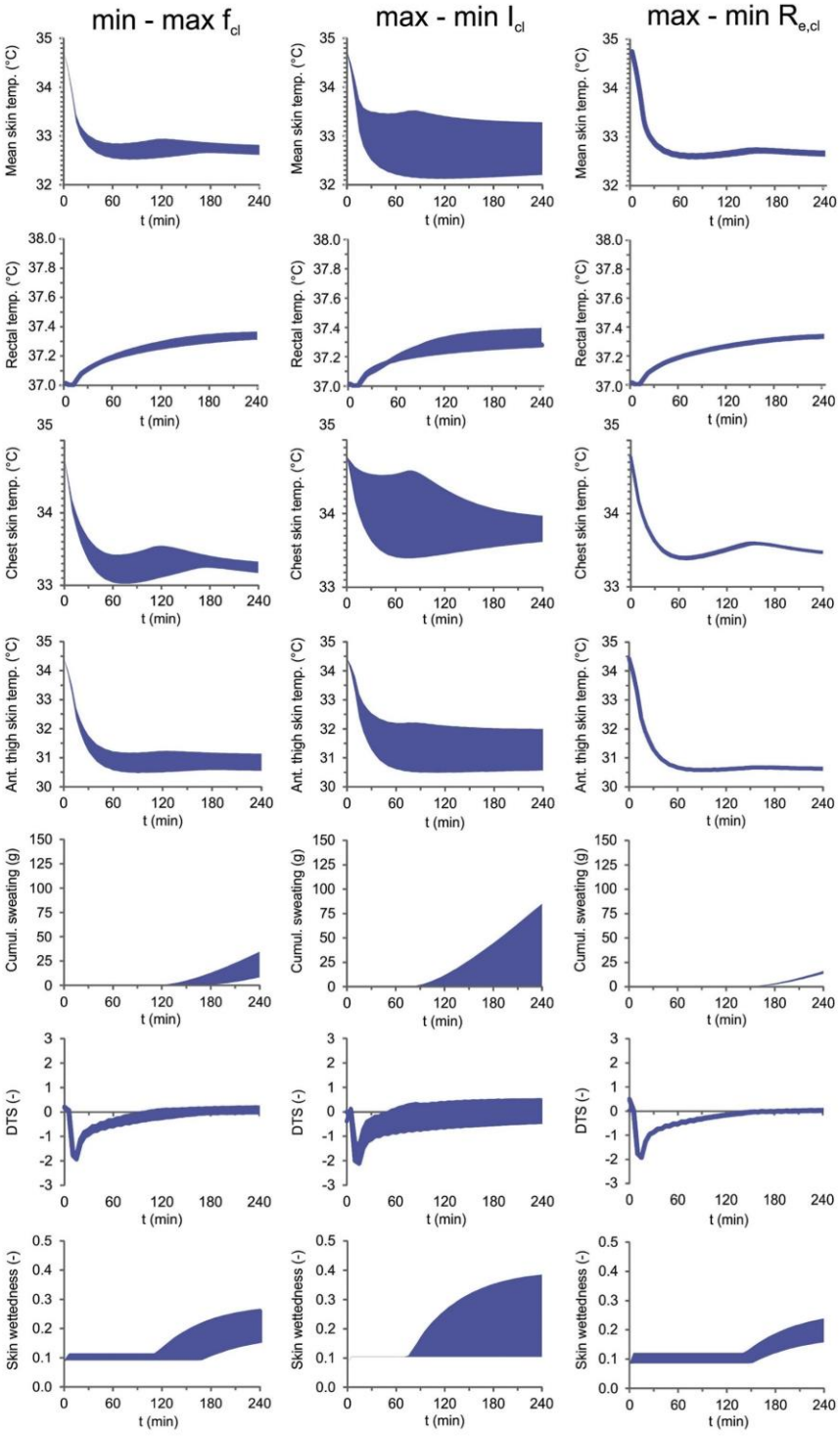

Fig. 6. Sensitivity of thermo-physiological responses to changes in individual clothing parameters.

predictions of thermal sensation, comfort or performance of the occupants [58,60]. This applies for instance in free running buildings with a larger temperature range, vehicles, and industrial spaces with special conditioning due to technological processes.

4.4. Sensitivity analysis

In order to examine the sensitivity of the physiological response to variations in clothing parameter inputs, we reproduced the winter case using upper and lower extremes of the clothing parameters out of the 8 cases. Only one clothing parameter was changed at a time (for instance f_{cl}) while keeping the rest (in this case I_{cl} and $R_{e,cl}$) as the reference – *Case 1* sitting.

The results are displayed in Fig. 6 and clearly show the variability of I_{cl} inducing the greatest effect on all monitored thermo-physiological parameters in thermo-neutral environmental conditions (Details in Section 2.11). Differences in skin temperatures and DTS exceeded 1 °C and 1 unit, respectively. As previously discussed, such discrepancies have measurable impact on the perceived thermal sensation and/or comfort. Despite high deviations in f_{cl} (up to 43%) and $R_{e,cl}$ (up to 233%), the effect of these two parameters on thermo-physiology is practically negligible. However, it can be expected that the importance of $R_{e,cl}$ in warm conditions will play a more significant role, as a larger amount of sweat is excreted and needs to be transported through the clothing system. Secondly, the variation of $R_{e,cl}$ between methods might be larger when protective clothing with higher evaporative resistance is considered, since this clothing is less represented and more difficult to unambiguously identify in databases used in regression and reference table methods.

4.5. Reliability of the reference methods

Despite using the state-of-the-art methods as a reference, several remarks should be noted on their reliability. Firstly, the precision of 3D scanning method – used in this study to determine clothing area factor – is typically better than 1.7 mm [28,61]. Based on the dimensions of the passive body geometry in the Fiala model [46], an addition of 1.7 mm to the body part radius causes a change in f_{cl} as low as 0.01 units. This increment is, thus, negligible compared to observed f_{cl} variation between examined methods and we conclude high reliability of this method. Secondly, the measurement of I_{cl} has the typical error among the repeated measurements of less than 4% that is recommended by the standard ISO 15831 [32]. The only two local extremes of 10% were found at the *Abdomen* and *Back*. Finally, the precision of the methodology to determine $R_{e,cl}$ has several methodological limitations that are bound to complexity of the heat and mass transfer through the garment, such as heat pipe effect, wicking, partial drying, wet conduction [62], evaporative heat energy taken from the environment [53], and inability to control the temperature of the wetted manikin's skin [63,64]. Thus, the skin temperature might be lower than assumed and introduce an error in $R_{e,cl}$ of up to 14% [63]. Nevertheless, according to our sensitivity analysis in mild thermal environments, the errors in $R_{e,cl}$ have only a minor impact on the physiological response.

5. Conclusions

Eight typical approaches to determine clothing properties for thermo-physiological and thermal sensation predictions were examined, both in sitting and standing body positions, using two sets of indoor clothing. Considerable differences among the eight examined methods in clothing area factor, intrinsic clothing thermal insulation, and evaporative resistance were found. Next, the findings from the study also confirm a need to differentiate between the local clothing inputs in seated and standing positions and urge to avoid using the whole body values that are not sufficient for local thermo-physiological modelling. The impact of the variation of the clothing parameters was shown in the simulations of physiological responses in thermo-neutral, homogeneous, and steady conditions. Consequently, due to differences in the clothing inputs, we found major deviations of skin temperatures, skin wettedness, and global thermal sensation votes. Furthermore, sensitivity analysis revealed a dominant influence of intrinsic clothing thermal insulation on the simulated responses, while clothing area factor and evaporative resistance had minor influences. Therefore, we recommend using the highest precision method available to determine I_{cl}, such as a manikin measurement, physical modelling or regression modelling. Nonetheless, it can be expected that discrepancies among the methods will be stressed out in heterogeneous and extreme ambient conditions, for instance in vehicular cabins exposed to hot or cold weather conditions, free running buildings or specific working environments.

The findings from this study are beneficial for a broad variety of research and engineering applications, where a design of a thermal environment is essential to ensure comfort and performance of the occupants, such as multiple sitting occupations (office work, assembly or sewing work, driving) and passenger transportation. Here, the acceleration of innovation cycles and reduction of costs for physical studies is advanced by the selection and use of reliable thermo-physiological models, which incorporate realistic clothing boundary conditions whilst also accounting for body position.

Acknowledgements

The part of work conducted at Empa was supported by the [HEATSHIELD project within EU Horizon 2020 program] under Grand [RIA 668786–1]. The experimental part of the work conducted at Brno University of Technology was supported by the [Ministry of Education project Youth and Sports of the Czech Republic] under the "National Sustainability Programme I" [LO1202 Netme Centre Plus]; and the [Brno University of Technology] under the project Reg. No. [FSIeS-17-4444]. The authors would like to thank Ankit Joshi from Empa, St. Gallen for help with calculating clothing thermal properties in *Cases 3 and 4*.

References

[1] M. Veselý, W. Zeiler, Personalized conditioning and its impact on thermal comfort and energy performance - a review, Renew. Sustain. Energy Rev. 34 (2014) 401–408, https://doi.org/10.1016/j.rser.2014.03.024.
[2] M. Veselý, P. Molenaar, M. Vos, R. Li, W. Zeiler, Personalized heating – comparison of heaters and control modes, Build. Environ. 112 (2017) 223–232, https://doi.org/10.1016/j.buildenv.2016.11.036.
[3] W. Pasut, H. Zhang, E. Arens, Y. Zhai, Energy-efficient comfort with a heated/cooled chair: results from human subject tests, Build. Environ. 84 (2015) 10–21, https://doi.org/10.1016/j.buildenv.2014.10.026.
[4] M. Luo, E. Arens, H. Zhang, A. Ghahramani, Z. Wang, Thermal comfort evaluated for combinations of energy-efficient personal heating and cooling devices, Build. Environ. 143 (2018) 206–216, https://doi.org/10.1016/j.buildenv.2018.07.008.
[5] A. Psikuta, J. Allegrini, B. Koelblen, A. Bogdan, S. Annaheim, N. Martínez, D. Derome, J. Carmeliet, R.M. Rossi, Thermal manikins controlled by human thermoregulation models for energy efficiency and thermal comfort research – a review, Renew. Sustain. Energy Rev. 78 (2017) 1315–1330, https://doi.org/10.1016/J.RSER.2017.04.115.
[6] E. Foda, K. Sirén, Design strategy for maximizing the energy-efficiency of a localized floor-heating system using a thermal manikin with human thermoregulatory control, Energy Build. 51 (2012) 111–121, https://doi.org/10.1016/j.enbuild.2012.04.019.
[7] D. Fiala, A. Psikuta, G. Jendritzky, S. Paulke, D.A. Nelson, W.D. van Marken Lichtenbelt, A.J.H. Frijns, Physiological modeling for technical, clinical and research applications, Front. Biosci. S2 (2010) 939–968.
[8] C. Huizenga, Z. Hui, E. Arens, A model of human physiology and comfort for assessing complex thermal environments, Build. Environ. 36 (2001) 691–699, https://doi.org/10.1016/S0360-1323(00)00061-5.
[9] M. Hepokoski, A. Curran, D. Dubiel, Improving the accuracy of physiological response in segmental models of human thermoregulation, in: S. Kounalakis, M. Koskolou (Eds.), XIV Int. Conf. Environemntal Ergon. Nafplio, Nafplio, 2011, pp. 102–103.
[10] B. Koelblen, A. Psikuta, A. Bogdan, S. Annaheim, R.M. Rossi, Thermal sensation models: a systematic comparison, Indoor Air 27 (2016) 1–10, https://doi.org/10.1111/ina.12329.
[11] S. Veselá, B.R., A.J. Frijns Kingma, Local thermal sensation modeling: a review on the necessity and availability of local clothing properties and local metabolic heat

production, Indoor Air 27 (2017) 261–272, https://doi.org/10.1111/ina.12324.
[12] G. Havenith, D. Fiala, Thermal indices and thermophysiological modeling for heat stress, Comp. Physiol. 6 (2015) 255–302, https://doi.org/10.1002/cphy.c140051.
[13] G. Havenith, R. Heus, W.A. Lotens, Resultant clothing insulation: a function of body movement, posture, wind, clothing fit and ensemble thickness, Ergonomics 33 (1990) 67–84, https://doi.org/10.1080/00140139008927094.
[14] G. Havenith, R. Heus, W.A. Lotens, Clothing ventilation, vapour resistance and permeability index: changes due to posture, movement and wind, Ergonomics 33 (1990) 989–1005, https://doi.org/10.1080/00140139008925308.
[15] Y.S. Wu, J.T. Fan, W. Yu, Effect of posture positions on the evaporative resistance and thermal insulation of clothing, Ergonomics 54 (2011) 301–313, https://doi.org/10.1080/00140139.2010.547604.
[16] E. Mert, A. Psikuta, M.A. Bueno, R.M. Rossi, The effect of body postures on the distribution of air gap thickness and contact area, Int. J. Biometeorol. (2016) 1–13, https://doi.org/10.1007/s00484-016-1217-9.
[17] E. Mert, A. Psikuta, M.A. Bueno, R.M. Rossi, Effect of heterogenous and homogenous air gaps on dry heat loss through the garment, Int. J. Biometeorol. 59 (2015) 1701–1710, https://doi.org/10.1007/s00484-015-0978-x.
[18] International Organization for Standardization, ISO 9920 Ergonomics of the Thermal Environment - Estimation of Thermal Insulation and Water Vapour Resistance of a Clothing Ensemble, (2007), p. 104.
[19] J.S. Curlee, An Approach for Determining Localized Thermal Clothing Insulation for Use in an Element Based Thermoregulation and Human Comfort Code, Master Thesis Michigan Technological University, 2004.
[20] G. Havenith, D. Fiala, K. Blazejczyk, M. Richards, P. Bröde, I. Holmér, H. Rintamaki, Y. Benshabat, G. Jendritzky, The UTCI-clothing model, Int. J. Biometeorol. 56 (2012) 461–470, https://doi.org/10.1007/s00484-011-0451-4.
[21] S. Veselá, A. Psikuta, A.J.H. Frijns, Local clothing thermal properties of typical office ensembles under realistic static and dynamic conditions, Int. J. Biometeorol. (2018) 15, https://doi.org/10.1007/s00484-018-1625-0.
[22] Y. Lu, F. Wang, X. Wan, G. Song, C. Zhang, W. Shi, Clothing resultant thermal insulation determined on a movable thermal manikin, Part II: Eff. Wind Body Mov. Local Insul. 59 (2015) 1487–1498, https://doi.org/10.1007/s00484-015-0959-0.
[23] D.A. Nelson, J.S. Curlee, A.R. Curran, J.M. Ziriax, P.A. Mason, Determining localized garment insulation values from manikin studies : computational method and results, Eur. J. Appl. Physiol. 95 (2005) 464–473 https://doi.org/10.1007/s00421-005-0033-4.
[24] E. McCullough, B. Jones, A comprehensive data base for estimating clothing insulation, ASHRAE Res. Proj. Rep. RP 411 (1985) 162.
[25] J. Pokorný, J. Fišer, M. Fojtlín, B. Kopečková, R. Toma, J. Slabotínský, M. Jícha, Verification of Fiala-based human thermophysiological model and its application to protective clothing under high metabolic rates, Build. Environ. (2017), https://doi.org/10.1016/j.buildenv.2017.08.017.
[26] E. Mert, S. Böhnisch, A. Psikuta, M.-A. Bueno, R.M. Rossi, Contribution of garment fit and style to thermal comfort at the lower body, Int. J. Biometeorol. 60 (2016) 1995–2004, https://doi.org/10.1007/s00484-016-1258-0.
[27] A. Psikuta, E. Mert, S. Annaheim, R.M. Rossi, Local air gap thickness and contact area models for realistic simulation of human thermo-physiological response, Int. J. Biometeorol. (2018) 1–14 https://doi.org/10.1007/s00484-018-1515-5.
[28] E. Mert, A. Psikuta, M. Bueno, R.M. Rossi, The effect of body postures on the distribution of air gap thickness and contact area, Int. J. Biometeorol. 61 (2017) 363–375, https://doi.org/10.1007/s00484-016-1217-9.
[29] E. Mert, S. Böhnisch, A. Psikuta, M.-A. Bueno, R.M. Rossi, Contribution of garment fit and style to thermal comfort at the lower body, Int. J. Biometeorol. 60 (2016) 1995–2004, https://doi.org/10.1007/s00484-016-1258-0.
[30] A. Joshi, A. Psikuta, M.A. Bueno, S. Annaheim, R.M. Rossi, Mathematical formulation of sensible heat transfer in the spatially heterogeneous skin-clothing-environment system, in: A. Psikuta (Ed.), 12th International Manikin and Modelling Meeting (12i3m), St. Gallen, Switzerland, 2018 https://doi.org/10.5281/zenodo.1404475.
[31] International Organization for Standardization, EN ISO 14505-2 Ergonomics of the Thermal Environment - Evaluation of Thermal Environments in Vehicles - Part 2: Determination of Equivalent Temperature, (2006), p. 25.
[32] International Organization for Standardization, ISO 15831 Clothing - Physiological Effects - Measurement of Thermal Insulation by Means of a Thermal Manikin, (2004), p. 11.
[33] K. Katic, R. Li, W. Zeiler, Thermophysiological models and their applications: a review, Build. Environ. 106 (2016) 286–300, https://doi.org/10.1016/j.buildenv.2016.06.031.
[34] H. Zhang, E. Arens, C. Huizenga, T. Han, Thermal sensation and comfort models for non-uniform and transient environments: Part I: local sensation of individual body parts, Build. Environ. 45 (2010) 380–388, https://doi.org/10.1016/j.buildenv.2009.06.018.
[35] H. Zhang, E. Arens, C. Huizenga, T. Han, Thermal sensation and comfort models for non-uniform and transient environments, part II: local comfort of individual body parts, Build. Environ. 45 (2010) 389–398, https://doi.org/10.1016/j.buildenv.2009.06.015.
[36] Q. Jin, X. Li, L. Duanmu, H. Shu, Y. Sun, Q. Ding, Predictive model of local and overall thermal sensations for non-uniform environments, Build. Environ. 51 (2012) 330–344, https://doi.org/10.1016/j.buildenv.2011.12.005.
[37] H.O. Nilsson, I. Holmér, Comfort climate evaluation with thermal manikin methods and computer simulation models, Indoor Air 13 (2003) 28–37, https://doi.org/10.1034/j.1600-0668.2003.01113.x.
[38] Thermetrics, Seat Test Automotive Manikin, Prod. Broch. (2015) 2. http://www.thermetrics.com/sites/default/files/product_brochures/STAN Manikin Thermetrics 2015.pdf (accessed March 2, 2018).
[39] V.T. Bartels, Thermal comfort of aeroplane seats: influence of different seat materials and the use of laboratory test methods, Appl. Ergon. 34 (2003) 393–399, https://doi.org/10.1016/S0003-6870(03)00058-9.
[40] M. Fojtlín, A. Psikuta, R. Toma, J. Fiser, M. Jícha, Determination of car seat contact area for personalised thermal sensation modelling, PLoS One 13 (2018), https://10.1371/journal.pone.0208599.
[41] E.A. McCullough, B.W. Olsen, S. Hong, Thermal insulation provided by chairs, ASHRAE Trans. Soc. Heat. Refrig. Aircond. Engin. 100 (1994) 795–804 http://www.cbe.berkeley.edu/research/other-papers/McCullough et al 1994 Thermal insulation provided by chairs.pdf.
[42] T. Wu, W. Cui, B. Cao, Y. Zhu, Q. Ouyang, Measurements of the additional thermal insulation of aircraft seat with clothing ensembles of different seasons, Build. Environ. 108 (2016) 23–29, https://doi.org/10.1016/j.buildenv.2016.08.008.
[43] E. Mert, A. Psikuta, M.-A. Bueno, R.M. Rossi, Effect of heterogenous and homogenous air gaps on dry heat loss through the garment, Int. J. Biometeorol. 59 (2015) 1701–1710, https://doi.org/10.1007/s00484-015-0978-x.
[44] ASTM, F2370-16 Standard Test Method for Measuring the Thermal Insulation of Clothing Using a Heated Manikin, (2015), pp. 1–7, https://doi.org/10.1520/F1291-15.1.
[45] A. Psikuta, Local air gap thickness and contact area models for realistic simulation of thermal effects in clothing, Int. J. Biometeorol. (2018) 1–14 https://doi.org/10.1007/s00484-018-1515-5.
[46] D. Fiala, G. Havenith, Modelling human heat transfer and temperature regulation, Mechanobiol. Mechanophysiology Mil. Inj, Springer, Berlin, 2015, pp. 265–302, , https://doi.org/10.1007/978-3-319-33012-9.
[47] D. Fiala, K.J. Lomas, M. Stohrer, Computer prediction of human thermoregulatory and temperature responses to a wide range of environmental conditions, Int. J. Biometeorol. 45 (2001) 143–159, https://doi.org/10.1007/s004840100099.
[48] A. Psikuta, D. Fiala, G. Laschewski, G. Jendritzky, M. Richards, K. Blazejczyk, I. Mekjavič, H. Rintamäki, R. de Dear, G. Havenith, Validation of the Fiala multi-node thermophysiological model for UTCI application, Int. J. Biometeorol. 56 (2011) 443–460, https://doi.org/10.1007/s00484-011-0450-5.
[49] N. Martínez, A. Psikuta, K. Kuklane, J.I.P. Quesada, R.M.C.O. de Anda, P.P. Soriano, R.S. Palmer, J.M. Corberán, R.M. Rossi, S. Annaheim, Validation of the thermo-physiological model by Fiala for prediction of local skin temperatures, Int. J. Biometeorol. 60 (2016) 1969–1982, https://doi.org/10.1007/s00484-016-1184-1.
[50] H.A.M. Daanen, A. Psikuta, 3D body scanning, Autom. Garment Manuf, first ed., Woodhead Publishing, 2017, pp. 237–252, , https://doi.org/10.1016/B978-0-08-101211-6.00010-0.
[51] M. Fojtlín, J. Fišer, M. Jícha, Determination of convective and radiative heat transfer coefficients using 34-zones thermal manikin: uncertainty and reproducibility evaluation, Exp. Therm. Fluid Sci. 77 (2016) 257–264, https://doi.org/10.1016/j.expthermflusci.2016.04.015.
[52] M.G.M. Richards, R. Rossi, H. Meinander, P. Broede, V. Candas, E. den Hartog, I. Holmér, W. Nocker, G. Havenith, Dry and wet heat transfer through clothing dependent on the clothing properties under cold conditions, Int. J. Occup. Saf. Ergon. 14 (2015) 69–76, https://doi.org/10.1080/10803548.2008.11076750.
[53] F. Wang, C. Gao, K. Kuklane, I. Holmer, Determination of clothing evaporative resistance on a sweating thermal manikin in an isothermal Condition : heat loss method or mass loss method? Ann. Occup. Hyg. 55 (2011) 775–783, https://doi.org/10.1093/annhyg/mer034.
[54] B. Koelblen, A. Psikuta, A. Bogdan, S. Annaheim, R.M. Rossi, Comparison of fabric skins for the simulation of sweating on thermal manikins, Int. J. Biometeorol. 61 (2017) 1519–1529, https://doi.org/10.1007/s00484-017-1331-3.
[55] A. Mark, The Impact of the Individual Layers in Multi-Layer Clothing Systems on the Distribution of the Air Gap Thickness and Contact Area, Master Thesis Albstadt-Sigmaringen University of Applied Science, 2013.
[56] International Organization for Standardization, ISO 7730 Ergonomics of the Thermal Environment — Analytical Determination and Interpretation of Thermal Comfort Using Calculation of the PMV and PPD Indices and Local Thermal Comfort Criteria vol 3, (2005), p. 52.
[57] B.E. Ainsworth, W.L. Haskell, M.C. Whitt, M.L. Irwin, A.M. Swart, S.J. Strath, O.W. L, Compendium of Physical Activities: an update of activity codes and MET intensities, Med. Sci. Sports Exerc. 32 (2000) 498–516.
[58] B. Koelblen, A. Psikuta, A. Bogdan, S. Annaheim, R.M. Rossi, Thermal sensation models: validation and sensitivity towards thermo-physiological parameters, Build. Environ. 130 (2018) 200–211, https://doi.org/10.1016/j.buildenv.2017.12.020.
[59] T. Fukazawa, G. Havenith, Differences in comfort perception in relation to local and whole body skin wettedness, Eur. J. Appl. Physiol. 106 (2009) 15–24, https://doi.org/10.1007/s00421-009-0983-z.
[60] H.A.M. Daanen, E. Van De Vliert, X. Huang, Driving performance in cold, warm, and thermoneutral environments, Appl. Ergon. 34 (2003) 597–602, https://doi.org/10.1016/S0003-6870(03)00055-3.
[61] A. Psikuta, J. Frackiewicz-Kaczmarek, E. Mert, M.A. Bueno, R.M. Rossi, Validation of a novel 3D scanning method for determination of the air gap in clothing, Meas. J. Int. Meas. Confed. 67 (2015) 61–70, https://doi.org/10.1016/j.measurement.2015.02.024.
[62] G. Havenith, M.G. Richards, X. Wang, P. Brode, V. Candas, E. den Hartog, I. Holmer, K. Kuklane, H. Meinander, W. Nocker, Apparent latent heat of evaporation from clothing: attenuation and "heat pipe" effects, J. Appl. Physiol. 104 (2007) 142–149, https://doi.org/10.1152/japplphysiol.00612.2007.
[63] S. Ueno, S.I. Sawada, Correction of the evaporative resistance of clothing by the temperature of skin fabric on a sweating and walking thermal manikin, Textil. Res. J. 82 (2012) 1143–1156, https://doi.org/10.1177/0040517511427966.
[64] F. Wang, K. Kuklane, C. Gao, I. Holmér, Development and validity of a universal empirical equation to predict skin surface temperature on thermal manikins, J. Therm. Biol. 35 (2010) 197–203, https://doi.org/10.1016/j.jtherbio.2010.03.004.

Paper III

Thermal model of an unconditioned, heated and ventilated seat to predict human thermo-physiological response and local thermal sensation.

Miloš Fojtlín[1,2], Agnes Psikuta[2*], Jan Fišer[1], Jan Pokorný[1], Róbert Toma[1], Simon Annaheim[2], Miroslav Jícha[1], and René M. Rossi[2]

[1]Brno University of Technology, Faculty of Mechanical Engineering, Energy Institute, Department of Thermodynamics and Environmental Engineering, Czech Republic

[2]Empa Swiss Federal Laboratories for Material Science and Technology, Laboratory for Biomimetic Membranes and Textiles, St. Gallen, Switzerland

*Corresponding author: agnes.psikuta@empa.ch; Empa Swiss Federal Laboratories for Material Science and Technology, Lerchenfeldstrasse 5, 9014 St. Gallen, Switzerland

ABSTRACT

Local conditioning technologies such as seat heating and ventilation have been shown to improve thermal sensation and comfort, with reduced energy demands compared to conventional methods of heating and cooling. Investigation of the conditioning effectivity is demanding in terms of time and resources, as it is mainly based on human subject or thermal manikin testing. More effective modelling approaches are therefore needed for the development and assessment of novel solutions. One promising method of rapidly investigating a wide range of environmental conditions is thermo-physiological and thermal sensation modelling. Until now, however, one of the most important properties of the seat, its thermal diffusivity, has been neglected in such simulations. We therefore developed a methodology that involves the seat thermal capacity and seat conditioning, coupled with a multi-node thermo-physiological model and thermal sensation models, to demonstrate the importance of these factors. The modelling results were validated against our own experimental data and data from the literature for unconditioned, heated and ventilated automotive seats. The root mean square deviation (RMSD) and bias of the local skin temperatures were within the standard deviation of the measurement, typically within 1°C. In the case of the predicted local thermal sensations, we found the RMSD and bias to be below two standard deviations of the human votes in two out of three of the thermal sensation models examined. Less accurate predictions were found for the seat contact, where further model refinement is needed.

KEYWORDS:

Heating; Ventilation; Seat; Human; Thermo-physiology; Fiala model; Thermal sensation

1 Introduction

Ensuring thermal comfort for occupants of indoor environments using heating ventilation and air-conditioning (HVAC) systems is typically related to substantial energy consumption and the production of environmental pollutants [1]. This topic is particularly critical in the development of electric mobility, where energy used for microclimate management is supplied at the expense of the vehicle's driving range. Here, the thermal management of a passenger compartment is challenging for the following reasons:

- The transient and asymmetric thermal environment;
- The broad range of radiant, air, and contact temperatures (between approximately −20° and 60°C);
- Substantial solar gains through windows and the greenhouse effect;
- Low thermal insulation of the cabin and the consequent high impact of ambient conditions on the cabin microclimate;
- High ventilation rates and local air velocities of up to 2 m/s [2];
- Contact with surrounding surfaces such as seats (18% of total body area [3]), and the application of local conditioning technologies such as heated and ventilated seats.

The conditions described above may cause thermal discomfort and negatively influence the cognitive abilities of a driver [4], [5]. According to Alahmer et al. [6], the most critical period of exposure is a transient and non-uniform phase with rapid cooling of a *hot-soaked cabin*. Furthermore, approximately 85% of car trips made within Europe are shorter than 18 km and no longer than 30 minutes [7], and highly transient situations involving intensive cooling or heating are most likely to occur. New solutions with localised delivery of heat or cold are therefore being investigated in order to address these situations. Research done on heated and ventilated (cooled) seats indicates their potential in rapidly enhancing thermal comfort while requiring low energy consumption [8]–[14]. The lower energy demands are possible through targeted delivery of the heating or cooling power exactly where needed, rather than treating the entire air volume around the occupant. This broadens the boundaries of comfortable ambient temperatures and may bring energy savings of up to 40% on the conventional HVAC systems [12], [13]. Such studies are normally carried out with human participants or thermal manikins, making investigation of the effectivity of these local conditioning solutions time- and resource-consuming. Thus, tools for rapid design and optimisation of personalised thermal comfort systems are needed.

A promising solution to this demand is the modelling of the thermo-physiological response and local human thermal sensation in a dynamically changing thermal environment. The review paper by Katic et al. [15] lists and discusses differences among the contemporary thermo-physiological models in detail. For instance, the most frequently cited models are the

65MN model by Tanabe et al. [16], the Berkeley model [17], [18], and several Fiala-based models – ThermoSEM by Kingma [19], FPCm by ErgonSim [20], [21], Fiala-FE by Theseus FE [22], FMTK by Pokorny et al. [23], and the Human Thermal Module in TAITherm by Thermoanalytics Inc. [24]. These models are all segmented into at least ten body parts, in order to cover the main body segmentation of the upper and lower limbs, torso and head, thus allowing the investigation of local thermal responses and the consequent modelling of local thermal sensation. However, for reliable applications of the models, their validation is crucial. One of the best documented and often implemented models is the FPCm5.3 (Fiala Physiological and Comfort model – FPCm5.3, Ergonsim, Germany [20], [21]). The major advantage of FPCm5.3 is its broad validation of both mean and local responses in a range of air temperatures from 5 to 50°C, exercise levels from 0.8 met to 10 met, and for steady and transient conditions [25]–[28].

Although numerous thermal sensation models are available [29], the number of well-documented and validated local thermal sensation models is limited [30]. One of the models developed specifically for automotive applications is the MTV model by Nilsson [31], [32], which later became part of the ISO 14505 standard [33]. This model correlates the mean thermal vote with an equivalent temperature (t_{eq}), defined as the temperature of a uniform enclosure in which a person would lose heat at the same rate as in the actual environment [34]. The advantage of this method in practical applications is that the calculation of t_{eq} can be based on heat flux data from a human body, a thermal manikin, or an equivalent temperature sensor [35]. Another automotive-oriented approach is the thermal sensation and comfort (TSZ) model proposed by Zhang et al. [36], [37]. The major focus of the development of this model was the local heterogeneous cooling conditions, with rather high gradients typical of car cabins. Here, the thermal sensation is predicted on the basis of multiple regressions of skin and core temperatures with human thermal sensation votes. Finally, the TSV model proposed by Jin et al. [38] represents an approach predicting local and global thermal sensation on the basis of skin temperatures only. The model was developed based on a pool of Chinese subjects by applying local ventilation to various body parts, thus creating asymmetric thermal conditions.

Transparently validated and well documented methodology to model the effects of conditioned seats on human thermophysiology is scarcely available in the literature. An example of a one-dimensional dynamic thermal model to predict skin temperatures, heat fluxes, and thermal sensation in the seat-occupant interface with heating and ventilation was proposed by Karimi et al. [39], [40]. While the paper described a broad physical background of the heat and mass transfer, the particular material properties and validation data to achieve presented results were absent. The model validation for winter and summer driving conditions showed the estimated average error below 21% in skin temperatures. The study demonstrated

advantages of one-dimensional modelling such as a low number of input parameters, low computational power demands, and potentially realistic outputs in a defined range of conditions.

A more advanced approach based on three-dimensional transient numerical model to resolve the seat-occupant contact of a ventilated seat was proposed by Shin et al. [41]. The model validation with human data revealed large discrepancies of up to 12°C for skin and seat surface temperatures, which significantly limits the model for thermal sensation modelling applications. Further, the higher resolution of the model also requires both precise boundary conditions addressing conduction, convection, evaporation, and radiation in three-dimensional space, which are difficult to obtain as well as lead to higher computing demands and times.

The human subject studies on thermo-physiological responses to seats with conditioning technologies seldom report the full set of information that could be used for validation of modelling [8], [12], [42]–[45]. This information includes the time-dependent skin and seat surface temperatures, detailed information about clothing, local thermal sensation, and heat exchange at the contact with body parts. The last parameter is the most critical, and is usually unknown or is presented as the heating power delivered to the seat rather than the heat exchanged with a human body [8], [42]. Since the seat has a substantial heat capacity and a heterogeneous structure, an unknown proportion of the delivered heat dissipates into the seat. Additionally, in the first moments of contact with the seat, the temperature gradient between the seat surface and skin can be high, and may be accompanied by rapid cooling or heating of the skin and intense discomfort. This important heat exchange during the first contact is dependent on the thermal diffusivity of the seat, which is calculated from the thermal conductivity, the density, and the heat capacity of the seat. However, the seat boundary condition is usually addressed in the form of thermal and evaporative resistances [33], [34], [46], [47], which are dependent only on the thermal conductivity of the seat, and are therefore clearly insufficient.

The aim of this study is to present a complex methodology for reliable and efficient simulations of the effects of unconditioned, heated, and ventilated seats on human thermo-physiology and thermal sensation in steady-state and transient conditions. To do so, we proposed and transparently validated a physical one-dimensional model of transient local heat transfer between a seat and its occupant. Most importantly, a complete information package was presented, which enables instant model implementation. Secondly, to demonstrate the model´s applicability in real-life situations, the coupling methodology of the physical model and the model of human thermoregulation FPCm5.3 was devised to provide the local boundary conditions at the regions of the body that are affected by the seat. The thermo-physiological model outputs were supplied to three local thermal sensation models (MTV, TSZ, and TSV) to predict local thermal sensation. Finally, we conducted own human

trials to validate in detail the developed simulation aproach using comparison of heat fluxes, skin and seat temperatures, and thermal sensation votes. The validation was carried out under both cool and hot environmental conditions, including conditioning technologies such as seat heating to a constant temperature, constant heat flux and seat ventilation.

2 Methods

2.1 Development of the seat heat transfer model

The heat transfer between a human body and a seat can be described by fundamental heat transfer principles in three-dimensional space. A thermal system consisting of a human body, clothing, seat and the ambient environment can be solved using energy conservation in control volumes for each node described by Equation (1):

$$Q_{stor,m} = Q_{gen,m} + Q_{cond,m} + Q_{conv,m} + Q_{evap,m} + Q_{rad,m} \quad (1)$$

where *m* denotes an arbitrary node, $Q_{stor,m}$ (W) is the stored heat within the volume, $Q_{gen,m}$ (W) the generated heat within the volume, $Q_{cond,i}$ (W) the heat transfer by conduction, $Q_{conv,i}$ (W) the heat transfer by convection, $Q_{evap,i}$ (W) the heat transfer by evaporation, and $Q_{rad,I}$ (W) the heat transfer by radiation.

Equation (1) can be simplified to a one-dimensional problem if we assume that the dominant heat flux is in a direction perpendicular to the plane of the seat. Compared to three-dimensional models, the simplifications are expected to be counterbalanced by substantially lower number of input parameters and lower computing power demands. Another simplification, in our model, was related to the evaporation, which was replaced by a heat sink or a prescribed temperature profile at the seat surface. While the main cause of cooling in the ventilated seat is sweat evaporation, in practical applications, it is not feasible to determine the parameters necessary for psychrometric calculations precisely. This is especially related to the measurement of the airflow, air humidity, and air temperature in the contact, which are burden with a substantial uncertainty. The proposed approach is expected to yield an equivalent heat flux density, as if the evaporation was assumed.

With respect to the previous assumptions, for any internal node *m* between two solid materials *A* and *B*, $Q_{conv,m}$, $Q_{evap,m,}$ and $Q_{rad,m}$ from Equation (1) can be neglected due to the high evaporative resistance of the seat and the negligible convection and radiation in the highly compressed layers of clothing and seat. The solution to Equation (1) under these conditions can be obtained using the finite-difference method; this yields an explicit finite-difference equation that considers half of the thickness of materials *A* and *B* for a node (2):

$$k_A \frac{T_{m-1}^p - T_m^p}{\Delta x_A} + k_B \frac{T_{m+1}^p - T_m^p}{\Delta x_B} + \dot{q}_{gen,A} \frac{\Delta x_A}{2} + \dot{q}_{gen,B} \frac{\Delta x_B}{2} = \left(\rho_A c_A \frac{\Delta x_A}{2} + \rho_B c_B \frac{\Delta x_B}{2}\right) \frac{T_m^{p+1} - T_m^p}{\Delta t} \quad (2)$$

where the subscripts *A, B* denote the materials; the superscript *p* is used to denote the time dependence of the temperature *T*, and the new time derivative is associated with p+1; *k* (W/mK) is the heat conductivity; *Δx* is the discretised thickness of the control volume; q_{gen} (W/m^3) is the heat generation per unit volume; ρ (kg/m^3) is the material density; and *c* (W/mK) is the specific heat of the material.

For nodes that lie at the border with the ambient air, such as at the back of the seat, we neglected evaporation due to the high evaporative resistance of the seat. Since a seat in the cabin is partially shaded from the sun, presumably meaning that the temperature difference between the seat and the adjacent surfaces in the cabin is low, we also neglected the contribution of the radiative heat exchange with the cockpit on the thermal balance of the seat. Thus, the explicit solution for heat exchange is described by Equation (3):

$$h\left(T_{\infty}^{p} - T_{m}^{p}\right) + k\frac{T_{m-1}^{p} - T_{m}^{p}}{\Delta x} + \dot{q}_{gen}\frac{\Delta x}{2} = \rho\frac{\Delta x}{2}c\frac{T_{m}^{p+1} - T_{m}^{p}}{\Delta t} \quad (3)$$

where *h* is a convective heat transfer coefficient (m^{2}K/W) and T_{∞}^{p} is the ambient air temperature.

Equations (2) and (3) were applied to solve for the heat transfer at the seat cushion and backrest, respectively, using a discretised time step of 0.05 sec. As a representative human body part in the contact with backrest, posterior thorax and abdomen were selected. Similarly, posterior thighs and pelvis were chosen to represent body parts in the contact with seat cushion. An overview of the nodes and constants used in this study is presented in Table 1. The properties of human tissues were adopted from Fiala et al. [48] and the properties of the seat from Kolich et al. [49]. The initial temperatures of the human tissues were taken from the Fiala Physiological and Comfort model (FPCm5.3, Ergonsim, Germany) [20], [21] at the moment of just before sitting down on the seat. The initial temperature distribution of the seat was assumed to be homogeneous and equal to the pre-conditioning air temperature in the chamber.

Table 1. Overview of the calculation nodes and their properties

BACKREST / SEAT CUSHION	**NODES OF HUMAN BODY** [48]					**NODES OF ADJACENT LAYERS**			
	LUNGS	BONE	MUSCLE	FAT	SKIN	CLOTHING [50] (cotton)	SEAT COVER [50] (leather/polyester)	HEAT SOURCE/SINK	PU CUSHION
Δx (m)	0.077 / -	0.012 / 0.022	0.034 / 0.026	0.003 / 0.005	0.002	< 0.001*	0.002‡	0.001	0.050‡
k (W/mK)	0.280	0.750	0.420	0.160	0.470	0.040	0.140 / 0.050	-	0.048
c_p (J/kgK)	3718	1700	3768	2300	3680	976	1500 / 976	-	1331
ρ (kg/m^3)	550	1357	1085	850	1085	365	365 / 365	-	62
q_{gen} (W/ m^3)	600	-	684	58	368	-	-	†	-

**assuming uniform clothing coverage; † value depending on the heating/cooling strategy, positive heat flux for heating;‡may vary for specific seats.*

2.2 Validation strategy and integration of the seat heat transfer model into FPCm5.3

The workflow of the validation strategy is depicted in Figure 1, and consists of three steps. The validity of the outputs was assessed against the experimental data after each step. Firstly, the heat flux density at the seat-human interface, calculated by the heat transfer model, was validated against our own measurements for cases at 18°C and 41°C, as other datasets were not available. Secondly, the time-dependent heat flux calculated by the seat heat transfer model was prescribed using the FPCm5.3 to predict the human thermal responses. Here, validation was focused on the predicted local skin temperatures, with and without seat contact. Thirdly, the FPCm5.3 was coupled with three local thermal sensation models to predict the thermal sensation at nine body sites. The pool of cases examined here comprises unconditioned seats, two modes of seat heating, and ventilated seats under a range of environmental conditions from 5°C to 41°C (details in Table 2).

Table 2. Complete overview of the cases used for validation of the methodology

	Case	Preconditioning of subjects 60 minutes t_{amb} (°C)/ t_{rad} (°C)/ Rh (%)/ w_{air} (m/s)	Chamber exp. t_{amb} (°C)/ Rh (%)/ w_{air} (m/s)	Seat conditioning	Males Un-cond./ Cond.	Females Un-cond./ Cond.	BMI M/ F ($kg.m^{-2}$)	Available data for validation
This study	18 °C	22.5 / 21 / 40 / 0.05	18 / 40 / 0.15	Uncond./ Heated const. temp.	8 / 14	2 / 6	25 / 23	8 skin temp**; backrest & seat cushion surf. temp and heat flux; TS votes
	41 °C	25 / 21 / 30 / 0.05	41-25* / 30 / 0.15	Uncond. / Ventilated	7 / 7	2 / 2	26 / 28	8 skin temp; backrest & seat surf. temp and heat flux; TS votes
Oi et. al [8]	5 °C	22 / 22 / 50 / 0.05	5 / 50 / 0.15	Uncond./ Heated const. HF	8 / 8	-	18.6 / -	Skin temp at backrest & seat cushion
	10 °C	22 / 22 / 50 / 0.05	10 / 50 / 0.15	Uncond./ Heated const. HF	8 / 8	-	18.6 / -	Skin temp at backrest & seat cushion
	15 °C	22 / 22 / 50 / 0.05	15 / 50 / 0.15	Uncond./ Heated const. HF	8 / 8	-	18.6 / -	Skin temp at backrest & seat cushion
	20 °C	22 / 22 / 50 / 0.05	20 / 50 / 0.15	Uncond./ Heated const. HF	8 / 8	-	18.6 / -	Skin temp at backrest & seat cushion

t_{amb} – ambient air temperature; t_{rad} – mean radiant temperature; Rh – relative air humidity; w_{air} – mean air speed; BMI – body mass index;

**25°C reached after 20 min of exposure; **skin temperatures unavailable for unconditioned case*

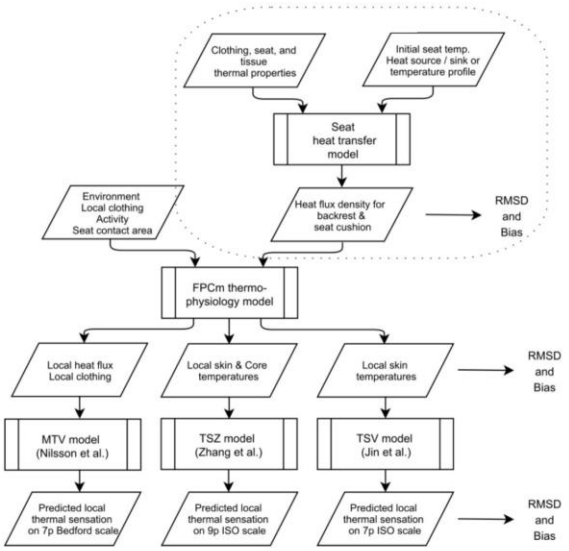

Figure 1. Overview of the methodology comprising the seat heat transfer model, FPCm model, and three thermal sensation models (references: MTV [31], TSZ [36], [37], and TSV [38]). The highlighted parts were developed in this study.

2.2.1 Human subjects and clothing

The first dataset was acquired at the Brno University of Technology (BUT) based on our own measurements in a climatic chamber (Figure 2). All participants were informed about the experiment and gave written consent for their voluntary participation in the study. The research was approved by the Ethical Committee at the Department of Biomedical Engineering, BUT. To ensure similar initial conditions, the participants were instructed not to eat, smoke, or exercise for at least two hours before the experiment as well as to wear their own indoor clothing for the relevant season (summer or winter). In the case of the cool condition, this was typically a cotton T-shirt or a short-sleeved shirt, light pullover, trousers, underwear, socks, and a pair of shoes (thermal insulation of 1.1 clo). In the hot condition, the clothing consisted of a T-shirt or a short-sleeved shirt, light trousers, underwear, socks, and a pair of light shoes (thermal insulation of 0.6 clo).

Figure 2 Experimental setup in the climatic chamber at BUT. Left – control/heated seat with textile upholstery. Right – ventilated seat with leather upholstery. Seats were placed in the geometrical centre of the chamber.

The second set of experimental data was collected from study by Oi et al. [8], who examined a pool of subjects consisting of eight male university students wearing an undershirt, long-sleeved shirt, jacket, underpants, trousers, socks and shoes, with an overall thermal insulation of 0.9 clo. The following mean characteristics were presented, with standard deviation indicated in brackets: age 22.5 years (1.1 years); height 175.0 cm (1.3 cm); weight 57.2 kg (3.2 kg).

2.2.2 Seat instrumentation and skin temperature measurements

In our experiments, serial-production front seats from a middle-range passenger car were used with following construction layers: a polyester cover, resistance heating wire, polyurethane foam cushioning, and metal inner chassis (Figure2, for more details on seat see [3] and chamber [51]). Exposures with the ventilated seat were equipped with a similar seat having perforated leather upholstery. In order to ensure identical initial conditions before the human exposures, the seats were conditioned in the climatic chamber for at least two hours. The seats were instrumented with two heat flux blankets (Mahöle Messtechnik, Germany), one of which was placed at the backrest and one at the seat cushion. The blanket had a resolution of 16 × 16 points distributed in a square grid of 48 × 48 cm. Each point measured heat flux indirectly using two thermistors (relative accuracy < 0.3°C; response time < 1.5 s) separated by a solid with a known thermal resistance. This allowed us to determine both the heat fluxes and seat temperatures simultaneously.

The participant's local skin temperature was measured at eight body sites according to the ISO 9886:2004 standard [52]: forehead, right scapula, left upper chest, right upper arm, left forearm, left hand, right anterior thigh, and left calf. The eight skin temperatures were averaged using the weighting coefficients from the standard [52] to calculate the mean skin temperature. The local skin temperatures were measured with oscillator-based digital thermometers (iButton, Maxim Integrated,

USA, accuracy ± 0.5 °C). The sensors were attached to the participants' skin using medical tape (Hypafix 16002, BSN Medical GmbH, Germany) made from nonwoven polyester with acrylic adhesive, cut to 35 mm × 50 mm patches [53].

Oi et al. [8] used automotive front seats for the experimental exposures with unconditioned (control) and heated seats. The seat construction comprised a leather upper cover, silicone rubber heating pads, polyurethane foam cushioning, and metal inner chassis. The heating was provided for both the seat cushion and the backrest with an equal heating power density of 268 W/m^2 [8]. The skin temperature was measured at 16 body sides using epoxy-coated thermistor probes (Nikkiso-Therm, Musashino, Japan) attached to the skin surface by surgical tape.

2.2.3 Human exposures with unconditioned (control) seat

The cool exposure at 18°C was carried out at BUT. The participants were pre-conditioned in thermo-neutral conditions for one hour while sitting. The chamber session was designed as a benchmark case for steady indoor environments with ambient temperature below thermo-neutrality and duration of 30 minutes. This measurement provided crucial data on heat flux density in the seat contact, development of local skin temperatures as well as subjective local thermal sensation votes.

The hot exposure at 41°C was also carried out at BUT. This case was design to mimic hot summer conditions, and the rapid cooling of an overheated cabin by a conventional air-conditioning system. Here, the chamber exposure consisted of 10 minutes of walking at a pace of 4 km/h to initiate sweating, after which the participants were seated on an seat for 30 minutes. At this point, chamber cooling was initiated (at a cooling rate of −0.8 °C/min) for the first 20 minutes of the exposure to reach the pre-conditioning conditions (t_{air} = 25°C, Rh 30%, w = 0.15 m.s^{-1}). A detailed summary of the exposures is presented in Table 2.

The last dataset for unconditioned seats was adopted from Oi et al. [8] (Table 2), including data about global thermal sensation and comfort in a climatic chamber at constant environmental conditions at 5°C, 10°C, 15°C and 20°C. Local skin temperature, for buttocks and back, were obtained based on a personal communication with the main author of 24th October 2017. The experimental procedure started with one hour of subject´s preconditioning under thermo-neutral conditions (Table 2). After this period, the participants were exposed to the automotive seat in the climate chamber for 20 minutes.

2.2.4 Human exposures with seat heated to constant heat flux and constant temperature

For the case at 18°C, the experimental procedure started in the same way as for the unconditioned seat, followed by 30 min of chamber exposure with heated seats to constant temperature of 38°C. The seat heating was initiated immediately after the participants took their seats in the climate chamber. To maintain the seat surface temperature, a feedback sensor (DS18S20, Dallas Semiconductor, USA, accuracy ± 0.5°C) was sewn onto the seat cushion in the contact area of the buttocks

and was used. The standard deviations of the seat surface temperatures at the seat cushion and the backrest were 0.8°C and 1.8°C, respectively. The participants could turn off the heating at any time; however, none of them used this option. The data from the constant heat flux heating mode were adopted from Oi et al. [8]. The experimental protocol and the equipment were identical to the unconditioned seat cases at 5°C, 10°C, 15°C and 20°C (Section 2.2.3).

2.2.5 Human exposures with ventilated seat

The experimental protocol for the exposure using the ventilated seat is identical as the procedure from the unconditioned seat at 41°C (Section 2.2.3). The seat was set to its maximal ventilation rate, extracting approximately 18 m^3/h of air from the seat and back cushion when occupied. However, this value depends on the proportions of the occupant´s body and one has to be cautious in its interpretation. The resulting airflow through the seat ventilation system also contains a part of the air that passes through the unoccupied parts of the seat. Therefore, it should not be used as a boundary condition for the ventilated seat modelling.

2.2.6 Thermo-physiological modelling

We used the Fiala-based thermo-physiological model (FPCm5.3, Ergonsim, Germany) [21] to reproduce the human trials listed in Table 2 and described in Sections 2.2.3–2.2.5. The model was selected based on its extensive validation and documentation in a range from 5 to 50°C and exercise levels from 0.8 met to 10 met [25]–[28]. The model yields predicted thermal responses for an average person (height 1.69 m, weight 71.4 kg and skin surface 1.83 m^2) for 13 individual body parts, which are further divided into spatial sectors. The local clothing thermal properties were adopted from our previous study [54], in which we examined comparable garments to the ones in this study using state-of-the-art methods. To achieve the most realistic results, measurements were carried out in the sitting position, since body posture has a strong influence on the local thermal and evaporative resistance of clothing.

The boundary condition at the seat contact was treated as a prescribed heat flux to the posterior thighs, posterior hip, posterior abdomen and posterior thorax [3]. The corresponding heat fluxes were calculated using the seat heat transfer model presented in Section 2.1. Additionally, to illustrate the difference between our new approach to seat simulation and previous methods, such as treating the seat as an additional resistance, we carried out two simulations based on the 5°C case and reported the temperatures at the seat contact, with and without use of the seat heat transfer model. To achieve this, the unconditioned seat in the 5°C case was approximated as additional thermal and evaporative resistances of 0.7 $m^2K \cdot W^{-1}$ and 120 $m^2Pa \cdot W^{-1}$, respectively [46]. The clothing area factor f_{cl} of the seat, defined as the ratio of the seat surface area to the body surface area, was estimated as 2.0 units. In the same case with heating, a heat flux density of 268 W/m^2 was applied directly to the skin in the FPCm5.3. This simulation was carried out to demonstrate the differences between the complex approach

represented by the seat heat transfer model with heat generation and the assumption of adiabatic behaviour of the seat cushioning. In this way, a constant heat flux is transferred to the human body, disregarding the thermal effects of the seat.

2.3 Coupling with the thermal sensation models

The outputs from the seat heat transfer model and FPCm5.3 indicate the thermal state of a human body. Despite the complex mechanisms responsible for human thermal perception, this information can be translated into an average predicted thermal sensation vote using a thermal sensation model [55]. Such an approach is applicable to a given set of conditions defined by metabolic activity, clothing and a range of environmental conditions. In asymmetric thermal environments such as cabins, it is meaningful to use local thermal sensation predictions rather than global ones, due to the difficulties in identifying the prevailing thermal sensation when contradictory sensations are perceived [56].

As shown in the diagram in Figure 1, the outputs from thermo-physiological modelling were processed using three local thermal sensation models for a seated position, to investigate their performance. Firstly, the model by Nilsson [31] was used; this is based on heat transfer (MTV) as part of the ISO 14505 [33], and was implemented due to its standardisation and practical applicability. The model uses a seven-point Bedford scale that combines thermal sensation votes with thermal comfort (much too cold, too cold, cold but comfortable, neutral, hot but comfortable, too hot, much too hot). The model is applicable over a range of ambient temperatures from 19°C to 29°C. Next, we applied the model by Zhang (TSZ) [36], [37] dedicated to vehicular cabins, which predicts local thermal sensation using an extended nine-point ISO scale with two additional extreme thermal sensation votes (very cold, very hot). The model was developed for a range of air temperatures between 20°C and 33°C. Finally, we implemented the model by Jin et al. (TSV) [38], which uses local skin temperatures as inputs and yields a local thermal sensation on the seven-point ISO scale (cold, cool, slightly cool, neutral, slightly warm, warm, hot) [57]. Since the division of a human body into segments is not identical in each model, in some cases two body parts (e.g. upper and lower arms) were merged into a single segment and the area-weighted average was used to obtain the resulting thermal sensation.

2.3.1 Verification of skin temperatures and thermal sensation predictions

Before using the outputs from the FPCm5.3 to model thermal sensation, the predicted local skin temperatures were verified against human data for the 18°C and 41°C cases, since the local skin temperatures for other cases, as reported by Oi et al., were not available. Similarly, in order to verify the predicted local thermal sensation votes, local human thermal sensation votes were collected from the participants for the 18°C and 41°C cases at major body sites (back/backrest, buttocks/ seat cushion, face, chest, arms, hands, anterior thighs, lower legs, and feet). The votes were recorded at the end of the preconditioning phase and every three minutes during the actual chamber exposure, using the seven-point ISO scale [57] (*−3 Cold, −2 Cool, −1 Slightly cool, 0 Neutral, 1 Slightly warm, 2 Warm, 3 Hot*).

2.3.2 Statistical analysis of thermo-physiological and thermal sensation responses

One-minute averages and their standard deviation were calculated for each parameter measured. The accuracy of all parameters predicted by the seat heat transfer model, FPCm5.3, and the thermal sensation models (heat flux, seat temperatures, skin temperatures, and thermal sensation votes) was assessed by means of root mean square deviation (RMSD), which measures the average difference between the measured and predicted values. The second descriptor examined here, bias, is expected to be close to zero for unbiased simulations, and a negative value indicates an over-prediction of the examined value. Predictions were assumed to have high precision if the RMSD and bias were within the standard deviation of the measurement.

3 Results

3.1 Validation of the seat heat transfer model and its integration into FPCm5.3

The validation of the seat heat transfer model was carried out on the basis of heat fluxes measured separately at the surface of the backrest (corresponding body parts: posterior thorax and abdomen) and seat cushion (corresponding body parts: posterior thighs and pelvis). These measurements were available only for cases at 18°C and 41°C. In the next step, the predicted heat fluxes from the seat heat transfer model were used as a seat boundary condition in FPCm5.3. Here, cases from literature at 5°C, 10°C, 15°C, and 20°C were available as well as our own measurement at 18°C and 41°C.

Exposure to the unconditioned seat and a summary of the RMSD and bias of the simulations with the FPCm5.3 model for all control seat cases is depicted in Figure 3, where the development of the contact skin temperatures at 5°C, seat surface temperatures at 18°C and 41°C, and heat fluxes at 5°C, 18°C and 41°C over 20 minutes are shown. A positive heat flux represents heat loss from the skin. To quantify the error induced by addressing the seat by thermal and evaporative resistances, neglecting the seat thermal mass, we carried out such case at 5°C (Figure 3, dotted line) and compared it to the proposed methodology (Figure 3, dashed line).The experimental data were depicted as circles.

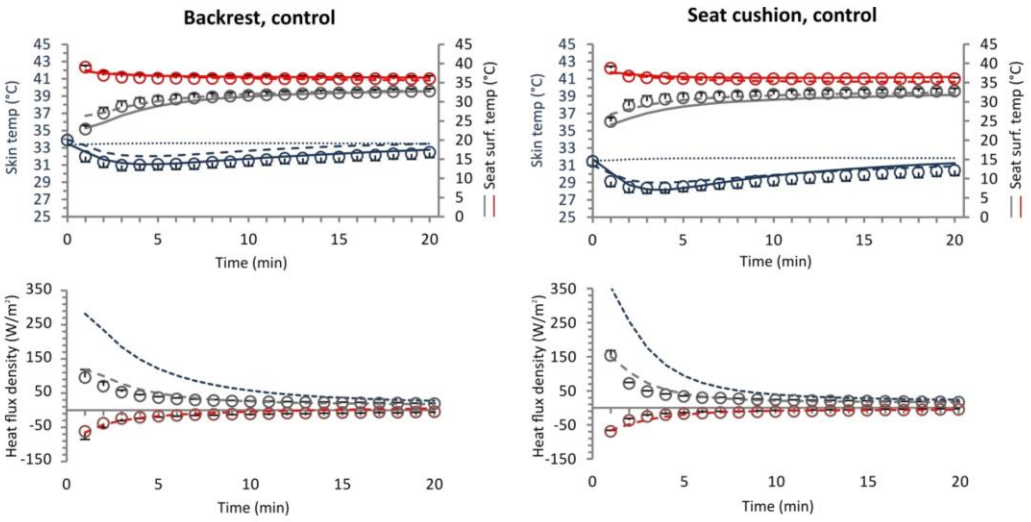

		Backrest, control			Seat cushion, control		
	Case	RMSD	Bias	SD	RMSD	Bias	SD
Contact temp. (°C)	5°C	0.3	-0.2	0.6	0.6	-0.5	0.7
	5°C *	1.9	-1.8	0.6	2.5	-2.4	0.7
	10°C	0.5	-0.5	0.5	0.7	-0.7	0.4
	15°C	0.4	-0.4	0.5	0.4	-0.4	0.6
	18°C	0.8	0.4	0.9	1.5	1.3	0.5
	20°C	0.2	-0.2	0.3	0.4	-0.3	0.6
	41°C	0.5	-0.4	0.9	0.5	-0.4	0.4
Contact heat flux (W/m²)	18°C	9.2	-3.3	2.9	8.1	-2.1	1.6
	41°C	12.6	10.0	7.6	3.5	1.5	3.5

Figure 3 Unconditioned (control) seats: skin (5°C case) and seat surface temperatures (18°C and 41°C cases), and heat fluxes (5°C, 18°C and 41°C cases) at the seat-body contact area as well as RMSD, bias, and standard deviation (SD, also shown as error bars in the graphs) of the data. Seating began at time 0 min. Case 5°C * depicts results of simulations where the seat was represented by thermal and evaporative insulation.

Figure 4 depicts the development of the contact skin temperatures (5°C case) and seat surface temperatures (18°C case), and heat fluxes (18°C and 41°C cases) for 20 minutes of exposure to the heated seat, together with a summary of the RMSD and bias of the simulations from the thermo-physiological model from all heated seat cases. In addition to the measured data (circles), the FPCm5.3 simulation results (continuous line), corresponding calculations using the seat heat transfer model (dashed lines), and dotted lines illustrate the development of skin temperature when the heat flux density of 268 W/m^2 (reported by Oi et al. [9]) is prescribed in the FPCm5.3 simulations directly at the skin, neglecting the presence of the seat.

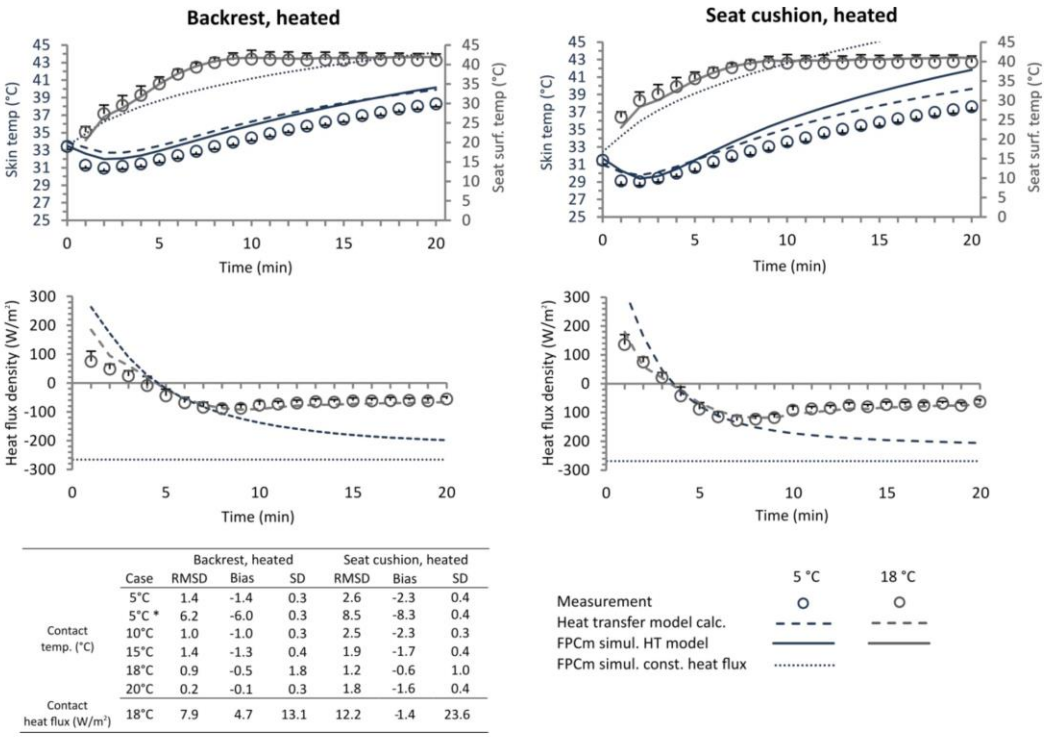

		Backrest, heated			Seat cushion, heated		
	Case	RMSD	Bias	SD	RMSD	Bias	SD
Contact temp. (°C)	5°C	1.4	-1.4	0.3	2.6	-2.3	0.4
	5°C *	6.2	-6.0	0.3	8.5	-8.3	0.4
	10°C	1.0	-1.0	0.3	2.5	-2.3	0.3
	15°C	1.4	-1.3	0.4	1.9	-1.7	0.4
	18°C	0.9	-0.5	1.8	1.2	-0.6	1.0
	20°C	0.2	-0.1	0.3	1.8	-1.6	0.4
Contact heat flux (W/m²)	18°C	7.9	4.7	13.1	12.2	-1.4	23.6

Figure 4 Heated seats: skin temperatures (5°C case), seat surface temperatures (18°C case), and heat fluxes (5°C and 18°C cases) at the seat-body contact area and the RMSD, bias and standard deviation (SD, also shown as error bars in the graphs) of the data. Seating started at time 0 min. The 5°C * case depicts results of simulations where the heated seat was represented by a constant heat flux applied to the skin.

Figure 5 shows the seat surface temperatures and heat fluxes for 20 minutes of exposure to the ventilated seat (41°C case) together with an overview of the RMSD and bias of the FPCm5.3 simulations. The measured data are depicted via circles, FPCm5.3 simulation results via continuous lines, and calculations using the seat heat transfer model by dashed lines.

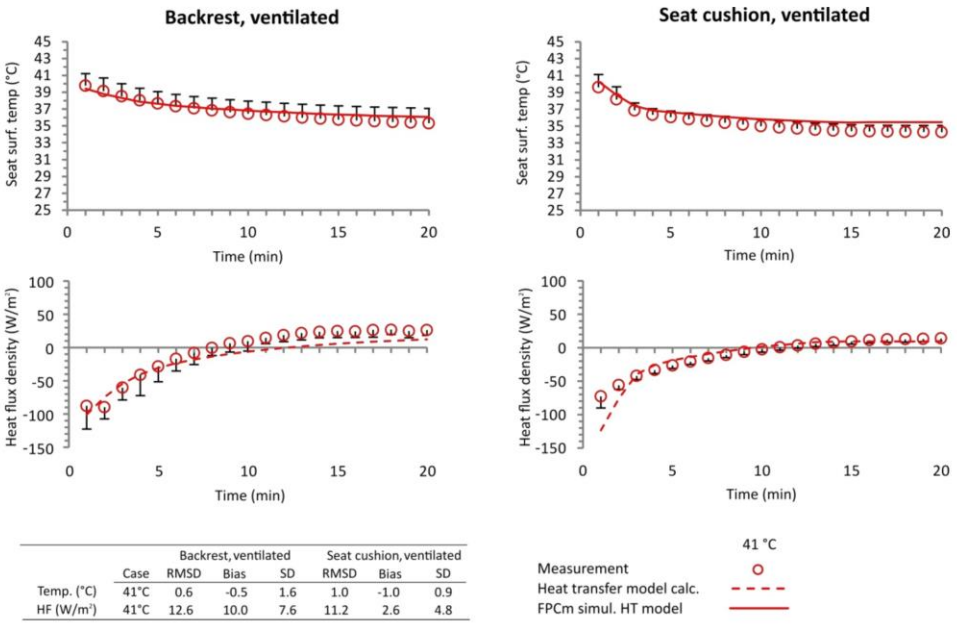

		Backrest, ventilated			Seat cushion, ventilated		
	Case	RMSD	Bias	SD	RMSD	Bias	SD
Temp. (°C)	41°C	0.6	-0.5	1.6	1.0	-1.0	0.9
HF (W/m²)	41°C	12.6	10.0	7.6	11.2	2.6	4.8

Figure 5 Ventilated seats: seat surface temperatures and heat fluxes in contact with the ventilated seat and the RMSD and bias for temperatures and heat fluxes from the FPCm simulations. The error bars depict standard deviation. Seating began at time 0 min.

Table 3 presents the RMSD, bias and mean standard deviation of the predicted data in comparison with the experimental data for skin temperatures in regions without seat-body contact, which were available only for the 18°C and 41°C cases. The RMSD and bias were calculated throughout the whole duration of exposure in the climate chamber and compared to the average SD of the measurements.

Table 3 RMSD and bias of eight local skin temperatures at regions without seat-body contact and mean skin temperatures in the 18°C and 41°C cases. The bold values indicate a low accuracy of prediction (greater than two standard deviations of the corresponding value).

		UNCONDITIONED EXPOSURE			EXPOSURE WITH COND.		
Case	Skin temperatures (°C)	RMSD	Bias	AVG SD	RMSD	Bias	AVG SD
18°C	Forehead	1.9	-1.9	1.5	-	-	-
	Chest	0.1	-0.1	1.6	-	-	-
	Upper arm	0.4	0.4	1.2	-	-	-
	Lower arm	0.6	0.5	1.4	-	-	-
	Hand	0.7	-0.7	1.8	-	-	-
	Anterior thigh	0.2	-0.2	0.9	-	-	-
	Calf	**2.4**	**-2.4**	0.4	-	-	-
	Mean skin temp. (mTsk)	0.5	-0.4	0.4	-	-	-
41°C	Forehead	0.4	0	0.6	0.5	-0.2	0.7
	Chest	0.8	-0.8	1.3	0.7	-0.7	1.3
	Upper arm	0.7	0.6	0.5	0.5	0.4	0.6
	Lower arm	0.9	0.8	0.6	1.3	1.2	0.8
	Hand	0.5	-0.3	0.5	0.5	0.0	0.5
	Anterior thigh	0.3	0.1	0.8	0.4	0.2	0.8
	Calf	**1.4**	**-1.4**	0.7	0.9	-0.9	1
	Mean skin temp. (mTsk)	0.5	-0.4	0.4	0.4	-0.3	0.5

3.2 Coupling with the thermal sensation models

Figure 6 depicts local thermal sensations at four body sites: two body parts in contact with the seat (backrest and seat cushion), one uncovered body part (hand) and one body part covered with clothing (chest), as predicted by the three thermal sensation models (details in Section 2.2.5) for both the 18°C and 41°C cases. In the case of heating at constant heat flux, the local thermal sensation votes were not available. The RMSD, bias, and mean standard deviation for all body parts are presented in Table 4. The thermal sensation scales of individual models were left in the original form, without scaling.

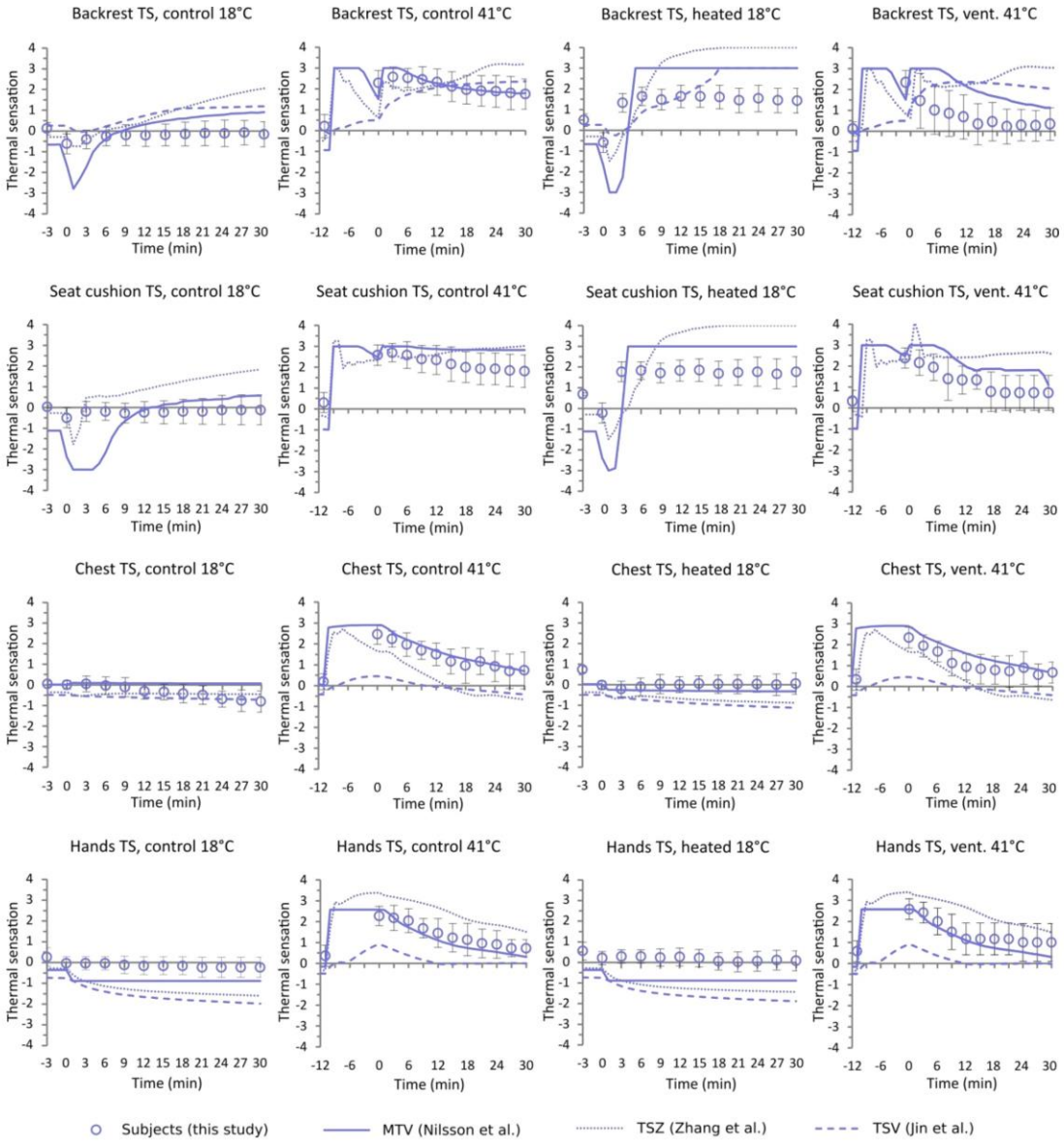

Figure 6 Thermal sensation votes at the seat cushion (posterior thighs and pelvis), backrest (posterior thorax and abdomen), hand and chest, as predicted by three thermal sensation models for unconditioned (at 18°C and 41°C), ventilated (at 41°C) and heated seats at a constant temperature (obtained for the 18°C case). The error bars indicate the standard deviation. Please note that MTV uses a seven-point Bedford scale, TSZ uses a nine-point ISO 10551 scale, and TSV uses a seven-point ISO 10551 scale.

Table 4 RMSD, bias and mean standard deviation of the experimental data for local thermal sensation at 18°C and 41°C. The values in brackets indicate the RMSD and bias within the first six minutes of exposure. The bold values indicate low accuracy of the predictions, greater than two standard deviations of the corresponding value.

	Thermal sens. (-)	MTV RMSD	MTV BIAS	TSZ RMSD	TSZ BIAS	TSV RMSD	TSV BIAS	AVG SD
Unconditioned 18°C	Backrest	0.8 (1.0)	-0.2 (0.8)	**1.2** (0.2)	-0.9 (-0.2)	1.0 (0.6)	-0.9 (-0.6)	0.5
	Seat cushion	**1.2** (**2.2**)	0.4 (**2.2**)	**1.3** (0.6)	**-1.1** (-0.6)	-	-	0.5
	Face	0.5	-0.5	0.7	0.7	0.2	0.1	0.5
	Chest	0.5	-0.4	0.3	0.1	0.4	0.3	0.4
	Arms average	0.1	0.0	1.0	1.0	**1.7**	**1.7**	0.5
	Hands	0.7	0.7	**1.1**	**1.1**	**1.5**	**1.4**	0.4
	Anterior thighs	0.7	-0.6	0.5	-0.4	-	-	0.5
	Lower legs	0.3	-0.3	0.1	0.1	**1.3**	**1.3**	0.5
	Feet	0.3	0.3	0.5	0.5	0.7	0.7	0.9
Unconditioned 41°C	Backrest	0.4 (0.5)	0.1 (0.0)	1.0 (**1.1**)	-0.2 (0.9)	0.7 (**1.3**)	0.0 (**1.3**)	0.6
	Seat cushion	0.8 (0.3)	-0.5 (-0.2)	0.7 (0.2)	-0.4 (0.2)	-	-	0.7
	Face	0.7	-0.7	0.4	0.3	1.2	1.1	0.7
	Chest	0.2	-0.2	1.2	1.1	**1.4**	**1.4**	0.6
	Arms average	0.4	-0.2	0.7	-0.7	**1.6**	**1.5**	0.6
	Hands	0.3	0.3	1.0	-0.9	**1.2**	**1.2**	0.6
	Anterior thighs	0.4	0.0	0.4	0.3	-	-	0.6
	Lower legs	0.5	-0.4	0.9	0.8	1.3	1.2	0.7
	Feet	0.3	-0.1	0.3	0.3	**1.8**	**1.7**	0.6
Heated 18°C	Backrest	**1.7** (**2.3**)	-0.6 (**1.1**)	**2.0** (0.9)	**-1.4** (0.5)	**1.1** (**1.0**)	-0.5 (0.4)	0.5
	Seat cushion	**1.5** (**1.9**)	-0.4 (1.0)	**2.0** (**1.3**)	**-1.5** (-0.5)	-	-	0.5
	Face	0.3	-0.2	0.9	0.8	0.3	0.3	0.5
	Chest	0.3	0.3	0.8	0.7	**0.9**	**0.9**	0.4
	Arms average	0.1	0.0	0.9	0.9	**1.7**	**1.7**	0.5
	Hands	**1.0**	**1.0**	**1.3**	**1.3**	**1.7**	**1.7**	0.4
	Anterior thighs	0.5	0.4	0.5	0.4	-	-	0.5
	Lower legs	0.2	-0.1	0.2	0.2	**1.5**	**1.5**	0.5
	Feet	0.4	0.4	0.6	0.5	0.9	0.9	0.9
Ventilated 41°C	Backrest	1.4 (1.5)	-1.0 (-0.9)	**2.0** (1.3)	-1.5 (-0.1)	1.6 (1.3)	-1.2 (0.1)	0.9
	Seat cushion	0.9 (0.8)	-0.7 (-0.7)	1.3 (0.3)	-1.1 (-0.2)	-	-	0.7
	Face	0.9	-0.8	0.4	0.2	**1.8**	**-1.8**	0.6
	Chest	0.5	-0.4	0.9	0.9	**1.2**	**1.2**	0.6
	Arms average	0.5	-0.4	0.6	-0.5	**1.5**	**1.4**	0.7
	Hands	0.4	0.4	1.0	-0.8	1.3	1.3	0.7
	Anterior thighs	0.5	-0.3	0.2	0.0	-	-	0.5
	Lower legs	0.8	-0.7	0.8	0.5	0.9	0.9	0.6
	Feet	0.4	-0.4	0.2	0.0	**1.5**	**1.4**	0.6

4 Discussion

4.1 The seat heat transfer model and its integration into FPCm5.3

4.1.1 Validation of the seat heat transfer model

The seat heat transfer model was developed to calculate the time-dependent thermal interaction between the seat and its occupant. The human tissue layers represented an average unisex human, based on the FPCm5.3 [21], and the seat was composed of individual clothing and seat construction layers (Table 1). In total, four validation cases were available, including unconditioned, heated, and ventilated seats. In all cases, the predicted heat fluxes exhibited a good fit to the experimental data, and the RMSD and the bias were generally within two standard deviations of the measurement (Figures 3-5). The only exception was found in the case of the unconditioned seat at 18°C, where the RMSD was 9.2 W/m^2 (SD 2.9 W/m^2) at the backrest and 8.1 W/m^2 (SD 1.6 W/m^2) at the seat cushion. This discrepancy was still less than 10% of the peak heat flux density after sitting, and we considered that the heat flux predictions were sufficiently accurate to be coupled with the FPCm5.3 to obtain the local thermo-physiological responses for the whole body.

In comparison to the study by Shin et al. [41], we achieved realistic heat flux predictions (Figure 5) in the complex heat and mass transfer situation in the ventilated seat despite using a one-dimensional model. Thus, from the point of heat transfer, it seems to be possible to use the proposed simplifications to obtain realistic results while avoiding the elaborative determination of the parameters necessary for the calculation of the evaporative cooling. Our solution predicted a heat flux equivalent to the measurement using only the input parameter of the seat surface temperature. Finally, in our model, seat cooling can be represented using a heat sink if the cooling power is known.

4.1.2 Exposures with unconditioned seat

The predicted skin and seat surface temperatures from the FPCm5.3 simulations coupled with the seat heat transfer model were in good agreement with measurements (Figure 3). The RMSD and bias of the predicted seat contact temperatures were mostly lower than 1°C, and at the same time were lower than the standard deviation of the measurement. The only outlier was found in the 18°C case, where the RMSD and bias of the seat cushion temperature reached 1.5°C and 1.3°C, respectively. Here, the predictions were inaccurate only between the first and fourth minutes (Figure 3), and the rest of the exposure simulation agreed with the experiment. The SD was also typically higher in the first six minutes after sitting down than during the rest of the exposure, and mostly overlapped with the predictions. These findings can be directly related to the quality of the input, the calculated heat flux, which had an error of between 3% and 10%. In comparison to a similar study using one-dimensional model by Karimi et al. [40], we achieved consistent results throughout the temperature range from 5°C to 41°C.

The simulation carried out using the thermal and evaporative insulation as a seat boundary condition did not capture the substantial drop of 3°C in the contact skin temperature (Figure 3 – FPCm simul. insulation) as opposed to the seat heat transfer model approach coupled with FPCm5.3 (Figure 3 – FPCm simul. HT model). This confirms our hypothesis that neglecting the thermal diffusivity and the low initial seat temperature of 5°C leads to a critical error. Furthermore, the actual skin temperature recovery to the initial state took more than 20 minutes. According to Koelblen et al. [58] and Veselá et al. [59], a skin temperature deviation of 1°C can be related to a considerable change in local thermal sensation from approximately 0.5 to 1.5 units, depending on the thermal sensation model and its scale, meaning that the neglected temperature drop would naturally lead to a faulty thermal sensation prediction. This shows the importance of addressing the thermal mass of contact surfaces in thermo-physiological modelling, especially when examining environments that are exposed to conditions far from thermo-neutrality, such as vehicular cabins and a range of occupational settings.

4.1.3 Exposures with seat heating to constant heat flux or constant temperature

In the 18°C case, where the seat is heated to a constant temperature, very good agreement was found between the measured and simulated contact temperatures, as indicated by the RMSD and bias being below the experimental standard deviation (Figure 4). In the 5°C, 10°C, 15°C and 20°C cases with constant heat flux control, the predicted contact temperatures were on average up to 2.3°C higher than the experimental values in the coldest case. The simulations, however, agreed with the measurements until approximately the fifth minute of the exposure, and were over-predicted towards the end of the exposure, when the heating started to have a major impact on the development of temperature (Figure 4). We can also observe a decreasing trend in the RMSD and bias with an increase in the temperature of the exposure (see the table in Figure 4). Since the seat heat transfer model neglects the lateral heat losses from the seat, which may be influential especially at lower temperatures, this is a likely reason for the discrepancy. Secondly, the seat heat transfer model is based on constant thermal properties of human tissues, whereas the FPCm5.3 contains an active thermoregulation system that influences the thermal properties of tissue depending on the thermal state of the body. A combination of both of these factors might explain the higher predicted skin temperature that is apparent in Figure 4 at 5°C.

Figure 4, FPCm simul. const. heat flux demonstrates the error of assuming an adiabatic boundary condition at the seat cushioning, thus setting the seat heating power purely to the skin of the seat's occupant. This approach causes not only an unacceptable overestimation of the contact skin temperature by more than 8°C, but also an immediate steep increase in the skin temperature, rather than its initial cooling by the thermal diffusivity of the cold seat. Under the same conditions, the FPCm5.3 coupled with the seat heat transfer model provides results that are four times more accurate in terms of RMSD and bias (Figure 4, FPCm simul. HT model). This approach was shown to deliver realistic outputs also in the cases taken from the

literature, where very little qualitative information about the experiment was available, such as a basic description of the seat, clothing, and the environment [8].

4.1.4 Exposures with ventilated seat

In the 41°C case, we obtained accurate predictions for the seat surface temperatures where the RMSD and bias were within the standard deviation of the measurement (Figure 5). In the study by Shin et al. [41], where three-dimensional model of ventilated seat was used, the good agreement in the seat and skin temperatures were found only within the first two minutes of exposure, followed by an error of up to 12°C in the fifth minute. We achieved consistent results despite simplifying the heat and mass transfer to the resulting heat flux density between the seat and the occupant. The 41°C case also confirms the applicability of this approach at high ambient temperatures.

4.1.5 Predicted skin temperatures at the body sites without seat contact

The skin temperatures for eight main body parts without seat contact were predicted very accurately in both cases, i.e. at 18°C and 41°C. The RMSD and bias of the FPCm5.3 simulations were mostly below the standard deviation of the measurements, with an average of 0.9°C (Table 3). To put this into the context of the previous FPCm5.3 validation studies, such as the study by Martínez et al. [27], an average RMSD of 1.3°C for local skin temperatures was determined based on 43 distinct human exposures. The study reported an increased RMSD at the forehead of 1.6°C, which is in line with our findings (RMSD 1.9, bias −1.9°C, SD 1.5). This discrepancy can be explained by the variations in the hair coverage of the forehead and the evaporative cooling capacity of sweat [60]. At the calves, the simulation results exhibited constant over-predictions of 2.4°C and 1.8°C for the cases of 18°C and 41°C, respectively (Table 3). This contradicts the findings of a prior validation study [60], where good prediction power was found at the calves. An explanation can be found in a possible discrepancy in the local clothing input. The participants were instructed to wear their own clothing, consisting of typical garments for the appropriate season, and we did not control for the fit of the clothing. The fit defines the size of the air gaps between the skin and clothing, and consequently influences the resulting thermal and evaporative insulation of the clothing [61]. Finally, the predicted mean skin temperature was satisfactory in both cases, with an RMSD and bias close to the experimental SD of 0.5°C (Table 3).

4.2 Coupling with the thermal sensation models

Overall, the most realistic performance under all conditions examined here was found in MTV and TSZ, where in the vast majority of cases, the RMSD and bias were within two standard deviations of the human votes (with an average of 1.1 thermal sensation units, Table 4). The two standard deviations of the thermal sensation votes were selected to cover 95% of their dispersion due to the relatively low number of participants (details of this are given in Table 2). High accuracy of the thermal sensation predictions was also found for body parts with less precisely predicted skin temperatures, namely the lower legs

and forehead. The only outliers were the hands, which were under-predicted by approximately 1.3 units in the case of 18°C. This phenomenon was apparent in all three models, and can be attributed to the higher local activity of the hands (filling out questionnaires and usage of smart devices) and the subconscious resting of the hands on the warmer thighs.

Despite the realistic predictions of the skin temperatures at the seat contact, the predicted thermal sensation was clearly less accurate than for body parts without seat contact (Table 4). To differentiate between the entire duration of the seat exposure and the first six minutes after taking the seat, when rapid changes of thermal sensation took place, the RMSD and bias were calculated separately for these periods (Table 4). In both the cool conditions (18°C) and the hot conditions (41°C), TSZ performed well in the first six minutes, with an RMSD and bias within two standard deviations. However, after this period, TSZ tended to drift towards higher thermal sensation votes and exceeded the limit of two standard deviations. The MTV model, on the other hand, over-estimated the effects of the cold seat by between 0.8 to 2.3 units in the first six minutes of the cool exposure, mainly because the initial cooling was as high as 150 W/m^2. The rest of the cool exposure typically mirrored the trends of the experimental data. Under hot conditions, predictions by MTV were the most accurate of the three models, and good accuracy was achieved, with an RMSD and bias of approximately one standard deviation (Table 4 and Figure 6).

In the case of the TSV model, the RMSD and bias exceeded two standard deviations in more than half of the body parts examined. More importantly, TSV did not respond either to the temperature step change or to the cooling ramp (Figure 6). Secondly, the segmentation of the model allows us to examine only one contact part, namely the backrest. These findings mean that TSV is less suitable for applications in vehicular cabins than the two other examined models. One of the major parameters influencing the results of the TSV model is the neutral skin temperature that is used to measure the deviation from the thermo-neutral state for a given body part. The TSV model was developed based on data from 40 Chinese participants, as opposed to the central European population investigated in this study. Using the baseline thermo-neutral skin temperature directly from FPCm5.3, which was on average 1.1°C higher, did not provide any major improvements to the predicted thermal sensation. Koelblen et al. showed that this model did not perform better for the Asian population than for the other two thermal sensation models developed based on white or mixed populations.

One possible reason for the low precision of all models in the seat contact may stem from the broader range of skin temperatures in the contact compared to the non-contact ones (Figure 3). Thus, at the seat contact, the thermal sensation models were at or beyond their limit of applicability. Another explanation for this lower accuracy has been proposed by Oi et al. [8], who concluded that there was a need for higher skin temperatures at the seat contact at lower ambient temperatures to

achieve optimal thermal sensation in the contact parts. Similar conclusions were also presented by Zhang et al. [10] for heated and cooled seats in a range of temperatures of between 15°C and 45°C. However, this relativity is not captured in any of the examined models, and further work is needed on the extension of the current thermal sensation models.

4.3 Practical implications

As opposed to the detailed three-dimensional computing methods, the main advantages using the proposed models can be summarized in following points:

- Easily accessible input parameters and boundary conditions;
- Low computing power demands;
- Quick results with an acceptable error margin within defined conditions;
- Simple implementation.

The proposed methodology was validated in a range of conditions between 5°C and 41°C. This range is not only typical in automotive applications, but also in occupational environments with higher heat strain due to a technological process installed. Therefore, a broad community of environmental engineers can benefit from our findings. Next, thanks to the rapid calculation times, it is possible to run parametric studies and studies focused on optimisation of the environmental parameters with respect to energy savings. These are the priorities in diminishing the carbon foot print and in the development of electric vehicles. Finally, the methodology has a great potential to significantly reduce needs for human studies and prototyping, and thus accelerate product development.

4.4 Limitations

The aim of the proposed model is to approximate the heat transfer between a solid with considerable thermal mass (seat) and an adjacent body part, rather than to act as a substitute for complex thermo-physiological models such as the FPCm5.3. For this reason several simplifications had to be assumed. On the site of the human, the model calculates the heat transfer for individual body parts and does not assume any connection with the rest of the human body by blood circulation. Next, the tissue thermal properties were constant, which is not the case in reality if a thermoregulatory action (such as vasomotor response, sweating, and shivering) occurs. Therefore, the seat heat transfer model may be prone to error under conditions where the human core temperature is changing substantially and thermoregulatory actions are present. On the site of the seat, the simplifications were mainly related to the assumption of one-dimensional heat flux. This might be influential under cold conditions with heating, where we found an increasing trend in the skin temperature error with decreasing ambient temperature (overestimation of 2.3°C found at 5°C of ambient temperature). In case of the seat ventilation, the sweat evapo-

ration was substituted by a heat sink or a temperature profile prescribed at the seat. This approach was shown to yield an equivalent heat flux, which can be used as a heat flux boundary condition in thermo-physiological modelling. It has to be noted that this boundary condition type restricts evaluation of the sweating and moisture propagation. Although contemporary thermal sensation models do not account for moisture, skin wettedness is one of the parameters influencing human comfort. For this reason, future advancements should also comprise humidity at the skin.

5 Conclusions

For the first time, this study has demonstrated a thorough methodology for simulating the human thermal response and thermal sensation in contact with heated and ventilated seats. This was done under a broad variety of environmental conditions ranging from 5°C to 41°C, including transient and thermally asymmetric exposures with and without local seat conditioning technologies. The seat heat transfer model was found to be a key component in calculating realistic boundary conditions for body contact with a seat, for the accurate prediction of thermo-physiological responses and thermal sensation. The typical error in the calculated heat flux between the seat and the occupant was less than two standard deviations of the measurement. Consequently, the error in the predicted seat contact temperatures using the FPCm5.3 was typically lower than 1°C, or within the standard deviation of the measurement in the majority of cases. Furthermore, the benefits of the model were underlined by comparing it with the conventional way of treating the seat as a thermal and evaporative resistance and, in the heated case, as a constant heat flux applied directly to the skin. These conventional approaches lead to an unrealistic development of the skin temperatures and errors four times higher than those obtained using the seat heat transfer model.

The high precision of the FPCm5.3 model in predicting skin temperatures at eight main body parts without seat contact was also confirmed, with an RMSD and bias typically within the SD of the measurement and below 1°C. This verification was necessary to provide reliable inputs to the thermal sensation models. Overall, the best performing models were MTV and TSZ, while TSV performed the worst. The predictions were less accurate in the seat contact area, especially under cool conditions at 18°C. Here, all models typically exceeded two standard deviations of the human votes. Within the six-minute highly transient period after taking the seat, the best performing model was TSZ. After this phase, MTV provided robust and acceptably accurate results that realistically mirrored the human thermal sensation votes. A further extension of the current models is therefore needed to improve their performance under conditions with local conditioning.

Since the proposed methodology is valid in conditions between 5°C and 41°C, we can assume that the set of models can be used in a broad variety of environments, such as passenger transportation and occupational environments with higher heat

strain. The approach presented here can be of great merit within rapidly developing industries such as electric vehicle engineering. The virtual optimisation of the seat conditioning strategies reduces the need for human studies and prototyping, and may allow for energy savings and potentially increase the driving range.

Acknowledgements

The part of this work conducted at Empa was supported by the HEAT-SHIELD project within the EU Horizon 2020 program, under grant no. RIA 668786-1. The experimental part of the work conducted at Brno University of Technology was supported by the Ministry of Education Project Youth and Sports of the Czech Republic, under the "National Sustainability Programme I" [LO1202 Netme Centre Plus]; and the Brno University of Technology under project Reg. No. FSI-S-17-4444. We would like to thank to Dr. Hajime Oi for providing us with an additional set of data on seat contact skin temperatures.

6 Bibliography

[1] R. Farrington and J. Rugh, "Impact of Vehicle Air-Conditioning on Fuel Economy, Tailpipe Emissions, and Electric Vehicle Range: Preprint," *Natl. Renew. Energy Lab., Golden, CO*, pp. 1–12, 2000.

[2] M. Fojtlín, M. Planka, J. Fišer, J. Pokorný, and M. Jícha, "Airflow Measurement of the Car HVAC Unit Using Hot-wire Anemometry," in *EFM15 – Experimental Fluid Mechanics 2015*, 2016, vol. 114, p. 6.

[3] M. Fojtlín, A. Psikuta, R. Toma, J. Fiser, and M. Jícha, "Determination of car seat contact area for personalised thermal sensation modelling," *PLoS One*, vol. In press, 2018.

[4] S. Milosević, "Drivers' fatigue studies.," *Ergonomics*, vol. 40, no. 3, pp. 381–9, 1997.

[5] H. A. M. Daanen, E. Van De Vliert, and X. Huang, "Driving performance in cold, warm, and thermoneutral environments," *Appl. Ergon.*, vol. 34, no. 6, pp. 597–602, 2003.

[6] A. Alahmer, A. Mayyas, A. A. Mayyas, M. A. Omar, and D. Shan, "Vehicular thermal comfort models; a comprehensive review," *Appl. Therm. Eng.*, vol. 31, no. 6–7, pp. 995–1002, 2011.

[7] M. Cisternino, "Thermal climate in cabins and measurement problems," in *Assessment of thermal climate in operator's cabs, Seminar Florence; JTI-rapport*, 1999, pp. 15–23.

[8] H. Oi, K. Tabata, Y. Naka, A. Takeda, and Y. Tochihara, "Effects of heated seats in vehicles on thermal comfort during the initial warm-up period," *Appl. Ergon.*, vol. 43, no. 2, pp. 360–367, 2012.

[9] H. Oi, K. Yanagi, K. Tabat, and Y. Tochihar, "Effects of heated seat and foot heater on thermal comfort and heater energy consumption in vehicle," *Ergonomics*, vol. 54, no. 8, pp. 690–699, 2011.

[10] Y. F. Zhang, D. P. Wyon, L. Fang, and A. K. Melikov, "The influence of heated or cooled seats on the acceptable ambient temperature range," *Ergonomics*, vol. 50, no. 4, pp. 586–600, 2007.

[11] J. E. Brooks and K. C. Parsons, "An ergonomics investigation into human thermal comfort using an automobile seat heated with encapsulated carbonized fabric (ECF)," *Ergonomics*, vol. 42, no. 5, pp. 661–673, 1999.

[12] W. Pasut, H. Zhang, E. Arens, and Y. Zhai, "Energy-efficient comfort with a heated/cooled chair: Results from human subject tests," *Build. Environ.*, vol. 84, pp. 10–21, 2015.

[13] M. Veselý and W. Zeiler, "Personalized conditioning and its impact on thermal comfort and energy performance - A review," *Renew. Sustain. Energy Rev.*, vol. 34, pp. 401–408, 2014.

[14] S. Shahzad, J. K. Calautit, A. I. Aquino, D. S. N. M. Nasir, and B. R. Hughes, "A user-controlled thermal chair for an open plan workplace: CFD and field studies of thermal comfort performance," *Appl. Energy*, vol. 207, 2017.

[15] K. Katic, R. Li, and W. Zeiler, "Thermophysiological models and their applications: A review," *Build. Environ.*, vol. 106, pp. 286–300, 2016.

[16] S. I. Tanabe, K. Kobayashi, J. Nakano, Y. Ozeki, and M. Konishi, "Evaluation of thermal comfort using combined multi-node thermoregulation (65MN) and radiation models and computational fluid dynamics (CFD)," *Energy Build.*, vol. 34, no. 6, pp. 637–646, 2002.

[17] C. Huizenga, Z. Hui, and E. Arens, "A model of human physiology and comfort for assessing complex thermal environments," *Build. Environ.*, vol. 36, no. 6, pp. 691–699, 2001.

[18] S. Tanabe, M. E. ASHRAE Arens, M. H. ASHRAE Zhang TL Nladsen Member A SHRA E FS Bauman, P. Member ASHRAE, and T. Madsen, "Evaluating thermal environments by using a thermal manikin with controlled skin surface temperature," *Ashrae*, vol. 100 Part 1, pp. 39–48, 1994.

[19] B. Kingma, "Human thermoregulation: a synergy between physiology and mathematical modelling," PhD thesis, Maastricht University, 2012.

[20] ErgonSim, "FPC - model user manual,Version 2.5." p. 60, 2013.

[21] D. Fiala and G. Havenith, "Modelling Human Heat Transfer and Temperature Regulation," in *The Mechanobiology and Mechanophysiology of Military-Related Injuries*, vol. 19, Berlin: Springer, 2015, pp. 265–302.

[22] S. Paulke, "Finite element based implementation of fiala's thermal manikin in THESEUS-FE," in *VTMS 8 - Vehicle Thermal Management Systems Conference and Exhibition, Nottingham, United Kingdom*, 2007, pp. 559–566.

[23] J. Pokorný *et al.*, "Verification of Fiala-based human thermophysiological model and its application to protective clothing under high metabolic rates," *Build. Environ.*, vol. 126, pp. 13–26, 2017.

[24] M. Hepokoski, A. Curran, and D. Dubiel, "Improving the accuracy of physiological response in segmental models of human thermoregulation," in *XIV International Conference on Environemntal Ergonomics, Nafplio*, 2011, pp. 102–103.

[25] D. Fiala, K. J. Lomas, and M. Stohrer, "Computer prediction of human thermoregulatory and temperature responses to a wide range of environmental conditions," *Int. J. Biometeorol.*, vol. 45, no. 3, pp. 143–159, 2001.

[26] A. Psikuta *et al.*, "Validation of the Fiala multi-node thermophysiological model for UTCI application," *Int. J. Biometeorol.*, vol. 56, no. 3, pp. 443–460, 2011.

[27] N. Martínez *et al.*, "Validation of the thermophysiological model by Fiala for prediction of local skin temperatures," *Int. J. Biometeorol.*, vol. 60, no. 12, pp. 1969–1982, 2016.

[28] D. Fiala *et al.*, "Physiological modeling for technical, clinical and research applications," *Front. Biosci. S2*, pp. 939–968, 2010.

[29] Y. Cheng, J. Niu, and N. Gao, "Thermal comfort models: A review and numerical investigation," *Build. Environ.*, vol. 47, pp. 13–22, 2012.

[30] B. Koelblen, A. Psikuta, S. Annaheim, and R. M. Rossi, "Comparison and performance evaluation of local thermal sensation models," *Build. Environ.*, vol. Accepted m, 2018.

[31] H. O. Nilsson, "Thermal comfort evaluation with virtual manikin methods," *Build. Environ.*, vol. 42, no. 12, pp. 4000–4005, 2007.

[32] H. O. Nilsson, "Comfort climate evaluation with thermal manikin methods and computer simulation

models.," PhD Thesis, University of Gavle, 2004.

[33] International Organization for Standardization, "EN ISO 14505-2 Ergonomics of the thermal environment - Evaluation of thermal environments in vehicles - Part 2: Determination of equivalent temperature." European Committee for Standardization, Brussels, p. 25, 2006.

[34] H. O. Nilsson and I. Holmér, "Comfort climate evaluation with thermal manikin methods and computer simulation models.," *Indoor Air*, vol. 13, no. 1, pp. 28–37, 2003.

[35] M. Fojtlín, J. Fišer, J. Pokorný, A. Povalač, T. Urbanec, and M. Jícha, "An innovative HVAC control system: Implementation and testing in a vehicular cabin," *J. Therm. Biol.*, vol. 70, no. Part A, pp. 64–68, 2017.

[36] H. Zhang, E. Arens, C. Huizenga, and T. Han, "Thermal sensation and comfort models for non-uniform and transient environments: Part I: Local sensation of individual body parts," *Build. Environ.*, vol. 45, no. 2, pp. 380–388, 2010.

[37] Y. Zhao, H. Zhang, E. A. Arens, and Q. Zhao, "Thermal sensation and comfort models for non-uniform and transient environments, part IV: Adaptive neutral setpoints and smoothed whole-body sensation model," *Build. Environ.*, vol. 72, pp. 300–308, 2014.

[38] Q. Jin, X. Li, L. Duanmu, H. Shu, Y. Sun, and Q. Ding, "Predictive model of local and overall thermal sensations for non-uniform environments," *Build. Environ.*, vol. 51, pp. 330–344, 2012.

[39] G. Karimi, E. C. Chan, J. R. Culham, I. Linjacki, and L. Brennan, "Thermal Comfort Analysis of an Automobile Driver with Heated and Ventilated Seat," *SAE Tech. Pap. 2002-01-0222*, no. 1988, 2002.

[40] G. Karimi, E. C. Chan, and J. R. Culham, "Experimental Study and Thermal Modeling of an Automobile Driver with a Heated and Ventilated Seat," *SAE Tech. Pap.*, no. 2003-01–2215, p. 13, 2003.

[41] K. Shin, H. Park, J. Kim, and K. Kim, "Mathematical and Experimental Investigation of Thermal Response of an Automobile Passenger With a Ventilated Seat," no. November, pp. 529–539, 2008.

[42] Y. F. Zhang, D. P. Wyon, L. Fang, and A. K. Melikov, "The influence of heated or cooled seats on the

acceptable ambient temperature range.," *Ergonomics*, vol. 50, no. 4, pp. 586–600, 2007.

[43] T. Lund Madsen, "Thermal effects of ventilated car seats," *Int. J. Ind. Ergon.*, vol. 13, no. 3, pp. 253–258, 1994.

[44] S. Shahzad, J. K. Calautit, A. I. Aquino, D. S. N. M. Nasir, and B. R. Hughes, "A user-controlled thermal chair for an open plan workplace: CFD and field studies of thermal comfort performance," *Appl. Energy*, vol. 207, pp. 283–293, 2017.

[45] S. Watanabe, T. Shimomura, and H. Miyazaki, "Thermal evaluation of a chair with fans as an individually controlled system," *Build. Environ.*, vol. 44, no. 7, pp. 1392–1398, 2009.

[46] V. T. Bartels, "Thermal comfort of aeroplane seats: Influence of different seat materials and the use of laboratory test methods," *Appl. Ergon.*, vol. 34, no. 4, pp. 393–399, 2003.

[47] M. Scheffelmeier and E. Classen, "Development of a method for rating climate seat comfort," *IOP Conf. Ser. Mater. Sci. Eng.*, vol. 254, no. 18, 2017.

[48] D. et al. Fiala, "UTCI-Fiala multi-node model of human heat transfer and temperature regulation.," *Int. J. Biometeorol.*, no. Special Issue, pp. 1–13, 2011.

[49] M. Kolich, D. Dooge, M. Doroudian, E. Litovsky, R. Ng, and J. Kleiman, "Thermophysical Properties Measurement of Interior Car Materials vs. Temperature and Mechanical Compression," *SAE Int.*, vol. 2014-01–10, p. 9, 2014.

[50] International Organization for Standardization, "ISO 9920 Ergonomics of the thermal environment - Estimation of thermal insulation and water vapour resistance of a clothing ensemble." Geneva, p. 104, 2007.

[51] M. Fojtlín, J. Fišer, and M. Jícha, "Determination of convective and radiative heat transfer coefficients using 34-zones thermal manikin: Uncertainty and reproducibility evaluation," *Exp. Therm. Fluid Sci.*, vol. 77, pp. 257–264, 2016.

[52] E. of the physical environment. Technical Committee ISO/TC 159, Ergonomics, Subcommittee SC 5, *EN-ISO 9886:2004, Ergonomics - evaluation of thermal strain by physiological measurements.*, vol. 3, no. 1. 2004.

[53] B. A. Macrae, R. M. Rossi, A. Psikuta, C. M. Spengler, and S. Annaheim, "Contact skin temperature measurements and associated effects of obstructing local sweat evaporation during mild exercise-induced heat stress," *Physiol. Meas.*, vol. 39, no. 7, p. 12, 2018.

[54] M. Fojtlín, A. Psikuta, J. Fišer, R. Toma, S. Annaheim, and M. Jícha, "Clothing boundary conditions for thermo-physiological modelling: comparison of methods and body postures.," *Build. Environ.*, vol. 155, pp. 376–388, 2019.

[55] B. Koelblen, A. Psikuta, A. Bogdan, S. Annaheim, and R. M. Rossi, "Thermal sensation models: A systematic comparison," *Indoor Air*, vol. 27, no. 3, pp. 1–10, 2016.

[56] H. Zhang, E. Arens, C. Huizenga, and T. Han, "Thermal sensation and comfort models for non-uniform and transient environments, part III: Whole-body sensation and comfort," *Build. Environ.*, vol. 45, no. 2, pp. 399–410, 2010.

[57] International Organization for Standardization, "ISO 7730 Ergonomics of the thermal environment — Analytical determination and interpretation of thermal comfort using calculation of the PMV and PPD indices and local thermal comfort criteria," vol. 3. Geneva, p. 52, 2005.

[58] B. Koelblen, A. Psikuta, A. Bogdan, S. Annaheim, and R. M. Rossi, "Thermal sensation models: Validation and sensitivity towards thermo-physiological parameters," *Build. Environ.*, vol. 130, no. December 2017, pp. 200–211, 2018.

[59] S. Veselá, B. R.; Kingma, and A. J. Frijns, "Local thermal sensation modeling: a review on the necessity and availability of local clothing properties and local metabolic heat production.," *Indoor Air*, vol. 27, no. 2, pp. 261–272, 2017.

[60] N. Martínez *et al.*, "Validation of the thermophysiological model by Fiala for prediction of local skin temperatures," *Int. J. Biometeorol.*, vol. 60, no. 12, pp. 1969–1982, 2016.

[61] A. Psikuta, E. Mert, S. Annaheim, and R. M. Rossi, "Local air gap thickness and contact area models for realistic simulation of human thermo-physiological response," *Int. J. Biometeorol.*, pp. 1–14, 2018.

Paper IV

Experimental Thermal and Fluid Science 77 (2016) 257–264

Contents lists available at ScienceDirect

Experimental Thermal and Fluid Science

journal homepage: www.elsevier.com/locate/etfs

Determination of convective and radiative heat transfer coefficients using 34-zones thermal manikin: Uncertainty and reproducibility evaluation

Miloš Fojtlín *, Jan Fišer, Miroslav Jícha

Department of Thermodynamics and Environmental Engineering, Energy Institute, Faculty of Mechanical Engineering, Brno University of Technology, Technická 2, 616 69 Brno, Czech Republic

ARTICLE INFO

Article history:
Received 15 October 2015
Received in revised form 13 April 2016
Accepted 17 April 2016
Available online 19 April 2016

Keywords:
Thermal manikin
Heat transfer coefficient
Experimental work
Thermal comfort
Uncertainty evaluation

ABSTRACT

A lot of research has been done in order to investigate heat transfer coefficients of a human body in various postures, wind speeds and wind directions. However, there has not been any reference to measurement reproducibility and measurement confidence intervals. The purpose of this study is to determine heat transfer coefficients of a thermal manikin experimentally, while focusing on the repeated determination of the coefficients and statistical data evaluation. The manikin imitates human metabolic heat production; it measures combined dry heat flux from its surface and also its surface temperature.

The major part of the radiative heat flux was eliminated by a low-emissivity coating applied to the surface of the nude manikin. The tests were performed across 34 zones that correspond to parts of a human body. Both standing and seated postures were investigated. The tests were conducted at constant air temperature (24 °C) and constant wind speed (0.05 m s^{-1}). Based on three repetitions of each case, the mean values of heat transfer coefficients, with their uncertainty intervals, were calculated. Next, the results of this paper were compared to the results of similar experimental work of de Dear et al. (1997) and Quintela et al. (2004). A mismatch of the values is up to 1 W m^{-2} K^{-1}, while an extreme was found on the manikin's seat with a difference of over 1 W m^{-2} K^{-1}. The outcomes of this study provide essential information in form of separated values of the convective and radiative heat transfer coefficients that enable us to create detailed computational models of a thermal comfort.

1. Introduction

The analysis of heat exchange from a human body has been drawing a lot of interest for decades. Through the years, plentiful approaches have been developed to determine the heat transfer (eg., [1–15]). Clearly, motivation for this is simple. Urbanization made people to spend less of their time outdoors where the ambient conditions are given by the actual weather. Today, statistics show that average European citizens spend 80–90% of their workday time indoors, in buildings or vehicles [16]. Owing to this, a building design in terms of thermal comfort, air quality, and low energy demands is important. In addition, many independent studies provide evidence of improper thermal environment and its negative influence on the human body (e.g., [17,18]). However, such situations can be tackled, in the future, using modern computational methods. To do so, there is a need for anatomically detailed heat transfer coefficients.

The heat transfer coefficients represent an amount of heat transferred between the body and the ambient environment. The majority of the heat is exchanged via convection and radiation. In case the convection and radiation are not sufficient to cool down a human body, excretion of sweat and its evaporation takes place. Evaporation is based on mass transfer during which the latent heat is consumed. Since, there is a focus on the cases close to a thermal comfort state, only dry heat loss will be further examined—the cases disregarding sweating. The third mode of heat transfer, conduction, can be neglected, when there is a minor contact with solid objects. It is also the case of this study.

The very first studies, to determine the heat transfer coefficients, involved experimental subjects exposed to various thermal conditions [3–5]. Later on, simple heat emitting devices were used to simulate heat transfer, such as Stolwijk's 25-node model [19]. Nowadays, there is a greater demand for anatomically detailed and accurate heat transfer coefficients, resulting in the use of

* Corresponding author.
E-mail address: fojtlin@eu.fme.vutbr.cz (M. Fojtlín).

http://dx.doi.org/10.1016/j.expthermflusci.2016.04.015
0894-1777/

modern technologies, typically thermal manikins of different kinds. Current manikin constructions resulted in the segmentation of their bodies into zones (segments) representing major human body parts (upper lower limbs, chest, back, etc.). Consequently, manikins have been examined in various body postures, with moving limbs, and under various air flow regimes. A full scale of possible manikins' applications is addressed, for instance, in Wyon's work [20]. On the other hand, the thermal manikin is not designed to measure the radiative or convective heat transfer coefficients directly. It determines heat flux from its surface in a combined form via radiation, convection, and conduction. Neglecting the conduction, the combined heat flux from the manikin is represented by the convection and radiation only. Because of a small temperature difference of the system, the manikin and the air, a linear description of the heat transfer in the following form is used.

$$Q_0 = Q_c + Q_r = h_c.(T_{sk} - T_a) + h_r.(T_{sk} - T_r) \quad (1)$$

Q_0 combined heat flux density (W m^{-2}),
Q_c convective heat flux density (W m^{-2}),
Q_r radiative heat flux density (W m^{-2}),
h_c convective heat transfer coefficient (W m^{-2} K^{-1}),
h_r radiative heat transfer coefficient (W m^{-2} K^{-1}),
T_{sk} manikin surface temperature (°C),
T_a ambient air temperature (°C),
T_r mean radiant temperature (°C).

Certain steps must be taken to separate the combined heat flux into radiative and convective parts. Generally, one of the heat transfer modes must be eliminated or calculated first. Thus, it is possible to determine the remaining mode. Commonly used approaches are briefly described in the following paragraphs.

1.1. Radiative heat transfer coefficient (h_r)

Some authors (e.g., [6]) calculate values of the whole body h_r from ASHRAE Handbook of Fundamentals [7]. This approach is quite simple and efficient; however, it does not allow examining the individual body parts, which is nowadays essential. The second known approach [8] was used to determine radiative heat fluxes within 16 segments of a standing thermal manikin by eliminating convective heat fluxes. Convection was suppressed through setting $T_{sk} = T_a$ in formula (1). This was achieved inside a climate chamber with independently controlled temperatures of $T_a = 34$ °C and $T_r = 27$ °C. The third known approach, presented by Kurazumi et al. [9], uses a radiant flux meter to determine local radiative heat fluxes from a surface of a thermal manikin. The manikin is set to a constant surface temperature of 33 °C. The mean local h_r was calculated for 11 body parts with regards to various manikin body postures.

1.2. Convective heat transfer coefficient (h_c)

In this section three experimental approaches to determine h_c are presented. The first approach is based on the use of heat flux sensors placed on the surface of a thermal manikin or a real human subject [10]. In order to eliminate Q_r, the heat flux sensors were covered with low emissivity aluminum foil ($\varepsilon = 0.04$). The major advantage of this method is that the heat flux sensor can be placed on moving objects (e.g., parts of human body, manikin). On the other hand, heat flux is recorded only at one spot, and to achieve a better resolution, several sensors must be involved. Since the flux meters are not immersed into the surface of a certain object, they can interfere with the airflow around the body as well as with the temperature of the surface [10]. Secondly, Chang et al. [11] and Nishi and Gagge [12] use a naphthalene sublimation method as a representative of convection process. Likewise, this method, again, allows examining only the local convection on the parts of the body where the naphthalene disc is stuck. Another disadvantage is a need for the extra laboratory equipment. The third approach involves thermal manikins with controlled skin temperature. This method is nowadays preferred by the majority of researchers (e.g., [1,2,6,14,15]). The Q_0 measurements are performed across the whole surface of the manikin with precise body segmentation. Accuracy of such measurements is, thus, much higher compared to the spot measurements. Yet, as previously mentioned, the manikins are not able to measure the convective heat flux directly. Consequently, the radiative heat flux must be eliminated, or it must be calculated. ASHRAE formula [7] for the whole body h_r is quite well accepted, but not sufficient for detailed examination. For a comprehensive calculation of h_r, Francisco et al. [13] present their own computational method. The third known approach is to cover the whole manikin with a low emissivity coating [1,2] suppressing the radiative flux. Finally, another possible method to eliminate radiative heat flux is to set the radiant temperature of the environment equal to the manikin's surface temperature. At the same time, an ambient air temperature is controlled to be lower than the mean radiant temperature. However, examples of such have not been found.

The available studies present results from experiments without any specification of the number of measurement repetitions. Evaluation of the uncertainties is also unavailable. Although, all the experiments were carried out in laboratory conditions with very precise equipment, repeatability and uncertainty of the measurements are still questionable. The aim of this study is to involve a computer-controlled thermal manikin Newton to determine the convective and radiative heat transfer coefficients repeatedly. Thus, the repeatability of the measurements can be critically reviewed. The following cases are to be investigated: (a) standing, (b) sitting thermal manikin in natural convection environment with resolution of 34 segments. These cases were opted to enable comparing the results with the generally accepted values of h_r and h_c.

2. Methods

The presented study involves a state-of-the-art thermal manikin Newton that replaces a human in order to simulate a metabolic heat production. The manikin measures the combined dry heat flux from its surface together with its surface temperature. To separate the combined flux (Q_0) to its parts (Q_r, Q_c), the approach of eliminating the radiative heat flux by the low-emissivity coating was selected.

The low-emissivity coating was created using thin aluminum cooking foil applied to the surface of the manikin with the exception of its hands (zones 11 and 12) and nose. Segmentation and curvature of these parts did not allow us to achieve a desired coating quality. Consequently, hands were not examined and the nasal area is negligible compared to the total face area. To fix the coating, sodium alginate mixed with water was used (in total around 7 g). A very tight fit of the coating was ensured by the foil polish (Fig. 1). Regarding several independent sources [1,2,10], the aluminum foil emissivity (ε) fits the range from 0.025 to 0.1. Our estimate is $\varepsilon = 0.025$ (polished foil [2]).

After the coating was finished, the manikin was placed into a calibration box, which itself was built inside a climatic chamber. The main role of the assembly was to maintain desired radiant and ambient temperature equal. Because of the equal radiant and ambient temperatures, the manikin's heat loss can be split into the convective and the radiative heat portions respectively using the low-emissivity coating. Next, three ambient temperature

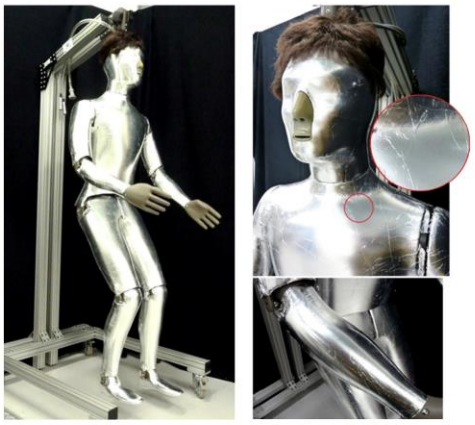

Fig. 1. Application of the low emissivity coating in detail.

probes were installed vertically, next to the manikin, in order to indicate a possible temperature gradient. The installation height of the probes represented an ankle, chest, and head posture. The ambient air speed was sensed by omnidirectional (spherical) anemometric probe set in front of the manikin's chest.

2.1. Determination of the radiative and convective heat transfer coefficients

Regarding the Stefan–Bolzmann law, reducing the surface emissivity of a body proportionally reduces its radiative heat flux. Thus, the heat production of the manikin with the low-emissivity coating is propagated mainly through convection. The radiative heat transfer coefficient can be expressed as below (2, 3, 4) applying the linearized formula of the heat transfer from the manikin (1) under the following conditions: (a) $T_a = T_r$; (b) h_c for the uncoated and coated manikin ($h_{c,foil}$) is the same; (c) the uncoated manikin's emissivity is $\varepsilon = 0.95$ (determined by separate measurement with an IR camera), and the polished foil emissivity is estimated to $\varepsilon = 0.025$.

$$h_0 = h_c + h_r \tag{2}$$

$$h_{0,foil} = h_{c,foil} + \frac{0.025}{0.95} h_r = h_c + \frac{0.025}{0.95} h_r \tag{3}$$

$$h_r = 1.027(h_0 - h_{0,foil}) \tag{4}$$

Convective heat transfer coefficient, h_c, is given by subtraction of h_r from the total heat transfer coefficient, h_0.

$$h_c = h_0 - h_r \tag{5}$$

2.2. Procedure

Firstly, the calibration box was assembled onto a geometric center of the climate chamber. Next, the manikin was hung by a head-mounted hook in the center of the calibration box facing the inlet nozzles of the chamber. Two postures were examined, seated with forearms in horizontal position, and standing with arms next to the manikin's body. To ensure its stability during the tests, the manikin had to be supported by its feet. Then, the box was equipped with the additional temperature probes together with the anemometric probe. After the box was closed, the climate chamber was initiated to maintain a desired temperature level. At the same time, the manikin was switched on to reach thermal equilibrium. A homogenous environment inside the calibration box was designed obeying standard ISO 14505 [21], and to have the following characteristics:

$$t_a = t_r = 24\ ^\circ\text{C} \pm 0.2\ ^\circ\text{C};\ v_a = 0.05\ \text{m s}^{-1};\ \Delta t_{0.1-1.1m} < 0.4\ ^\circ\text{C}$$

t_a ambient air temperature (°C),
t_r mean radiant temperature inside the box (°C),
v_a local air speed (m s^{-1}),
$\Delta t_{0.1-1.1m}$ temperature gradient; from 0.1 to 1.1 m above floor (°C).

The assembly preconditioning lasted typically around 2 h. Once the equilibrium was achieved, the data from all probes were recorded for one hour with 1 Hz frequency. The cases with the low emissivity coating were examined first; then, the coating was removed and the measurement scheme was repeated with the nude manikin. This procedure involved manipulation with the manikin before every test.

2.3. Equipment

The climate chamber located in the Laboratory of thermal comfort at Brno University of Technology was used as an ambient temperature regulator with precision of an automatic temperature controller limited to ±0.5 °C. Regarding the standard ISO 14505-2 [21], it was necessary to achieve precision within ±0.2 °C in the examined space. This was accomplished by a manual control mode with the additional temperature probes placed in the chamber. Moreover, the chamber was used in a recirculation mode without fresh air supply; this improved the stability of the ambient conditions. However, the air speed in the chamber was relatively high, up to 3 m s^{-1} and its deceleration was necessary (Fig. 2).

Nilsson [22] created a methodology to determine an equivalent temperature using a defined room—calibration box. The calibration box passively maintains the ambient air temperature and the mean radiant temperature of its walls equal. Not only temperature stabilization, but also ambient air speed deceleration and homogenization were crucial to create desired conditions. Both functions were achieved through lightweight construction of the calibration box, and its walls and floor micro ventilation. The walls were made of black breathable nonwoven fabric (density around 50 g m^{-2}, negligible heat capacity). This fabric had to be perfectly stretched on the skeleton in order to prevent its fluttering that caused unwanted turbulences inside the box. The skeleton was made of square aluminum profiles (45 × 45 mm). Inner dimensions of the box were 2 × 2 × 2 m. The ceiling was equipped with a small ventilation hole (0.5 × 0.5 m). To support the manikin's feet, square plywood (1 × 1 m) was used as a part of the floor. The rest of the floor consisted of the nonwoven fabric to supply a thermal plume with the air.

The thermal manikin Newton comprises 34 independently controlled zones, self-supporting construction and 10 movable joints (ankles, knees, hips, elbows, shoulders). Its body is made of several heat conducting carbon composite layers with a copper filling agent. Under the uppermost layer of every zone, a combined heating and temperature measuring system is embedded, where electric power is converted into heat. Under the steady state conditions, the amount of the supplied power is equal to the heat loss from the given zone. Indication of each zone and its surface area is given in Fig. 3. This configuration provides a uniform heat distribution within the zone and a very quick response to a change of ambient conditions. The manikin was examined nude, except for the head, which was covered with artificial short hair (Fig. 1). A control mode of the manikin was set to a constant surface temperature of 34 °C, as it is the closest approximation of a human skin

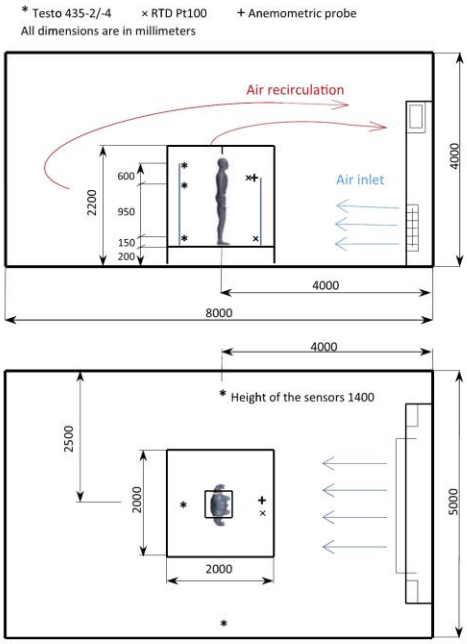

Fig. 2. The experimental assembly with positioning of the sensors.

temperature in thermal neutral conditions [7,22]. The temperatures around 34 °C are also used by other researchers [1,2,8,9].

Description and positioning of the temperature, anemometric, and heat flux sensors are summarized in Table 1 and in Fig. 2. All sensors were calibrated prior to the measurements, except for the heat fluxes measured by the manikin. The temperatures and air speed are logged via independent systems in a period of one second.

2.4. Statistical data evaluation

The main focus of the statistical data processing was on the heat fluxes, where the variability was the greatest. Typical sample standard deviation (SSD) of the heat flux was around 1.5 W m^{-2}; upper extreme on the feet 4 W m^{-2}. The ambient temperatures showed good stability typical SSD 0.03 °C, and the mean temperatures fitted into the recommended interval of 24 ± 0.2 °C [21]. Moreover, a very good stability of the manikins' surface temperatures was found, typical SSD 0.01 °C.

The purpose of the statistical data evaluation is following:

(a) To test a normal distribution of the data. Normality is a premise for the further calculations of the type A uncertainty, homogeneity of variances, and test for the means.
(b) To test homogeneity of variances. If the homogeneity is not rejected, the variances of the populations from which different samples are drawn are equal. This is also the second premise for the test for the means.
(c) To test if the population means are equal.

Firstly, the mean value representing one zone and one measurement was calculated from randomly selected thirty samples out of a pool of 1800 samples (the last thirty minutes of the measurement). This was done 408 times for the following situations: 3× nude standing; 3× nude sitting; 3× standing with the cover; 3× sitting with the cover, ×34 zones.

Secondly, the normal distribution of the randomly selected samples was tested using the Kolmogorov–Smirnov test at a significance level of 0.05. The null hypothesis, the data comes from standard normal distribution, was rejected only in the case of the zone 2 (head) by the first measurement with the nude manikin in the sitting position.

Next, for the purposes of the type A uncertainty evaluation, it is necessary to prove also the normal distribution of the mean values of three repeated measurements. This is, however, insignificant when less than ten repetitions are made. The actual testing was executed indirectly using data from hands that were not covered with the low emissivity foil. For the sitting and standing cases respectively, 12 + 12 independent samples were available from the hands. Normality in both cases was tested by the Anderson–Darling test. In both cases, the null hypothesis was not rejected

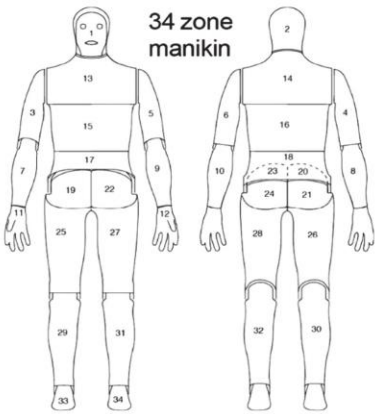

no.	ZONE	S [m²]	no.	ZONE	S [m²]
1	Face	0.0436	18	Lower Back	0.0503
2	Head	0.0939	19	R Up Thigh Fr	0.0487
3	R Up Arm Fr	0.0519	20	R Up Thigh Grd	0.0309
4	R Up Arm Bk	0.0317	21	R Up Thigh Bk	0.0274
5	L Up Arm Fr	0.0519	22	L Up Thigh Fr	0.0487
6	L Up Arm Bk	0.0317	23	L Up Thigh Grd	0.0309
7	R Forearm Fr	0.0384	24	L Up Thigh Bk	0.0274
8	R Forearm Bk	0.0264	25	R Lwr Thigh Fr	0.1032
9	L Forearm Fr	0.0384	26	R Lwr Thigh Bk	0.0488
10	L Forearm Bk	0.0264	27	L Lwr Thigh Fr	0.1032
11	R Hand	0.0461	28	L Lwr Thigh Bk	0.0488
12	L Hand	0.0461	29	R Calf Fr	0.0823
13	Upper Chest	0.092	30	R Calf Bk	0.0528
14	Shoulders	0.0793	31	L Calf Fr	0.0823
15	Stomach	0.1019	32	L Calf Bk	0.0528
16	Mid Back	0.0634	33	R Foot	0.0596
17	Waist	0.0468	34	L Foot	0.0596

Fig. 3. Manikin's zones indication and surface area dimensions.

Table 1
Temperature, anemometric, and heat flux sensors, types, accuracy and positioning.

Probe	Qty.	Uncertainty	Conf. (%)	Range	Placement
RTD TM Newton	2	±0.1 °C	95	−30 to 80 °C	80 cm in front of manikin's chest; 15 and 60 cm above box floor
Heat flux from a zone	34	±1% of value	95	–	–
Temperature of a zone	34	±0.1 °C	95	–	–
Wireless temp. TESTO 435-2/-4	3	±0.3 °C	95	−20 to 70 °C	80 cm behind manikin's back; chest, head and ankle level
Wireless temp. TESTO 435-2/-4	2	±0.3 °C	95	−20 to 70 °C	Outside the box on its L and R side, 1.4 m above floor
Anemometer – Value Tester, 8475	1	±1% of value	95	0.05 to 0.5 m s^{-1}	80 cm in front of manikin's chest; 80 cm above box floor

at a significance level of 0.05. Based on these findings, the normal distribution of the means is assumed across all zones.

Next, groups consisting of three means representing one particular zone and one case (eg., zone 1, sitting nude manikin) were examined exploiting the Bartlett test of homogeneity of variances. Homogeneity of variances was rejected 54 times at a significance level of 0.05. This means that at least one variance out of three is significantly different. The best matches were found on the Face, Front Forearms, Chest, Hands, Waist, Lower thighs. On the other hand, the worst were on Back forearms, Upper thighs, Back Calves.

Finally, the One way ANOVA test was applied to test the three means against the null hypothesis, the means are equal at a significance level of 0.05. The null hypothesis was rejected 130 times and only six were not rejected. This means that majority of the mean values are significantly different. This also means that further uncertainty evaluation is necessary.

2.5. Uncertainty evaluation

Type A uncertainty evaluation is an evaluation method of uncertainty through the statistical analysis of series of observations and is represented by a statistically estimated sample standard deviation of the mean $u_A(x)$ (6) [23]. This statement applies only to the following cases: (a) the data origin from independent observations under the same conditions of measurements; (b) variable x obeys the normal probability distribution. Based on the statistical tests, it is expected that the probability distribution characterized by the variable x and its standard uncertainty $u_A(x)$ (6) is approximately normal (Gaussian, confidence level ca 68.3%).

$$u_A(x) = \left[\frac{1}{n(n-1)}\sum_{i=1}^{n}(x_i - \bar{x})^2\right]^{\frac{1}{2}} \tag{6}$$

$u_A(x)$ type A uncertainty of variable x,
n number of independent observations, measurements,
x_i value of i variable x,
$\bar{x}$ mean value of variable x.

Formula (6) is not applicable if measurements are not repeated at least 10 times. This is due to insufficient evidence that the variable x is Gaussian. However, proving the opposite, as it was done in the subchapter 2.2, formula (6) can be used without any corrections.

Type B uncertainty evaluation is an evaluation method by means other than the statistical analysis of series of observations. To express the type B uncertainty, partial uncertainties of the heat flux, temperature of the zone, and ambient temperature were considered. Values of the uncertainties are shown in Table 1.

Uncertainties of indirect measurements were evaluated under the condition that the data from measurements were not correlated; to measure each physical value, a separate device was used. Uncertainty of indirect independent measurements is a function of each uncertainty from which the final uncertainty is calculated. If the final quantity x is a function of quantities $a, b, c, \ldots$, the final uncertainty u_x is calculated as follows [23].

$$x = f(a, b, c \ldots) \tag{7}$$

$$u_x = \sqrt{\left(\frac{\partial f}{\partial a}u_a\right)^2 + \left(\frac{\partial f}{\partial b}u_b\right)^2 + \left(\frac{\partial f}{\partial c}u_c\right)^2 + \ldots} \tag{8}$$

Combined standard uncertainty is calculated according to formula (9).

$$u_c = \sqrt{(u_A)^2 + (u_B)^2} \tag{9}$$

Further multiplication of standard uncertainty $u(x)$ by coverage factor $k = 2$ defines the expanded uncertainty $U(x)$ having the level of confidence of 95% [23].

$$U = k.u \tag{10}$$

Systematic errors stem from the selected approach, faulty laboratory equipment or insufficient knowledge of laboratory attendants. To start with, the radiation heat flux was eliminated by the low emissivity coating. Therefore, the residual radiative heat flux was non-zero and was compensated in the calculation, however, it is a source of uncertainty. Secondly, the additional layer of the aluminum coating increased thermal resistance on the surface of the manikin. However, this layer was composed of few micrometers thin aluminum foil and water based adhesive. It was assumed that the layer had an insignificant influence on the measurements. Thirdly, the surface structure of the manikin was changed due to the aluminum coating. Yet, this error was hardly describable, and negligible influence on the convection was assumed.

3. Results and discussion

The standard ISO 14505-2 [21] defines a segment as the manikin's portion that logically represents a part of human body (leg, chest, etc.). Hence, the segment is composed of one or more zones. If all zones of one segment have the same surface temperature, we can determine the segment total heat flux. This heat flux is given by the weighted average of each zone's flux where the "weight" is the surface area of the corresponding zone. The heat fluxes, coupled with corresponding temperatures, provided sufficient information to calculate h_c and h_r. The data were processed for each zone (segment), except for hands (zones 11, 12). Table 2 indicates the segmentation that was made by the authors of this paper; however, different definitions of the segmentation exist depending on the manikin physical construction. The pair zones are shown only for the right-hand side in the table. Please note that the segments "thighs" and "seat" vary when sitting or standing. This is

Table 2
Segmentation of the manikin Newton.

Segment Fojtlin (de Dear)	Zones
Head	Face (1), Head (2)
R Up Arm	R Up Arm Fr, (3) R Arm Bk (4)
R Forearm	R Forearm Fr, (7) R Forearm Bk (8)
Chest	Up Chest (13), Stomach (15) Waist (17)
Back	Shoulders (14), Mid Back (16), Lower Back (18)
R Thigh –Sitting	R Lwr Thigh Fr (25), R Lwr Thigh Bk (26)
R Thigh – Standing	R Up Thigh Fr (19), R Lwr Thigh Fr & Bk (25, 26)
Seat – Sitting	L & R Up Thigh Grd, (20, 21)
(Pelvic area – de Dear)	L & R Up Thigh Bk, (23, 24)
Seat – Standing	L & R Up Thigh Bk (21, 24)
(Pelvic area – de Dear)	
R Calf	R Calf Fr (29), R Calf Bk (30)
R Foot	R Foot (33)

due to the rigid body construction of the manikin, zones 19, 20, 22, 23 are activated or deactivated on purpose.

3.1. Convective heat transfer coefficients

Fig. 4 shows the mean values of h_c in complete overview of 34 zones, sitting and standing postures with combined uncertainty at a significance level of 0.05. The results of this work were compared with the results of two authors [1,2] in Fig. 6. Both works were selected because of the similar methodology used to determine heat transfer coefficients. On the other hand, different manikins with different segmentations were involved.

Firstly, de Dear et al. [1] and Quintela et al. [2] used in their papers the segment "pelvic area" whereas we use the term "seat". Regarding very different results ($h_{c\text{-}seat} = 4.40 \pm 0.27$ W m^{-2} K^{-1} for the sitting posture that is 1.6 times higher than those of the others), we assume a different physical constitution of these segments. Similar situation is also obvious on the manikin's back for sitting posture and feet. However, the anomalously high values of h_c of the feet, and segments closest to the floor indicate formation of local turbulence in the box. Later, an insufficient overlap of the nonwoven floor was found resulting in the actual turbulence. This was confirmed by the homogeneity tests and type A expanded uncertainty evaluation, where the uncertainty is notably high, up to ±4.37 W m^{-2} K^{-1}. Secondly, Quintela et al. [2] used the thermal manikin Maria without hair, de Dear et al. [1] operated with the manikin Monika with shoulder length hair, and the Newton had short hair. The differences in the results were obvious on the head; the highest h_c was found on the standing manikin Maria (h_c = 5.05 - W m^{-2} K^{-1}), lower values were determined with the Newton and Monika ($h_c \leqslant 3.70$ W m^{-2} K^{-1}) with the hair.

Next, Quintela et al. [2] applied a comfort control mode of the manikin's surface temperature. Therefore, the surface temperature of the manikin decreases with rising heat flux. However, the control model was not described in detail. The control mode of de Dear's experiment was not explicitly stated in his paper [1], only skin-to-air temperature gradient of 12 K was mentioned in the Conclusions. To support the stability of the temperature regulation during our tests, a constant surface temperature control mode of 34 °C was used. As a result, our h_c values are slightly higher compared to those of Quintela et al. [2].

Penultimately, it is assumed that the air entered the calibration box from the floor and the facial side of the manikin, and left the box through the ceiling opening. Consequently, the front parts of the manikin had lower fluctuation of h_c—lower type A uncertainty values. On the contrary, dorsal segments values varied more. De Dear et al. also present similar conclusions. The pair parts of the manikins show a very good match, what proves symmetrical conditions during the measurements. The maximum mismatch between pair body parts is always less than 0.3 W m^{-2} K^{-1}. The width of the uncertainty bars ranged up to circa ±1 W m^{-2} K^{-1}. In the most cases (disregarding seat, back, feet and head where different geometry applies), combined expanded uncertainties overlap with values of the other authors.

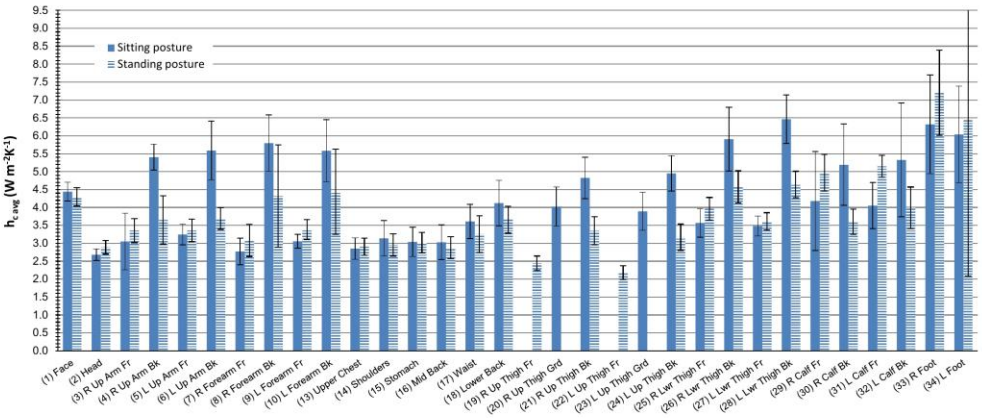

Zone	1	2	3	4	5	6	7	8	9	10	13	14	15	16	17	18	19	20	21	22	23	24	25	26	27	28	29	30	31	32	33	34
$U_{A\text{-}SIT\text{-}CONV}$	0.13	0.10	0.77	0.26	0.21	0.78	0.33	0.74	0.05	0.82	0.22	0.44	0.37	0.43	0.43	0.58	-	0.50	0.51	-	0.49	0.42	0.36	0.85	0.21	0.61	1.36	1.11	0.59	1.57	1.34	1.31
$U_{B\text{-}SIT\text{-}CONV}$	0.23	0.13	0.19	0.25	0.19	0.26	0.17	0.26	0.19	0.27	0.20	0.22	0.17	0.21	0.20	0.26	-	0.22	0.26	-	0.22	0.27	0.18	0.26	0.18	0.29	0.26	0.23	0.26	0.24	0.30	0.29
$U_{A\text{-}STND\text{-}CONV}$	0.08	0.13	0.27	0.63	0.25	0.18	0.41	1.40	0.19	1.16	0.12	0.22	0.20	0.22	0.47	0.30	0.11	-	0.31	0.11	-	0.28	0.21	0.35	0.05	0.22	0.44	0.23	0.15	0.50	1.13	4.37
$U_{B\text{-}STND\text{-}CONV}$	0.24	0.14	0.19	0.24	0.20	0.24	0.19	0.27	0.20	0.27	0.20	0.22	0.20	0.21	0.20	0.23	0.17	-	0.24	0.16	-	0.24	0.24	0.28	0.24	0.30	0.26	0.27	0.27	0.29	0.36	0.33

*all units [W/m^2.K]

Fig. 4. Overview of mean values of convective heat transfer coefficients in sitting and standing posture, combined uncertainty bars (95% conf.). Type A and B uncertainty evaluation in the table (95% conf.).

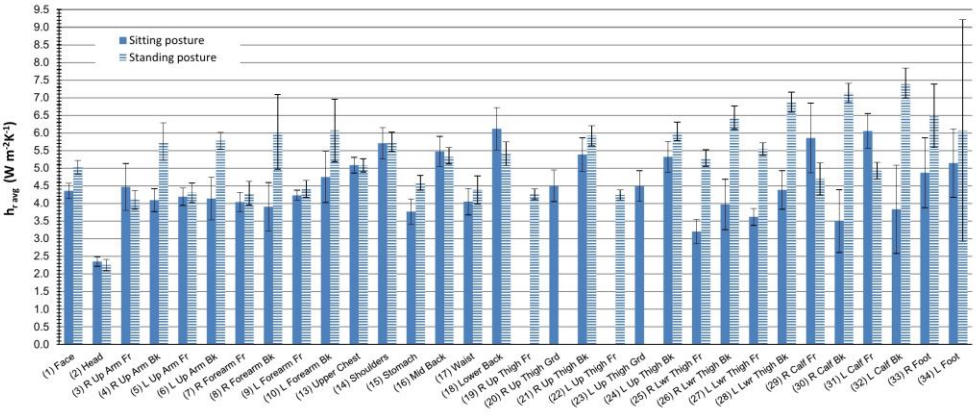

Zone	1	2	3	4	5	6	7	8	9	10	13	14	15	16	17	18	19	20	21	22	23	24	25	26	27	28	29	30	31	32	33	34
$U_{A\text{-}SIT\text{-}RAD}$	0.13	0.09	0.65	0.26	0.20	0.57	0.24	0.66	0.05	0.70	0.16	0.41	0.33	0.40	0.34	0.57	-	0.42	0.43	-	0.41	0.39	0.32	0.69	0.19	0.50	0.97	0.87	0.46	1.24	0.97	0.94
$U_{B\text{-}SIT\text{-}RAD}$	0.17	0.10	0.14	0.19	0.14	0.20	0.13	0.20	0.14	0.21	0.15	0.16	0.13	0.16	0.15	0.19	-	0.17	0.20	-	0.16	0.20	0.13	0.20	0.14	0.22	0.19	0.18	0.19	0.19	0.23	0.22
$U_{A\text{-}STND\text{-}RAD}$	0.06	0.12	0.22	0.50	0.23	0.16	0.30	1.04	0.18	0.86	0.11	0.21	0.15	0.17	0.37	0.29	0.08	-	0.23	0.08	-	0.20	0.15	0.25	0.04	0.18	0.41	0.18	0.12	0.36	0.86	3.14
$U_{B\text{-}STND\text{-}RAD}$	0.18	0.11	0.15	0.18	0.15	0.18	0.14	0.20	0.15	0.20	0.15	0.16	0.15	0.16	0.15	0.17	0.13	-	0.18	0.12	-	0.17	0.18	0.21	0.18	0.22	0.19	0.20	0.20	0.22	0.28	0.25

*all units [W/m^2.K]

Fig. 5. Overview of mean values of radiative heat transfer coefficients in sitting and standing posture, combined uncertainty (95% conf.). Type A and B uncertainty evaluation in the table (95% conf.).

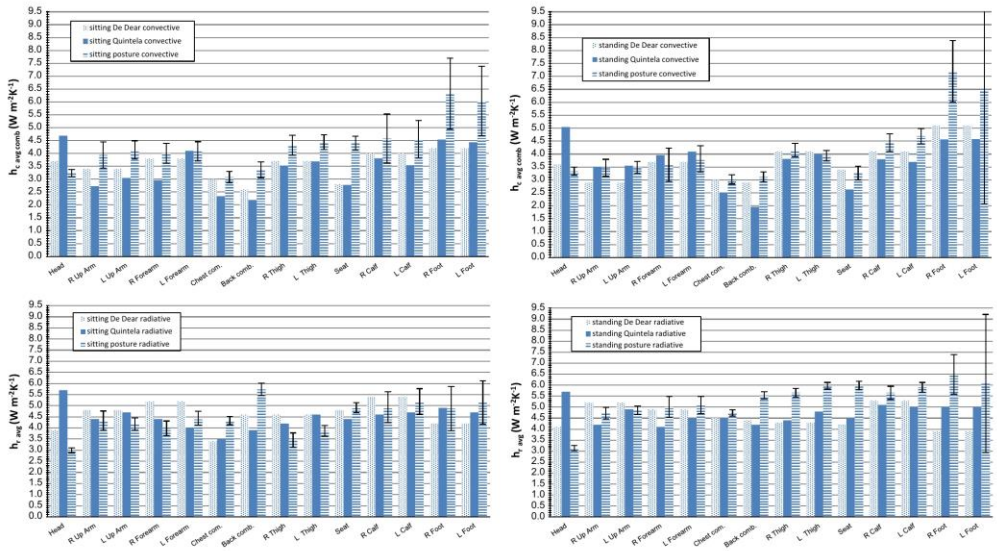

Fig. 6. Comparison of combined heat transfer coefficients de Dear et al. [1], Quintela et al. [2], Fojtlin combined uncertainty (95% conf.).

In conclusion, the sitting manikin has slightly higher h_c values than those of the standing. Particularly, limbs have a higher rate of cooling which corresponds with their geometry and theoretical expectations. Convective heat transfer coefficients match well with generally accepted wholebody values of around 3.7 W m^{-2} K^{-1}.

3.2. Radiative heat transfer coefficients

Values of h_r for 34 zones for the standing and sitting postures are listed in Fig. 5. Values for 14 segments are listed and compared with two other authors in Fig. 6.

Again, the values of h_r confirm theoretical expectations. The higher the view factor of the segment is, the more heat is emitted (e.g., face, lower thighs back). Overall, the manikin in standing posture has higher values of h_r compared to the sitting one. Despite the unlike geometries and the control mode of the manikins, the mismatch of the mean h_r results is lower than 1 W m^{-2} K^{-1}. Exceptions are found on the head and the feet where different conditions apply. We ascribe large values of the type A uncertainty on the lower limbs to the air fluctuation in the floor area. Yet, again, we assume a good match with generally accepted values ranging from 3 to 6 W m^{-2} K^{-1}.

To sum up, we provided the evidence that the repeatability of the measurements with the manikins is feasible even if only three measurements take place. Next, we showed that it is necessary to process the data statistically, even though the experiments were carried out in fine laboratory conditions. Statistics are the only way to reveal the confidence and accuracy of the results.

4. Conclusion

1. The thermal manikin Newton was involved to analyze dry heat transfer coefficients. Two cases were examined: sitting and standing postures. The ambient conditions were selected to represent thermal neutral environment; the air temperature was equal to the radiant temperature of 24 °C, and the air speed was maintained at 0.05 m s^{-1}. The measurements were repeated three times to express the type A uncertainty of the results.
2. The low emissivity coating was applied to the surface of the manikin to enable separation of the dry heat flux into the convective and radiative fraction.
3. The convective heat transfer coefficients of the sitting manikin were slightly higher than those of the standing. Opposite applies in the case of the radiative heat transfer coefficients. The same conclusions are also stated in the papers of other authors [1,8,9].
4. Mean values of heat transfer coefficients are in a very good match with other authors [1,2]. A mismatch varies between 0 and 1 W m^{-2} K^{-1} per segment; however, the extremes were found on the head, feet, seat and back where different conditions applied. Reproducibility of the measurements was achieved.
5. The type A and B uncertainties of the measurements were expressed at the 95% confidence level. Thanks to the uncertainty evaluation and statistics, we were able to indicate errors in the measurements (feet, calves). Even in the laboratory conditions, heat transfer coefficients vary significantly. Statistical data evaluation is thus essential.

Acknowledgements

The research was supported by the project LO1202 NETME CENTRE PLUS with the financial support from the Ministry of Education, Youth and Sports of the Czech Republic under the "National Sustainability Programme I".

References

[1] R.J. de Dear et al., Convective and radiative heat transfer coefficients for individual human body segments, Int. J Biometeorol., 40, 1997, pp. 141–156. ISB.
[2] D. Quintela et al., Analysis of sensible heat exchanges from a thermal manikin, Eur. J. Appl. Physiol. 92 (2004) 663–668, http://dx.doi.org/10.1007/s00421-004-1132-3.
[3] J.D. Hardy, The radiation of heat from the human body. I, J. Clin. Invest. 13 (1934) 593–604.
[4] J.D. Hardy, The radiation of heat from the human body. II, J. Clin. Invest. 13 (1934) 605–614.
[5] J.D. Hardy, The radiation of heat from the human body. III. The human skin as a black body radiator, J. Clin. Invest. 13 (1934) 605–620.
[6] M.C.G. Silva, J.A. Coelho, Convection coefficients for the human body parts determined with a thermal mannequin, in: 8th International Conference on Air Distribution in Rooms, Copenhagen, Denmark, 2002, pp. 277–280.
[7] American Society of Heating Ventilation and Air-Conditioning Engineers (ASHRAE), Thermal comfort, in: ASHRAE Fundamentals Handbook, ASHRAE, Atlanta, Ga, 2001 (Chapter 8).
[8] M. Ichihara, M. Saitou, S. Tanabe, M. Nishimura, Measurement of convective heat transfer coefficient and radiative heat transfer coefficient of standing human body by using thermal manikin, in: Proceedings of the Annual Meeting of the Architectural Institute of Japan, 1995, pp. 379–380.
[9] Y. Kurazumi et al., Radiative and Convective Heat Transfer Coefficients of the Human Body in Natural Convection, vol. 43, Elsevier Ltd.: Building and Environment, 2008.
[10] U. Danielsson, Convection Coefficients in Clothing Air Layers, Thesis, Royal institute of technology, Stockholm, 1993.
[11] S.W.K. Chang et al., Determination of the effect of walking on the forced convective heat transfer coefficient using an articulated manikin, ASHRAE Trans. 94 (1988) 71–81.
[12] Y. Nishi, A.P. Gagge, Direct evaluation of convective heat transfer coefficient by napthalene sublimation, ASHRAE Trans. 88 (1970) 120–130.
[13] S.C. Francisco, A.M. Raimundo, A.R. Gaspar, D.A. Quintela, Calculation of detailed radiative heat exchanges using Stokes theorem, in: 7th International Thermal Manikin and Modelling Meeting – University of Coimbra, 2008.
[14] A.R. Gaspar, A.V.M. Oliviera, D.A. Quintela, Effects of walking and air velocity on convective heat transfer from a nude manikin, in: Windsor Conference: Comfort and Energy Use in Buildings: Getting Them Right-International Conference, Windsor Great Park, UK, 2006, pp. 27–30.
[15] N. Luo, W.G. Weng, M. Yang, Experimental study of the effects of human movement on the convective heat transfer coefficient, Exp. Therm. Fluid Sci. 57 (2014) 40–56.
[16] Office for Official Publications of the European Communities, How Europeans Spend Their Time, Luxemburg: European Communities, 132 s, 2004. ISBN 92-894-7235-9.
[17] Ormandy David, Veronique Ezratty, Health and Thermal Comfort: From WHO Guidance to Housing Strategies, University of Warwick, UK, 2011.
[18] A. Chen et al., Human health and thermal comfort of Office workers in Singapore, Build. Environ. 58 (2012) 172–178.
[19] J.A.J. Stolwijk, Mathematical model of thermoregulation, in: J.D. Hardy, Gagge, J.A.J. Stolwijk (Eds.), Physiological and Behavioral Temperature Regulation, Thomas, Springfield, 1970, pp. 703–721.
[20] D.P. Wyon, Use of thermal manikins in environmental ergonomics, Scand. J. Environ. Health 15 (Suppl 1) (1989) 84–94.
[21] ISO 14505-2:2006 Ergonomics of the Thermal Environment – Evaluation of Thermal Environments in vehicles Part 2: Determination of Equivalent Temperature. Technical Committee ISO/TC 159.
[22] H.O. Nilsson, Comfort Climate Evaluation with Thermal Manikin Methods and Computer Simulation Models. Ph.D. Thesis, University of Gävle, 2004.
[23] JCGM 100, Evaluation of Measurement Data – Guide to the Expression of Uncertainty in Measurement, Paris: Joint Committee for Guides in Metrology (JCGM/WG 1), 2008.

Paper V

Journal of Thermal Biology 70 (2017) 64–68

Contents lists available at ScienceDirect

Journal of Thermal Biology

journal homepage: www.elsevier.com/locate/jtherbio

An innovative HVAC control system: Implementation and testing in a vehicular cabin

Miloš Fojtlín[a,*], Jan Fišer[a], Jan Pokorný[a], Aleš Povalač[b], Tomáš Urbanec[b], Miroslav Jícha[a]

[a] Department of Thermodynamics and Environmental Engineering, Energy Institute, Faculty of Mechanical Engineering, Brno University of Technology, Czechia
[b] Department of Radio Electronics, Faculty of Electrical Engineering and Communication, Brno University of Technology, Czechia

ARTICLE INFO

Keywords:
Vehicular cabin
Thermal manikin
Equivalent temperature
Thermal comfort

ABSTRACT

Personal vehicles undergo rapid development in every imaginable way. However, a concept of managing a cabin thermal environment remains unchanged for decades. The only major improvement has been an automatic HVAC controller with one user's input – temperature. In this case, the temperature is often deceiving because of thermally asymmetric and dynamic nature of the cabins. As a result, the effects of convection and radiation on passengers are not captured in detail what also reduces the potential to meet thermal comfort expectations. Advanced methodologies are available to assess the cabin environment in a fine resolution (e.g. ISO 14505:2006), but these are used mostly in laboratory conditions. The novel idea of this work is to integrate equivalent temperature sensors into a vehicular cabin in proximity of an occupant. Spatial distribution of the sensors is expected to provide detailed information about the local environment that can be used for personalised, comfort driven HVAC control. The focus of the work is to compare results given by the implemented system and a Newton type thermal manikin. Three different ambient settings were examined in a climate chamber. Finally, the results were compared and a good match of equivalent temperatures was found.

1. Introduction

A keyword Thermal comfort typed into a scientific database yields several hundreds of entries in which numerous methods have been proposed to predict thermal sensation and thermal comfort. The most relevant approaches to the subject of this work are well described in recent overview papers (Alahmer et al., 2011; Cheng et al., 2012; Croitoru et al., 2015; Hintea et al., 2014;). On the contrary, thermal management of the cabins remains almost unchanged for decades. Admittedly, CFD simulations and optimization processes resulted in an enhanced thermal experience, but the potential of available methodologies have not been exploited to the full.

The motivation for substantial interest in thermal comfort of passengers has several grounds. Firstly, microclimatic parameters in vehicular cabins are specific with respect to a wide range of air temperatures, radiant temperatures, air velocities and their spatial asymmetry (Alahmer et al., 2012; Ružić and Časnji, 2012; Simion et al., 2015). Moreover, majority of European car trips are shorter than 20 min (Cisternino, 1999) and such a short period is usually insufficient to ensure steady environment. Secondly, inappropriate environmental parameters account for thermal stress and negatively influence driver's cognitive abilities (Daanen et al., 2003; Milosević, 1997; Sheridan et al., 1991). Thus, a state of thermal comfort is not only important for passengers but also for prevention of driver's fatigue in personal, commercial and working vehicles. In addition, quality of microclimate is often a parameter which may influence preferences of a potential customer. Finally, the thermal management contributes to considerable energy drains. In steady thermal conditions, this may reach about 7% of a vehicle total energy consumption, whereas, the consumption could be quadruped (Farrington and Rugh, 2000; Kambly and Bradley, 2014) in peak loads. Compared to conventional automobiles, the situation is even more challenging in electric vehicles with a limited amount of energy stored in accumulators. As a result, new concepts of efficient energy utilisation are investigated.

Contemporary cabins are largely managed using manual or automatic HVAC systems that supply heat or cold based on passengers' preset. However, the incoming air is treated and distributed according to one user input – temperature. Certainly, there are also system inputs such as exterior and interior temperatures, air humidity, solar intensity, etc. (Daly, 2006). On the other hand, such a cluster of general information can provide only limited insight into the spatial effects of radiation and convection on the passengers. Moreover, these two parameters, together with clothing insulation, have a major impact on local thermal comfort. Hence, detailed resolution of the environ-

* Corresponding author. Address: OTTP 13302, Technická 2, Brno, Czechia.
E-mail address: milos.fojtlin@vutbr.cz (M. Fojtlín).

http://dx.doi.org/10.1016/j.jtherbio.2017.04.002
Received 12 January 2017; Received in revised form 11 April 2017; Accepted 12 April 2017
Available online 13 April 2017

mental parameters should be helpful for effective HVAC control and ventilation strategies, e.g. localized air-conditioning (Oh et al., 2014).

Higher spatial resolution of environmental parameters (air speed, air temperature, radiant temperature, and intensity of turbulence) can be achieved using state-of-the-art methodologies that are already available, but mostly in laboratory conditions. One of the most advanced devices to examine complex thermal environments is a thermal manikin (Nilsson and Holmér, 2003; Psikuta et al., 2015; Silva, 2002). In principle, the manikin generates artificial metabolic heat that is measured together with its surface temperature. To allow examining individual body parts, the surface of the manikin is usually divided into several independent segments. This enables the most accurate imitation and sensing of heat transfer from an artificial human body. On the other hand, manikins are expensive and suitable for laboratory use rather than field testing or permanent installation in the cabin. Therefore, a set of flat (directional) or ellipsoidal (omnidirectional) sensors can be used instead.

In case of measurement with the sensors, a total of six or more points are recommended for acceptable coverage of the body surface (Holmér et al., 1999). Next, the study concludes that each measurement approach yields significantly different results, yet, all of the methods can be useful for thermal comfort evaluation. Further, sensors are usually placed on an unheated manikin (a dummy) or a human-shaped stand (Mayer and Schwab, 1999; Silva, 2002; Zimny et al., 1999). This configuration promises better applicability in field conditions compared to the manikins. However, examples of measurements with the individual flat sensors installed in proximity of an occupant have not been found.

Nonetheless, information about heat transfer is insufficient to describe thermal comfort and it needs to be correlated with subjective perception of the environment. To do so, a concept of equivalent temperature (t_{eq}) can be exploited which has been shown to correlate with Mean Thermal Vote (Mayer and Schwab, 1999; Nilsson, 2007; Nilsson and Holmér, 2003).

The equivalent temperature is based on a physical phenomenon expressing the effect of the environment on dry heat transfer from a human body. According to the paper of Nilsson and Holmér (2003), it is defined as follows: *The equivalent temperature is the temperature of an imaginary enclosure with the mean radiant temperature equal to the air temperature and still air in which a person has the same heat exchange by convection and radiation as in the actual conditions.* This definition is depicted in Fig. 1, where the thermal manikin is exposed to two unlike environments. The situation on the left shows actual non-uniform environment, for instance a typical car cabin. The right picture illustrates an imaginary uniform enclosure in which the t_{eq} is equal to the t_{eq} of the left one. However, it must be assumed that the clothing, the posture, and the activity level are the same in both spaces.

Next, the standard 14505-2 (EN ISO, 14505-2, 2006) introduces four different definitions of the t_{eq} according to its means of determination. As there is no method to measure the t_{eq} directly, it can be calculated as: (a) whole-body; (b) segmental; (c) directional; (d) omnidirectional. Indeed, all definitions of the t_{eq} are principally the same, only the surface engaged in the sensing process is different.

The t_{eq} is defined by formula (1), where t_s is the temperature of a heated surface (normally 34 ± 0.1 °C). The surface temperature of 34 °C is considered as a good approximation of a mean skin temperature close to thermal neutral conditions. Next, Q represents the total dry heat flux density (W.m^{-2}) determined from the heated surface. Finally, h_{cal} is defined as the combined heat transfer coefficient obtained from a calibration in a standard environment.

$$t_{eq} = t_s - \frac{Q}{h_{cal}} \quad (1)$$

The content of this work follows the iHVAC project (Fišer et al., 2015) in which a system of cost-effective equivalent temperature sensors enables precise evaluation of the environment. This information can be used, in the future, for personalised, comfort driven HVAC control. Next, the t_{eq} was opted as it is correlated with Mean Thermal Vote (MTV), allows assessing thermal comfort via Comfort zone diagrams (Nilsson, 2007; Nilsson and Holmér, 2003) and the evaluation procedure is standardised (EN ISO, 14505-2, 2006). In addition, this approach has been recognised as a relatively new and promising method that is suitable primarily for non-uniform indoor environments (Cheng et al., 2012).

2. Methodology

The aim of this is study is to compare the performance of the implemented t_{eq} sensors system with a 34-zone Newton type thermal manikin seated on a driver's seat. In the first step, sixteen directional t_{eq} sensors are distributed along main body parts (head, chest, back and limbs) to allow spatial examination of the t_{eq} in the cabin. In total, one HVAC setting and three ambient conditions are studied in the Brno University of Technology climate chamber. Finally, signals from the sensors are optimized to match the output from the thermal manikin.

As two measurement systems were engaged in the study, h_{cal} had to be determined for each one of them. Firstly, the thermal manikin was calibrated in the climate chamber under standardized conditions: ambient temperature equals mean radiant temperature of 24 ± 0.2 °C; air velocity of 0.05 m s^{-1}; temperature gradient from 0.1 to 1.1 m above floor is less than 0.4 °C. Next, the manikin was wearing light summer clothing which consisted of cotton T-shirt, shorts, underpants, socks and sandals, and short hair (Fig. 2). The total clothing insulation was 0.21 Clo. Segmentation and dimensions of the manikin are described in detail in the publication by Fojtlín et al. (2016).

Further, the 34 zones of the manikin were merged into 16 segments that represent major human body parts (Table 1). The resulting segmental equivalent temperature is given by the weighted average of each zone's t_{eq} where the *weight* is the surface area of the corresponding zone (Fojtlín et al., 2016). However, body parts in direct contact with the seat cushion (back and seat) are excluded from the study, thus, results from 14 segments are presented. Firstly, it is because of the manikin rigid body construction that does not fit the seat

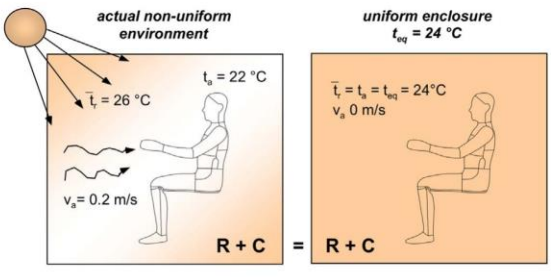

Fig. 1. Illustrated definition of the equivalent temperature, adopted from Nilsson (2004)

Fig. 2. Clothing and positioning of the manikin in the cabin.

Table 1
Aggregation maps of the sensors, pre and post optimization.

Body part	Pre-optimization map						Optimized map		
Scalp	16	23	34				16	23	
Face	16	23	24	31	32		16	23	31
Chest	11	16	23	31	32	33	11	23	33
Arm Upper Left	31	33					23	31	33
Arm Upper Right	14	16	32				14	16	32
Forearm Left	31	33					22	31	33
Forearm Right	14	32					14	22	32
Hand Left	11	31					11	31	
Hand Right	11	32					11	32	
Thigh Left	15	22	33				22	33	
Thigh Right	13	14	15				11	14	
Calf Left	15	21	22				21	22	
Calf Right	13	15	22				21	22	
Feet	12	21					12	21	22

perfectly. Secondly, the weight of the manikin is lower compared to a real person. This influences deformation and insulation properties of the seat cushion. Consequently, the heat fluxes from the manikin and the sensors are not representative and so are the equivalent temperatures. Finally, the h_{cal} values were defined for a free air boundary condition, not for contact with another solid body.

The calibration of the custom made t_{eq} sensors, developed by Department of Radio Electronics[2], was carried out under the same conditions as for the manikin.

The thermal manikin is suitable to determine the segmental or the whole-body t_{eq}, whereas, this work proposes exploitation of the directional t_{eq} using the equivalent temperature sensors with the flat heated surface (Fig. 3). To enable comparing these two systems, the directional t_{eq} values had to be allocated to the corresponding body parts (Table 1). Signals from the sensors were scaled to match the segmental equivalent temperatures determined by the thermal manikin. In the first run, the allocation and scaling were based on an estimate. In the second run, Generalized Reduced Gradient (GRG) algorithm with a variable step was applied to find the optimal scaling of the sensors. In addition, this approach has been shown as helpful to identify redundant signals from the sensors.

2.1. Construction of the equivalent temperature sensors

The custom made t_{eq} sensor consists of two circuit boards (Fig. 3, centre). The upper board is the actual equivalent temperature sensor heated by resistors. Its surface is encapsulated by a heat conducting composite to enable better heat distribution across the surface. The lower circuit board is embedded in the plastic body of the sensor. This board controls the upper board and sends signals to a central data concentrator. To avoid transferring heat from the electronics to the sensor board, the boards are separated by a thermal insulation. Such separation is crucial not to influence the sensor by parasitic heat flux during measurements.

The system was developed as a compact and modular solution where new sensors can be easily added or removed from a communication network. Apart from the boxed version of the sensor, there was also a need for a construction that would allow implementing the sensing circuit board onto the seat surface and into the HVAC vents (Fig. 3, right). Placing the sensors inside the vents guarantees quick response to the change of HVAC settings. For this reason, four sensors (31, 32, 35, 36) were modified and the sensor circuit board was extended from the sensor body by a wire. On the other hand, the control circuit board should be as close as possible to the heating element. It is because of an extension wires resistance that negatively influences precision of the heat flux measurement.

The measurement system was designed to be used in three basic working modes: (a) constant surface temperature; (b) constant heat flux; (c) passive thermometer. The presented work provides results from a constant surface temperature mode set to 34 °C. Sensors were calibrated against the nude manikin with the same setup. Further, design of the sensors allows thermal loads up to 1000 W m^{-2} while maintaining the sensor surface temperature at 60 ± 0.1 °C.

2.2. Measurement procedure

Firstly, the sensors were installed and their placement was opted to copy position of the major body parts. The spatial distribution of the 16 sensors in the cabin is shown in Fig. 4. In addition, the positioning was made with respect to possible permanent integration of the same type of sensors into the interior surfaces. The allocation of the sensors to the body parts is proposed in Table 1. The table shows the maximalist layout of the system and the optimized layout with regards to the number of the sensors.

Secondly, the Newton type manikin was seated on the driver seat in the mid-size experimental vehicle. The tests took part in the climate chamber by three ambient conditions: (a) Cold case, 10 °C; (b) Neutral case, 20 °C; (c) Hot case, 25 °C with a solar simulator set to 700 W m^{-2} and 70° above horizon facing the left side of the car. The cabin environment was managed by the HVAC unit pre-set to regime Automatic 22°.

Prior to the measurements, the car was preconditioned to reach ambient conditions with the running manikin on board. Next, the vehicle was started and the HVAC system was switched on. Data from the sensors and the manikin were recorded for one hour. Only stationary conditions were examined that were reached after approximately 40 min. Data from the last 5 min of the measurements are presented in this study. Transient cases are subject to the further research. Finally, the equivalent temperatures from the sensors and the manikin were determined for each body part.

3. Results and discussion

The results are summarised in Fig. 5, where there are shown differences between equivalent temperatures determined by the manikin and the on-board system. This study reveals behaviour of the system valid for the stationary conditions in the climate chamber obtained from single measurement. The repeatability and reproducibility of measurements with the Newton type manikin was shown in work by Fojtlín et al. (2016).

It is widely believed that a thermal manikin is the best tools to emulate thermal behaviour of a human with respect to radiative and convective heat losses. For this reason, it was opted as a benchmark for the testing. Nevertheless, from the perspective of heat transfer, the manikin behaves rather differently than the sensor. Firstly, the manikin, as well as a human, generates a thermal plume around its body. Resulting t_{eq}, determined by the sensor in the proximity of the manikin or the human, is thus affected by the plume. According to the study with Dressman and Newton type manikins (Fišer et al., 2014), t_{eq}

Fig. 3. Dimensions of the equivalent temperature sensor (left); insight into the sensor electronics (centre); application of the wired sensor into a HVAC vent (right).

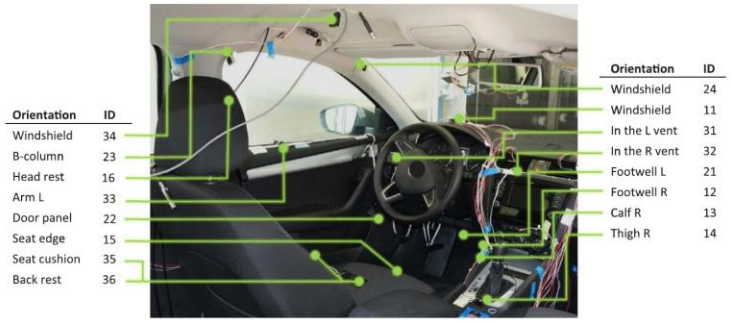

Fig. 4. A spatial distribution of the equivalent temperature sensors in the cabin.

determined by the sensors should be corrected to match the one determined by the manikin, however, this applies only to air velocities up to 0.5 m s^{-1}. Car cabins are typically supplied by large airflows (Fojtlín et al., 2015), so the air velocity is usually sufficient to mitigate effects of the plume and the correction is not necessary. Moreover, the sensors *11, 13, 14, 15, 22* are not influenced by the plume because of their placement in the cabin and at the same time they are not directly influenced by the airflow from the HVAC vents. Secondly, the human-like geometry of the manikin's surface has, naturally, a greater ability to realistically respond to the effects of convection and radiation, while, the sensors respond rather to spot changes. Therefore, it was vital to find representative placement of the sensors in the cabin.

Next, Fig. 5 shows that the first estimate of the sensor aggregation map (Table 1) yields results that differ from the manikin significantly. The greatest differences were found on the chest and limbs under all environmental conditions with extremes on the Chest and Right thigh of 4 K (Hot case). On the other hand, the smallest differences between the manikin and the system were found under thermal neutral conditions (Chamber 20 °C, no solar radiation). This was expected because of thermally symmetric ambient conditions, where the air temperature is close to the mean radiant temperature.

In the next step, the GRG optimization with a variable optimization step algorithm was applied to find the best solution for the scale coefficients under all ambient cases. In other words, it should find a universal solution to minimize differences between the t_{eq} obtained from the manikin and the on-board system.

Further, according to the thermal comfort evaluation via the comfort zones diagram, the width of the comfort zones varies depending on the selected clothing and the body-part sensitivity. Naturally, the bare parts have the narrowest comfort zones, except for hands that tolerate heat and cold well. Therefore, the correct comfort evaluation depends on precise determination of the corresponding t_{eq}. The target value for the t_{eq} differences was opted ± 1 K. On the other hand, the focus of the further research comprises testing of the system performance against a pool of volunteers in a real driving environment.

The optimization was found successful under cold conditions apart from the L (+2.33 K) and R (+1.57 K) calf. In the case of the Neutral conditions, the greatest differences were found on L (−1.40 K) and R (−2.28 K) thigh. Other body-parts were successfully optimized to desired differences. The optimization of the Hot case showed the best results having all the t_{eq} differences smaller than the target value ± 1 K.

The results from the optimization indicated that the optimal scale coefficients of the sensors *13, 15, 24, 34* were zero. This also means that the signals from these were redundant. At the same time, sensors *11, 22, 23* were allocated to the aggregation map to reduce peaks in the results of the optimization on the Left arm and the Right thigh (Table 1).

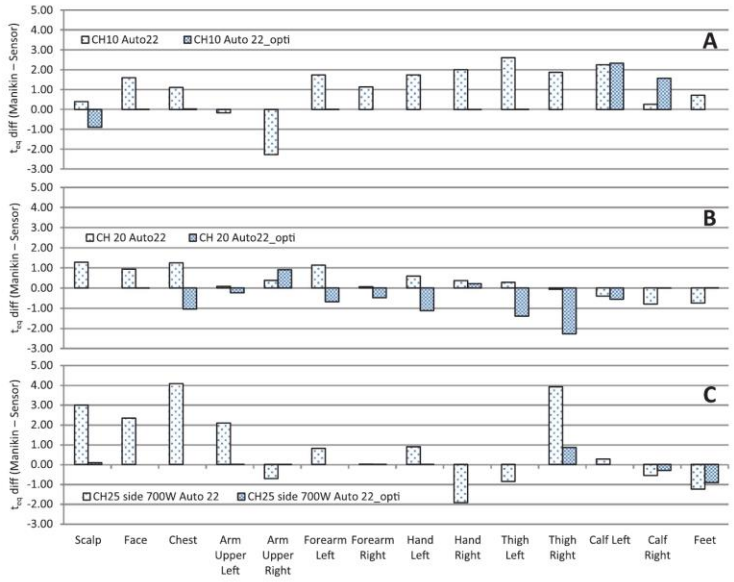

Fig. 5. Comparison of the cases: A – Chamber 10 °C; B – Chamber 20 °C; C – Chamber 25 °C, 700 W m^{-2}; pre and post optimization.

Generally, the most problematic parts to capture are the limbs. The main reason for this is their cylindrical shape and complicated positioning in the cabin. Therefore, the flat surface of the sensors struggles to follow the results from the manikin under variety of the environmental scenarios.

Finally, it should be noted that the Hot case was carried out with the solar simulator. It is of further investigation if the selected sensor surface temperature (34 °C) is suitable for a real cabin use. The interior temperatures in the car cabins can easily reach temperatures over 34 °C when exposed to direct sunlight. Under such solar loads, it is highly likely that the sensor surface temperature exceeds its prescribed value and it becomes *"blind"*. Therefore, for exposed sensors it might be useful to set a higher surface temperature. Another solution, proposed by the author of the method, H.O. Nilsson (Nilsson, 2004), is to switch the overheated sensor to the passive thermometer mode (pages 58–61 and Appendix D).

4. Conclusions

Presented study shows pilot results from the experiments carried out in the climate chamber using the experimental vehicle, the thermal manikin and the on-board system comprising 16 equivalent temperature sensors. The on-board system was designed as a cost effective modular solution available for permanent installation in the cabin. The study shows that the sensors are capable of detailed spatial evaluation of the equivalent temperature.

Additionally, the system outputs are aimed to be used, in the future, for comfort driven control actions of the cabin HVAC system. To do so, a comfort zone diagram that correlates the t_{eq} with the MTV (Mean Thermal Vote) or other suitable approach can be exploited. Compared to the contemporary HVAC management, this should result in personalised thermal comfort experience. Moreover, precise application of heat and cold is also believed to help reduce energy consumption of the HVAC system.

Next, the contact parts of the manikin body were excluded from the evaluation as proper h_{cal} values must be determined first. Secondly, it was found that in the thermally neutral environment the proposed system of sensors yields the equivalent temperatures almost identical as the manikin. The greatest differences were found under the cold and hot conditions. Thirdly, the system was optimized using the GRG algorithm to minimize differences between the manikin and the on-board system. This was achieved under all environmental conditions apart from the calves in the cold and the thighs in the neutral conditions (difference ± 2 K). Moreover, the optimization helped to identify four redundant sensors that were excluded from the study.

Penultimately, the system might be vulnerable to malfunction in the extremely hot environment, when the surface temperature exceeds 34 °C. This could be solved by switching the sensors to the passive thermometer mode. However, from the perspective of thermal comfort, equivalent temperatures over 34 °C always result in discomfort of an occupant, as there is no way of body cooling apart from evaporation by heavy sweating.

Finally, further experiments are aimed to evaluate the thermal comfort using the comfort zone diagram and the mean thermal vote. The real performance of the system will be tested based on the comparison of the comfort votes and the online evaluation from the on-board system.

Acknowledgement

The research is supported by the project Innovative Control of HVAC as the Part of Driver Assistance System, TA04031094. The authors gratefully acknowledge support from the projects Reg. No. FSI-S-14–2355 of the Brno University of Technology, and Josef Bozek Competence Centre for Automotive Industry" TE01020020 of the Technology agency of the Czech Rep. For simulations and experiments, equipment of the SIX Center was used (the grant LO1401).

References

Alahmer, A., Mayyas, A., Mayyas, A.A., Omar, M.A., Shan, D., 2011. Vehicular thermal comfort models; a comprehensive review. Appl. Therm. Eng. 31, 995–1002. http://dx.doi.org/10.1016/j.applthermaleng.2010.12.004.

Alahmer, A., Abdelhamid, M., Omar, M., 2012. Design for thermal sensation and comfort states in vehicles cabins. Appl. Therm. Eng. 36, 126–140. http://dx.doi.org/10.1016/j.applthermaleng.2011.11.056.

Cheng, Y., Niu, J., Gao, N., 2012. Thermal comfort models: a review and numerical investigation. Build. Environ. 47, 13–22. http://dx.doi.org/10.1016/j.buildenv.2011.05.011.

Cisternino, M., 1999. Thermal climate in cabins and measurement problems. In: Assessment of Thermal Climate in Operator's Cabs, Seminar Florence; JTI-Rapport. Swedish Institute of Agricultural and Environmental Engineering, Florence, pp. 15–23.

Croitoru, C., Nastase, I., Bode, F., Meslem, A., Dogeanu, A., 2015. Thermal comfort models for indoor spaces and vehicles — Current capabilities and future perspectives. Renew. Sustain. Energy Rev. 44, 304–318. http://dx.doi.org/10.1016/j.rser.2014.10.105.

Daanen, H.A.M., Vliert, Van De, Huang, X, E., 2003. Driving performance in cold, warm, and thermoneutral environments. Appl. Ergon. 34, 597–602. http://dx.doi.org/10.1016/S0003-6870(03)00055-3.

Daly, S., 2006. Automotive Air-conditioning and Climate Control Systems. Elsevier Ltd, Oxford, UK.

EN ISO 14505-2, 2006. Ergonomics of the thermal environment - Evaluation of thermal environments in vehicles - Part 2: Determination of equivalent temperature.

Farrington, R., Rugh, J., 2000. Impact of Vehicle Air-Conditioning on Fuel Economy, Tailpipe Emissions, and Electric Vehicle Range. In: Earth TechnologiesForum, Washington D.C.

Fiser, J., Thomschke, C., Bader, V., 2014. Impact of convective plume around human body on Teq measured by equivalent temperature sensors. Proc. Ambience14 10i3m. Tampere. 100–104.

Fišer, J., Povalač, A., Urbanec, T., Pokorný, J., Fojtlín, M., 2015. Implementation of the equivalent temperature measurement system as a part of the vehicle Heating, ventilation and Air-conditioning unit. Extrem. Physiol. Med. 4, A159. http://dx.doi.org/10.1186/2046-7648-4-S1-A159.

Fojtlín, M., Planka, M., Fišer, J., Pokorný, J., Jícha, M., 2015. Airflow measurement of the car HVAC unit using hot-wire anemometry. Exp. Fluid Mech. 2015, 173–178. http://dx.doi.org/10.1051/epjconf/201611402023.

Fojtlín, M., Fišer, J., Jícha, M., 2016. Determination of convective and radiative heat transfer coefficients using 34-zones thermal manikin: uncertainty and reproducibility evaluation. Exp. Therm. Fluid Sci. 77, 257–264. http://dx.doi.org/10.1016/j.expthermflusci.2016.04.015.

Hintea, D., Kemp, J., Brusey, J., Gaura, E., Beloe, N., 2014. Applicability of thermal comfort models to car cabin environments. ICINCO 2014 - In: Proceedings of the 11th International Conference Informatics Control. Autom. Robot. 1, 769–776. doi:http://dx.doi.org/10.5220/0005101707690776.

Holmér, I., Nilsson, H., Bohm, M., Norén, O., 1999. Equivalent temperature in vehicles – conclusions and recommendations for standard, In: Assessment of Thermal Climate in Operator's Cabs, Seminar Florence; JTI-Rapport. Swedish Institute of Agricultural and Environmental Engineering, Florence, pp. 89–94.

Kambly, K.R., Bradley, T.H., 2014. Estimating the HVAC energy consumption of plug-in electric vehicles. J. Power Sources 259, 117–124.

Mayer, E., Schwab, R., 1999. Correlation between thermal response and teq, In: Assessment of Thermal Climate in Operator's Cabs, Seminar Florence; JTI-Rapport. Swedish Institute of Agricultural and Environmental Engineering, Florence, pp. 63–70.

Milosević, S., 1997. Drivers' fatigue studies. Ergonomics 40, 381–389. http://dx.doi.org/10.1080/001401397188215.

Nilsson, H.O., 2004. Comfort climate evaluation with thermal manikin methods and computer simulation models. (Thesis) University of Gavle.

Nilsson, H.O., 2007. Thermal comfort evaluation with virtual manikin methods. Build. Environ. 42, 4000–4005. http://dx.doi.org/10.1016/j.buildenv.2006.04.027.

Nilsson, H.O., Holmér, I., 2003. Comfort climate evaluation with thermal manikin methods and computer simulation models. Indoor Air 13, 28–37. http://dx.doi.org/10.1034/j.1600-0668.2003.01113.x.

Oh, M.S., Ahn, J.H., Kim, D.W., Jang, D.S., Kim, Y., 2014. Thermal comfort and energy saving in a vehicle compartment using a localized air-conditioning system. Appl. Energy 133, 14–21. http://dx.doi.org/10.1016/j.apenergy.2014.07.089.

Psikuta, A., Kuklane, K., Bogdan, A., Havenith, G., Annaheim, S., Rossi, R.M., 2015. Opportunities and constraints of presently used thermal manikins for thermo-physiological simulation of the human body. Int. J. Biometeorol. 60, 435–446. http://dx.doi.org/10.1007/s00484-015-1041-7.

Ružić, D., Časnji, F., 2012. Thermal interaction between a human body and a vehicle cabin. Heat. Transf. Phenom. Appl. 295–318. http://dx.doi.org/10.5772/51860.

Sheridan, T., Meyer, J., Roy, S., Decker, K., Yanagishima, T., Kishi, Y., 1991. Physiological and Psychological evaluations of driver fatigue during long term driving. SAE Trans. 10. http://dx.doi.org/10.4271/910116.

Silva, M.C.G. Da, 2002. Measurements of comfort in vehicles. Meas. Sci. Technol. 13, R41–R60. http://dx.doi.org/10.1088/0957-0233/13/6/201.

Simion, M., Socaciu, L., Unguresan, P., 2015. Factors which influence the thermal comfort inside of vehicles. Energy Proc. 85, 472–480. http://dx.doi.org/10.1016/j.egypro.2015.12.229.

Zimny, K., Zenker, H., Doemoek, S., Ellinger, M., 1999. Comparison between Measured and Computer Simulated teq, In: Assessment of Thermal Climate in Operator's Cabs, Seminar Florence; JTI-Rapport. Swedish Institute of Agricultural and Environmental Engineering, Florence, pp. 71–81.